
# Functionalization of titanium surfaces with TGF-β inhibitor peptides

PhD thesis dissertation

**Pablo Sevilla Sánchez**

Supervisors:
Professor Conrado José Aparicio Bádenas, PhD
Professor Francisco Javier Gil Mur, PhD

Departament de Ciència dels Materials i Enginyeria Metal.lúrgica
E.T.S. d'Enginyeria Industrial de Barcelona
Universitat Politècnica de Catalunya

July 2013

*El infinito ciclo de las ideas y de los actos,*
*infinita invención, experimento infinito,*
*Trae conocimiento de la movilidad, pero no de la quietud;*
*Conocimiento del habla, pero no del silencio;*
*Todo nuestro conocimiento nos acerca a nuestra ignorancia,*

Del poema La roca, de T.S. Eliot (1934)

*A mis padres, Luis y Encarna*

*A mis hermanas, Marta y Susana*

*A mi sobrina, Sara*

*A Cristina*

# Agradecimientos, Aknowledgements, Agraïments

El día que comencé mi tesis doctoral me imaginé a mi mismo escribiendo estas palabras, las cuales, aunque abran éste manuscrito han sido redactadas en último lugar. Una tesis doctoral no se puede llevar a buen término sin la ayuda y colaboración de múltiples personas. Es por ello que me corresponde a mí el gesto de agradecer a todas aquellas personas que de alguna manera han participado y compartido este trabajo conmigo. He de reconocer que los agradecimientos de ésta tesis son las palabras que más ilusión me hace escribir de todo este documento.

En primer lugar quiero dar las gracias al director esta tesis, el profesor Francisco Javier Gil, no sólo por haberme dado buenos consejos y no haber dudado de mi capacidad para realizar este trabajo sino también por todos los años en los que ha sido mi mentor, mi amigo y por haber velado siempre por mis intereses. No tengo ninguna duda de que si no fuera el profesor Gil esta tesis nunca se hubiera realizado y yo no sería la persona que soy ahora. Por todo ello y mucho más: Gracias, Javier.

No menos intenso es mi agradecimiento al co-director de esta tesis, el profesor Conrado Aparicio. Sin la participación del profesor Aparicio esta tesis no tendría la calidad, rigurosidad y nivel científico que tiene. Hace ya más de 10 años que nos conocimos y desde entonces no ha dejado de apoyarme, ofrecerme oportunidades profesionales, darme buenos consejos y obsequiarme con su amistad incondicional. Estas palabras se quedan cortas para describir la admiración y agradecimiento que siento por el profesor Conrado Aparicio.

Quiero agradecer también a la Sra. Leonora Saavedra por su insuperable ayuda en la corrección lingüística de esta tesis la cual ha analizado con ojo clínico, por ayudarme a mejorar mi inglés, tanto escrito como hablado y por darme ánimos y apoyo en momentos difíciles. Y sobre todo por su absoluta hospitalidad y la de su familia que me conmovió verdaderamente.

Un especial agradecimiento al Dr. Daniel Rodríguez, quien desinteresadamente participó en muchas ocasiones en las actividades de codirección de esta tesis siempre con un punto de vista pragmático, útil y constructivo.

Le idea principal y más revolucionaria de esta tesis nació en Pamplona durante una estancia en el departamento de cirugía ortopédica traumatología de la Universidad de Navarra cuyo grupo de investigación está dirigido por el Dr. Iñigo Izal, quien, conociendo mis inquietudes me puso

en contacto con el profesor Francisco Borrás-Cuesta y el doctor Javier Dotor quienes junto con otros colaboradores crearon los péptidos inhibidores del TGF-β y los pusieron a mi disposición. Adicionalmente quiero agradecer a las investigadoras del departamento de traumatología Pury Ripalda, Patricia Sanz, Ana Zabalza, Carlos Arregui y Eduardo del Pozo por el buen ambiente que viví en Pamplona durante mi estancia gracias a todas estas personas.

Igualmente me gustaría agradecer a la profesora Mª Pau Ginebra por ser un ejemplo de liderazgo, dedicación, profesionalidad y buenas intenciones. Por haberme permitido formar parte del BiBiTe y estar siempre dispuesta a facilitar el trabajo de investigación.

Al profesor José María Manero, jefe de la línea de metales, por su buena disposición para solucionar todo tipo de dificultados y dudas siempre con buen humor y mucha paciencia.

Quiero hacer un especial agradecimiento al profesor Josep Anton Planell, uno de los más grandes investigadores que he conocido, por haberme acogido en el grupo de Biomateriales como técnico de laboratorio cuando él era el director y por haberme permitido utilizar los recursos y el equipamiento del IBEC sin los cuales esta tesis no habría sido posible.

Extiendo mi agradecimiento al grupo de biomateriales para terapias regenerativas del IBEC, dirigido por el profesor Planell, por su ayuda y por los buenos momentos que he pasado en el laboratorio con las Doctoras Elisabeth Engel y Melba Navarro, los doctores Miguel Ángel Mateos y Oscar Castaño y los investigadores Xavier Puñet en especial, Arlyng González, Riccardo Levato, Nadège Sachot, Aitor Sánchez, Tiziano Serra, Belén González, Laura Gómez y Giovanna Tormen.

My 5 months stay in Minneapolis was intense. The work done in the Minnesota Dental Research Center for Biomaterials and Biomechanics of the University of Minnesota was a key factor for the accomplishment of the objectives of this thesis. I had the opportunity to work with a big number of great researchers and I also made really good friends there. First, I want to thank Prof. Alex Fok, the director of the center, for accepting me. To Dr. Aparicio for supervise my work and Yu Ping Li, Xi Chen, Kyle Holmberg, Bao Hui, Lan Pham, Erik Jensen, Maria Pintado, Binna Han and Tamzid Mafiz whose were really helpful and kind anytime I needed them. Also, I spent a really happy time in Minneapolis thanks to the hospitality and good heart of many people such Conrado Aparicio, Jane Lewis, Lan Pham, Minh Hong, Arash Jafarian, Mahsa Abdolhosseini, Maria Pintado, Kyle Holmberg and Tamzid Mafiz. I have so many happy memories that won't ever forget. Vull agrair especialment a la Gemma Mestres per tots els moments passats amb ella, que van ser bonics i intensos.

He pasado cerca de 10 años en el grupo de Biomateriales del departamento de Ciencia de los Materiales e ingeniería metalúrgica de la UPC, más tarde acuñado como BiBiTe. Durante todos estos años mis actividades dentro del grupo han sido innumerables y he conocido y colaborado con muchísimas personas. Guardo una cantidad infinita de buenos recuerdos pasados en el grupo y en el departamento. Todos esos buenos momentos me ayudaron a tomar la decisión de realizar la tesis doctoral. Por eso quiero agradecer a todas las personas que trabajan o han trabajado en el departamento durante estos 10 años. En especial a la gente del grupo de biomateriales: Marta Pegueroles, Aleix Mestre, Carles Mas, Maria Godoy, Meritxell Molmeneu, Marc Fernández, Miquel Punset, Emiliano Salvagni, Jordi Guillem, Javier Peña, Marta González, Gemma Mestres, Yassine Maazouz, Edgar Montufar, Noelia Aparicio, Damien Lacroix, Montse Espanyol, Jérôme Noailly, Cristina Canal, Andrea Malandrino, Kiara Ricardi, Maite Valderas, Carolina Herranz, Sara Gallineti, Luis Delgado, Milena Arciniegas, Clara Sandino, David Pastorino, Judit Buixadera y Mónica Ortiz. Un agradecimiento especial al grupo de biofuncionalización con los que he pasado grandes momentos en el despacho y el laboratorio: Emiliano Salvagni, Virginia Paredes, Nathalia Marín y Mª Isabel Castellanos.

No puedo olvidar a los estudiantes de proyecto de final de carrera, master y doctorado que me acompañaron y colaboraron en este trabajo u otros trabajos relacionados durante su periplo estudiantil: Maria Godoy, Carlos Suárez, Magalí Forton, Maite Barrabès, Marta Díaz, Clemence Campion, Santiago Trigo y Gerard Fabregat.

Actualmente me encuentro trabajando de profesor en el departamento de mecánica de la Escola Universitaria Salesiana de Sarriá y todos mis compañeros de la escuela han sido también partícipes de esta tesis de alguna manera. A ellos quiero agradecer su paciencia, apoyo y ánimos para terminar esta tesis, lo cual no ha sido fácil debido a las múltiples actividades que he debido desarrollar durante este último año. En especial quiero agradecer su confianza y apoyo al director de la escuela, el Dr. Carles Rubio y a mis compañeros del departamento de mecánica: Marta Mata, Elena Bartolomé, Inma Ortigosa, Ignasi Florensa y Arkaitz Fano.

I would like to thank to Dr. Chiara Tonda-Turo and Dr. Helena Sepulveda Azevedo for reviewing this thesis and giving me their udeful advice and opinion.

También quiero dar las gracias al Ministerio de Educación y Ciencia por haberme concedido una beca FPU que me permitió realizar esta tesis de manera independiente y a la Universitat

Politècnica que Catalunya por haber puesto a mi disposición los recursos necesarios para realizar este trabajo de investigación.

Al escribir estos agradecimientos me he dado cuenta de que una tesis, al menos de la manera en que yo la he vivido, no es solamente un trabajo de investigación. Una tesis es en realidad una filosofía de vida que dura entre 3 y 8 años aproximadamente. Todos los demás aspectos importantes de mi vida se han visto afectados o influenciados de alguna forma por esta actividad. Una tesis no se queda en el laboratorio. Una tesis es algo que llevas puesto las 24 horas del día. Te acuestas y te levantas con ella, está en tu cabeza cuando comes con tu familia y cuando estas tomando una cerveza con tus amigos. Planificas una vida a corto plazo alrededor de esta actividad. Por tanto, hay personas ajenas a la investigación que participan activamente en una tesis y sin las cuales esta tesis no habría sido posible. En especial quiero agradecer a mi familia por que han sufrido mis ausencias y no han dejado de quererme y de apoyarme en ningún momento. Gracias Luis y Encarna por criarme, quererme y comprarme zapatos, gracias Marta y Susana por haberme aguantado y querido desde el día en que nací. Gracias también a Miguel, Sara, Jordi, Ana, Bernat y todos los tíos, tías, primos y primas que tengo, que son muchos.

Una filosofía de vida basada en una tesis doctoral requiere de evasión puntual o puede llegar a ser contraproducente. Mi vía de escape han sido siempre mis amigos y a ellos les debo, en este caso, que mi salud mental no se haya visto afectada, aunque ellos creen que nunca he gozado de una psique equilibrada. Gracias Cristian, Miquel, Alberto, Rubén, Marina, Carlos, Mercè, Lluis, Sergi, Opi, Ojeda, Delek, Alba, Sandra, Marcos, Isma y a todos los demás por todas las historias que hemos pasado juntos.

Y gracias a ti, Cristina, porque el día en que te conocí mi vida cambió y sigue cambiando sin cesar, siempre a mejor. Te quiero.

Gracias a todos.

# Abstract

This thesis is framed in the field of metallic biomaterials, specifically on titanium surfaces developed for bone regeneration. The most common applications of titanium as a biomaterial are dental implants and hip and knee prostheses. These components clinically require good stability and fixation to the bone in the long term. Titanium is an ideal material for these applications as it has high mechanical strength, toughness, corrosion resistance and, above all, a high capacity for osseointegration.

In general, titanium is a bioinert material where, once implanted, the living tissue generates a thin layer of fibrous tissue around the implant which separates the bone to the implant. An excessive thickness of this layer of fibrous tissue can compromise the stability and integration of the implant leading to the failure of the biomedical treatment.

The main objective of this thesis is the development of a new titanium surface with control and inhibition of the generation of fibrous tissue on the surface of the implant. We aim improving the osseointegration of implants and prostheses by benefiting cellular responses on the surface of the implant.

For the control of the formation of fibrous tissue on the surface we have developed new biofunctional titanium surfaces by covalently immobilizing two different short peptides on the metallic substrate. These two peptides are inhibitors of the effect of the cytokine TGF-β1, which increases the production of fibrous tissue by the activity of fibroblastic cells. These peptides, P17 and P144, have been developed by the team of our collaborators at the Dr. Francisco Borrás-Cuesta's lab, in the Centro de Investigación Médica Aplicada of the Universidad de Navarra

This thesis is divided into 6 chapters describing the development and characterization of titanium surfaces functionalized with TGF-β inhibitor peptides:

- Chapter 1: Introduction to the areas and important concepts of the thesis.
- Chapter 2: Design and development of a method of covalent immobilization of short peptides on titanium surfaces.
- Chapter 3: Study of the factors involved in the immobilization of short peptides on the titanium surfaces.
- Chapter 4: Physical-chemical characterization of titanium surfaces functionalized with the P17 peptide.
- Chapter 5: Physical-chemical characterization of titanium surfaces functionalized with the P144 peptide.
- Chapter 6: *In vitro* biological response of titanium surfaces functionalized with P17 and P144.

The most relevant results in the development of this thesis are:

- The development of a new method of covalent immobilization of peptides on titanium surfaces with a high density of peptide on the surface and with a good mechanical and thermal-chemical stability.
- The development of titanium surfaces with inhibitory action of TGF-β activity.
- The developed new surfaces are able to increase osteoblast differentiation, thereby potentially enhancing osseointegration of the biofunctionalized titanium implants and prostheses.

This research work contributes to increase the knowledge on covalent and non-covalent immobilization of short peptides on titanium surfaces. It also helps in increasing the knowledge of the action and inhibition of TGF-β on fibroblastic and osteoblastic cells; the later seeded on titanium surfaces. The developed material is an excellent candidate for its application in implantology and orthopedics.

# Resumen

Esta tesis queda enmarcada en el ámbito de los biomateriales metálicos, concretamente en superficies de titanio desarrolladas para la regeneración ósea. Las aplicaciones más habituales del titanio como biomaterial son los implantes dentales y las prótesis de cadera y rodilla. Estos componentes requieren, en servicio, buena estabilidad y fijación al hueso a largo plazo. El titanio es un material idóneo para el cumplimiento de estos requisitos gracias a su alta resistencia mecánica, tenacidad, resistencia a la corrosión y, sobre todo, por su alta capacidad de osteointegración.

En general, el titanio es un biomaterial bioinerte donde, una vez implantado, el tejido vivo genera una fina capa de tejido fibroso alrededor del implante la cual separa el hueso del implante. Un espesor excesivo de esta capa de tejido fibroso puede comprometer la estabilidad e integración del implante y conllevar el fracaso del tratamiento.

El objetivo principal de esta tesis es el desarrollo de una nueva superficie de titanio que sea capaz de controlar e inhibir la generación de tejido fibroso en la superficie del implante. De esta manera, tratamos de mejorar la osteointegración de implantes y prótesis mediante la mejora de la respuesta celular sobre la superficie del implante.

Para el control del crecimiento de tejido fibroso en la superficie se han desarrollado nuevas superficies de titanio donde se han inmovilizado dos tipos de péptidos cortos capaces de inhibir la interacción de la citoquina TGF-β, la cual incrementa la producción de este tipo de tejido por parte de las células fibroblásticas. Estos péptidos, llamados P17 y P144 han sido desarrollados por el equipo de nuestro colaborador el Dr. Francisco Borrás-Cuesta, en el Centro de Investigación Médica Aplicada de la Universidad de Navarra.

Esta tesis está dividida en 6 capítulos donde se describe el desarrollo y caracterización de las superficies de titanio funcionalizadas con péptidos inhibidores del TGF-β:

- Capítulo 1: Introducción a los ámbitos y conceptos importantes de la tesis.
- Capítulo 2: Diseño y desarrollo de un método de inmovilización covalente de péptidos cortos sobre superficies de titanio.
- Capítulo 3: Estudio de los factores que intervienen en la inmovilización de péptidos cortos sobre las superficies de titanio.
- Capítulo 4: Caracterización físico-química de las superficies de titanio funcionalizadas con el péptido P17.
- Capítulo 5: Caracterización físico-química de las superficies de titanio funcionalizadas con el péptido P144.
- Capítulo 6: Respuesta biológica *in vitro* de las superficies de titanio funcionalizadas con P17 y P144.

Los resultados más relevantes en el desarrollo de esta tesis han sido:

- El desarrollo de un nuevo método de inmovilización covalente de péptidos sobre superficies de titanio obteniendo una alta densidad de péptido en superficie con una buena estabilidad mecánica y termoquímica.
- La consecución de superficies de titanio capaces de inhibir la acción del TGF-β.
- Las nuevas superficies desarrolladas son capaces de incrementar la diferenciación osteoblástica y así, potencialmente mejorando la capacidad de osteointegración de implantes y prótesis de titanio.

Este trabajo de investigación contribuye a aumentar el conocimiento sobre la inmovilización covalente y no covalente de péptidos cortos en superficies de titanio. También contribuye en aumentar el conocimiento de la acción e inhibición del TGF-β en células fibroblasticas y osteoblásticas, estas últimas sembradas sobre superficies de titanio. El material desarrollado es un excelente candidato para su aplicación en implantología y traumatología ósea.

# 1. Introduction

## Contents

## 1.1. Scope

Metallic implant materials are, nowadays, completely established in the human society. A vast amount of metallic medical devices interact with the human body in order to repair, substitute or enhance biological functions or body parts. Among all of them, we can highlight hip and knee prostheses, dental implants, heart valves and cardiovascular stents [1].

The need for biomedical devices that integrate with the body tissues and avoid foreign body reactions, infection or inflammation is currently a reality. Therefore, the number of metallic materials which can opt to be good biomaterial candidates is limited but constantly growing thanks to the progress in science and technology. Among all the metals used as biomaterials, the most used are titanium and its alloys, stainless steel and cobalt based alloys [1].

In the case of metallic biomaterials that interact with bone, titanium has demonstrated its enormous capacity to integrate with hard tissues, making possible a myriad of new applications in the field of biomaterials as Brånemark stated in 1964 [2].

Currently, the new advances in biochemistry and materials science have enabled the modification of titanium surfaces in order to improve in many ways the host response to a biomaterial. The biofunctionalization of titanium surfaces in particular is at present an exciting field where the frontiers of knowledge expand every day and consists on tethering active biomolecules on the titanium surface in order to tailor the cell and tissue response to the surface.

## 1.2. Objectives

The improvement of the host tissue response to a titanium implant, such hip or knee prostheses and dental implants, is highly dependent on the modification of the implant surface. Biofunctionalization is a key process to achieve better osseointegration, less or null bacterial infection and hence, improve the performance of the titanium implant.

In this PhD thesis both the biofunctionalization processes of titanium surfaces and the parameters to achieve a successful biofunctionalization are studied. Furthermore, a new method to properly anchor oligopeptides on titanium surfaces has been developed. Also, a new titanium surface, biofunctionalized with TGF-β inhibitor peptides has been generated. We have evaluated its physicochemical properties and the in vitro response of various cell types to these newly developed titanium surfaces.

This chapter guides the reader through the main aspects of the thesis. The first section is a review of biofunctionalization processes focusing on biofunctionalization of titanium surfaces. The following section describes tissue response to titanium surfaces including cell material interactions. Finally, a description of the TGF-β superfamily and its effects on cell response is given. The aspects included in this introduction are dealt with in greater detail in the corresponding chapters where more specific information can be found.

## 1.3. Endosteal metallic implants

Most metallic biomaterials used in biomedical applications [3-5] are considered to be almost inert. Its biological activity, as regards the formation of a bone-implant interface, is much lower than other compounds such as calcium phosphates [6]. However, metals remain the most widely used material for implants which require mechanical toughness (dental, arthroplasties or cardiovascular) (Figure 1-1) due to their combination of mechanical properties such high

mechanical strength, high fracture toughness and low Young's modulus [7]. The main biocompatible metals are stainless steel, cobalt-based alloys and titanium-based alloys [1]. Titanium-based alloys have become the most widely used in orthopedic applications because of their high strength and low elastic modulus which is closer to the bone than other metal alloys. Moreover, corrosion is one of the major degradation processes that might occur in vivo, and should thus be considered when evaluating new biomaterials and new designs of medical devices. The bio-environment may be described as "aggressive" and is associated with a variety of salts and appreciable changes in the local pH conditions. Metals and alloys, which are extensively used in medical devices, might corrode severely in this bio-environment in accordance with both thermodynamic and kinetic considerations. This degradation process is undesirable firstly because it limits the functionality and lifetime of medical devices, and secondly because it releases corrosion products that may elicit an adverse biological reaction in the host [8]. The above mentioned titanium alloys have an excellent corrosion resistance due to the spontaneous formation of a passive oxide layer [5,9,10].

***Figure 1-1****: Left: Dental implant (Klockner) [11], middle: Hip prosthesis (Sony surgical) [12] , right: coronary stent (Boston Scientific) [13].*

The biocompatibility of a material is largely related to the reactions between the material surface and the host tissue inflammatory response [14]. This response depends on several factors, not only having to do with the biomaterial, but also with the characteristics of the patient and the surgical procedure [15]. If only the material is taken into account, the biocompatibility of a metal is mainly determined by the toxicity of the metals present, and their surface chemical reactions, corrosion, roughness and porosity [16,17].

The quasi-inert response of bio-metals is due to the encapsulation process that takes place after implantation, whereby the metal is surrounded and isolated from the surrounding tissue [18]. The first step of this process is that the implant is covered by blood clots containing

leukocytes, erythrocytes, platelets and coagulation proteins. Both implant and surgery trigger an inflammatory reaction which removes damaged tissue, clots and bacteria. Inflammatory cells, first as polymorphonuclear granulocytes and then as monocytes, reach the damaged area to purge debris and foreign material. If there is too much foreign substance for granulocytes to eliminate it, monocytes differentiate into macrophages. If there is a delay in removing the substance, the enzymes of activated macrophages affect the fibroblasts to make a fibrous capsule around the implant [19]. As long as phagocytic activation is maintained, the capsule becomes thicker. The inert material is encapsulated by a thin fibrous layer around the implant, which can be ideal for implants in contact with soft tissues. By contrast, hard tissue fibrous layer prevents the integration of the implant to the bone, weakening the implant to bone bonding [20,21].

### 1.3.1. Metal to bone interactions

In an ideal implant, bone would be expected to follow the processes described hereinafter. An inflammatory reaction, which is a reparative response, starts to take place between 2-3 days after the implant is placed. Then, the pluripotent cells from bone marrow differentiate into osteoblasts, forming a layer near the surface of the implant together with fibroblasts. Osteoblasts, fibroblasts and capillaries penetrate into the clot layer, replacing and filling the space between the bone and the implant with a collagen-rich extracellular matrix, which subsequently mineralizes [22]. Normally, there are vesicles in the extracellular matrix (ECM) and some of them include calcification focuses. So the presence of vesicles on the biomaterial implant in the early stages is a good sign of primary acceptance of the material. When the membranes of these vesicles burst, apatite crystals ($Ca_5$ ($PO_4$) $_3$ (F, Cl, OH)) emerge forming calcified structures [23]. These continue to grow and mineralize to reach and bind directly to the implant surface. In an ideal situation, the material would be covered by bone instead of by a fibrous layer.

Changes in the local environment, such as acidity, content of oxygen, electric charge, ion concentration, enzymes, growth factors, etc. have a strong effect on the differentiation and

migration of stem cells, precursors of osteoblasts [24-26]. The adhesion of these precursor cells to the substrate along with the formation of the mineralized ECM is essential for the differentiation of osteoblasts. In ideal biomaterials, there is an abundance of ECM and osteoblasts around their surface, which is confirmed by studying the adhesion [27] and proliferation of these cells on the surface [26,28].

Clinically, the process of direct bonding between the bone and the implant without the growth of a fibrous capsule between them was defined as osseointegration by Brånemark [29]. Osseointegration was originally defined as a direct structural and functional connection between ordered living bone and the surface of a load-carrying implant [30]. It is now said that an implant is regarded as osseointegrated when there is no progressive relative movement between the implant and the bone with which it has direct contact [31]. In practice, this means that in osseointegration there is an anchorage mechanism whereby non-vital components can be reliably and predictably incorporated into living bone and that this anchorage can persist under all normal conditions of loading. In non-ideal conditions, non osseointegrated implants biometals generally have a thick fibrous layer between the implant and the bone which makes them "quasi-inert" but not mechanically stable, despite having excellent mechanical properties to withstand loads. A different situation is observed with bioactive glasses which form a chemical bond between the implant and bone, but with mechanical properties inferior to those of metals, mainly, due to its high fragility [32]. Another cause of rejection of metallic implants is due to the release of biologically active substances (metal ions) or micro-particles of the worn surface [17,33-35]. Even micro-particles that are made of non-toxic materials can trigger a detrimental inflammatory response due to their size. These particles cause irritation and activate phagocytic cells, thereby initiating the production of inflammatory factors, which eventually leads to chronic inflammation, fibrosis, and osteolysis in bone porosity. Particles released from wear prevent the formation of an interface between the prosthesis and the implant, which induces the loss of the prosthesis. Furthermore, the wear of the metal increases its surface area and therefore the amount of released metal ions.

## 1.3.2. Titanium in implantology

Until the eighteenth century metallic materials used in surgical implants were mainly gold and silver, while steel began to be used in the nineteenth century. In the 20$^{th}$ century stainless steels, chromium, cobalt and molybdenum alloys made their debut, but it wasn't until the 40's that titanium and its alloys were introduced in the medical field [1]. It was Bothe, Beaton and Davenport who first observed the excellent biocompatibility of these metals, comparable to that of stainless steel or of Vitallium (CoCrMo) in their implants in animals [36].

Additionally, titanium has low density, 4.7 g/cm$^3$, when it is compared to 7.9 g/cm$^3$ of AlSl 316 stainless steel, 8.3 g/cm$^3$ CoCrMo alloy and 9.2 g/cm$^3$ CoNiCrMo alloy.

Its good mechanical properties and, mainly, its excellent corrosion resistance, make titanium a biomaterial of great interest for use in surgical implants [37].

### 1.3.2.1. Mechanical properties

There are four grades of commercially pure titanium (c.p. Ti) for surgical implants available, with increasing amount of interstitial or sustitutional elements (O, N, C, H and Fe) as the number of the grade increases. The impurity content determines the mechanical properties of commercially pure titanium (Table 1-1):

***Table 1-1:*** *Mechanical properties of commercially pure titanium*

| Property | Grade 1 | Grade 2 | Grade 3 | Grade 4 |
|---|---|---|---|---|
| Ultimate resistance (MPa) | 240 | 345 | 450 | 550 |
| Elastic limit (MPa) | 170 | 275 | 380 | 485 |
| Elongation (%) | 24 | 20 | 18 | 15 |
| Necking (%) | 30 | 30 | 30 | 25 |

The resistance of titanium and its alloys is generally inferior to that of stainless steel AISI 316 and cobalt based alloys, but in relation to its specific strength (strength/ density), titanium alloys are superior to others [38]. Another advantage of titanium in biomedical applications,

compared to stainless steel and cobalt-based alloys is that its Young's modulus is lower than that of these other metals (110 GPa for Ti in comparison to 200 GPa for stainless steel and 220 GPa for Co-based alloys). When a rigid implant is inserted in bone, the loads that the implant receives are absorbed by itself, transferring a low part of these loads to the surrounding bone due to the low elastic deformation of the implant. This effect is called stress shielding [39]. A lower elastic modulus, closer to the bone's Young modulus (around 20 GPa), lets the implant to transfer higher loads to its bone bed. This effect generates a higher stimulus on bone cells and improves bone remodelling [40]. However, titanium has a poor shear resistance, so that it is not suitable for bone screws and nails [41].

#### 1.3.2.2. Corrosion resistance

In a chemical point of view, in the biological environment where it is placed, the prosthesis or implant acts as an assembly of different metals and alloys within a liquid aqueous phase called electrolyte. This will produce corrosion, i.e. degradation or destruction of metals by reaction with their environment. Moreover, when a metal is in an aqueous solution, such as blood, metal ions form a lattice which allows electrons to move freely. An electric field is generated at the interface. Thus, as a result of power fluctuations due to random thermal agitation, a metal ion can escape from the metal and pass into the solution, and conversely, a metal ion from the solution can place itself somewhere on the metal surface. This transfer corresponds to the movement of electric charges from one phase to the other [42-44].

The excellent corrosion resistance of titanium alloys results from the formation of very stable, continuous, highly adherent, and protective oxide films on metal surfaces. Because titanium metal is highly reactive and has an extremely high affinity for oxygen, these beneficial surface oxide films form spontaneously and instantly when fresh metal surfaces are exposed to air and/or moisture. In fact, a damaged oxide film can generally reheal itself instantaneously if at least traces of oxygen or water are present in the environment. However, anhydrous conditions in the absence of a source of oxygen may result in titanium corrosion, because the protective film may not be regenerated if damaged [45,46].

### 1.3.3. Implant surface

The implant surface quality depends on its physicochemical properties and topography (Table 1-2). Both types of properties are relevant in the biological behavior of c.p. Ti [47].

Of particular importance is the fact that the early events that occur after implantation (contact with the blood, adsorption of proteins and other biological molecules, cell adhesion, etc...) are due to the interaction between the biological environment and the surface synthetic material. Likewise, the response of the biological reactions and pathways choosing particular cells and living organisms and, therefore, the sequence of events that lead to an appropriate osseointegration depend on a variety of surface properties. However, it is still not known in depth which of these factors is the most clinically relevant, and how they influence the body's response.

***Table 1-2:*** *Properties and information necessary to describe the surface quality of an implant [40]*

| Surface Properties | Information |
|---|---|
| **Chemical composition** | Atomic composition |
| | Chemical state of the elements |
| **Structure** | Cristalinity |
| **Order** | Inclusions |
| **Disorder** | Vacancies |
| | Grain boundaries |
| **Morphology** | 2D and 3D shape of the surface details |
| **Texture** | Surface index |
| **Roughness** | Porosity |
| **Shape** | |
| **Surface energy** | Wettability |
| | Adsorption capability |
| | Surface energy |
| **Electrical** | Surface potential |
| | Surface charges |
| | Corrosion behavior |
| **Mechanical** | Elasticity |
| | Plasticity |
| | Residual stresses |

#### 1.3.3.1. Topographical properties

The surface topography (surface roughness and texture) can be considered one of the most important surface properties which influence the body's response to the presence of an implant. The effect of surface topography on cell and tissue response has been extensively studied, both in vitro and in vivo [40,48-51]. It is well known, for example, that increasing the roughness of the c.p. Ti, enhances the osteoblastic response in vitro and in vivo, and improves mechanical anchoring to the implant. In fact, the surface topographies of commercial Ti implants, in most cases, have been specially designed and manufactured to produce topographic irregularities, at nanometric to micrometric scale.

#### 1.3.3.2. Physicochemical properties

A thorough description of the physicochemical properties of c.p. Ti surfaces should study the properties of the titanium oxide layer which develops naturally and spontaneously in contact with air and other media. This layer isolates the metal from the environment so that chemical and biological agents do not interact directly with the metal, but with this stable oxide layer, thus protecting the metal against oxidation that could provoke undesirable chemical and biological reactions and furthermore corrosion.

A number of different stoichiometries of titanium oxide can be identified on the surface of c.p.Ti ($Ti_3O$, $Ti_2O$, $Ti_3O_2$, TiO, $Ti_2O_3$, $Ti_3O_5$ and $TiO_2$) [52]. The most stable of them is $TiO_2$, with the titanium in the oxidation state +IV. Table 1-2 details the surface properties of titanium that have shown their influence on the interaction between the metal and the proteins and cells and thus, affecting its biological integration.

From the analysis of all these properties, the following conclusions can be drawn: [40,53]:

(1) The highly protective nature of the oxide layer, usually only a few nanometers thick, is responsible for its natural integrity and chemical stability in a wide range of pHs, electrolytes and fluids.

(2) The titanium oxide surface rapidly repassivates after local passivation loss, for example due to the effect of mechanical wear.

(3) The low solubility of hydrated titanium oxides, along with an even lower tendency to form loaded titanium compounds are very important aspects of the biocompatibility of titanium.

(4) It can be assumed that there is a certain physicochemical similarity between clean titanium oxide surface and water as a result of extensive hydroxylation / oxide hydration and moderate hydrophilicity. This entails a certain interaction with the surface and the water shell formed around the biomolecules, such as proteins.

(5) The dielectric constant of this oxide is similar to that of water. In aqueous fluids, this provokes the reduction of polarization and shielding of electrostatic forces between charged particles.

(6) The low surface charge, due to the isoelectric point of titanium oxide being only slightly below physiological pH, is believed to reduce the risk of establishing strong interaction between the titanium surface and the charged domains of proteins.

(7) After treating titanium surface with a strong base and temperature, a layer of carbonated calcium-phosphate is formed, giving to titanium the ability to form a surface apatite layer when immersed in a simulated (but protein and cell—free) body fluid ex vivo.

***Table 1-3:*** *Selected physicochemical properties of titanium and its oxide [47,53]*;

| Most stable oxide | TiO2 |
|---|---|
| Isoelectric point | 3.5-6.7 |
| Charge at pH=7 | negative |
| Oxide's dielectric constant | 86-170 |
| Solubility at pH=7 (mol/l) | $3 \cdot 10^{-6}$ |
| Charge of the dissolving species | 0 |
| Contact angle in water | 54 |
| Surface free energy ($mJ/m^2$) | 50 |
| Polar component ($mJ/m^2$) | 31.7 |
| Dispersive component ($mJ/m^2$) | 18.3 |

# 1.4. Biochemical surface modifications

Biomimetic surface modifications are those that try to mimic natural materials which have multifunctional hierarchical morphologies [54-57]. Bio-mimetics involve the study of biological microstructures to find the correlation between the structure with the physical and chemical processes carried out and to use this knowledge to design and synthesize new materials.

The objective in the development of bio-mimetic surfaces is to emulate nature to design biomaterials with increased functionality. A common example of modification to improve the biomimetic biofunctionality of natural or synthetic materials is to promote adhesion interactions between cells and the surface. This can be achieved by immobilizing peptides or extracellular matrix components on the surfaces that bind specific cell adhesion receptors promoting cell adhesion [58-60].

The goal of biochemical surface modification is to immobilize proteins, enzymes, or peptides on biomaterials for the purpose of inducing specific cell and tissue responses or, in other words, to control the tissue implant interface with molecules delivered directly to the interface. In contrast to other bioactive surfaces, such bioactive glasses or calcium phosphate coatings,

biochemical surface modification utilizes critical organic components of the body to affect tissue response [61].

### 1.4.1. Biomimetic coatings – biomolecule immobilization

The most promising process for increasing the bioactive properties of metallic implants is the immobilization of biomolecules, such as peptides, proteins or growth factors, mimicking the biochemical composition of the extracellular matrix at the molecular level, especially the adhesion of signals that the extracellular matrix presents to the cells. A key role of extracellular matrix in tissue repair is the production of adhesive proteins. The discovery of this function has resulted in many approaches to incorporate various proteins or their isolated adhesive domains on biomaterial surfaces [62].

The research and development on adhesive proteins led the discovery of the amino acid sequence most responsible of the adhesion between cells and tissues: The sequence RGD (Arginine-glycine-aspartic acid) [63]. Proteins that contain the RGD attachment site, together with the integrins that serve as receptors for them, constitute a major recognition system for cell adhesion. The RGD sequence is the cell attachment site of a large number of adhesive extracellular matrix, blood, and cell surface proteins, and nearly half of the over 20 known integrins recognize this sequence in their adhesion protein ligands. The integrin-binding activity of adhesion proteins can be reproduced by short synthetic peptides containing the RGD sequence. Such peptides promote cell adhesion when insolubilized onto a surface [64].

Besides studying the binding of natural enzymes or proteins to the surface of implants and prostheses, the research has mostly focused on binding short RGD containing peptides [65]), to prostheses, or immobilizing peptides that target specific binding to integrin receptors and other cell adhesion molecules.

Other important considerations to take into account so as to achieve the required biofunctionality have been reported by Porté-Durrieu et al.: The chemistry used to immobilize the biomolecule must provide a stable bond that is not susceptible to hydrolysis and that does

not denature or inactivate the biomolecule interfering with the functional domain structure. For effective interaction between the immobilized biomolecules and cell receptors there has to be a minimum number of bioactive species on the surface. The distance between these surface functional groups and the implant must be sufficient to allow flexible movement. Additionally, a particular orientation of the molecules and a specific configuration or structure is required [66].

The most widespread practices for immobilizing biomolecules is adsorb the biomolecules to the surface by physisorption taking advantage of electrostatic or hydrophobic interactions or to bond the biomolecules to the surface covalently by means of terminal amino groups, such as APTES, using carbodiimides or glutaraldehyde as binding agents [67,68]. The APTES (Aminopropyltriethoxy silane) is a silane having an amine as a terminal functional group. Another widely used strategy is to functionalize the metal oxide with maleimides and bind biomolecules via thiol (-SH) of cysteine [22,69].

#### 1.4.1.1. Immobilization of enzymes and proteins

The application of immobilization via glutaraldehyde terminated surfaces of several proteins on previously silanized metallic oxide has proven successful. Through this method researchers have adhered trypsin proteins [67], albumin and alkaline phosphatase [68] which has resulted in a stable link retaining the enzymatic activity of the protein for a period of 7 days.

The in vitro response of these new materials with proteins attached to previously silanized metal oxide surfaces has also been evaluated. Puleo et al. reported a significant induction of osteoblastic activity on C3H10T1/2 cells on samples functionalized by titanium plasma with bone morphogenetic protein (BMP-4) linked via amino groups using a carbodiimide crosslinker [70].

### 1.4.1.2. Immobilization of peptides on biomaterial surfaces

The immobilization of short peptides on metal oxide surfaces differs in some aspects to the immobilization of proteins. Being short molecules, they have greater mobility in solution enabling one to exploit the amino groups and carboxyl termini of the peptide for binding to the functional group of the substrate. This allows for greater control over the orientation and spatial configuration of the peptide attached to the surface. It is also possible to have more control over the junction points between the peptide and the functional groups of the substrate surface and therefore greater mobility control of the peptide once bound to the substrate.

Moreover, there is the possibility to cover the surface with different types of peptides for signaling domains for specific cellular functions, thereby making it possible to have a high cell behavior control on the surface. Xiao et al. linked RGDC (the cell adhesion RGD motif -arginine-glycine-aspartic acid-, plus a cysteine) to titanium functionalized with APTES [69,71]. The adhesion peptides containing the RGD domain have been shown to induce the cellular response, especially attachment in short cultivation times, obtaining different types of adhesion depending on the sequence and form of the peptide.

The immobilized RGD sequence also appears to trigger certain cellular signaling cascades, resulting in long-term events such as differentiation. The process is not known in detail, but the results suggest that the mode of immobilization of the peptide plays an important role [66,72].

Another approach to which many researchers are nowadays dedicating effort and achieving successful results is the development of new surfaces that avoid bacteria in several ways [73-77]. The development of new antimicrobial peptides (AMPs) that exhibit bactericidal, fungicidal, viricidal and tumoricidal properties, that act at a very low concentration, and that are less likely to promote bacterial resistance is a promising field of research. The immobilization of such peptides on biomaterial surfaces could improve biomaterial integration and avoid mid-term failures.

# 1.5. Cytokines and TGF-β superfamily

This section is an introduction to the cytokines and more specifically to the TGF-β superfamily of cytokines. As has been previously said, two titanium surfaces, biofunctionalized with TGF-β inhibitor peptides, have been developed. So it is convenient to understand the properties and functions of these proteins in the body. More information about TGF-β and TGF-β inhibitor peptides can be found in chapter 6.

## 1.5.1. Cytokines

Cytokines are low molecular weight proteins, typically between 15-30 kDa, consisting of 120-180 amino acids. Although they are in general produced by leukocytes, certain cytokines can also be secreted by many other cell types. The term originally established to designate biological products produced by lymphocytes in response to antigen was lymphokine. Subsequently its use was extended to similar molecules secreted by other cell types, which are included within the broader term cytokine. The term interleukin (IL) was applied to those molecules that serve as communication signals between leukocyte types, numbering them in correspondence to the order in which they were discovered (IL-1, IL-2, etc.). Some of them, despite being initially detected in *in vitro* functional assays, have nevertheless retained their original names according to their biological function so as to enable identification, as is the case with TNF (tumour necrosis factor) and TGF (transforming growth factor)[78].

The expression of most of the cytokines is strictly regulated by cells. In general, no significant production of these molecules can be detected, making cellular activation necessary to produce cytokines in sufficient quantities to exert biological effects. Most cytokines are secreted into the extracellular space in a glycosylated form that increases their stability and solubility. However, certain cytokines can accumulate inside the cell, or, alternatively, remain anchored to the membrane or to the extracellular matrix. In general, these molecules have a very short life span and operate at very low concentrations, on a picogram scale, by binding to high affinity

receptors present on the surface of the producer cell itself or other varied cell types [79]. Cytokines exert autocrine effect when they bind to receptors present in the producer cell itself. They may also have a paracrine effect by acting on different cell types found in their vicinity. In some cases they can be released into the blood or lymphatic circulation, exerting their effect on other organs and tissues, thus acting as endocrine hormones (Figure 1-2).

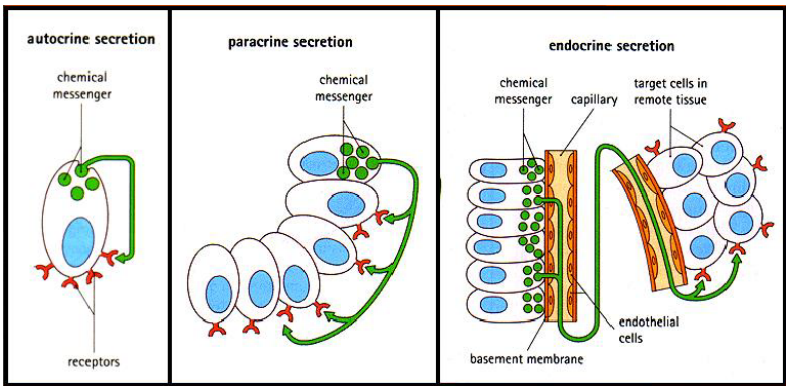


***Figure 1-2**: Cytokines can exert their effect in three ways: autocrine (same cell), paracrine (neighbouring cells) and endocrine (distant cells through the blood) [80]*

Two important functional characteristics of cytokines are their pleiotropy [81], such that a single cytokine is able to exert biological effects by acting on various different cell types, and their redundancy, i.e. several cytokines that may contribute to the development of the same function in a given cell type. One consequence of these properties is that in the absence of a particular cytokine, its functions can be wholly or partially replaced by others. Many of these biological characteristics of cytokines can be explained by the cellular structure and wide distribution of its receptors. The actions of cytokines are encompassed within a system or functional network, where the effect of a molecule is closely regulated, positively or negatively, by other molecules in the system. Thus, the secretion of a cytokine can be induced, enhanced or inhibited by other cytokines, which in turn may increase or inhibit the expression of its receptors.

The biological effects of cytokines can be varied, since they not only play an essential role in immune responses, but some of them are also involved in embryogenesis and development of organs (e.g., angiogenesis), while others play a key role in neuroimmune and neuroendocrine processes. Many are also important regulators, both positive and negative, of cellular events

such as mitosis, differentiation, migration, survival, cell death, and even its malignant transformation.

The biological activity of cytokines can be measured by different types of bioassays, using, for example, cell lines whose function depends on the presence of the factor under study. Currently, the most common technique used is solid phase immunoassays such as ELISA to measure the concentration of cytokines in biological fluids, and the ELISPOT to quantify cytokine-producing cells. It is also possible to quantify and characterize identifying cells producing intracellular cytokines by flow cytometry. Another possibility is the use of RT-PCR techniques to detect and quantitatively measure mRNA levels encoding a particular cytokine [82,83].

While most cytokines possess no sequence homology among themselves, some have been grouped into families based on their three-dimensional structure. With regards to the secondary structure of the molecule, cytokines are grouped according to whether they have an alpha-helical conformation (IFN-alpha, IFN-gamma, IL-2, IL-3, IL-4, IL-5, IL-6, IL-7, IL-9, G-CSF, M-CSF and GM-CSF), a beta-sheet structure (IL-1-alpha, IL-1-beta, TNF-alpha, TNF-beta and TGF-beta) or a composite structure alpha / beta (IL-8 and IFN-gamma). Moreover, the available gene analysis has led to the definition of groups of cytokines that are associated genetically.

#### 1.5.1.1. Cytokine receptors

Communication between the different cell types of the immune system and other body systems is mediated by cytokines. These molecules exert their biological effects through binding to specific receptors expressed at the cell surface. Cytokine receptors are membrane proteins which comprise a glycosylated extracitoplasmic binding region with the cytokine, a transmembrane region and a cytoplasmic region involved in the transmission of signals within the cell. The cloning of these receptors and many of its structure analysis has allowed it to be classified into four families according to common regions of homology within members of the same family [84].

The functional receptors have a high affinity to cytokines. Only low concentrations of cytokines are necessary for effective binding to their receptors ($10^{-9}$-$10^{-11}$M) and for triggering a corresponding biological effect. Moreover, these receptors are expressed in low numbers on the cell surface generally from a few hundred to a few thousand receptors per cell. The distribution of some of them, such as the IL-2 and IL-5, is restricted to a few cell types whereas others, amongst them IL-1, IL-4 and IL-6, are distributed in a wide variety of cell types [82]. The expression of cytokine receptors at the cell surface may be constitutive, i.e. regardless of any physiological stimulus, the cytokines will be produced or synthesized at a constant level. However, in some cases the cell may require previous activation as this generally tends to increase the number of receptors per cell.

Many cytokine receptors are complex multicatenary compounds of a chain that binds specifically to the cytokine (chain specific) and a chain that transduces signals into the cell and that is shared by other cytokine receptors (common chain). In general, for signal transduction, the specific binding of several chains (homodimers) or a specific chain with the common one (heterodimers) is required. In some cases, the interaction of three chains is involved in the formation of high affinity receptors. Signal transduction can occur by mechanisms common to all the families of receptors or by specific mechanisms of each of them. Many of the functional characteristics of cytokines, such as redundancy and pleiotropy, can now be explained by the current understanding of the composition and signalling mechanisms of its receptors [78].

Depending on their structure, cytokine receptors can be grouped into four different families: The immunoglobulin superfamily, the receptor family of tumour necrosis factor (TNFR), the family of receptors of hematopoietic growth factor (HGFR) including most cytokine receptors also referred to as receptor superfamily of cytokines and, finally, the family of chemokine receptors. Within each family, the homology between the different members is approximately 15 to 25%. There exist receptors that cannot be grouped in any of these families, for example: the receptor for epidermal growth factor (EGF), the A chain of the IL-2 receptor, and the receptor for transforming growth factor β (TGF-β).

### 1.5.2. TGF-β superfamily

There are two types of transforming growth factors, TGF-alpha and TGF-beta, which possess no structural similarity or share the same effects. Only TGF-beta has immunomodulatory effects. It is produced by T lymphocytes, platelets and numerous other cell types. Its name comes from the initial observation of phenotypic changes induced in rat fibroblasts. It increases proliferation of fibroblasts, osteoblasts and smooth muscle cells and increases the synthesis of extracellular matrix proteins, which promotes the healing of wounds. This cytokine also has immunosuppressive effects already observed to inhibit the growth and function of many cell types. In the immune system it seems to inhibit the synthesis and/or the effect of IFN-gamma, TNF-alpha, TNF-beta, IL-1, IL-2 and IL-3 [79].

The transforming growth factor beta (TGF-β) superfamily is a large family of structurally related cell regulatory proteins that was named after its first member, TGF-β1, originally described in 1983 [85].

Many proteins have since been described as members of the TGF-β superfamily in a variety of species, including invertebrates as well as vertebrates and categorized into 23 distinct gene types that fall into four major subfamilies [86-88]:

- The decapentaplegic-Vg-related (DVR) related subfamily (including the bone morphogenetic proteins and the growth differentiation factors)
- The activin/inhibin subfamily
- The TGF-β subfamily
- A group encompassing various divergent members

BMPs, GDFs, activins, and TGF-βs are homodimers, consisting of two extended monomers held together in most, but not all cases, by an inter-chain disulfide bond (Figure 1-3).

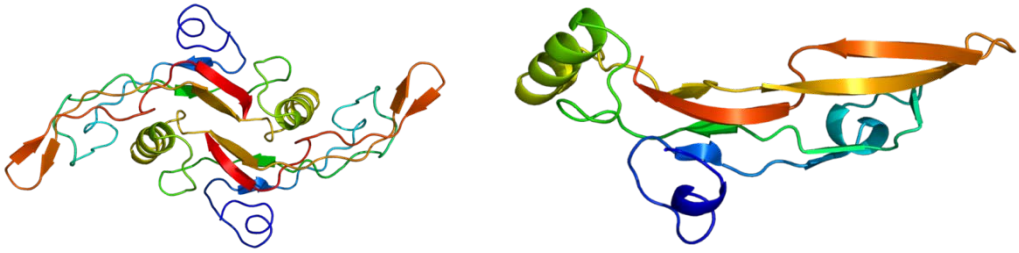

***Figure 1-3**: Left: structure of TGF-β1 homodimer. Right: Structure of TGF-β2 monomer [89]*

TGF-βs and related factors induce their response by assembling a heterotetrameric complex comprised of two type I - type II receptor pairs (Figure 1-4). Type I and type II receptors have the same overall domain structure, including a cysteine-rich extracellular domain that adopts a three-finger toxin fold, a single transmembrane helix, and an intracellular serine-threonine kinase domain. The human genome encodes seven type I and five type II receptors. Through cell based crosslinking studies, the BMPs and GDFs have been shown to bind multiple type I and type II receptors in mixed order, while the TGF-βs bind a single type I and a single type II receptor in a pronounced sequential order, first by binding the type II, TβR-II, followed by the type I, TβR-I. These biochemical findings provided the first hint that growth factor receptor complexes of the family might differ structurally [90].

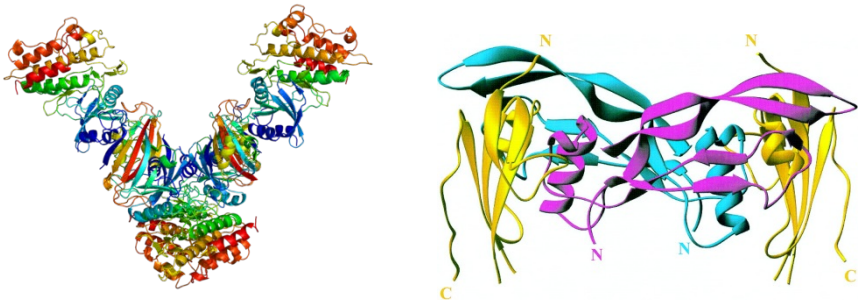


***Figure 1-4**: Left: Structure of TGF beta receptor 1 (TGFBR1) heterotetramer. Right: The structure of the bone morphogenetic protein (BMP)-2:BMPR-IA ectodomain complex. The two BMP-2 monomers forming the homodimer are shown in blue and magenta, and the two ectodomain molecules of BMPR-IA are in gold. The view is from the side with the C-termini of the receptor chains pointing toward the cell membrane [91].*

### 1.5.2.1. TGF-β subfamily

Transforming Growth Factor Beta 1, 2, and 3 (TGF-β1, TGF-β2, and TGF-β3) are highly pleiotropic cytokines that virtually all cell types secrete. TGF-beta molecules are proposed to act as cellular switches that regulate processes such as immune function, proliferation, and epithelial-mesenchymal transition. Targeted deletions of these genes in mice show that each TGF-beta isoform has some non-redundant functions: TGF-beta 1 is involved in hematopoiesis, endothelial differentiation and fibrotic response in different tissues; TGF-beta 2 affects development of cardiac, lung, craniofacial, limb, eye, ear, and urogenital systems; and TGF-beta 3 influences palatogenesis and pulmonary development [92]. The full range of *in vitro* biological activities of TGF-beta 5 has not yet been explored. However, TGF-beta 1, TGF-beta 2, TGF-beta 3, and TGF-beta 5 have been found to be largely interchangeable in an inhibitory bioassay, and it is anticipated that TGF-beta 5 will show a spectrum of activities similar to the other TGF-beta family members [93].

TGF-beta ligands are initially synthesized as precursor proteins that undergo proteolytic cleavage. The mature segments form active ligand dimers via a disulfide-rich core consisting of the characteristic 'cysteine knot'. TGF-beta signaling begins with binding to a complex of the accessory receptor betaglycan (also known as TGF-beta RIII) and a type II serine/threonine kinase receptor termed TGF-beta RII. This receptor then phosphorylates and activates a type I serine/threonine kinase receptor, either ALK-1 or TGF-beta RI (also called ALK-5). The activated type I receptor phosphorylates and activates SMAD proteins that regulate transcription. Use of other signaling pathways that are SMAD-independent allows for distinct actions observed in response to TGF-beta in different contexts [94]. TGF-beta signaling pathway is more widely treated in chapter 6.

#### *1.5.2.1.1. Inhibition of TGF-β*

During development, growth factors and hormones cooperate to establish the unique sizes, shapes and material properties of individual bones. Among these, TGF-β has been shown to developmentally regulate bone mass and bone matrix properties. However, the mechanisms

that control postnatal skeletal integrity in a dynamic biological and mechanical environment are distinct from those that regulate bone development. In addition, despite advances in understanding the roles of TGF-β signaling, the net effects of altered postnatal TGF-β signaling remain unclear [95]. Although, inhibition of TGF-β subfamily has demonstrated to provoke beneficial effects in many tissues [96,97].

There are, basically, three strategies to inhibit TGF-β:

1 - The use of peptides or antibodies that interact with TGF-β receptors (TGF-beta RI, RII or RIII) impeding them of interacting with TGF-β. This, usually, totally blocks the signaling pathway of all proteins related to the receptor [98].

2 - The use of peptides or antibodies which bind to TGF-βs at the sites where the cytokine interacts with the TGF-β receptors. This strategy can be more specific than the previous one due to the possibility of inhibit only one type of cytokine leaving the signaling pathway open for the interaction of the other proteins [99].

3 – The inhibition of SMADs through antibodies which interact with these proteins inside the cell skeleton. This approach requires a profound knowledge of TGF-β signaling pathway but provides the possibility of inhibit specific pathways in order to gain knowledge about the effects of TGF-β on cell and tissue response [100].

TGF-β inhibition is a promising strategy to inhibit undesired effects on bone regeneration such the production of excessive fibrous tissue or to accelerate osteoblastic and osteoclastic activity [101-103].

# 1.6. Conclusions

Implant success is intimately related to its surface properties. The cell response *in vitro* and *in vivo* will be determined by a number of physical and chemical properties of the implant. Of all surface properties, chemical composition and surface topography may be the most important for implant purposes.

Biochemical surface modification of metallic biomaterials is a promising approach to develop new devices and improve the biological response to metallic implants. Two currently developed tendencies seem to be the most auspicious: the immobilization of adhesive peptides to promote cell adhesion on biomaterial surface, and the immobilization of antimicrobial peptides to avoid bacterial infection.

TGF-β inhibition opens a new perspective to improve the regeneration of bone and other tissue regeneration. Combined with biochemical surface modification, TGF-β inhibition can be an innovative and promising approach to improve the integration and performance of implants and prostheses.

# 1.7. References

1. Ratner B, Hoffman A, Schoen F, Lemons J. Biomaterials science, third edition: An introduction to materials in medicine. : Academic Press, 2012.

2. Brånemark PI, Breine U, Johansson B, Roylance PJ, Röckert H, Yoffey JM. Regeneration of bone marrow. Acta Anatomica 1964;59:1-46.

3. Kasemo B, Gold J. Implant surfaces and interface processes. Adv Dent Res 1999;13:8-20.

4. Navarro M, Michiardi A, Castano O, Planell JA. Biomaterials in orthopaedics. J R Soc Interface 2008;5:1137-1158.

5. Geetha M, Singh AK, Asokamani R, Gogia AK. Ti based biomaterials, the ultimate choice for orthopaedic implants – A review. Progress in Materials Science 2009;54:397-425.

6. Lin D, Ju C, Huang S, Tien Y, Yin H, Chen W, Chern Lin J. Mechanical testing and osteointegration of titanium implant with calcium phosphate bone cement and autograft alternatives. Journal of the Mechanical Behavior of Biomedical Materials 2011;4:1186-1195.

7. Burg KJL, Porter S, Kellam JF. Biomaterial developments for bone tissue engineering. Biomaterials 2000;21:2347-2359.

8. Blackwood D.J. Biomaterials: Past Successes and Future Problems. Corr Rev 2011;21:97.

9. Kim T, Han J, Lee I, Lee K, Shin M, Choi B. New titanium alloys for biomaterials: A study of mechanical and corrosion properties and cytotoxicity. Biomed Mater Eng 1997;7:253-263.

10. Contreras R, Sahlin H, Frangos JA. Titanate biomaterials with enhanced antiinflammatory properties. Journal of Biomedical Materials Research Part A 2007;80A:480-485.

11. Klockner. Klockner Implant system. http://www.klockner.es/. 2012.

12. Sony. Sony Surgicat PVT. http://www.sonysurgical.com/Orthopaedic-Hip-Prosthesis.html. 2012.

13. Boston S. Boston Scientific. http://www.bostonscientific-international.com/home.bsci. 2012.

14. Rodil SE. Modificación superficial de biomateriales metálicos. Revista Latinoamericana de Metalurgia y Materiales 2009;29:67-83.

15. Covani U, Giacomelli L, Krajewski A, Ravaglioli A, Spotorno L, Loria P, Das S, Nicolini C. Biomaterials for orthopedics: A roughness analysis by atomic force microscopy. Journal of Biomedical Materials Research Part A 2007;82A:723-730.

16. Zreiqat H, Valenzuela SM, Nissan BB, Roest R, Knabe C, Radlanski RJ, Renz H, Evans PJ. The effect of surface chemistry modification of titanium alloy on signalling pathways in human osteoblasts. Biomaterials 2005;26:7579-7586.

17. Virtanen S. Corrosion of Biomedical Implant Materials. Corrosion reviews 2008;26:147-171.

18. Kasemo B. Biocompatibility of titanium implants: Surface science aspects. J Prosthet Dent 1983;49:832-837.

19. Anderson JM, Rodriguez A, Chang DT. Foreign body reaction to biomaterials. Semin Immunol 2008;20:86-100.

20. Lee TM, Tsai RS, Chang E, Yang C,Y., Yang MR. The cell attachment and morphology of neonatal rat calvarial osteoblasts on the surface of Ti-6Al-4V and plasma-sprayed HA coating: Effect of surface roughness and serum contents. J Mater Sci Mater Med 2002:341-350.

21. Santavirta S, Takagi M, Konttinen YT, Sorsa T, Suda A. Inhibitory effect of cephalothin on matrix metalloproteinase activity around loose hip prostheses. Antimicrob Agents Chemother 1996;40:244-246.

22. Rezania A, Johnson R, Lefkow AR, Healy KE. Bioactivation of Metal Oxide Surfaces. 1. Surface Characterization and Cell Response. Langmuir 1999;15:6931-6939.

23. Sela J, Gross UM, Kohavi D, Shani J, Dean DD, Boyan BD, Schwartz Z. Primary mineralization at the surfaces of implants. Crit Rev Oral Biol Med 2000;11:423-436.

24. Chai C, Leong KW. Biomaterials Approach to Expand and Direct Differentiation of Stem Cells. Mol Ther 2007;15:467-480.

25. Manso M, Ogueta S, Pérez-Rigueiro J, García JP, Martínez-Duart JM. Testing biomaterials by the in-situ evaluation of cell response. Biomol Eng 2002;19:239-242.

26. Tognarini I, Sorace S, Zonefrati R, Galli G, Gozzini A, Carbonell Sala S, Thyrion GDZ, Carossino AM, Tanini A, Mavilia C, Azzari C, Sbaiz F, Facchini A, Capanna R, Brandi ML. In vitro differentiation of human mesenchymal stem cells on Ti6Al4V surfaces. Biomaterials 2008;29:809-824.

27. Bigerelle M, Anselme K. A kinetic approach to osteoblast adhesion on biomaterial surface. Journal of Biomedical Materials Research Part A 2005;75A:530-540.

28. Chang EJ, Kim HH, Huh JE, Kim IA, Seung Ko J, Chung CP, Kim HM. Low proliferation and high apoptosis of osteoblastic cells on hydrophobic surface are associated with defective Ras signaling. Exp Cell Res 2005;303:197-206.

29. Davies JE. Bone bonding at natural and biomaterial surfaces. Biomaterials 2007;28:5058-5067.

30. Branemark PI, Hansson BO, Adell R, Breine U, Lindstrom J, Hallen O, Ohman A. Osseointegrated implants in the treatment of the edentulous jaw. Experience from a 10-year period. Scand J Plast Reconstr Surg Suppl 1977;16:1-132.

31. Branemark R, Branemark PI, Rydevik B, Myers RR. Osseointegration in skeletal reconstruction and rehabilitation: a review. J Rehabil Res Dev 2001;38:175-181.

32. Kim H, Song J, Kim H. Bioactive glass nanofiber?collagen nanocomposite as a novel bone regeneration matrix. Journal of Biomedical Materials Research Part A 2006;79A:698-705.

33. Beech IB, Sunner JA, Arciola CR, Cristiani P. Microbially-influenced corrosion: damage to prostheses, delight for bacteria. Int J Artif Organs 2006;29:443-452.

34. Jacobs JJ, Hallab NJ, Urban RM, Wimmer MA. Wear particles. J Bone Joint Surg Am 2006;88 Suppl 2:99-102.

35. Doorn PF, Campbell PA, Amstutz HC. Metal versus polyethylene wear particles in total hip replacements. A review. Clin Orthop Relat Res 1996;(329 Suppl):S206-16.

36. Bothe RT, Beaton LE, Davenport HA. Reactionofbonetomultiplemetallicimplants. Surgery gynecology and obstretics 1940;71:598-602.

37. Gil FJ, Planell JA. Aplicaciones biomédicas del titanio y sus aleaciones. Biomecánica 1993;1:34-42.

38. Donachie MJ. Titanium and titanium alloys (source book). : Asm Intl, 1982.

39. Chapter 3. designs of joint endoprostheses. Tribology and Interface Engineering Series: Elsevier. p. 75-129.

40. Brunette D, Tengvall P, Textor M. Titanium in medicine: Material science, surface science, engineering, biological responses and medical applications (engineering materials). : Springer, 2001.

41. Niinomi M. Mechanical properties of biomedical titanium alloys. Materials Science and Engineering: A 1998;243:231-236.

42. Great Britain Committee oC. Corrosion control in engineering design / department of industry, committee on corrosion. London : H.M. Stationery Off, 1978.

43. Stratmann M. Lectures on electrochemical corrosion. Von M. Pourbaix, 3rd english edition, expanded, 342 Seiten, NACE International, Houston 1995, ISBN 1-877914-91-6. Materials and Corrosion 1996;47:717-717.

44. Diamanti MV, Pedeferri MP. Effect of anodic oxidation parameters on the titanium oxides formation. Corros Sci 2007;49:939-948.

45. Burstein GT, Liu C, Souto RM. The effect of temperature on the nucleation of corrosion pits on titanium in Ringer's physiological solution. Biomaterials 2005;26:245-256.

46. Simka W, Sadkowski A, Warczak M, Iwaniak A, Dercz G, Michalska J, Maciej A. Characterization of passive films formed on titanium during anodic oxidation. Electrochim Acta 2011;56:8962-8968.

47. Aparicio Bádenas C. Tratamientos de superficie sobre titanio comercialmente puro para la mejora de la osteointegración de los implantes dentales.

48. Aparicio C, Rodriguez D, Gil FJ. Variation of roughness and adhesion strength of deposited apatite layers on titanium dental implants. Materials Science and Engineering: C 2011;31:320-324.

49. Aparicio C, Padrós A, Gil F. In vivo evaluation of micro-rough and bioactive titanium dental implants using histometry and pull-out tests. Journal of the Mechanical Behavior of Biomedical Materials ;In Press, Corrected Proof.

50. Pegueroles M, Gil FJ, Planell JA, Aparicio C. The influence of blasting and sterilization on static and time-related wettability and surface-energy properties of titanium surfaces. Surface and Coatings Technology 2008;202:3470-3479.

51. Pegueroles M, Aparicio C, Bosio M, Engel E, Gil FJ, Planell JA, Altankov G. Spatial organization of osteoblast fibronectin matrix on titanium surfaces: Effects of roughness, chemical heterogeneity and surface energy. Acta Biomaterialia 2010;6:291-301.

52. Luckey HA, Kubli FJ. Titanium alloys in surgical implants. : ASTM International, 1983.

53. Tengvall P, Lundstrom I. Physico-chemical considerations of titanium as a biomaterial. Clin Mater 1992;9:115-134.

54. Stevens B, Yang Y, Mohandas A, Stucker B, Nguyen KT. A review of materials, fabrication methods, and strategies used to enhance bone regeneration in engineered bone tissues. Journal of Biomedical Materials Research Part B: Applied Biomaterials 2008;85B:573-582.

55. Eisenbarth E, Velten D, Breme J. Biomimetic implant coatings. Biomol Eng 2007;24:27-32.

56. Zhu L, Ye X, Tang G, Zhao N, Gong Y, Zhao Y, Zhao J, Zhang X. Biomimetic coating of compound titania and hydroxyapatite on titanium. Journal of Biomedical Materials Research Part A 2007;83A:1165-1175.

57. Alvarez K, Sato K, Hyun SK, Nakajima H. Fabrication and properties of Lotus-type porous nickel-free stainless steel for biomedical applications. Materials Science and Engineering: C 2008;28:44-50.

58. Alves CM, Yang Y, Carnes DL, Ong JL, Sylvia VL, Dean DD, Agrawal CM, Reis RL. Modulating bone cells response onto starch-based biomaterials by surface plasma treatment and protein adsorption. Biomaterials 2007;28:307-315.

59. Bagno A, Piovan A, Dettin M, Chiarion A, Brun P, Gambaretto R, Fontana G, Di Bello C, Palù G, Castagliuolo I. Human osteoblast-like cell adhesion on titanium substrates covalently functionalized with synthetic peptides. Bone, 2007;40:693-699.

60. Bessa PC, Casal M, Reis RL. Bone morphogenetic proteins in tissue engineering: the road from laboratory to clinic, part II (BMP delivery). J Tissue Eng Regen Med 2008;2:81-96.

61. Morra M. Biochemical modification of titanium surfaces: peptides and ECM proteins. Eur Cell Mater 2006;12:1-15.

62. Hubbell JA. - Biomaterials for tissue engineering. - World Journal of Urology :- 2.

63. Pierschbacher MD, Hayman EG, Ruoslahti E. Location of the cell-attachment site in fibronectin with monoclonal antibodies and proteolytic fragments of the molecule. Cell 1981;26:259-267.

64. Ruoslahti E. RGD and other recognition sequences for integrins. Annu Rev Cell Dev Biol 1996;12:697-715.

65. Albelda SM, Buck CA. Integrins and other cell adhesion molecules. FASEB J 1990;4:2868-2880.

66. Porté-Durrieu MC, Guillemot F, Pallu S, Labrugère C, Brouillaud B, Bareille R, Amédée J, Barthe N, Dard M, Baquey C. Cyclo-(DfKRG) peptide grafting onto Ti–6Al–4V: physical characterization and interest towards human osteoprogenitor cells adhesion. Biomaterials 2004;25:4837-4846.

67. Puleo DA. Biochemical surface modification of CoCrMo. Biomaterials 1996;17:217-222.

68. Nanci A, Wuest JD, Peru L, Brunet P, Sharma V, Zalzal S, McKee MD. Chemical modification of titanium surfaces for covalent attachment of biological molecules. J Biomed Mater Res 1998;40:324-335.

69. Xiao SJ, Textor M, Sencer ND, Wieland M, Keller B, Sigrist H. Immobilization of the cell-adhesive peptide Arg–Gly–Asp–Cys (RGDC) on titanium surfaces by covalent chemical attachment. J Mater Sci Mater Med 1997;8:867-872.

70. Puleo DA, Kissling RA, Sheu M-. A technique to immobilize bioactive proteins, including bone morphogenetic protein-4 (BMP-4), on titanium alloy. Biomaterials 2002;23:2079-2087.

71. Thid D, Bally M, Holm K, Chessari S, Tosatti S, Textor M, Gold J. Issues of Ligand Accessibility and Mobility in Initial Cell Attachment. Langmuir 2007;23:11693-11704.

72. Pallu S, Bourget C, Bareille R, Labrugère C, Dard M, Sewing A, Jonczyk A, Vernizeau M, Christine Durrieu M, Amédée-Vilamitjana J. The effect of cyclo-DfKRG peptide immobilization on titanium on the adhesion and differentiation of human osteoprogenitor cells. Biomaterials 2005;26:6932-6940.

73. Costa F, Carvalho IF, Montelaro RC, Gomes P, Martins MCL. Covalent immobilization of antimicrobial peptides (AMPs) onto biomaterial surfaces. Acta Biomaterialia 2011;7:1431-1440.

74. Harris LG, Tosatti S, Wieland M, Textor M, Richards RG. Staphylococcus aureus adhesion to titanium oxide surfaces coated with non-functionalized and peptide-functionalized poly(l-lysine)-grafted-poly(ethylene glycol) copolymers. Biomaterials 2004;25:4135-4148.

75. Héquet A, Humblot V, Berjeaud J, Pradier C. Optimized grafting of antimicrobial peptides on stainless steel surface and biofilm resistance tests. Colloids and Surfaces B: Biointerfaces 2011;84:301-309.

76. Kazemzadeh-Narbat M, Kindrachuk J, Duan K, Jenssen H, Hancock REW, Wang R. Antimicrobial peptides on calcium phosphate-coated titanium for the prevention of implant-associated infections. Biomaterials 2010;31:9519-9526.

77. Onaizi SA, Leong SSJ. Tethering antimicrobial peptides: Current status and potential challenges. Biotechnol Adv 2011;29:67-74.

78. Sherbet GV. 11 - cytokines. Growth Factors and Their Receptors in Cell Differentiation, Cancer and Cancer TherapyLondon: Elsevier, 2011. p. 115-132.

79. Dunlop RJ, Campbell CW. Cytokines and Advanced Cancer. J Pain Symptom Manage 2000;20:214-232.

80. Paper6. Autocrine, Paracrine, Endocrine. http://paper6-textcube.blogspot.com.es/2009/10/autocrine-paracrine-endocrine.html. 2012.

81. Tayal V, Kalra BS. Cytokines and anti-cytokines as therapeutics — An update. Eur J Pharmacol 2008;579:1-12.

82. Mire-Sluis AR. Cytokines: from technology to therapeutics. Trends Biotechnol 1999;17:319-325.

83. Meager A. Measurement of cytokines by bioassays: Theory and application. Methods 2006;38:237-252.

84. LeRoy E, Trojanowska M, Smith E. Cytokines and human fibrosis. Eur Cytokine Netw 1990;1:215-219.

85. Assoian RK, Komoriya A, Meyers CA, Miller DM, Sporn MB. Transforming growth factor-beta in human platelets. Identification of a major storage site, purification, and characterization. Journal of Biological Chemistry 1983;258:7155-7160.

86. Herpin A, Lelong C, Favrel P. Transforming growth factor-beta-related proteins: an ancestral and widespread superfamily of cytokines in metazoans. Dev Comp Immunol 2004;28:461-485.

87. Burt DW. Evolutionary grouping of the transforming growth factor-beta superfamily. Biochem Biophys Res Commun 1992;184:590-595.

88. Burt DW, Law AS. Evolution of the transforming growth factor-beta superfamily. Prog Growth Factor Res 1994;5:99-118.

89. Rutgers R. Protein data Bank, http://www.pdb.org/pdb/home/home.do. 2012.

90. Hinck AP. Structural studies of the TGF-βs and their receptors – insights into evolution of the TGF-β superfamily. FEBS Lett 2012;586:1860-1870.

91. Nickel J, Dreyer MK, Kirsch T, Sebald W. The Crystal Structure of the BMP-2:BMPR-IA Complex and the Generation of BMP-2 Antagonists. The Journal of Bone & Joint Surgery 2001;83:S7-S14.

92. Dennler S, Goumans M, ten Dijke P. Transforming growth factor β signal transduction. Journal of Leukocyte Biology 2002;71:731-740.

93. Kazue M, Madoka G, Eri O, Yoshitaka A, Shigeo T, Ryuji T. Xenopus neurula left-right asymmetry is respeficied by microinjecting TGF-β5 protein. 2003;47:15; 15-29.

94. Odell W. TGF beta signaling pathway. http://www.biocarta.com/pathfiles/h_tgfbpathway.asp. 2012.

95. Mohammad KS, Chen CG, Balooch G, Stebbins E, McKenna CR, Davis H, Niewolna M, Peng XH, Nguyen DHN, Ionova-Martin S, Bracey JW, Hogue WR, Wong DH, Ritchie RO, Suva LJ, Derynck R, Guise TA, Alliston T. Pharmacologic Inhibition of the TGF-β Type I Receptor Kinase Has Anabolic and Anti-Catabolic Effects on Bone. PLoS ONE 2009;4:e5275.

96. Santiago B, Gutierrez-Cañas I, Dotor J, Palao G, Lasarte JJ, Ruiz J, Prieto J, Borrás-Cuesta F, Pablos JL. Topical application of a peptide inhibitor of transforming growth factor-beta1 ameliorates bleomycin-induced skin fibrosis. J Invest Dermatol 2005;125:450-455.

97. Vicent S, Luis-Ravelo D, Antón I, García-Tuñón I, Borrás-Cuesta F, Dotor J, De Las Rivas J, Lecanda F. A novel lung cancer signature mediates metastatic bone colonization by a dual mechanism. Cancer Res 2008;68:2275-2285.

98. Gellibert F, de Gouville AC, Woolven J, Mathews N, Nguyen VL, Bertho-Ruault C, Patikis A, Grygielko ET, Laping NJ, Huet S. Discovery of 4-{4-[3-(pyridin-2-yl)-1H-pyrazol-4-yl]pyridin-2-yl}-N-(tetrahydro-2H- pyran-4-yl)benzamide (GW788388): a potent, selective, and orally active transforming growth factor-beta type I receptor inhibitor. J Med Chem 2006;49:2210-2221.

99. Vicent S, Luis-Ravelo D, AntÃ³n I, GarcÃa-TuÃ±Ã³n I, BorrÃ¡s-Cuesta F, Dotor J, De LR, Lecanda F. A novel lung cancer signature mediates metastatic bone colonization by a dual mechanism. Cancer Res 2008;68:2275-2285.

100. Tojo M, Hamashima Y, Hanyu A, Kajimoto T, Saitoh M, Miyazono K, Node M, Imamura T. The ALK-5 inhibitor A-83-01 inhibits Smad signaling and epithelial-to-mesenchymal transition by transforming growth factor-beta. Cancer Sci 2005;96:791-800.

101. Nikolidakis D, Meijer GJ, Oortgiesen DAW, Walboomers XF, Jansen JA. The effect of a low dose of transforming growth factor β1 (TGF-β1) on the early bone-healing around oral implants inserted in trabecular bone. Biomaterials 2009;30:94-99.

102. Shen Z, Kook Kim S, Youn Jun D, Park W, Ho Kim Y, Malter JS, Jo Moon B. Antisense targeting of TGF-β1 augments BMP-induced upregulation of osteopontin, type I collagen and Cbfa1 in human Saos-2 cells. Exp Cell Res 2007;313:1415-1425.

103. Filvaroff E, Erlebacher A, Ye J, Gitelman S, Lotz J, Heillman M, Derynck R. Inhibition of TGF-beta receptor signaling in osteoblasts leads to decreased bone remodeling and increased trabecular bone mass. Development 1999;126:4267-4279.

# 2. Immobilization of oligopeptides on titanium surfaces

## CONTENTS

# 2.1. Introduction

## 2.1.1. Scope

Implantology therapies have come to be widely accepted in the orthopedic and odonthologic communities. As a consequence, it has become an important alternative to the rehabilitation of patients with bone diseases or tooth loss. This advance has been made possible by the developments taking place in this field over the last 30 years, leading to a wide range of implant and prostheses types. This is especially so with c.p. titanium, the most used material for dental implants due to its biocompatibility and its incomparable bone integration.

Currently, the research community is focusing on improving short and long-term implant results. These efforts, aside from advances in surgery techniques, have become embodied in two tendencies that pursue a two-fold objective: achieving a better understanding of the implant tissue interactions and processes, and developing new materials and surfaces with better biological properties and service performance. The two tendencies are the following [1,2]:

- Biofunctional materials that incorporate biological motives, such as peptides, proteins, polymers and polysaccharides, which improve cell response to the implant material [3-5].

- Antibacterial materials that avoid or hinder the bacterial growth and infection of the implant environment [6,7].

The first tendency, biofunctionalization, was born when Pierschbacher and Ruoslahti discovered the cell adhesion RGD motif contained in many extracellular matrix proteins [8,9]. Over the last years, many researchers have been trying, with variable success, to adhere RGD containing peptides, proteins and polymers to different surfaces in order to improve cell adhesion [9-17].

The development of antibacterial surfaces, on the other hand, sprang from the need to avoid infections in the implants being used. The mouth is a noxious environment where thousands of bacteria types live [18] and these frequently attack implant sites, generating infection and bone loosening. To counter this problem, researchers worked on developing new materials, not only resorting to antibacterial agents such as silver, but going further into the research of biological antimicrobial motives [19-21].

Both of the above tendencies have one thing in common: the need to immobilize biological motives on the surface of the biomaterial. Over the last years, many functionalization processes have been created in order to study the effectiveness of new biological motives on tissue. However, as there are so far no available biofunctional implants in the commercial market for patients, it is still necessary to develop simple, reliable and viable functionalization processes to immobilize the new biologically effective motives on implant surfaces.

This chapter focuses on the functionalization process of c.p. Titanium surfaces. Moreover, it analyses the development of a new, simple and effective method to covalently immobilize oligopeptides on titanium surfaces.

### 2.1.2. Surface modification with oligopeptides and other biomolecules

The different strategies to modify surfaces can be classified as physicochemical (for example, altering the surface energy, surface charge, composition and surface morphology), or biochemical, according to the proposal made by Ito et. al [22]. The biochemical surface modification can be both an alternative and a supplementary treatment to the physicochemical and morphological modifications. The objective of the biochemical surface modification is to further current knowledge about cell behavior, biology and biochemistry so as to control and tailor the cell functions in order to induce a specific cell reaction like cell adhesion, migration or differentiation. This way, the extracellular matrix growth on non-biological materials can be

controlled. The surface biochemical modification aims to immobilize on the surface of biomaterials biofunctional molecules such as proteins, enzymes, and bioactive peptides which are able to induce specific reactions on the tissue, and thus control the interaction between tissue and biomaterial. Additionally, the nonspecific reactions of protein adsorption, which is known to occur immediately after implantation of the biomaterial, has to be controlled and minimized [23,24].

There are two important factors to be taken into account in the immobilization of biomolecules at the implant-tissue interface: the time that the molecules must remain fixed to the implant, and the spatial concentration and distribution of the bioactive sites. The colonizing cells of the adjacent tissue must have accessibility to these sites for a certain period of time to be able to initiate the different cell events. This entails that the fixed biomolecules on surface should be stable during a certain period of time. On the other hand, bioactive molecules must remain within a certain surface density range to ensure the accessibility of the biomolecules to the cells and, also, to maintain the stability of the bioactive species.

There are two main methods to distribute biomolecules on a biomaterial surface: physical adsorption, in which the adsorbate molecules are attracted to the surface by weak van der Waals forces, and covalent chemical bonding, a more complex process which actually involves chemical reactions between the molecules and the surface.

#### 2.1.2.1. Physical adsorption

When an implant is inserted in a biological environment, the proteins are adsorbed on the surface by weak bonds which depend mainly on the surface properties and the condition of the environment in contact with the surface [25,26]. Depending on the extent of change taking place in the biological environment due to cell activity on the implant, these proteins could be desorbed from the surface in an uncontrolled fashion, augmenting the risk of undesired desorption and diffusion of the biomolecules far from the implant surface [27,28]. Also, the adsorbed biomolecules could be exchanged with the proteins from the biological environment in a nonspecific manner. In a general way, the physical adsorption method has the

disadvantages of obtaining poor control over the retention and delivery of the adsorbed biomolecules as well as over the distribution and orientation of the biomolecules, which could be adsorbed in a way that would biologically inactivate them, [29] hampering characterization and surface functionality.

In an *in vitro* test, due to the fact that the micro-environment can be controlled, the protein adsorption is determined by means of the physicochemical changes of the surface. Titanium and its alloys are especially good candidates to be modified by protein adsorption because they spontaneously form an oxide layer which does not have electrical conductivity in physiological conditions, therefore inhibiting the possibility of redox processes between the metal and the adsorbed proteins, which do not tend to occur on cobalt based alloys and steels [30,31].

In spite of all these drawbacks, titanium with adsorbed biomolecules on its surface has demonstrated having bioactivity and being a clinically relevant biomaterial that promotes cell adhesion, osteoblast differentiation and *in vivo* osseointegration [32]. For this reason, coating titanium surfaces with physically adsorbed biomolecules is a worthwhile strategy to improve bone repair and implant integration [33,34].

#### 2.1.2.2. Chemical covalent immobilization

Covalent binding of biomolecules to the surface of an implant is experimentally more challenging than physical adsorption, due to the chemistry involved. Under physiological conditions covalently bound molecules have higher stability than physisorbed ones and this method contains the keys to control the orientation of immobilized bioactive molecules, such as the exposure of the active domains of the biomolecule, causing, thus, a more specific and quick reaction of the organism [35]. A large number of metal surfaces, including the common biomaterials such as Ti6Al4V, commercially pure titanium, nickel-titanium alloys and chromium-cobalt-molybdenum alloys, form a passivation layer of metal oxide hardly displays functional groups required for covalent attachment of molecules. However, the relatively inert oxide layers expose hydroxyl groups on their surface, allowing the binding of silanes on the metal

surface by chemical means [36]. Another possibility for covalently bonding molecules on the metal surface is to deposit amino, carboxyl or thiol groups by means of plasma; photo initiated polymerization or by ion projection etching [37,38].

Like most of the surfaces of metals used as biomaterials, titanium surfaces in contact with the atmosphere are coated spontaneously with an oxide layer which is amorphous and may vary in thickness, from 3 to 6 nm [39], and in composition. Typically, it is contaminated with elements in contact with the metal surface, resulting in a non-homogeneous and variable layer which can be different in each sample. Because the effectiveness of creating biomimetic coatings on oxidized metal surfaces depends on the reaction between the hydroxyl groups and chemicals used to form active sites for bonding [40], it is believed that a good cleaning process and/or a controlled oxidation, achieving a high degree of compositional homogeneity of the surface oxide layer, will significantly facilitate the reproducible manufacture of biofunctionalized implants and prostheses [41].

The controlled oxidation of titanium can produce a clean, homogeneous surface oxide layer, generating linking groups for the silanes. For the production of a controlled oxide layer, there are different chemical and electrochemical methods. Outstanding among the chemical methods is piranha etching with $H_2SO_4/H_2O_2$ resulting in clean and homogeneous oxide layers [41]. Electrochemical anodization can obtain amorphous oxide layers with a highly controlled thickness [42].

Performing a vacuum heat treatment on titanium subsequent to an acid attack seems to influence the chemical composition of the oxide layer closest to the surface, and it is beneficial for the binding of silanes. Porte-Durrieu et al. showed that the XPS analysis of titanium samples vacuum heat treated at 150 $^{o}$C contained a small proportion of contamination of carbon and an increase in $Ti_3^+$ defects, which are responsible for dissociative adsorption of water, improving the hydrophilicity and thus being suitable for condensation of silanes on the metal oxide surface [4].

#### *2.1.2.2.1. Depositing amino and carboxyl groups using plasma*

Depositing thin plasma polymer layers on titanium is another option for the limited amount of functional groups present on the surfaces of metal oxide. This technique produces of a uniform and adherent layer which does not undergo hydrolysis or delamination in aqueous environments. Morra and Cassinelli showed deposition of a 5 nm layer of plasma polymer from ethylene, which allows subsequent application of a variety of functionalization processes with organic material [37].

Puleo et al. deposited amino groups on Ti6Al4V by plasma polymerization, depositing 5-12 $NH_2$ groups per $nm^2$. In this way it is possible to bind proteins to obtain surfaces using carbodiimide as a cross-linker [43].

#### *2.1.2.2.2. Silanization*

The organosilanes are formed by two functional groups spaced at their ends by a ductile alkyl group. The silane group at one end is used for binding to the surface of titanium oxide while the other functional group at the opposite end serves to bind biomolecules, directly or via cross-linking. The diagram in figure 2-1 shows the configuration of a monolayer of silanes attached to a surface [35].

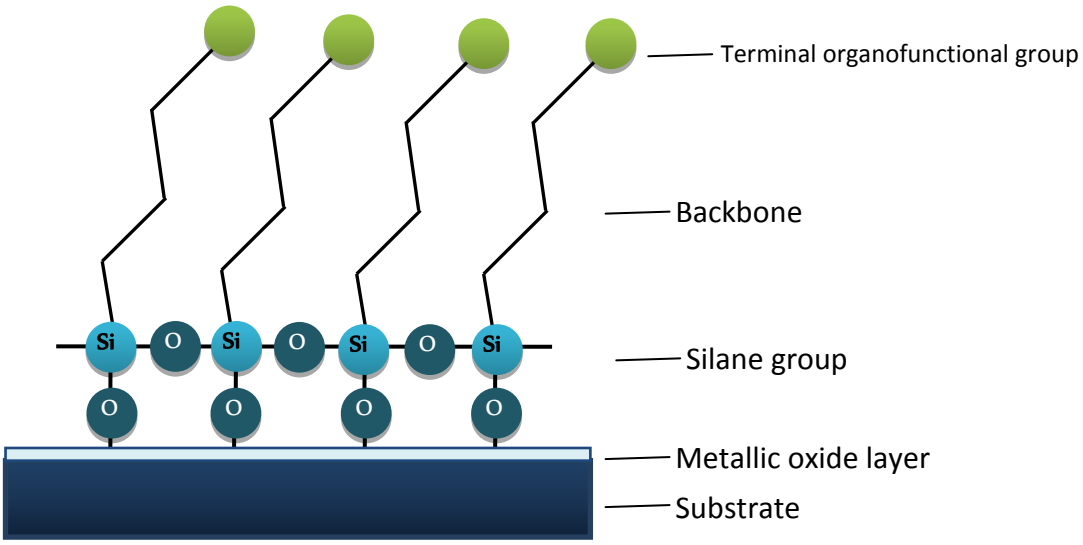


***Figure 2-1:*** *Organosilane layer scheme.*

The alkyl spacer body of silanes, being ductile, has the ability to partially absorb the stresses that occur in the tissue-biomaterial interface and can also serve to guide and properly expose the bioactive molecule bound to the silane, to induce the desired tissue reaction [41].

Strategies based on the covalent binding of biomolecules, forming biomimetic coatings on biomaterials, have been carried out successfully and have been documented in numerous studies. Silanization is a technique widely used for its high reproducibility in the functionalization of metal surfaces. However, the degree of coating, orientation and organization of the resulting layers has not yet been studied in detail. The generation of SAMs (Self-Assembled Monolayers) on surfaces such as monocrystalline gold models has been observed, but the formation of SAMs on imperfect actual polycrystalline metal surfaces used as biomaterials is more challenging to obtain [4,27].

#### 2.1.2.2.2.1. Properties affecting silanization of metallic surfaces

Studies of organosilane monolayer formation on model surfaces have identified that the water content and temperature are critical factors in the mechanism of formation and growth of the layers and the production of a monolayer or a multilayer. Two growth mechanisms can be distinguished in reference works: uniform growth, and growth in the form of islands. The formation of layers of silanes seems to be generated simultaneously by the two mechanisms, resulting in islands of silane with a relative alignment and vertical orientation of the alkyl, surrounded by unique disordered molecules with high tilt angles. It is often assumed that molecules bind to the surface via X-O-Si bonds and to each other through a Si-O-Si network as shown in figure 2-1, however, this scenario does not apply to all a coated surface [44]. The typical Si-O bond has a length of 1.6 Å, resulting in a distance of 3.2 Å between two oxygen atoms. This length does not allow sufficient space for the vertical positioning of the hydrocarbon chains. This implies that a monolayer that entirely covers the surface cannot be completely cross-linked. Schneider describes this organosilane monolayer exposing terminal methyl groups on silicon substrates and nearly vertically oriented molecules with a slope less than $20^{o}$. On a larger scale the monolayer shows a disordered structure but with hexagonal islands with an area of about 20 $Å^2$ where order is maintained locally [35].

*Water*

As it is further explained in section 2.3.1, water is necessary for the hydrolysis of the ethoxy or methoxy groups of most silanes. In the absence of water only an incomplete monolayer form is achieved, whereas excess water causes polymerization of the silane molecules in solution and the deposition of a polysiloxane multilayer [45].

During silanization of imperfect surfaces of metallic oxides two basic events occur: (1) The hydrolysis of the alkoxide groups followed by (2) condensation of the hydroxyl groups of the surface with silane molecules. In aqueous environments hydrolysis of alkoxide groups in solution occurs immediately, causing the condensation between silanol groups before contacting the metal surface, leading to an uncontrolled process of deposition of a non-homogeneous polymerized silane (polysiloxane) multilayer. In an anhydrous environment hydrolysis and condensation occur only when silane molecules come into contact with the layer of adsorbed water on the surface of metal oxide, favoring the formation of a uniform monolayer of silane, especially in polycrystalline surfaces. For this reason silanization in anhydrous surroundings appears to provide better and greater stability of the silane coating, in comparison with that afforded by an aqueous solution [46].

*Temperature*

Moreover, temperature also plays an important role in the process. At low temperatures, the silanized surface shows a heterogeneous structure with a high density of coverage with a multitude of islands of alkyl chains oriented approximately in a vertical direction. By increasing the temperature it produces a decrease in the ability to be coated completely and a greater disorder is obtained. Temperature threshold value below that at which an orderly monolayer is obtained is a function of the length of the alkyl chain. Long chains show a higher temperature threshold. The problem is the competition between the polymerization reaction of the hydrolyzed silane monomers and the reaction of silanes with the surface OH groups. A low temperature favors the reaction at the surface, but also slows down the reaction kinetics [35,45].

#### *2.1.2.2.3. Peptide immobilization on biomaterial surfaces*

The immobilization of oligopeptides on titanium surfaces has focused on two different approaches: cell adhesive surfaces and antimicrobial surfaces. Cell adhesion has been extensively achieved through the attachment of the RGD cell adhesive amino acid sequence on different biomaterial surfaces [3,7,12,47,48]. Antimicrobial surfaces have achieved only a partial success due to the fact that several antimicrobial peptides have been found to be cytotoxic [49-53].

All peptide-biofunctionalized surfaces share the need for effective interaction between the immobilized peptide and the target biological molecules. In the case of the RGD peptides the target are the cell receptor integrins, and in the case of the antimicrobial peptides, the target tends to be the bacterium membrane. In order to achieve effectiveness of the biofunctional surface, some parameters such as surface peptide density and accessibility need to be controlled.

As was discussed in section 1.4.1.2 and the previous paragraphs, the RGD sequence has been highly studied when immobilized on metallic and non-metallic surfaces. The improvement of RGD functionalized surfaces on cell adhesion is a reality. Despite the aim of this thesis wasn't the functionalization of titanium surfaces with RGD peptides, in this chapter a RGD peptide has been used. Due to the proved efficacy of the RGD peptides, a RGD containing peptide was selected as a model peptide to validate the biological effects of the peptides when immobilized on titanium surfaces with the proposed functionalization process.

#### *2.1.2.2.4. Surface density and accessibility*

In order to develop new materials that interact with cells in a predictable manner, deep knowledge on the effect of density of ligands (peptides) and on the kinetics of adhesion and other cellular functions is required. Some studies [12,54,55] determined the minimum surface density of ligands that are required for short-term events such as adhesion, extension,

formation of focal contacts and cell migration, and long-term events such as cell differentiation. The minimum values reported for cell adhesion are of the order of 1-10 fmol/cm$^2$ RGD ligand on osteoblastic and fibroblastic cells. The increased surface density of ligands leads to increased cell adhesion, but a clear and quantitative correlation has not yet been established between these two variables [54]. In addition to the extension and the formation of focal contacts, cell migration and adhesion strength have been correlated with the density of ligands and the affinity between integrins and ligands and the number of receptors per cell [56]. At low ligand density, mobility of the cells is limited due to the small amount of adhesion points; however, at high densities the mobility is strongly restricted because the surface is too sticky.

Long-term phenomena, such as cell differentiation or mineralization, are also affected by the density of ligands on the surface. In the case of peptides containing the RGD peptide, their density has clearly been shown to have an effect not only in the adhesion of osteoblastic cells, but also in the *in vitro* extension and mineralization of the cells [54]. The data showed that ligand densities higher than 0.6 pmol/cm$^2$ lead to increased mineralization. The main problem associated with these studies when assessing the cellular activity is the difficulty of quantifying the density of surface-active ligands and the lack of total control over the adsorption of other compounds on the surface, or over the direction that the peptides take to adhere to the surface.

In addition to the surface density, the accessibility of the ligands is crucial for the development of biomimetic surfaces. Thus, Houseman et. al. have studied the effect of using different cross-linkers and chain lengths bonding the ligand (peptide or protein) to the surface [57,58]. There is great controversy in determining the optimal length of the chain linking the ligand to the surface. A very short spatial chain produces inaccessibility of the ligand because it is very close to the surface, and therefore not sufficiently exposed to the receptors. In addition, it makes it easier for reactive compounds to interact with the surface beneath. A long chain may have the problem of not being rigid enough, allowing the ligand to adopt inadequate conformations, as well as occupying a greater surface area which prevents the ligand from being able to achieve a high surface density.

Another aspect to consider with regards to the accessibility of the ligands is the shielding effect which could be caused by the deposition of proteins and other biological molecules on the surface in contact with physiological fluids. These molecules, adsorbed on the surface, can shield the accessibility of cellular response by inhibiting the ligand. It is therefore necessary to design surfaces that minimize the adhesion of proteins when they come into contact with the physiological medium, as discussed below.

#### *2.1.2.2.5. Surface protein adsorption*

Some treatments have been developed to minimize non-specific interactions (such as protein adsorption) between the material and the biological environment to which it is exposed. Many of these surfaces are susceptible of being functionalized with a large number of macromolecules such as peptides or growth factors. These surfaces are ideal for the study of ligand-receptor interactions, annulling the side effects by exposing the biomaterial of study to the cells.

The most significant advance in this field was the discovery of the anti-bioadhesive properties of PEG (Poly ethylene glycol) [59]. The unique properties of PEG have shown a low protein, cells and bacteria adhesion due to its interaction with water. When PEG comes into contact with water it forms a protective hydrate capsule around the molecules of PEG. The reasons that PEG repels proteins, cell and bacterial adhesion are unclear but it is believed that when other molecules such as proteins run into this capsule, the adhesion is hindered due to a combination of water structure, entropic repulsion and osmotic pressure [60,61]. Because of this property PEG is an excellent candidate for producing anti-bioadhesive coatings. However, given that their use can affect the accessibility of biological ligands (peptide or protein), it is still necessary to carry out a thorough survey of these anti-adhesive properties.

## 2.2. Objectives

The main objective of the present chapter is to design and develop a reliable functionalization process in order to immobilize oligopeptides on a titanium surface. To achieve this aim, different products and processes have been studied and compared. To decide which process or product is best in comparison with the others in every step of the process, we have focused on the amount of peptide retained on the surface as the decisive factor. Other factors, such surface roughness, chemical composition and cell response have also been taken in account in order to select the best option in every step of the functionalization process.

As the functionalization process is composed of several steps or procedures in a sequential fashion, each step has been studied separately with a sequential analysis strategy. This means that in the first step of the functionalization process, several different procedures were tested and compared. After analysis and discussion of the results, one of the procedures was chosen to form part of the whole process and then, the analysis of the next step of the process was started including only the chosen procedure from the previous step.

Next, the different procedures and products compared in each step are shown. The ultimate functionalization process is composed by only one of the procedures or products from each step:

- Step 1: Surface activation
    - Plasma Cleaning
    - Piranha treatment
    - Sodium Hydroxide treatment
- Step 2: Silanization
    - 3-Aminopropyltriethoxysilane (APTES)
    - 3-Chloropropyltriethoxysilane (CPTES)

- Step 3: Crosslinking
    - Malonic acid
    - Glutaric acid
    - Diglycolic acid
- Step 4: Peptide immobilization
    - Only one procedure was tested which was dependent on the previously chosen procedures for steps 1, 2 and 3.

# 2.3. Design of the functionalization process

## 2.3.1. Overview

As previously described in the objectives section, the functionalization process is composed by a sequence of procedures that, combined, achieve the immobilization of the oligopeptides on the titanium surface. This section includes a description of the hypotheses of work of every procedure or product in each step of the functionalization process and the theoretical advantages and disadvantages of selecting one procedure over another in terms of the whole functionalization process.

It was decided that the functionalization process was able to perform a covalent immobilization of the peptides on the titanium surface. Thus, we decided to base the functionalization process on the most widely used strategy of immobilization of peptides and proteins on surfaces: silanization [62-65].

Silanization is a cheap, versatile and reliable method to link an organic molecule on a metallic, ceramic or polymeric surface. As its name indicates, silanes are coupling agents that have one or more silicon atoms ready to react with an active hydrogen on any organic chemical (e.g., alcohol, carboxylic acid, amine, phenol or thiol) via a process called silylation:

$$R_3Si\text{-}Cl + R'OH \Rightarrow R_3Si\text{-}OR' + HCl \qquad \textbf{Equation 2-1}$$

More concretely, alkoxysilane coupling agents contain three inorganic reactive groups on silicon (usually methoxy, ethoxy or acetoxy) and will bond well to the metal hydroxyl groups on most inorganic substrates, especially if the substrate contains silicon, aluminum or a heavy metal in its structure. The alkoxy groups on silicon hydrolyze to silanols, either through the addition of water or from residual water on the inorganic surface. Then the silanols coordinate with metal hydroxyl groups on the inorganic surface to form an oxane bond and eliminate water. See figure 2-2.

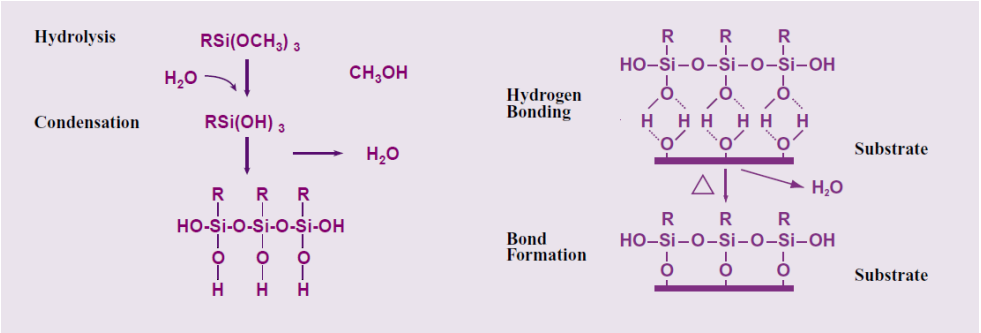


***Figure 2-2:*** *Hydrolysis of alkoxysilanes and bonding to an inorganic surface [66]*

As can be seen in figure 2-2 hydrolyzed silanes react with alkoxy groups present on the surface. Thus, we can infer that, the more OH groups on the surface, the better the silanization, and the greater the amount of silane on the surface. So, it was decided that, previous to silanization of the titanium surface, it had to be pretreated in order to increase the amount of OH groups on the surface. This first step was called: surface activation.

The second step of the functionalization process, silanization, is, indeed, the most important step of all. During the silanization procedure, the surface gets covered by a silane that reacts, by condensation, with the OH groups previously generated by the surface activation treatment. When the silanization process is finished, the surface is covered by silane molecules that are covalently bound to the surface and, on the other hand, silanes contain an organo-functional group that can react, in the subsequent step, with organic molecules. Section 2.3.3 describes in greater detail the studied silanes and the reactive containing groups.

Depending on the selected silane, the subsequent step entails a reaction with different organic groups such as amines, thiols, carboxylic acids, alcohol or others [67]. Depending on the organic group desired for binding to the surface, it is necessary, or not, to add an intermediate molecule, a cross-linker, that on the one hand, reacts with the organofunctional group of the silane and, on the other hand is able to react with the molecule that one wishes to immobilize on the surface. This optional third step was called: cross-linking.

Finally, once the surface is ready to react covalently with the desired molecule, in our case, an oligopeptide, the biomolecule binds to the surface by a nucleophilic substitution being immobilized on the titanium surface, achieving the objective of this chapter. The last step of the functionalization process has been called: peptide immobilization.

The following scheme (Figure 2-3) shows the steps of the functionalization process which will be evaluated in order to select the best conditions for immobilizing oligopeptides on titanium surfaces.

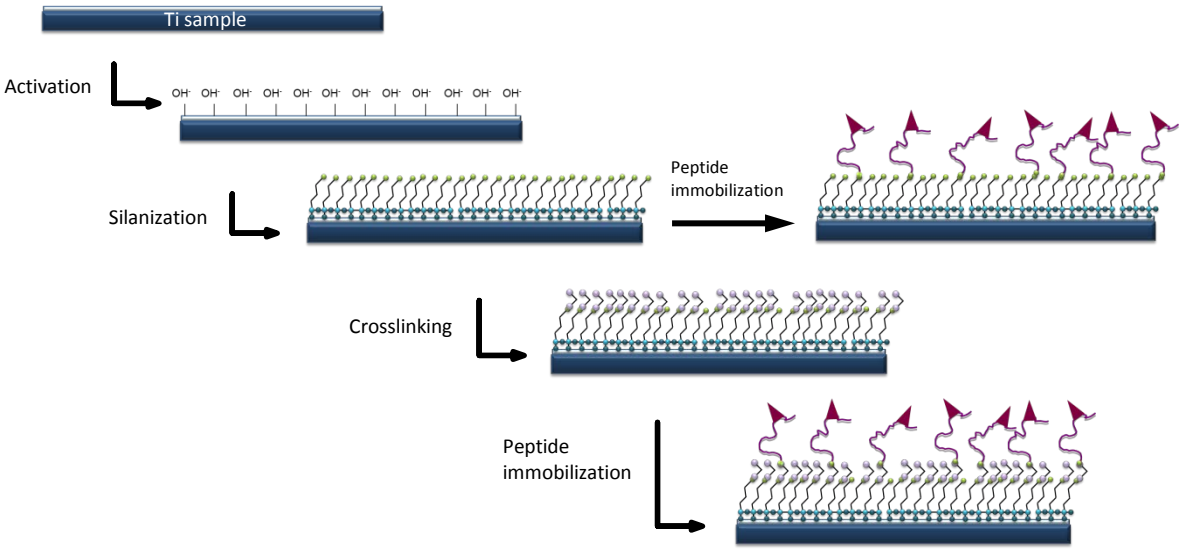


***Figure 2-3:*** *Scheme of the biofunctionalization process proposed.*

## 2.3.2. Step 1: Surface activation

C.p. titanium is a good material for being silanized because of the presence of OH groups on its surface [68,69]. However, several surface treatments are able to increase the amount of OH groups on titanium and other materials [69,70]. In order to increase the success probability on the silanization of titanium surfaces, it was decided to study 3 different activation methods that, a priori, should increase the amount of OH groups on the surface that are able to react with the silane on the subsequent silanization step.

### 2.3.2.1. Plasma cleaning

Plasma is a collection of freely moving charged particles which is, on the average, electrically neutral [71].

Plasma cleaning is a procedure in which a gas is ionized by a discharge produced by a radiofrequency (Rf) source, in order to create plasma which will interact with the surface (Figure 2-4). In plasma cleaning applications the most usual gases to be ionized are air, oxygen and argon.

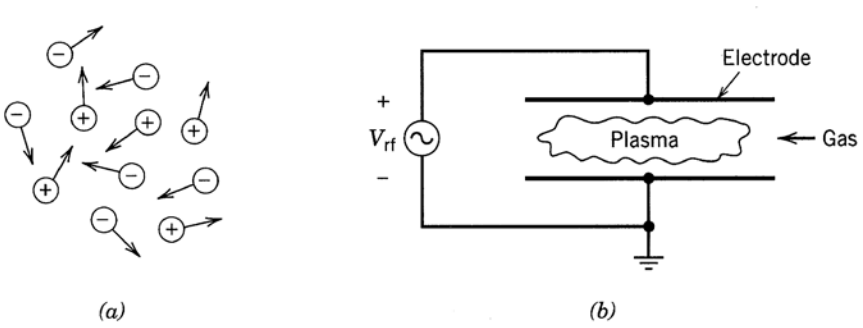


***Figure 2-4:*** *Scheme (a) accelerated plasma ions, (b) plasma generating device*

In plasma state, ions can react with the substrate compounds in order to neutralize its charge. The majority of product compounds are volatile. Once they take off from the surface, they are removed from the plasma chamber by vacuum.

Oxygen plasma cleaning is an effective procedure to remove carbonaceous species from the surface and to oxidize the surface of metals.

#### 2.3.2.1. Piranha treatment

Piranha solution, also known as piranha etch, is a mixture of sulfuric acid ($H_2SO_4$) and hydrogen peroxide ($H_2O_2$), which is commonly used to clean organic residues off substrates. Because the mixture is a strong oxidizer, it will remove most organic matter, and it will also hydroxylate most surfaces (add OH groups), making them highly hydrophilic [72,73].

The etching process can be understood as the sulfuric-acid boosted conversion of hydrogen peroxide from a relatively mild oxidizing agent into one sufficiently aggressive to dissolve elemental carbon, a material that is notoriously resistant to room temperature aqueous reactions. This transformation can be viewed as the energetically favorable dehydration of hydrogen peroxide to form hydronium ions, bisulfate ions, and, transiently, atomic oxygen:

$$H_2SO_4 + H_2O_2 \rightarrow H_3O^+ + HSO_4^- + O \qquad \textbf{Equation 2-2}$$

It is this extremely reactive atomic oxygen species that allows piranha solution to dissolve elemental carbon. Carbon allotropes are difficult to attack chemically because of the highly stable and typically graphite-like hybridized bonds that surface carbon atoms tend to form with each other. The most likely route by which piranha solution disrupts these stable carbon-to-carbon surface bonds is for an atomic oxygen first to attach directly to a surface carbon to form a carbonyl group:

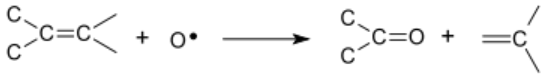

**Equation 2-3**

In the above process, the oxygen atom in effect “steals” an electron bonding pair from the central carbon, forming the carbonyl group and simultaneously disrupting the bonds of the

target carbon atom with one or more of its neighbors. The result is a cascading effect in which a single atomic oxygen reaction initiates significant “unraveling” of the local bonding structure, which in turn allows a wide range of aqueous reactions to affect previously impervious carbon atoms. Further oxidation, for example, can convert the initial carbonyl group into carbon dioxide and create a new carbonyl group on the neighboring carbon whose bonds were disrupted:

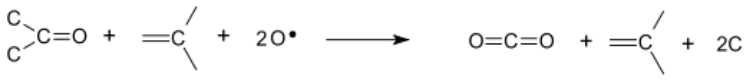

**Equation 2-4**

The carbon removed by piranha solution may be either original residues or char from the dehydration step. The oxidation process is slower than the dehydration process, taking place over a period of minutes. The oxidation of carbon exhibits itself as a gradual clearing of suspended soot and carbon char left by the initial dehydration process. In time, piranha solutions in which organic materials have been immersed typically will return to complete clarity, with no visible traces of the original organic materials remaining.

On metallic materials, such as titanium, piranha solution dissolves the oxidized surface and re-oxidizes it, roughening the surface during the process.

#### 2.3.2.2. Sodium Hydroxide treatment

The passive titanium oxide layer that spontaneously forms on the metal is very stable. However, the $TiO_2$ layer can react with a basic NaOH solution to form a sodium titanate gel. The research carried out by Aparicio et. al. [74] confirmed the generation of a sodium titanate layer when titanium was treated with NaOH 5 mol/l during 24 h at 60 $^{o}$C. The thickness of this layer was around 1 μm. During the treatment the $TiO_2$ is partially dissolved by the corrosive attack of the hydroxyl groups [75].

$$TiO_2 + OH^- \rightarrow HTiO_3$$ **Equation 2-5**

At the same time, Ti is hydrated following the reactions set down below:

$$Ti + 3OH^- \rightarrow Ti(OH)_3^+ + 4e^-$$

$$Ti(OH)_3^+ + e^- \rightarrow TiO_2\,H_2O + 0.5\,H_2\,(g) \qquad \textbf{Equations 2-6}$$

$$Ti(OH)_3^+ + OH^- \rightarrow Ti(OH)_4$$

If the attack continues on the already hydrated $TiO_2$, negatively charged hydrates are formed, giving to the surface a negative polarity.

$$TiO_2.nH_2O + OH^- \rightarrow HTiO_3^-.nH_2O \qquad \textbf{Equation 2-7}$$

These negatively charged molecules combine with sodium in the aqueous solution resulting in a hydrogel layer of sodium titanate ($Na_2Ti_3O_7$) [75]. This gel layer has very intricated topography, producing a surface a notably high real surface area including a high amount of OH groups.

### 2.3.3. Step 2: Silanization

As was explained in section 2.3.1 silanization is the central point on which the whole design of the functionalization process is based. The chemical process that allows the alkoxysilanes to bind to the titanium surface has already been explained in section 2.3.1. In this section the reactivity of the different organofunctional groups of the selected silanes will be discussed.

Two different silanes have been selected to be studied in order to select the best performer on the immobilization of short peptides on titanium surfaces. The first silane (3-Chloropropyltriethoxysilane) is a novel and promising silane which has the capability to bind nucleophiles such as amines or thiols directly in basic conditions. The second silane (3-Aminopropyltriethoxysilane) is the most used silane for the immobilization of biological molecules and has demonstrated an excellent performance on multiple oxide surfaces [65,76-

80]. 3-Aminopropyltriethoxysilane can react with esters in certain conditions leading to an amide bond or bind nucleophiles through the addition of a crosslinker.

### 2.3.3.1. 3-Chloropropyltriethoxysilane (CPTES)

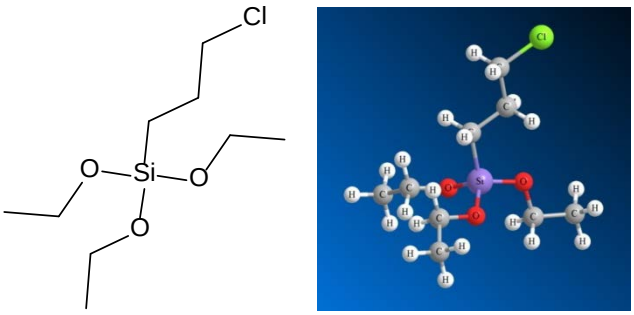


***Figure 2-5:*** *Scheme of CPTES silane in 2D (left) and 3D (right). Drawings performed with Chemdraw 12.0 CambridgeSoft (UK).*

3-Chloropropyltriethoxysilane (Figure 2-5), hereafter abbreviated as CPTES, contains a chlorine atom, a well know electron withdrawing group. Thus, chlorine draws the electronic density from the neighboring C, thereby yielding an electrophilic (electron deficient) -$CH_2$- group. Peptides and proteins contain free amino groups due to the presence of the N terminus and some amino acid side chains, which have nucleophilic properties and tendency to react with electrophiles. Therefore, the organo-functional group of CPTES will react with peptides and proteins through an $S_N2$ nucleophilic substitution. [81].

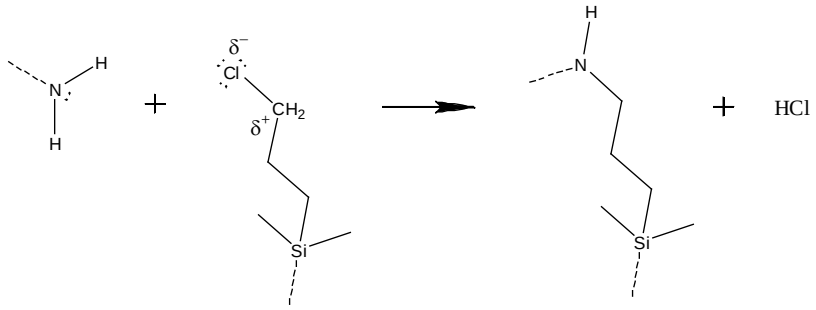


***Figure 2-6:*** *Scheme of the nucleophilic substitution between CPTES and the N-terminus of a peptide and the resulting covalent bond.*

The bond between the chlorine and carbon on CPTES is polarized due to the difference of electro-negativities between carbon and chlorine. The uneven share of electrons in this bond

creates a lack of electrons on the carbon atom. As a result, CPTES contains an electrophilic center. The free amine from the N-terminus (or from the lysine residues of a peptide) is a good nucleophile which has a free pair of electrons to share, thus making it a center with an excess of electronic density.

The $S_N2$ reaction is based on the interaction between a nucleophilic and an electrophilic group, upon which a new bond is formed between the two groups with simultaneous displacement of a leaving group (i.e. Cl) [81]. A scheme of the reaction is shown in figure 2-6.

#### 2.3.3.2. 3-Aminopropyltriethoxysilane (APTES)

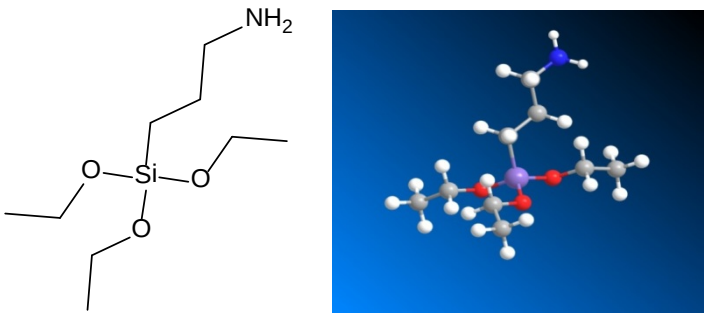


***Figure 2-7:*** *Scheme of APTES silane in 2D (left) and 3D (right).*

3-Aminopropyltriethoxysilane (Figure 2-7), hereafter abbreviated as APTES, is structurally very similar to CPTES except for the terminal organofunctional group. APTES contains a primary amino group at the end of the aliphatic chain. At neutral or basic pH, primary amines contain a free pair of electrons that can be shared to form a new covalent bond. Moreover, as indicated above, amines possess a nucleophilic character and hence may react with electrophiles. This is the case of carboxylic acid derivatives, such as esters or acid anhydrides, which contain an electrophilic C at the carbonyl group and a suitable leaving group. Thus, amines will nucleophilically attack the carbonyl group, with subsequent displacement of the leaving group, to form a stable amide bond. See figure 2-8. [81].

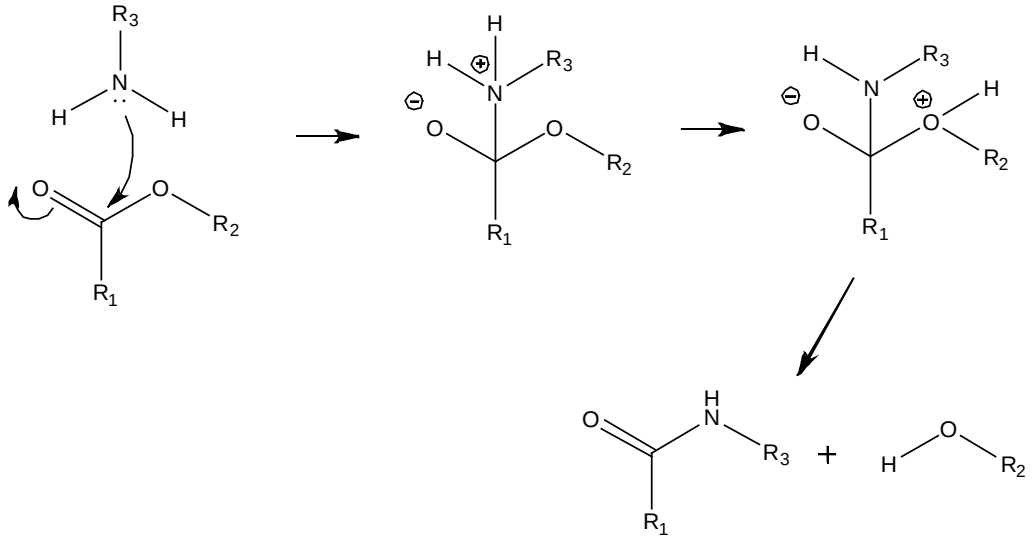


***Figure 2-8:*** *Scheme of the reaction between a primary amine and an ester group.*

Peptides and proteins contain numerous carboxylic acids, such as the C-terminus of an amino acid chain and aspartic and glutamic acid side chains. For this reason, a surface silanized with APTES could, in principle, establish covalent bonds with peptides and proteins that contain free carboxylic groups. However, carboxylic acids do not show the electrophilic properties required for such reaction. To circumvent this issue and confer them with the appropriate reactivity, carboxylic acids need to be derivatized into more reactive, electrophilic carboxylic acid derivatives. This process will be shortly discussed in the following section.

#### *2.3.3.2.1. Transforming carboxylic acids into their active derivatives*

There is nowadays a myriad of different coupling agents used to activate carboxylic acids and react with primary amines to yield amide bonds. These coupling agents have been developed to supply the peptide synthesis market, which has experienced an important growth over the last years [82],[83].

In this thesis, two coupling reagents have been selected to esterify carboxylic acids [84,85]:

- O-Benzotriazole-N,N,N’,N’-tetramethyl-uronium-hexafluoro-phosphate (HBTU)
- N-(3-Dimethylaminopropyl)-N’-ethylcarbodiimide (EDC) combined with N-Hydroxysuccinimide (NHS)

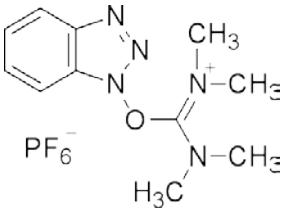

***Figure 2-9:*** *Scheme of O-Benzotriazole-N,N,N′,N′-tetramethyl-uronium-hexafluoro-phosphate (HBTU).*

HBTU is one of the most widely used coupling reagents in solid phase peptide synthesis. It is cheap, provokes very little racemization and it shows a very high efficiency [85]. Figure 2-9 shows HBTU's structure and figure 2-10 the mechanism of esterification of a carboxylic acid when using this coupling reagent. When HBTU reacts with a carboxylic acid, the molecule splits into two molecules: a carbodiimide and N-hydroxybenzotriazole (HOBt) #1. The resulting carbodiimide is unstable and can readily react with HOBt leading to an active benzotriazole-based ester #2, which has the required reactivity to react with nucleophilic amines #3.

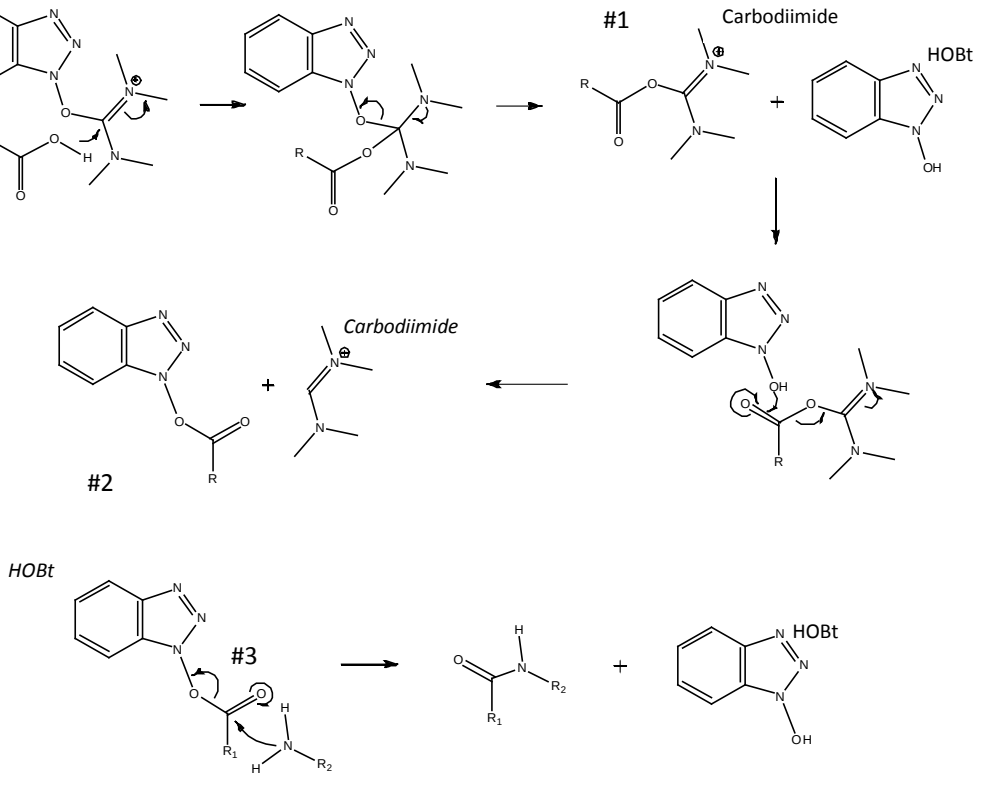


***Figure 2-10:*** *Scheme of HBTU esterification of a carboxylate and its subsequent reaction with a primary amine.*

For a long time, the active HBTU and its family were believed to possess an uronium structure, but intensive studies provided evidence for the formulation of guanidinium N-oxides. They are nevertheless still habitually called uronium type reagents. Unlike carbodiimides or phosphonium reagents, uronium salts may form tetramethylguanidinium derivatives with free amines. To circumvent this side reaction, base and excess reagent should be avoided, and pre-activation of the carboxylic acid component is recommended [83].

HBTU is insoluble in water and therefore requires the use of non-aqueous solvents such as dimethylformamide (DMF) or dimethyl sulfoxide (DMSO). When working in an aqueous media was necessary, HBTU was substituted by the water soluble reagent EDC+NHS. Although its efficiency is not as high as that shown by HBTU, EDC+NHS is cheaper and the methodology used is similar to that used for HBTU. Figure 2-11 shows the reaction pathway of EDC+NHS to create an amide bond.

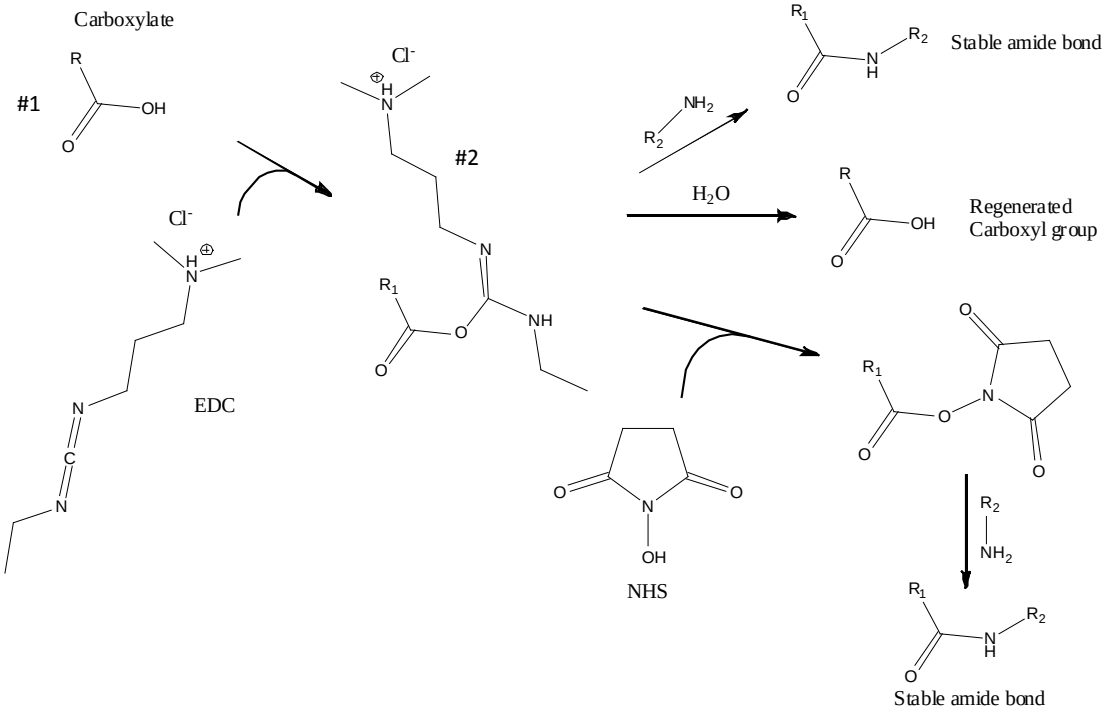


***Figure 2-11:*** *Scheme of EDC+NHS esterification of a carboxylate and its subsequent reaction with a primary amine.*

EDC reacts with a carboxyl group on molecule #1, forming an amine-reactive O-acylisourea intermediate (molecule #2). This intermediate may react with an amine, yielding a conjugate of the two molecules joined by a stable amide bond. However, it is also susceptible to hydrolysis,

making it unstable and short-lived in aqueous solution. The addition of NHS stabilizes the amine-reactive intermediate by converting it to an amine-reactive NHS ester, thus increasing the efficiency of EDC-mediated coupling reactions [86-88]. The amine-reactive NHS ester intermediate has sufficient stability to permit two-step crosslinking procedures, which allows the carboxyl groups on one protein to remain unaltered.

### 2.3.4. Step 3: Crosslinking

In the previous section, the guidelines regarding how to perform a covalent bond between the amino group of APTES and the carboxylic groups of a peptide in order to immobilize it on a titanium surface were described. As can be seen so far, CPTES can react directly with the amino groups of the peptide and APTES can react with carboxylic acids that have been previously activated by means of HBTU or EDC+NHS. The esterification of carboxylic acids leads to three problems that need to be solved in order to perform a controlled immobilization of the peptide on the surface:

- *Specificity:* Usually, peptides contain more than one carboxylic group. Many times, the carboxylic residues of the peptide form part of the biological motive that has to interact with the cells. The most direct example is the RGD sequence which contains an aspartic acid residue. When pre-activating a peptide with HBTU or EDC+NHS, there is no control on which carboxylic acids are activated and which not. Therefore, the aspartic acid residue of an RGD sequence may react with the amino group of APTES compromising its biological activity.
- *Peptide polymerization:* peptides contain both primary amines and carboxylic acids, as it the case for the C and N terminus of a peptide which are a carboxylic acid and a primary amine, respectively. Also, lysine residues contain a primary amine and aspartic and glutamic acid residues contain carboxylic acids. When pre-activating a peptide with HBTU or EDC+NHS, carboxylic acids get ready to react with amines which are present in the same amino acid chain or its neighbors in a concentrated

solution. Therefore, uncontrolled polymerization of the peptide may occur.

- *Racemization:* In chemistry, racemization refers to the converting of an enantiomerically pure mixture (one where only one enantiomer is present) into a mixture where more than one of the enantiomers are present. If the racemization results in a mixture where the enantiomers are present in equal quantities, the resulting sample is described as racemic or a racemate [89]. This effect has a paramount importance on biological molecules since the L form of amino acids and the D form of sugars (primarily glucose) are usually the biologically reactive form. The other form simply does not participate in biochemical reactions or can cause side-effects. While HBTU causes very little racemization it is recommended that N,N-Diisopropylethylamine (DIEA) be added to the solution to increase the HBTU's efficiency. DIEA can cause a very strong racemization [90] of the peptide. Also, EDC can produce racemization of the peptides in water [91,92].

In order to avoid these three problems, a new crosslinking method was developed and proposed here. This new method links the peptide on the APTES silanized surface in a specific way and thus, minimize the aforementioned drawbacks associated with the pre-activation of the peptides using HBTU or EDC+NHS.

Since the biological sequences that are used in this thesis contain numerous carboxylic acids and very few amine groups, it was decided that linking the peptide to the surface through its primary amines would create a more specific bond than linking the peptides through its carboxylic acids.

The idea, then, was to continue using the ester-amine reaction because of its high efficiency but applying a cross-linking molecule between the APTES amine and the amino group of the peptide. This cross-linking molecule was to have the following properties:

- Containing a carboxylic group capable of being esterified to link to the amino group APTES.

- Containing an additional carboxylic group to be esterified and thus, linked to the amino group of the peptide.
- One of the two aforementioned carboxylic groups of the cross-linker would react with APTES and the other carboxylic group would react with the peptide.

In order to get the best cross-linking performance, three crosslinkers were selected to be studied; i.e., malonic acid, glutamic acid, and diglycolic acid (Figure 2-12).

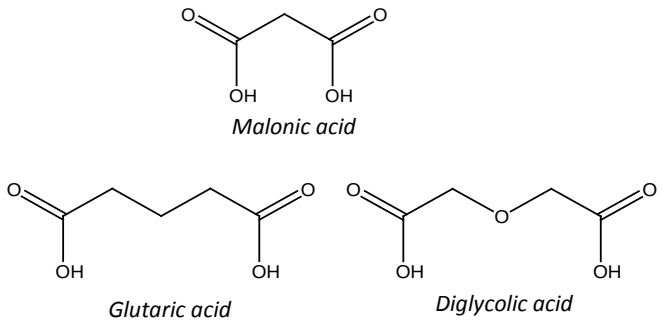


***Figure 2-12:*** *Chemical structures of the three cross-linkers evaluated in the study. Drawings performed with Chemdraw 12.0.*

As can be seen in figure 2-12, the three cross-linkers contain two carboxylic acids as terminal groups. Malonic acid is the shortest possible molecule and it is simply two carboxylic acids linked by a carbon atom. Glutaric and diglycolic acids have a longer intermediate chain which could better expose the free carboxylic acid to the peptide once they are already linked to APTES.

The lengths of the cross-linkers have been intentionally selected to be short in order to fulfill the third requirement, which is that only one of the carboxylic acids needs to link to APTES. Longer molecules have a higher probability of reacting with APTES on both of their sides as steric effects hinder short molecules from easily to do so.

So, our strategy is that the cross-linking step will activate both carboxylic acids of the cross-linker via HBTU or EDC+NHS and the cross-linker will react with APTES. Once this reaction is completed, the samples will be washed to remove all the products that could polymerize or

racemizate the peptides. In a final step, the previously activated free carboxylic acid of the cross-linker will react with the amino group of the peptide in a safe, oriented, and controlled fashion. Figure 2-13 shows the reaction pathway when malonic acid is used as the cross-linker.

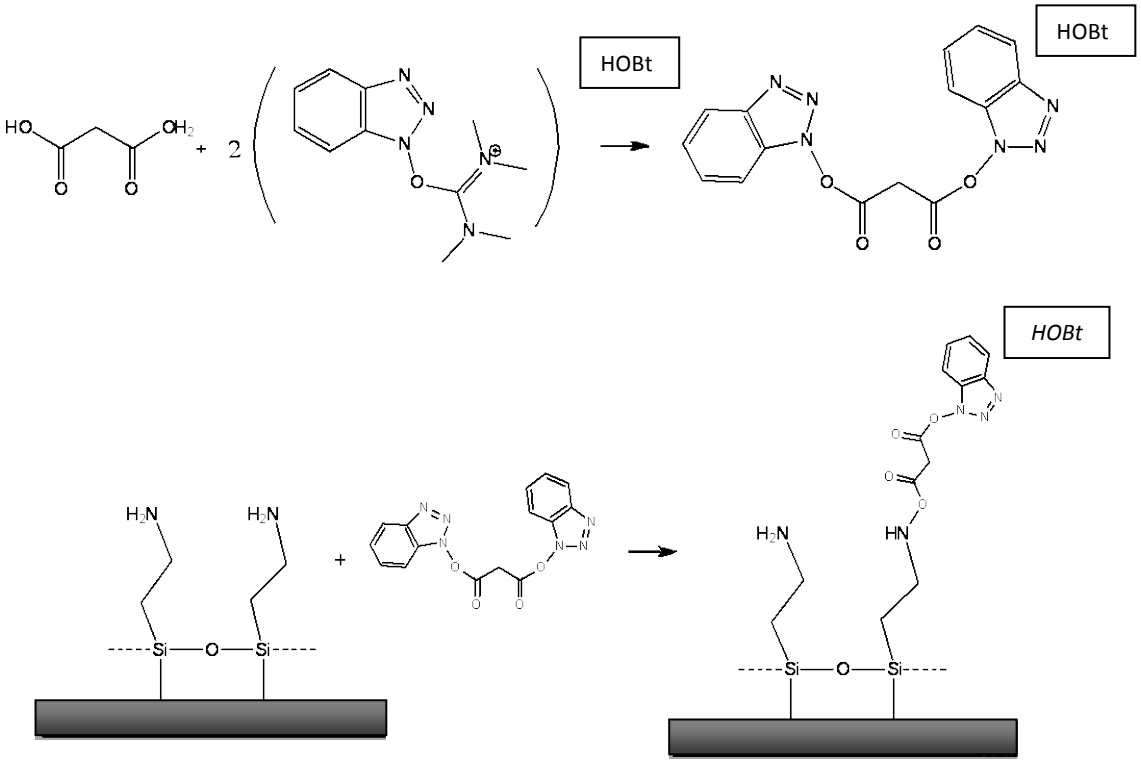


***Figure 2-13:*** *Reaction scheme of malonic acid with HBTU and its subsequent reaction with the anchored APTES amino group.*

## 2.3.5. Step 4: Peptide immobilization

The last step of the functionalization process is to immobilize the peptide on the surface. The peptide immobilization step can be performed, on a CPTES silanized surface, just after silanization, while on an APTES silanized surface it should be performed using a crosslinker molecule.

There are two elements of peptides which are essential for functionalization purposes. One is the biological motive of the peptide which will interact with cells or other biological elements in the body. The other is the linking site to the surface. This site should be specific and far from the biological motive in order to ensure that the biological elements have access to interact

with it. As was previously determined due to the assumptions of the functionalization process, the linking molecule would be a primary amine.

In order to accomplish an effective bioactive surface the peptides were designed with three generic blocks: -bioactive cue (RGDS), -spacer (G5), and –reacting site (K). The bioactive cue (RGDS) is the selected adhesion motive to evaluate the bioactivity of the biofunctionalized surfaces. The spacer (G5) is chain 5 glycines linked to the bioactive motive and its objective is to separate the bioactive motive RGDS from the surface in order to let more accessibility to the cell integrins for reacting with the bioactive cue. Finally, the reacting site (K), linked to the spacer (G5) contains two amino groups able to react with the surface in order to develop a covalent bond and ensure the immobilization of the peptides on the surface. Figure 2-14 shows a scheme of the reaction of the prepared surface with the designed peptide.

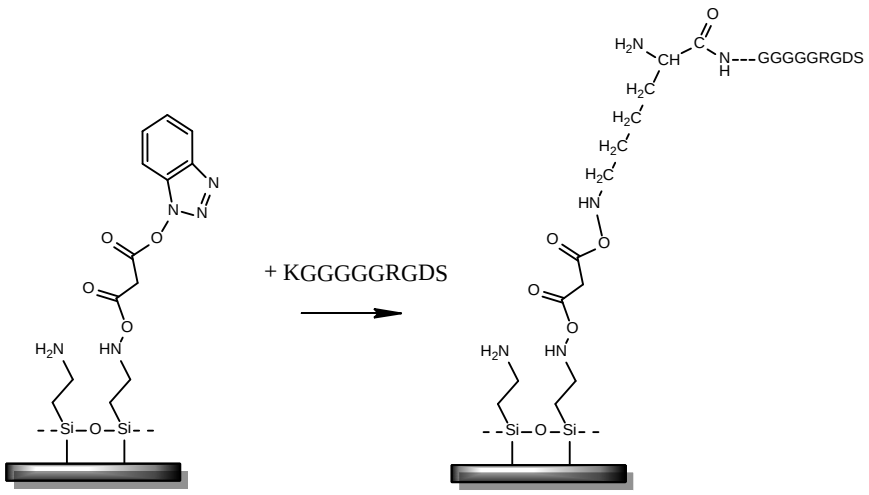


***Figure 2-14:*** *Reaction scheme of the APTES-malonic acid cross-linked surface with the KGGGGGRGDS peptide resulting in a covalent anchorage.*

# 2.4. Surface activation with Plasma, Piranha and Sodium hydroxide

## 2.4.1. Materials and Methods

### 2.4.1.1. Materials

The base material for the experiments was c.p. grade 2 titanium bars from Daido Steel Co. (Japan). The chemicals used to perform the different activation methods were sodium hydroxide pellets from Sigma-Aldrich (USA), 30% oxygen peroxide and 93-98% sulphuric acid from Panreac (Spain). To wash the titanium samples we used 96% ethanol, acetone PAI-ACS, Panreac (Spain), Milli-Q Water, Millipore (USA), 99% 2-propanol and 99.5% cylohexane anhydrous from Sigma-Aldrich (USA).

Other compounds used to characterize the surfaces were 98% 3-aminopropyltriethoxysilane (APTES) from Sigma-Aldrich (USA) and 5-(and-6)-Carboxyfluorescein succinimidyl ester, (5(6)FAM, SE) from Anaspec (USA).

### 2.4.1.2. Base material preparation

The titanium bars were cut in slides of 2 mm thickness with a Struers Accutom-50 diamond powder disk saw (Struers, Denmark). The disk spin velocity was 4500 rpm and the advance velocity was fixed at 0.05 mm/s. Next, the slide flashes were smoothened with a grit stone and one of the two sides of the slides was planned and polished with grit paper using a Buehler Ecomet 4 polishing machine (Buehler, Germany) and following the next procedure:

- Plane with P 240 SiC disk until all the slides had the same thickness
- Plane with P 400 SiC for 10 minutes
- Plane with P 600 SiC for 10 minutes
- Plane with P 800 SiC disk for 10 minutes

- Plane with P 1200 SiC disk for 20 minutes
- Polish with colloidal silica on a velvet cloth for 2 hours
- Washing on a clean velvet cloth with water for 15 minutes

Finally, the titanium samples were washed with ethanol, water and acetone and stocked for use. All the grit papers, cloths and colloidal silica were purchased from Buehler, Germany.

#### 2.4.1.3. Surface activation methods

In this section the three different activation methods studied are described.

##### *2.4.1.3.1. Plasma Cleaning*

In this thesis, the gas used for plasma cleaning the samples was 99,95 % pure oxygen. The device used was a PDC-02 plasma cleaner (Harrick, USA). The procedure is described as follows:

- Introduce the titanium samples into the chamber
- Generate vacuum for 5 minutes
- Inject oxygen for 3 minutes in the chamber
- Switch the Rf source on to generate the plasma for 5 minutes
- Switch the Rf source off
- Break the vacuum
- Extract the samples from the chamber and stock them in argon atmosphere

##### *2.4.1.3.2. Piranha treatment*

To treat the samples, piranha solution was prepared immediately prior to the treatment. Piranha solution was composed by 50 %.v of sulfuric acid and 50%.v of 30% oxygen peroxide.

After preparation, titanium samples were immersed in the piranha solution for 1 h. After piranha treatment, the samples were rinsed in milli-Q water, acetone and dried with nitrogen.

#### *2.4.1.3.3. Sodium hydroxide treatment*

To treat the samples, they were immersed in readily prepared sodium hydroxide 5 mol/l in a closed polypropylene flask. The flask was then introduced in a furnace at 60 $^{o}$C for 24 h. After the treatment the samples were immersed in Milli-Q water for 30 minutes, then the samples were immersed again in Milli-Q water for another 30 minutes and finally the samples were rinsed in Milli-Q water, acetone, dried with nitrogen and stocked in vacuum for their next use.

### 2.4.1.4. Characterization techniques

#### *2.4.1.4.1. Topography and roughness*

Surface topography plays a paramount role in biomaterials and the interactions between living tissues and biomaterial surface. The study of surface topography involves a wide variety of techniques in order to describe the roughness, homogeneity, porosity and other aspects. Although this work does not intend to focus on topography of the different surfaces developed, understand thorough study of the surface of a dental implant would require characterization of its roughness. Also, the topographical characterization of these surfaces is a key factor to analyze the effect of each activation treatment on the subsequent steps of the functionalization process.

Two different techniques were used to characterize surface topography, especially parameters of roughness. The techniques are described in the following section.

#### 2.4.1.4.1.1. Surface observation

The surfaces were studied by means of a scanning electron microscopy (SEM) (Zeiss Neon40, Zeiss, Germany) with an acceleration voltage of 8,0 keV in order to evaluate qualitatively the effect of the different surface treatments.

#### 2.4.1.4.1.2. Surface roughness

A description of the white light interferometry (LIM) technique to evaluate the surface roughness can be found in Annex A of this thesis in electronic format.

Roughness measurements were performed with an interferometer microscope (Optical Profiling System, Wyko NT1100, Veeco, USA). Three samples activated by each of the three different methods were analyzed and for every sample three measurements of roughness were carried out.

Surface analysis area was of 189,2×248,7 $mm^2$. Data analysis was performed with Wyko Vision 232TM software (Veeco, USA). A Gaussian filter was used to separate waviness and form from roughness of the surface by applying a cut-off value (λc) of 2,5 mm.

Roughness parameters were obtained from the 2D-profiles extracted from 3D images obtained by LIM. Surface index were calculated from the ratio of real surface area/geometric surface area, which were measured after obtaining 3D-topographical images of the surfaces by LIM.

### *2.4.1.4.2. Wettability*

A description of contact angle goniometry can be found in Annex A of this thesis in electronic format.

Surface wettability of the different titanium surfaces was measured with a contact angle goniometer (Contact Angle System OCA 15plus, Dataphysics, Germany) using the sessile drop method, in which a drop of milli-Q water of 3 µl was dispensed for each measurement. The contact angle was analyzed with SCA20 software (Dataphysics, Germany). A minimum of 9 measurements was performed on each surface.

#### *2.4.1.4.3. Chemical composition*

##### 2.4.1.4.3.1. X-ray photoelectron spectroscopy (XPS)

A description of the XPS technique can be found in Annex A of this thesis in electronic format.

Two samples of each condition were analyzed just after the activation treatment to avoid degradation or contamination of the surfaces. The equipment of analysis was a SAGE ESCA System, (SPECS, Germany). An aluminum source set at 1,5 KeV was used and the pressure of the chamber was, at most, $10^{-9}$ torr.

#### *2.4.1.4.4. Effectiveness on silanization*

In this work, the purpose of the activation methods is to prepare the titanium surface for the subsequent silanization. Therefore, the most direct way to evaluate the effectiveness of each activation method is to silanize the surface after performing each of the activation methods and characterize the silanized surface. The silanization process will be described in detail in section 2.5.1.2. In order to evaluate the silanized surface it was decided to use fluorescence microscopy. Fluorescence microscopy is a rapid and versatile method to obtain a semi-quantitative value for the amount and homogeneity of the silane on the surface.

The pre-activated surfaces were silanized with 3-aminopropyltriethoxy silane (APTES) as described next:

The activated surfaces were immersed in a solution of 99.8% anhydrous toluene (Sigma, USA) where APTES was diluted in a concentration of 30 mM [78]. The samples remained in the APTES solution for 1 hour at 70 $^{o}$C with agitation. After silanization, the samples were sonicated in anhydrous toluene for 15 minutes in order to eliminate the loosened silane from the surface. Subsequently the samples were sonicated for another 15 minutes in water and washed with ethanol, isopropanol, water and acetone and dried with nitrogen.

As was explained in section 2.3.3.2, APTES contains a primary amine that is able to react with a carboxylate in certain conditions. In order to visualize the surfaces using fluorescence microscopy, the silanized surfaces were treated overnight with a solution of 5-(and-6)-Carboxyfluorescein, Succinimidyl Ester (5(6)-FAM, SE) at a concentration of 50 mmol/l in 99.8% *N,N*-Dimethylformamide (DMF) purchased from Sigma, USA. After the treatment the samples were washed in ethanol, isopropanol, water and acetone and dried with nitrogen. To analyze the samples, an Olympus E600 upright microscope, equipped with an Olympus DP 25 digital camera (Olympus, Japan), was used. The green light (wavelengths between 500 and 550 nm) filter was selected in the microscope to take the micrographs. The fluorescence intensity of the images was obtained by means of Image J v.1.43u software (USA).

#### 2.4.1.5. Statistical analysis

A structured and sequential statistical analysis of the obtained results in the different experiments was performed.

First, it was necessary to determine whether parametric or non-parametric statistics should be used to analyze the results. To apply parametric statistics the values of study must fulfill a series of assumptions [93]:

- *Numeric variable:* The data of analysis are numeric.
- *Normality:* The values of the dependent variable come from a normal distribution.
- *Homoscedasticity:* The dependent variables have equal variances.

To determine if the variables of study came from a normal distribution the Kolmogorov-Smirnov test for normality [93,94] was performed. As the size of the sample per group was notably small there was not enough statistical confidence to assume that the variables followed a normal distribution. Thus, non-parametric statistics were used describe and compare results in this chapter.

Kruskal-Wallis test [95,96] of the equality of medians for two or more populations started the statistical analysis to evaluate significant differences ($p\text{-value}<0.05$) between experimental conditions the Kruskal-Wallis test is a non-parametric alternative for a one-way ANOVA table.

If the Kruskal-Wallis test showed statistical differences, then the multiple-comparison post-hoc Mann-Whitney test [95,97] was performed to determine which groups were statiscally different.

All statistical tests were performed using Minitab 16.1.1 software, Minitab Inc. (USA)

## 2.4.2. Results

In this section, the results with the different activation techniques are shown to select the best activation method for the purposes of this thesis.

### 2.4.2.1. Nomenclature

Whenever the space to describe the samples was limited, like in figures and tables, a nomenclature code was applied. Following, the abbreviators used are described:

**Ti:** *Titanium.* Polished and clean titanium as described in section 2.4.1.2.
**Ti Plasma:** Polished titanium treated with plasma cleaning as described in section 2.4.1.3.1.
**Ti Piranha:** Polished titanium treated with piranha as described in section 2.4.1.3.2.
**Ti NaOH:** Polished titanium treated with sodium hydroxide as described in section 2.4.1.3.3.

**APTES:** Polished titanium treated with the indicated activation treatment and silanized with APTES as described in section 2.4.1.4.4.

### 2.4.2.2. Topography and roughness

Figure 2-15 shows SEM pictures of the treated and untreated titanium surfaces, with the different activation methods studied. No difference between polished titanium and Plasma cleaned titanium was observed. Piranha treatment generates a high degree of roughness as a result of the preferential etching on the grain boundaries of the surface of the metal. Also, some pitting corrosion can be observed on these surfaces (marked with arrows in the figure). NaOH treatment generates a more homogeneous roughness on the Ti surface with a very intricate and nanoporous morphology.

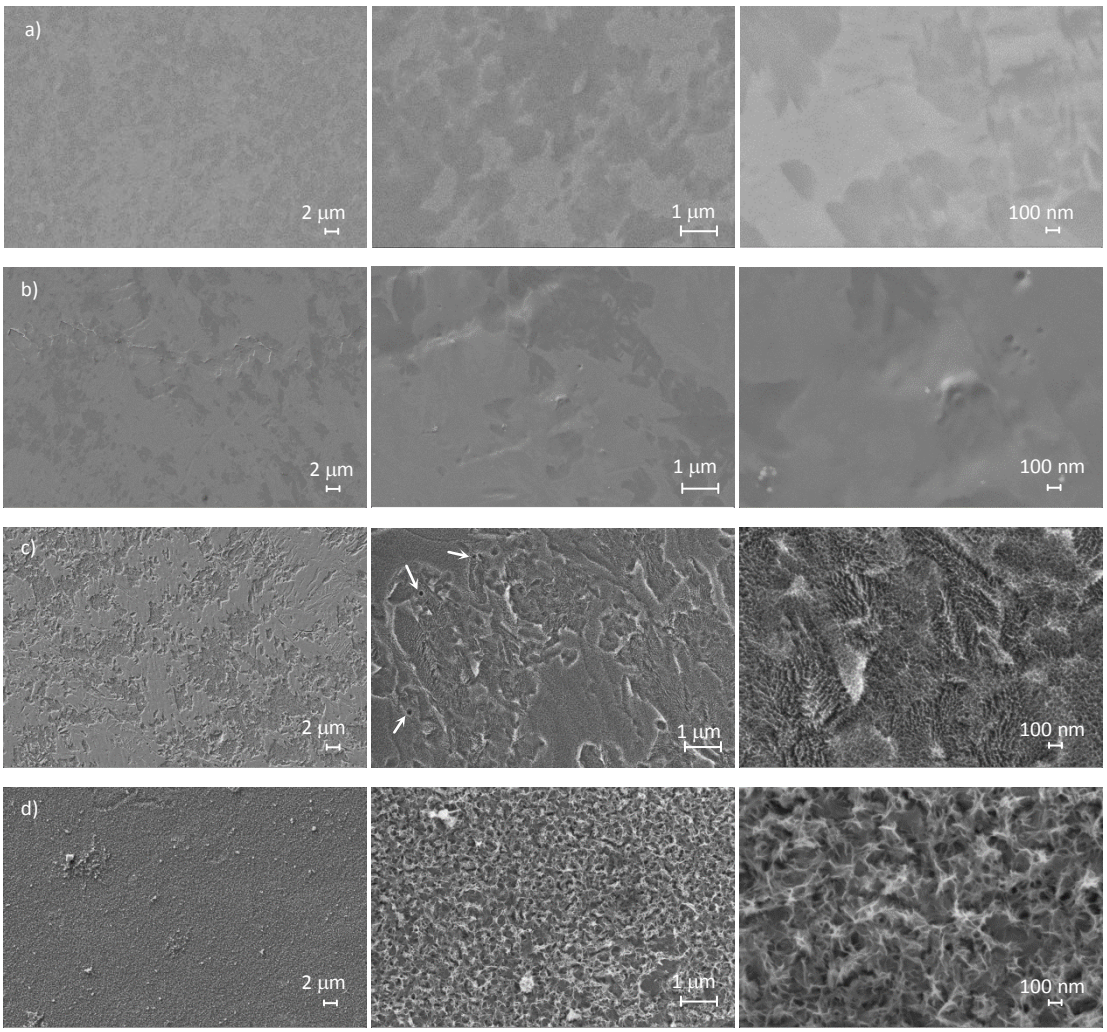


***Figure 2-15:*** *SEM images of a) Polished c.p. Ti; b) Plasma cleaned c.p. Ti; c) Piranha treated c.p. Ti; d) NaOH treated c.p. Ti*

Figure 2-16 shows the interferometry maps of the treated and untreated titanium surfaces, with the different activation methods. Table 2-1 shows the surface roughness data extracted from the interferometry images. As can be seen from these data, Plasma cleaning did not modify the surface roughness of titanium, while roughness of Piranha treated surfaces was approximately 10-fold higher. The homogeneity of the roughness achieved by the piranha treatment was lower than that of the other methods because $R_t$ was close to 1 μm. NaOH treatment increases titanium roughness about 5 times and the homogeneity of the roughness was sensibly better than the one gotten with piranha. Moreover, Piranha and NaOH treatments increased the surface index, with piranha being the treatment which produced a higher surface index. Interferometry is an optical technique which has its limitations regarding the resolution of the details on the surface. As can be observed from the SEM pictures, the surface treated with NaOH produced a very intricate tangle of sodium titanate plates with lengths of around 100 nm. Interferometric microscopy cannot resolve those topographical features and, hence, the surface index obtained is lower than the real one.

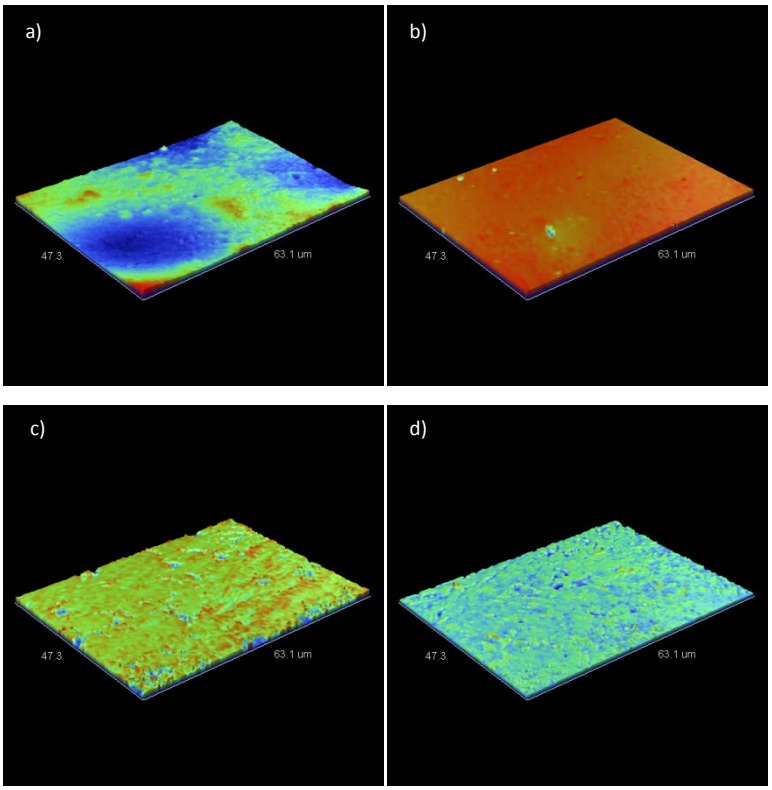


***Figure 2-16:*** *Interferometric images of a) Polished c.p. Ti; b) Plasma cleaned Ti; c) Piranha treated Ti and d) NaOH treated Ti.*

***Table 2-1*** *Mean-values ± standard deviation of the roughness parameters for all titanium surfaces studied. a,b and c mean statistically significant differences with regards to Ti, Plasma Ti and Piranha Ti respectively, using the Mann-Whitney test. Confidence interval: 0.95.*

| Surface | Ti | Plasma Ti | Piranha Ti | NaOH Ti |
|---|---|---|---|---|
| **Ra(nm)±SD** | 8.43±2.48 | 7.80±2.38 | 82.10±11.40$^{a,b}$ | 37.80±3.85$^{a,b,c}$ |
| **Rq(nm)±SD** | 9.21±2.68 | 8.47±2.31 | 124.40±13.81$^{a,b}$ | 52.88±7.15$^{a,b,c}$ |
| **Rt(nm)±SD** | 43.33±16.07 | 50.15±17.59 | 965.12±180.91$^{a,b}$ | 349.22±203.21$^{a,b,c}$ |
| **Surface Index±SD** | 1.0002±0.0000 | 1.0002±0.0000 | 1.0750±0.0106$^{a,b}$ | 1.0129±0.0016$^{a,b,c}$ |

### 2.4.2.3. Wettability

Water contact angle on polished titanium was 49.3 ± 1.5º (Figure 2-17). All the different activation treatments increased hydrophilicity on the titanium surface. Piranha treatment reduced the water contact angle to 34.5 ± 4.7º while plasma cleaning and NaOH reduced the contact angle to values near 0º and thus, immeasurable by contact angle goniometry.

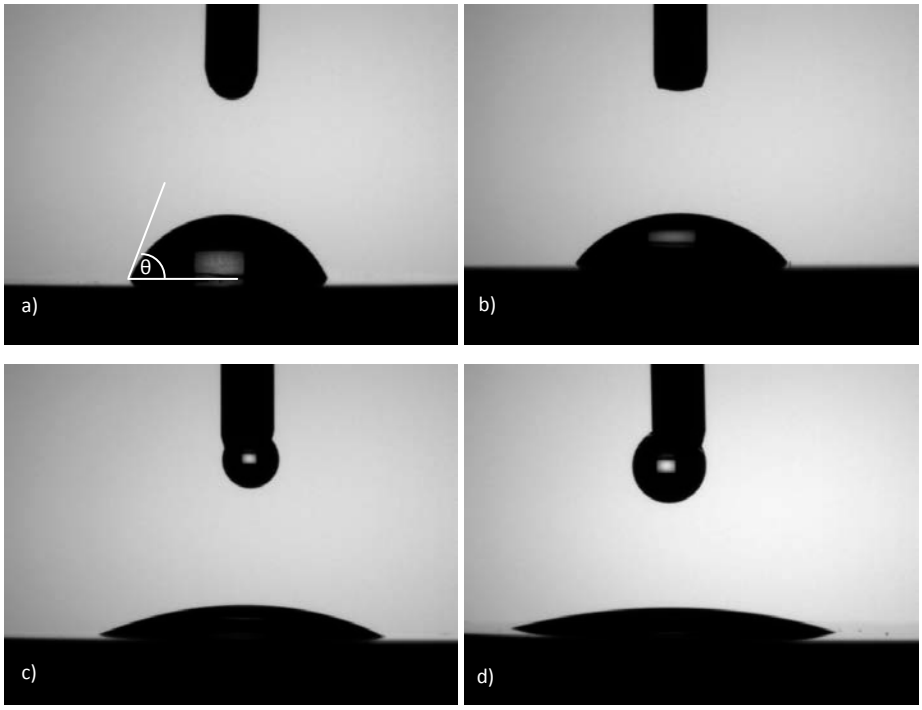


***Figure 2-17:*** *Water drops on a) polished Ti, b) piranha treated Ti, c) plasma cleaned Ti and d) NaOH treated Ti*

## 2.4.2.4. Chemical composition

### *2.4.2.4.1. X-ray Photoelectron Spectroscopy (XPS)*

#### 2.4.2.4.1.1. Survey analysis

Table 2-2 shows the chemical composition of the surfaces treated with the different activation techniques. Plain titanium shows a conventional composition with approximately 15% of carbon, which is low compared to other analyses [98,99]. All three activation techniques sensibly changed the chemical composition of the surface, but each one showing unique and specific chemical modifications.

Piranha treatment is believed to clean the surface by acid etching but an increase of carbon contamination was detected using this type of treatment. Also, surfaces treated with this method have approximately 1% of sulfur on the surface which could be noxious for living tissues and cells. Moreover, titanium signal was reduced due to the increase in contaminants and a thicker titanium oxide layer on the surface [72].

***Table 2-2*** *Chemical composition (% mol) of the titanium surfaces treated with the different activation methods. Data extracted from XPS survey spectra.*

| | C1s | Cl2p | N1s | Na1s | O1s | S2p | Si2p | Ti2p | Total | O/Ti |
|---|---|---|---|---|---|---|---|---|---|---|
| **Ti** | 16.7 | 0.4 | 0.7 | 0.1 | 57.3 | 0.0 | 0.5 | 24.4 | 100.0 | 2.35 |
| **Ti Piranha** | 24.8 | 0.0 | 0.8 | 0.0 | 54.0 | 0.9 | 0.2 | 19.4 | 100.0 | 2.78 |
| **Ti NaOH** | 7.8 | 0.0 | 0.6 | 3.6 | 65.9 | 0.2 | 0.6 | 21.2 | 100.0 | 3.11 |
| **Ti Plasma** | 13.8 | 0.2 | 1.3 | 0.8 | 61.8 | 0.3 | 0.0 | 21.7 | 100.0 | 2.85 |

Treating titanium with sodium hydroxide 5 mol/dm$^3$ for 24 h at 60 $^{o}$C generates a sodium titanate gel, $Na_2Ti_3O_7$, on the surface [74,75,100]. The percentage of carbon was very low suggesting that the NaOH treated surfaces were thoroughly cleaned. The relative percentage of sodium and oxygen sensibly increased, which is in agreement with the formation of a sodium titanate layer.

Oxygen plasma cleaning generates very reactive oxygen ions that can react with the contaminants and drag them from the surface. In fact, plasma cleaning reduced the carbon contamination on the surface. It also oxidized the surface since the percentage of oxygen increased and that for titanium was slightly reduced. However, plasma cleaning performs a less efficient surface modification than the other two treatments studied.

It has been shown that all activation treatments effectively oxidize the titanium surface since in all cases the O/Ti ratio increases with respect to non-activated Ti.

Following, the deconvolutions of the different peaks reveal more information about the composition of the surfaces activated with the different treatments and whether it increase the amount of OH groups on the surface.

2.4.2.4.1.1. Peak deconvolution

*Carbon C1s*

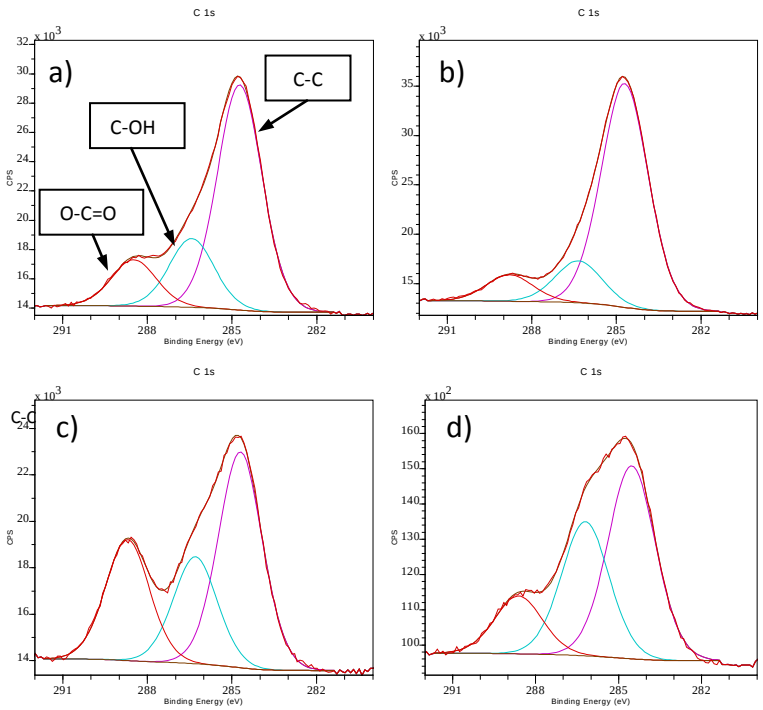


***Figure 2-18:*** *XPS Deconvolutions of the C1s peak of the titanium surfaces treated with the different activation methods. a) polished Ti, b)piranha treated Ti, c) NaOH treated Ti, d) plasma cleaned Ti.*

On titanium surfaces treated with these three activation methods, carbon should be treated as a contaminant. Nevertheless, it is interesting how the three different activation methods modified the composition of this contaminant on the titanium oxide surface. The deconvolutions of the carbon peak made evident the presence of species of with three different carbon groups (Figure 2-18 and table 2-3).

It was seen, in the previous section, that piranha treatment increased the carbon contamination. The deconvolution analysis revealed that species with C-C groups were prevalent. Those species are not reactive and therefore they will reduce the chances of a good silanization on the subsequent step of the functionalization process.

***Table 2-3*** *Deconvolution data of the carbon C1s for the different titanium surfaces*

| **Carbon C1s** | | | | |
|---|---|---|---|---|
| *Ti* | | | | |
| **Chemical State** | **Position (eV)** | **Area (pixel)** | **Area (%)** | **References** |
| C-C | 284.73 | 8606.83 | 66.19 | [101-103] |
| C-OH | 286.43 | 2628.59 | 20.21 | [102,104] |
| O-C=O | 288.48 | 1768.27 | 13.6 | [99,102,104] |
| | | | | |
| *Ti Piranha* | | | | |
| **Chemical State** | **Position (eV)** | **Area (pixel)** | **Area (%)** | **References** |
| C-C | 284.7 | 13348.3 | 76.61 | [101-103] |
| C-OH | 286.34 | 2498.03 | 14.34 | [101,102,105] |
| O-C=O | 288.78 | 1577.07 | 9.05 | [99,102,104] |
| | | | | |
| *Ti NaOH* | | | | |
| **Chemical State** | **Position (eV)** | **Area (pixel)** | **Area (%)** | **References** |
| C-C | 284.53 | 3316.3 | 50.13 | [99,102,104] |
| C-OH | 286.2 | 2304.8 | 34.84 | [101,102,105] |
| O-C=O | 288.61 | 994.383 | 15.03 | [99,102,105] |
| | | | | |
| *Ti Plasma* | | | | |
| **Chemical State** | **Position (eV)** | **Area (pixel)** | **Area (%)** | **References** |
| C-C | 284.7 | 5100.33 | 48.59 | [101-103] |
| C-OH | 286.3 | 2530.9 | 24.11 | [102,104] |
| O-C=O | 288.7 | 2866.01 | 27.3 | [99,102,104] |

As it was shown by the survey data, the surfaces showing least carbon presence were those treated with sodium hydroxide. However, the composition of the carbon peak on these surfaces revealed a high amount of C-OH groups which can react with the silanes at the silanization step, giving to the surface a high reactive potential.

Plasma cleaned surfaces showed the lowest concentration of C-C groups, showing therefore, a higher concentration of C-OH and O-C=O species which are more reactive.

*Oxygen O1s*

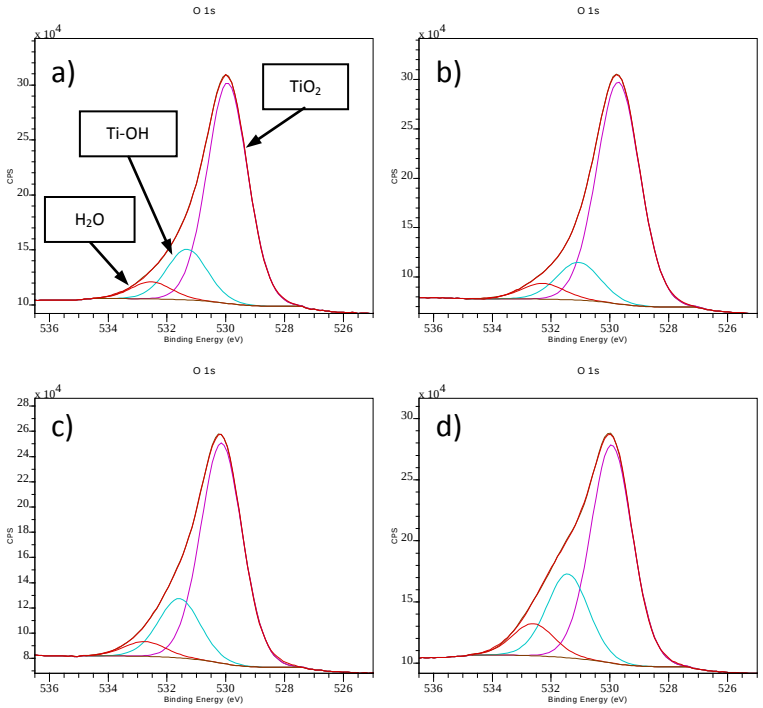


***Figure 2-19:*** *XPS Deconvolutions of the O1s peak of the titanium surfaces treated with the different activation methods. a)plain Ti, b)piranha treated Ti*

*c) NaOH treated Ti, d) plasma cleaned Ti.*

From the deconvolution of the oxygen peak, species with three different chemical groups were detected (Figure 2-19). Among them, Ti-OH group is the most important one in this work since, as it was explained in section 2.3.1, hydrolyzed silanes need to react with surface hydroxyl groups to generate a stable bond with the surface.

To achieve a proper immobilization of the silane in the subsequent functionalization step, a good activation method should generate a high amount of OH groups on the surface. As can be seen in table 2-4, piranha treatment did not increase OH groups on the surface, having an even lower percentage of OH groups than polished titanium. Sodium hydroxide treatment slightly increased the amount of OH groups on the surface, although the difference between plain

titanium and sodium hydroxide treated samples was not very high. Plasma cleaning has the highest activation potential of all three activation techniques according to the increase of OH groups.

***Table 2-4:*** *Deconvolution data of the carbon O1s for the different titanium surfaces*

| **Oxygen O1s** | | | | |
|---|---|---|---|---|
| *Ti* | | | | |
| **Chemical State** | **Position (eV)** | **Area (pixel)** | **Area (%)** | **References** |
| $TiO_2$ | 529.94 | 86939.1 | 76.5 | [99,104,106] |
| Ti-OH | 531.31 | 20002.3 | 17.6 | [99,107,108] |
| $H_2O$ | 532.54 | 6701.88 | 5.9 | [99,108] |
| *Piranha* | | | | |
| **Chemical State** | **Position (eV)** | **Area (pixel)** | **Area (%)** | **References** |
| $TiO_2$ | 529.72 | 122607 | 80.52 | [99,104,106] |
| Ti-OH | 531.06 | 20965 | 13.77 | [99,107,108] |
| $H_2O$ | 532.29 | 8692.68 | 5.71 | [99,108] |
| *NaOH* | | | | |
| **Chemical State** | **Position (eV)** | **Area (pixel)** | **Area (%)** | **References** |
| $TiO_2$ | 530.15 | 91881.3 | 74.77 | [99,104,106] |
| Ti-OH | 531.58 | 24798.8 | 20.18 | [99,107,108] |
| $H_2O$ | 532.76 | 6213.3 | 5.06 | [99,108] |
| *Plasma* | | | | |
| **Chemical State** | **Position (eV)** | **Area (pixel)** | **Area (%)** | **References** |
| $TiO_2$ | 529.94 | 94203.5 | 65.25 | [99,104,106] |
| Ti-OH | 531.43 | 36293.3 | 25.14 | [99,107,108] |
| $H_2O$ | 532.61 | 13869 | 9.61 | [99,108] |

*Titanium Ti2p*

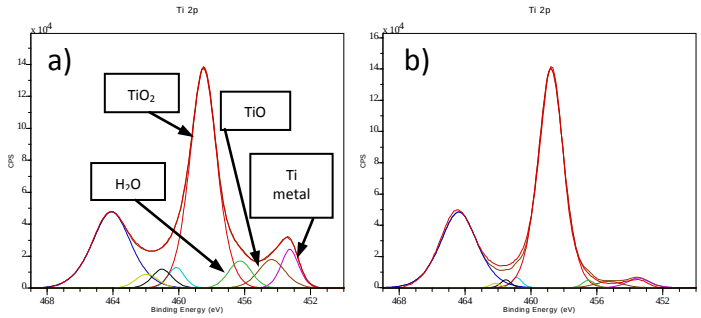


***Figure 2-20a:*** *XPS Deconvolutions of the Ti2p peak of the titanium surfaces treated with the different activation methods. a)Plain Ti, b)Piranha treated Ti.*

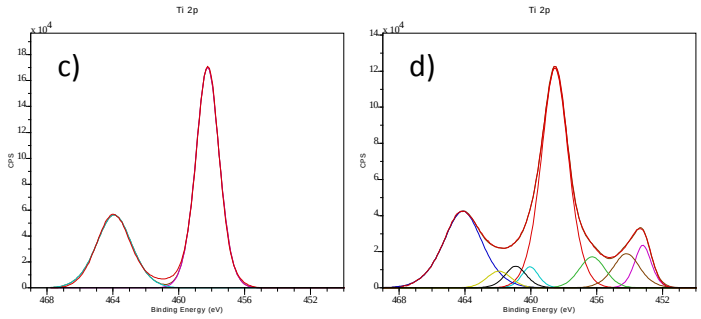


***Figure 2-20b:*** *XPS Deconvolutions of the Ti2p peak of the titanium surfaces treated with the different activation methods. c) NaOH treated Ti, d) Plasma cleaned Ti.*

***Table 2-5*** *Deconvolution data of Ti 2p3/2 for the different titanium surfaces*

| **Titanium Ti 2p3/2** | | | | |
|---|---|---|---|---|
| *Ti* | | | | |
| **Chemical State** | **Position (eV)** | **Area (pixel)** | **Area (%)** | **References** |
| Ti Metal | 453.27 | 1666.41 | 7.67 | [14,104,107] |
| TiO | 454.37 | 1860.58 | 8.57 | [14,109] |
| $Ti_2O_3$ | 456.29 | 7837.73 | 17.93 | [104,107] |
| $TiO_2$ | 458.51 | 14272.80 | 65.81 | [14,104,107-109] |
| | | | | |
| *Piranha* | | | | |
| **Chemical State** | **Position (eV)** | **Area (pixel)** | **Area (%)** | **References** |
| Ti Metal | 453.49 | 547.02 | 3.54 | [14,104,107] |
| TiO | 455.28 | 423.05 | 2.74 | [14,109] |
| $Ti_2O_3$ | 456.51 | 589.82 | 3.81 | [104,107] |
| $TiO_2$ | 458.79 | 13907.30 | 89.91 | [14,104,107-109] |
| | | | | |
| *NaOH* | | | | |
| **Chemical State** | **Position (eV)** | **Area (pixel)** | **Area (%)** | **References** |
| $Ti^{4+}$ | 457.87 | 17177.10 | 100 | [110] |
| | | | | |
| *Plasma* | | | | |
| **Chemical State** | **Position (eV)** | **Area (pixel)** | **Area (%)** | **References** |
| Ti Metal | 453.21 | 1538.23 | 7.42 | [14,104,107] |
| TiO | 454.20 | 1975.54 | 9.53 | [14,109] |
| $Ti_2O_3$ | 456.28 | 4426.02 | 21.34 | [104,107] |
| $TiO_2$ | 458.54 | 12800.20 | 61.72 | [14,104,107-109] |

Deconvolution of the titanium peak shows interesting differences among the activation methods (Table 2-5). Polished titanium surfaces were mainly composed of $TiO_2$ and $Ti_2O_3$ with lower percentages of TiO and metallic Ti. Piranha treatment effectively oxidized the surface, generating $TiO_2$ and therefore reducing the percentage of the other species. NaOH treatment shows only one peak corresponding to $Ti^{4+}$ from the sodium titanate ($Na_2Ti_3O_7$); and thus, the thickness of the sodium titanate layer is higher than the penetration depth of the X-ray beam

which is around 5 nm. Plasma cleaning did not modify the initial surface severely except for a slight increase of $Ti_2O_3$ and a decrease on $TiO_2$, suggesting that plasma cleaning tends to transform the $TiO_2$ into $Ti_2O_3$.

### 2.4.2.1. Effectiveness of activated surfaces on silanization

The subsequent step of the biofunctionalization process, after activation and washing, is silanization. In order to evaluate the effectiveness of each activation method to obtain a properly silanized surface, the different surfaces were silanized with APTES and treated with carboxyfluorescein to be able to evaluate them by fluorescence microscopy. Figure 2-21 shows the silanized surfaces pre-activated with the different methods. As can be seen, an activation treatment is mandatory to obtain subsequent silane immobilization on a titanium surface. Plasma cleaning had a very low effectiveness on silanizing the Ti surfaces, whereas piranha treatment produced a heterogeneous silanization on the surface as many fluorescent lumps on it could be seen. NaOH attack was, by far, the method which gave the notably highest fluorescence intensity while producing a more homogeneous silanized surface.

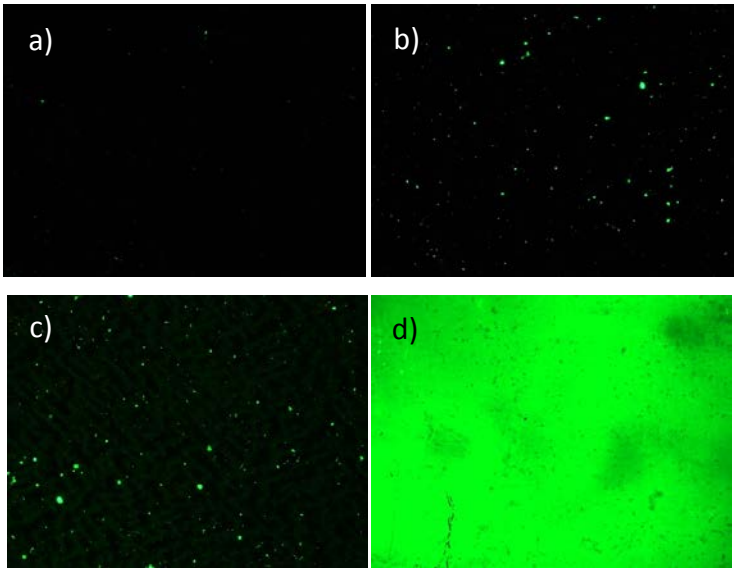


***Figure 2-21:*** *Fluorescence microscopy images of a) polished Ti, b) Plasma cleaned Ti, c) Piranha treated Ti and d) NaOH treated Ti*

Figure 2-22 shows the fluorescence intensity values for the different surfaces silanized and non silanized which have been treated with 5(6)-FAM, SE. Surfaces that were activated by NaOH treatment, without silanization, retained a significant amount of carboxyfluorescein. Nevertheless, after silanization, NaOH treated surfaces anchored a much higher amount of carboxyfluorescein.

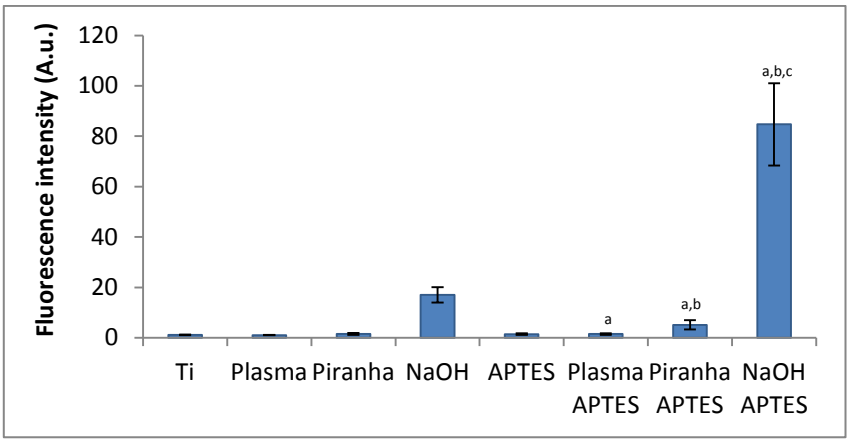


***Figure 2-22:*** *Fluorescence intensities of the different samples treated with carboxyfluorescein.* [a,b and c] *mean statistically significant differences with regards to Ti APTES, Plasma APTES and Piranha APTES, respectively, using the Mann-Whitney test. Confidence interval: 0,95*

## 2.4.1. Discussion

Three different activation methods have been compared in order to select the best choice for a proper biofunctionalization of titanium surfaces. Percentage of OH groups, amount of silanes immobilized, and physical and chemical homogeneity of the activated surfaces are the major criteria we considered for selecting the activation method.

Piranha treatment was discarded due to the fact that it increased the contamination of the titanium surfaces with carbon-containing species and more importantly, piranha treatment did not generate additional OH groups on the surface, which are the preferential reacting sites for forming silanols in the process of silanization. This was further confirmed by the low fluorescence intensity registered on Piranha activated titanium surfaces that were silanized with APTES and fluorescently labeled.

Plasma cleaning generated additional OH groups without modifying the surface topography. The fact that the topography is not modified with this method will be useful in posterior parts of this work for the analysis of the surfaces with techniques that require a flat and very smooth surface, such as AFM, Ellipsometry or Quartz-Crystal Microbalance, among others. The amount of silane immobilized on the surfaces treated with this method was notably lower compared to the other activation techniques. Thus, plasma cleaning although useful for characterization purposes it is not potentially appropriate for obtaining a high density of covalently-anchored peptides. The later can compromise the beneficial bioactive effects of these surfaces as the higher the number of peptides anchored on the surface, the higher the bioactive signaling, and the higher the potential clinical benefits of the coatings.

NaOH etching of the titanium surfaces was the one that resulted with the highest amount of immobilized silanes among the three activation methods studied. This is as a result of the synergistic effect that the formation of the titanate and the enormous increase in real surface area had on the total number of reacting OH groups this method produces. It is worth noting that the nanoporous topography, which confers the high real surface area to these surfaces, is homogeneously distributed on the surface and, therefore, will facilitate a homogenous coverage of the silanes on the treated surface.

For silanization purposes, most of titanium substrates are not pre-activated [111-113]. Although, to accomplish higher silanization efficiency several techniques such as acid attack, anodization or passivation have been applied [114-116].

Silanization treatments on titanium surfaces have been derived from works done on model surfaces such glass, gold and silicon [117-119]. Therefore, most of the activation and silanization treatments done on titanium surfaces have not been optimized for titanium surfaces. In this work, the NaOH treatment was decided to be tested for being a specific treatment which works efficiently only on titanium and its alloys.

NaOH attack was therefore the activation method selected for the first step in the protocol for biofunctionalizing titanium surfaces with oligopeptides. In some cases, however, the surfaces were plasma cleaned because NaOH treated surfaces imposed limitations in the quality and

reliability of the results obtained with certain characterization techniques. Water contact angle goniometry and spectroscopic ellipsometry are two of those techniques to add to the aforementioned in a previous paragraph.

# 2.5. Silanization with APTES and CPTES

In order to develop an effective biofunctionalization process, two silanes were compared on previously activated surfaces. For all the characterization techniques except for contact angle goniometry, the surfaces were pre-activated with NaOH as previously described. Samples for contact angle goniometry were pre-activated with plasma cleaning due to the fact that the samples activated with NaOH had an immeasurable contact angle. Also, in order to evaluate the effectiveness of both silanization methods, the silanized surfaces were, eventually, functionalized with a peptide containing an RGD sequence.

## 2.5.1. Materials and Methods

### 2.5.1.1. Materials

In addition to the materials mentioned in section 2.4.1.1, for CPTES silanization we used 3-chloropropyl triethoxy silane (CPTES), 99.8% anhydrous toluene and N-N-Diisopropylethylamine (DIEA) purchased from Sigma Aldrich (USA).

To characterize the surfaces, two fluorophores were used: 5-(and-6)-Carboxyfluorescein succinimidyl ester, (5(6)FAM, SE) and Fluorescein isothiocyanate cadaverine (FITC cadaverine) from Anaspec (USA). Also, a peptide containing the cell adhesion sequence RGD was produced by peptide solid-synthesis and purchased from Genscript (USA). The amino acid sequence of the peptide was $NH_2$-KGGGGGGRGDS-OH with a purity of 95%. For peptide immobilization O -

(Benzotriazol-1-yl) - N,N,N',N' - tetramethyluronium hexafluorophosphate (HBTU) was purchased from Sigma Aldrich (USA).

### 2.5.1.2. Silanization methods

#### *2.5.1.2.1. APTES silanization*

APTES silanization was performed on previously activated titanium surfaces following the guidelines of Song Y, et al. [78] to obtain a monolayer of silane on the surface as was described in section 2.4.1.4.4.

#### *2.5.1.2.2. CPTES silanization*

CPTES silanization was performed in a similar way to APTES silanization, but with several changes in the composition of the silane dissolution, made up by toluene as a solvent with 200 mM of CPTES and 100 mM of DIEA. The silanization was done exactly in the same fashion as APTES silanization, for 1 hour at 70 $^{o}$C and with the same washing.

### 2.5.1.3. Characterization of the surfaces

#### *2.5.1.3.1. Wettability*

As was reported in section 2.4.2.3, samples treated with NaOH pre-activation treatment were not proper to be studied by water contact angle goniometry due to the fact that contact angles were near zero and thus, the reliable visual assessment of those drops was compromised. Even after silanization, measuring the water contact angle of NaOH pretreated samples was not viable due to their high hydrophilicity. Therefore, it was decided to study the wettability of the

different silanized surfaces was studied by pre-activating them with plasma cleaning. This made possible the measurement of the contact angles of the surfaces of study.

After plasma cleaning, the titanium surfaces were silanized with APTES or CPTES as previously described in section 2.5.1.2. To evaluate the peptide retaining effectiveness of each method, some samples were also treated with the RGD peptide. The adsorption process of the RGD peptide on the different surfaces was performed as described here:

- CPTES silanized and non silanized samples
  - The samples were immersed in a pH 11 $Na_2CO_3$ solution with the dissolved RGD peptide at a concentration of 100 μmol/l overnight.
- APTES silanized samples
  - The samples were immersed overnight in a DMF solution of 100 μmol/l of the RGD peptide mixed with HBTU 100 μmol/l and DIEA 200 μmol/l

The contact angle measurements were performed as previously described in section 2.4.1.4.2.

#### *2.5.1.3.2. Chemical composition*

##### 2.5.1.3.2.1. X-Ray photoelectron spectroscopy

Samples pre-activated with NaOH etching and silanized with APTES or CPTES were analyzed as described in section 2.4.1.4.3.1. Two samples of each condition were analyzed.

##### 2.5.1.3.2.2. Time of Flight Secondary Ion Mass Spectroscopy (ToF SIMS)

A description of the Tof SIMS technique can be found in Annex A of this thesis in electronic format.

The previously activated titanium surfaces were analyzed by ToF SIMS twice. In the first analysis the detector was set as the anode, attracting and detecting the negative ions. In the second analysis the detector was set as the cathode attracting and detecting only the positive ions. For the analyses, the samples were submitted to a vacuum of $5 \cdot 10^{-9}$ mbar. The ion source was $Bi_3^{++}$ at energy of 25 KeV. The spectra was further normalized with respect to the highest intensity peak and presented with OriginPro 8 software (OriginLab, USA).

#### 2.5.1.3.2.3. Fourier Transform Infrared spectroscopy

A description of the FTIR technique can be found in Annex A of this thesis in electronic format.

Pre-activated titanium samples were analyzed using the Attenuated Total Reflectance Fourier Transform Infrared Spectroscopy (ATR-FTIR) technique using a Nicolet 6700 FTIR spectrometer equipped with the ATR Smart Saga accessory furnished with a diamond crystal (Thermo Fisher Scientific, USA). The sampling area was a circle of 1 mm of diameter, IR Beam Gain was set to 1, the scan resolution was set to a pass of 0.964 $cm^{-1}$ and each analysis was the average of 32 scans. To analyze the results the OMNIC 8 software (Thermo Scientific, USA) was used.

### *2.5.1.3.3. Effectiveness of silanized surfaces on tethering biomolecules*

After silanization, the experimental samples were exposed to a solution of a fluorescent probe at a concentration of 100 μmol/l of the fluorophore, overnight. In the case of silanized CPTES surfaces the fluorescent molecule was FITC cadaverine which contains an amino group that can react with the organofunctional CPTES group. The solvent was $Na_2CO_3$ at pH 11. In the case of silanized APTES surfaces the fluorophore was FAM, SE dissolved in DMF. FAM, SE contains a succidinimyl ester which acts as a very good leaving group when a nucleophilic group, i.e. APTES organofunctional amino group, is present, leading to the reaction of an amide bond.

The fluorescent microscopy analysis was performed as described in section 2.4.1.4.4.

#### *2.5.1.3.4. Biological viability*

##### 2.5.1.3.4.1. Cytotoxicity

Quantifying cell viability/cytoxicity via different assays is crucial for understanding the feasibility of a biomaterial when implanted in the body since the assessment of the proliferative or cytotoxic effect produced by a biomaterial or a medical product will determine the possibility of obtaining the required ISO standard.

Measurement of the degree of cytotoxicity was performed following the ISO 10993 standard corresponding to this evaluation [120]. The cell viability measurements were performed using the water-soluble tetrazolium salts (WST) method.

This assay is based on reducing a substrate, tetrazolium salt, through the action of mitochondrial dehydrogenases, forming a soluble colored product whose concentration is determined by measuring the optical density at 450 nm wavelength. High values are indicative of good cellular metabolic activity, while low values are indicative of cytotoxic effects in the system.

To avoid bacterial contamination, the titanium samples were sterilized immersing them in ethanol 70% for 30 minutes. After sterilization, the samples were rinsed twice with sterile PBS. The samples were then placed in sterile containers of 50 ml and incubated (37 ° C in 5% $CO_2$) for 72 hours in DMEM + 10% fetal bovine serum (FBS) supplemented with 1% L-Glutamine and 1% penicillin/streptomycin (Gibco life technologies, UK). The amount of medium was determined in relation to the total exposed area of the sample (Table 2-6), taking into account that the samples were metallic and had a diameter greater than 0.5 mm.

***Table 2-6:*** *Description of the amounts of extraction/area for biomaterials, in accordance with ISO 10993-12 p 10 [120].*

| **Thickness (mm)** | **Extract ratio (±10%)** | **Material example** |
|---|---|---|
| ≤ 0.5 | 6 $cm^2$/ml | Metal; synthetic polymer, ceramic, film, sheet and composite |
| > 0.5 | 3 $cm^2$/ml | Metal; synthetic polymer, ceramic, film, sheet and composite, molded parts |
| ≤ 1.0 | 3 $cm^2$/ml | Natural elastomer |
| > 1.0 | 1.25 $cm^2$/ml | Natural elastomer |
| Irregular | 0.1 g/ml to 0.2 g/ml; 6 $cm^2$/ml | Powder and sponges |

MG63 osteoblast-like cells were exposed to the extract for 24 hours at different concentrations. Upon completion of this period of exposure, the WST reagent was added directly to the culture medium (in the presence of the extract), reading the optical density with a spectrophotometer at 450 nm wavelength.

A range of 5 concentrations was established to determine the extract's cytotoxicity in the following intervals of dilution: full extract, 1:1, 1:10, 1:100, and the 1:1000 dilution of the extract provided in the culture medium. All measurements were performed in triplicate to obtain reliable statistics.

There were also measurements of positive and negative controls of cytotoxicity. The negative control consisted of submerging the cells in fresh medium, without any extract, whereas the positive control consisted of treating the cells with 1% Sodium dodecyl sulfate (SDS).

#### 2.5.1.3.4.2. Cell adhesion

To evaluate the biological viability of the silanization when immobilizing oligo-peptides on titanium surfaces NaOH pretreated samples were silanized and coated with RGD peptides as described in section 2.5.1.3.1. Afterwards, a cell adhesion assay was performed by exposing the samples to an osteoblastic cell line MG-63, for a period of 3 hours. Previous to cell exposure,

samples were sterilized immersing them in ethanol for 10 minutes and rinsing them twice with PBS. The non-specific adhesion points were blocked incubating the samples in 6% Bovine Serum Albumin (BSA) in PBS for 1 hour at 37 $^{o}$C.

Cells were exposed to the samples with DMEM/F12 medium, supplemented with 1% penicillin / streptomycin and 2% sodium pyruvate (Gibco life technologies, UK), without serum to avoid further unspecific protein adsorption, and kept in an incubator at 37 $^{o}$C for 3 hours.

After exposure, the samples were washed with 1x PBS (Gibco, UK) and then proceeded the fluorescent staining of cells. Nuclei were stained in blue with Hoetsch (Pierce, Thermo Scientific, USA). Actin cytoskeleton was stained in red with Texas Red-X phalloidin (Invitrogen, USA) and focal adhesion points were immuno-stained in green using mouse monoclonal anti-vinculin antibody (Sigma, USA) as primary antibody and Alexa Fluor 488 Goat anti-mouse $IgG_1$ as secondary antibody (Invitrogen, USA). Details of the staining protocol can be found in Santacruz Biotechnology [121]. Finally the samples were observed in a fluorescent lamp stereomicroscope SZX7 OLYMPUS (Japan) and micrographs were recorded using a personal computer. Cell number measurements were performed counting cell number using Image J ver. 1.45s from the images taken at the microscope. Cell extension (Cell ext) measurements were performed dividing the cell-covered are (Area covered by cells) by the total area scanned (Total Area). This ratio was then divided by the number of cells on each image analyzed (Cell number) as is shown in equation 2-8. At least four images of each condition were analyzed.

$$\text{Cell ext} = \frac{(\text{Total area} - \text{area covered by cells})}{\text{Cell number}} \qquad \textbf{Equation 2-8}$$

#### 2.5.1.1. Statistical analysis

The statistical analysis was conducted as previously described in section 2.4.1.5.

## 2.5.2. Results

The results regarding the silanization process are presented below. In this section, two silanes, APTES and CPTES, are compared in order to select the best one for our functionalization purposes.

### 2.5.2.1. Nomenclature

Like in the results regarding to the activation treatment, a nomenclature has been created in order to abbreviate the description of the different samples. Below, the abbreviation codes for every treatment are named and briefly described.

**Ti:** *Titanium.* Polished and clean titanium as described in section 2.4.1.2.
**Plasma or Pla:** Polished titanium treated with plasma cleaning as described in section 2.4.1.3.1.
**NaOH:** Polished titanium treated with sodium hydroxide as described in section 2.4.1.3.3.
**APTES:** Polished titanium treated with the indicated activation treatment and silanized with APTES as described in section 2.4.1.4.4.
**CPTES:** Polished titanium treated with the indicated activation treatment and silanized with CPTES as described in section 2.5.1.2.2.
**RGD:** Polished titanium previously treated with the indicated treatments with the RGD oligopeptide adhered to the surface as described in section 2.5.1.3.3.
**FITC:** Polished titanium previously treated with the indicated treatments with the FITC cadaverine fluorophore adhered to the surface as described in section 2.5.1.3.3.
**FAM:** Polished titanium previously treated with the indicated treatments with the FAM-X,SE fluorophore adhered to the surface as described in section 2.5.1.3.3.

### 2.5.2.2. Wettability

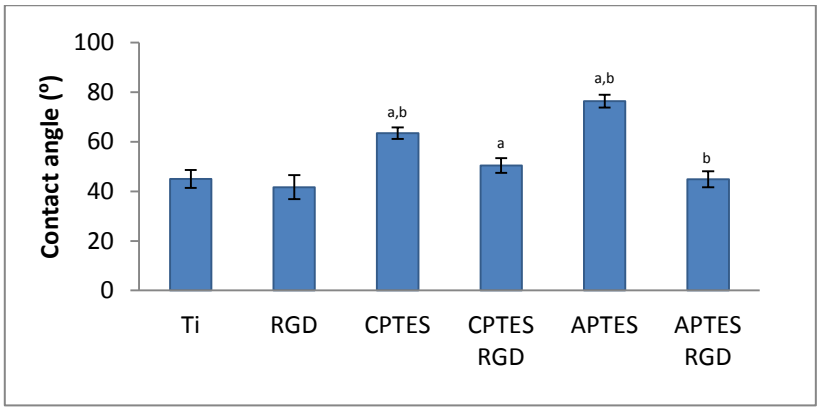


***Figure 2-23:*** *Contact angle values for plasma pre-activated surfaces silanized with CPTES or APTES with and without functionalization with RGD peptides.* [a,b]*: statistical differences between the groups using the Mann-Whitney test.*

On the one hand, silanes provided hydrophobicity to the surfaces due to their alkyl chain. On the other hand, the RGD peptides contain hydrophilic residues such as arginine and aspartic acid. As shown in figure 2-23, plain titanium surface with physisorbed RGD peptides were slightly more hydrophilic (lower contact angles) than without peptides. Silanized surfaces increased the water contact angle, especially when APTES was used to silanized the Ti surfaces. After anchoring RGD peptides on silanized surfaces, the water contact angle was reduced, mainly on APTES silanized surfaces. These results suggest that the APTES silanized surfaces were able to retain more peptide than CPTES silanized surfaces.

### 2.5.2.3. Chemical composition

#### *2.5.2.3.1. X-Ray photoelectron spectroscopy*

##### 2.5.2.3.1.1. Survey analysis

***Table 2-7*** *Chemical composition (%mol) of the titanium surfaces treated with the different activation methods. Data extracted from XPS survey spectra.*

| | C1s | Cl2p | N1s | Na1s | O1s | S2p | Si2p | Ti2p | Total |
|---|---|---|---|---|---|---|---|---|---|
| **APTES** | 21.1 | 0.0 | 4.0 | 0.4 | 54.5 | 0.2 | 4.5 | 15.4 | 100.0 |
| **CPTES** | 16.3 | 81.7 | 1.4 | 1.5 | 59.0 | 0.0 | 3.1 | 17.0 | 100.0 |

From the chemical composition shown on table 2-7, it can be seen that the two surfaces were properly silanized due to the fact that the titanium, sodium and oxygen signals decreased in comparison with NaOH activated surfaces, most notable on the APTES silanized surfaces. Also, the nitrogen is greatly increased on APTES surfaces due to the presence of the amino group of APTES silanes, while chlorine was increased on CPTES surfaces due to its respective terminal group. Additionally, the presence of silicon on both types of surfaces revealed the presence of the silane molecules. The theoretical ratio Si/N for APTES silanized surfaces is 1.0. The N percentage is slightly lower than the one for Si. The lower N1s percentage can be a consequence of the 0,6% residual silicon that was detected on the NaOH pre-activated surfaces. Si/Cl on CPTES surfaces was 1.8, but the theoretical ratio is 1.0. This might be due to partial displacement of leaving chlorine atoms by reaction of the silane molecules with water via Sn2 reaction.

2.5.2.3.1.1. Deconvolution of the peaks

*Carbon C1s*

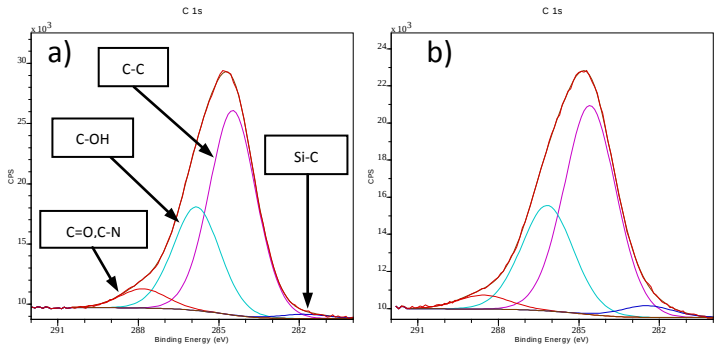


***Figure 2-24:*** *XPS Deconvolutions of the C1s peak of the titanium surfaces treated with the different silanization methods. a) APTES, b) CPTES*

***Table 2-8*** *Deconvolution data of the carbon C1s for the different titanium surfaces*

| **Carbon C1s** | | | | |
|---|---|---|---|---|
| *APTES* | | | | |
| **Chemical State** | **Position (eV)** | **Area (pixel)** | **Area (%)** | **References** |
| C-C | 284.5 | 16520.8 | 65.68 | [101-103] |
| C-OH. (CH2-CH2)n | 285.7 | 7058.28 | 28.06 | [101,102,104,122] |
| C=O. O=CN | 287.6 | 1348.75 | 5.36 | [99,102,104] |
| Si-C | 282.3 | 227.22 | 0.9 | [123] |
| | | | | |
| *CPTES* | | | | |
| **Chemical State** | **Position (eV)** | **Area (pixel)** | **Area (%)** | **References** |
| C-C | 284.5 | 7664.54 | 61.43 | [101-103] |
| C-OH. (CH2-CH2)n | 286.1 | 3871.4 | 31.03 | [101,102,104,122] |
| C=O. O=CN | 288.5 | 512.677 | 4.11 | [99,102,104] |
| Si-C | 282.4 | 427.307 | 3.43 | [123] |

In comparison with non silanized NaOH activated surfaces, both APTES and CPTES surfaces presented an additional peak approximately at 282,3 eV corresponding to the Si-C bond of the silanes [123,124]. The C-C peak, at 284,5 eV, increased its magnitude with respect to the non silanized surfaces (Table 2-4) due to the presence of the silane carbon chain. Finally, the C-OH peak, at around 286 eV slightly decreased in comparison with the activated surfaces. The decrease on this peak is explained by the reaction of the silanes with the OH groups on the surface. On the other hand, this peak could increase due to the presence of the carbon chain of the silanes, $(CH_2\text{-}CH_2)n$, which has a similar energy to that of C-OH bonds.

*Oxygen O1s*

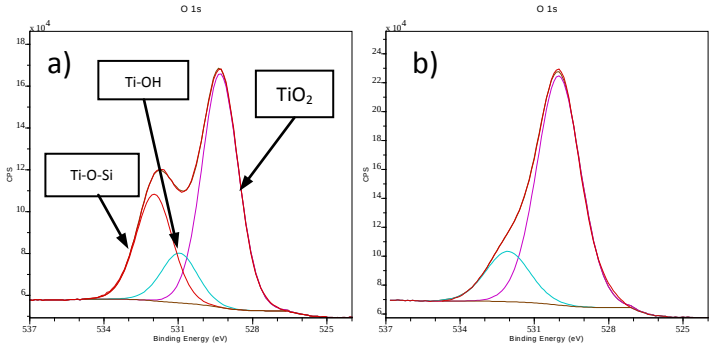


***Figure 2-25:*** *XPS Deconvolutions of the O1s peak of the titanium surfaces treated with the different silanization methods. a) APTES, b) CPTES*

***Table 2-9*** *Deconvolution data of the oxygen O1s for the different titanium surfaces*

| **Oxygen O1s** | | | | |
|---|---|---|---|---|
| *APTES* | | | | |
| **Chemical State** | **Position (eV)** | **Area (pixel)** | **Area (%)** | **References** |
| $TiO_2$ | 529.31 | 60765.5 | 59.91 | [99,104,106] |
| Ti-OH | 530.96 | 12919.9 | 12.74 | [99,107,108] |
| Ti-O-Si | 531.97 | 27744.9 | 27.35 | [99,108] |
| | | | | |
| *CPTES* | | | | |
| **Chemical State** | **Position (eV)** | **Area (pixel)** | **Area (%)** | **References** |
| $TiO_2$ | 530.02 | 103927 | 81.96 | [99,104,106] |
| Ti-O-Si | 532.07 | 22870.9 | 18.04 | [99,108] |

From the oxygen O1s peak deconvolution, it is possible to deduce that APTES silanes better covered Ti surfaces than CPTES silanes. The $TiO_2$ signal on APTES surfaces is lower than on CPTES surfaces indicating that the original signal of groups from the sodium titanate formed on the activated Ti surface got masked by a thicker top layer of APTES silanes. Also, the Ti-O-Si signal was higher on the APTES silanized surfaces indicating that the silane was properly bonded to the surface.

*Titanium Ti2p*

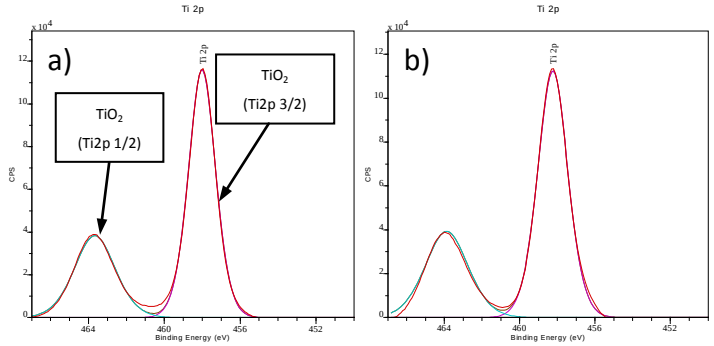


***Figure 2-26:*** *XPS Deconvolutions of the Ti2p peak of the titanium surfaces treated with the different silanization methods. a) APTES, b) CPTES*

Despite the fact that the percentage of titanium varied, the deconvolution of the titanium peak after silanization is the same as in the NaOH activated surfaces (Table 2-5). This was an expected result since the silanization process does not modify the titanium substrate.

*Nitrogen N1s and Chlorine Cl2p*

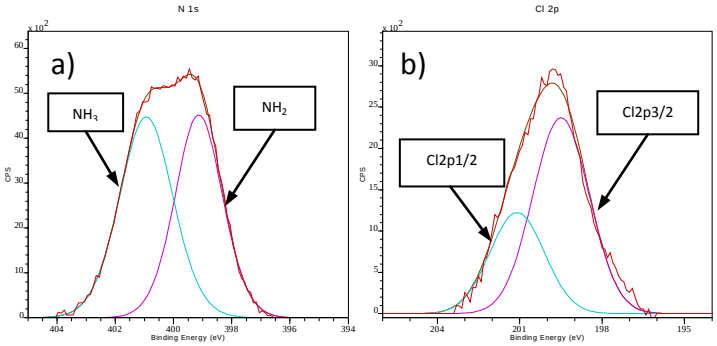


***Figure 2-27:*** *XPS Deconvolutions of the titanium surfaces treated with the different silanization methods. a)N1s on APTES surface, b)Cl2p on CPTES surface.*

The presence of nitrogen and chlorine on the silanized surfaces was evidence for the presence of both APTES and CPTES. Those are their signature groups as they are the corresponding terminal group of the two silanes. As can be seen, the amino group of the APTES is present in two states: the neutral $NH_2$, and the protonated $NH_3^+$ form. On CPTES surfaces only one species was detected, corresponding to the $CH_2$-Cl bond.

***Table 2-10*** *Deconvolution data of the nitrogen N1s and chlorine Cl2p for the different silanized surfaces*

| **Nitrogen N1s** | | | | |
|---|---|---|---|---|
| *APTES* | | | | |
| **Chemical State** | **Position (eV)** | **Area (pixel)** | **Area (%)** | **References** |
| $NH_2$ | 399.13 | 2462.94 | 47.28 | [125-127] |
| $NH_3$ | 400.93 | 2746.26 | 52.72 | [125-127] |
| | | | | |
| **Chlorine Cl2p3/2** | | | | |
| *CPTES* | | | | |
| **Chemical State** | **Position (eV)** | **Area (pixel)** | **Area (%)** | **References** |
| $CH_2$-Cl | 199.49 | 1743.54 | 100 | [128] |

*2.5.2.3.2. Time of Flight Secondary Ion Mass spectroscopy (ToF SIMS)*

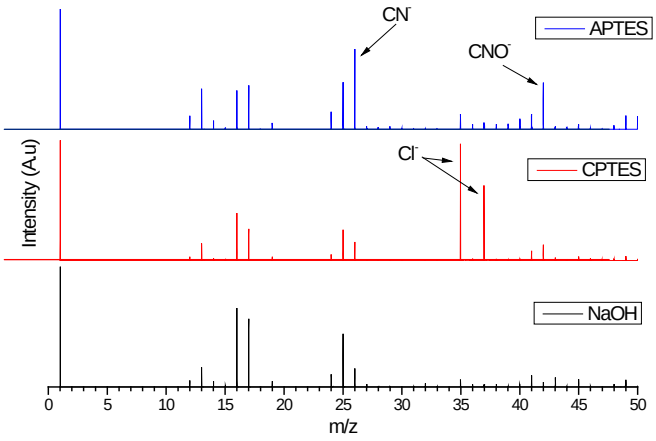


***Figure 2-28:*** *ToF SIMS spectra of the negative ions of Titanium samples treated with the different activation methods.*

ToF SIMS analysis revealed a significant presence of chlorine (m/z= 35 and 37) on CPTES surfaces, whereas APTES surfaces showed the presence of nitrogen containing species such as $CN^-$ and $CNO^-$ (m/z= 26 and 42, respectively). Positive spectra didn't show relevant differences. Also, it can be seen from figure 2-28 that OH groups (m/z= 17) have been reduced after both silanization processes.

The vertical resolution of ToF SIMS is higher than the obtained with XPS. This is due to the fact that the deepness of the volume of analysis is higher on XPS than that on ToF SIMS. Therefore, the most superficial atoms (chlorine on CPTES surfaces and nitrogen on APTES surfaces) are best detected with ToF SIMS.

#### *2.5.2.3.3. Fourier transform Infrared Spectroscopy (FTIR)*

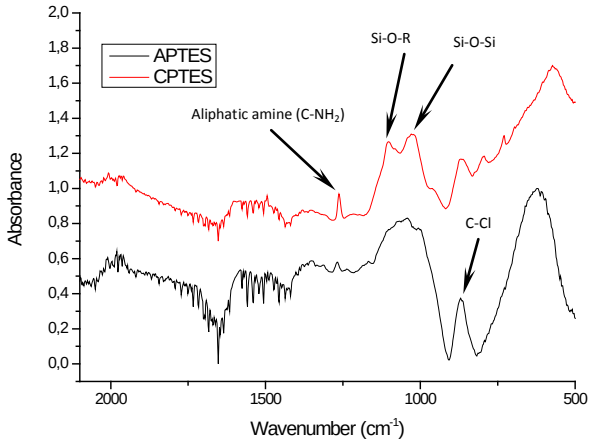


***Figure 2-29:*** *FTIR spectra of the silanized surfaces with CPTES and APTES. The spectrum of the NaOH treated surface was taken as the background.*

ATR-FTIR spectra correlated the results obtained by XPS and ToF SIMS. Si-O-Si and Si-O-R peaks (1025 and 1100 $cm^{-1}$ respectively) from the silane on the surface [65,76] were clearly detected in the FTIR spectra. The even clearer definition of these peaks on the APTES surface suggests a better coverage of the surface by APTES silane than by CPTES silane. Also, on the APTES silanized surface the terminal amino group of the silane was detected at the 1263 $cm^{-1}$ wavelength, while the terminal chlorine group from the CPTES silanes was detected at the 870 $cm^{-1}$ wavelength [129].

### 2.5.2.1. Effectiveness on tethering biomolecules

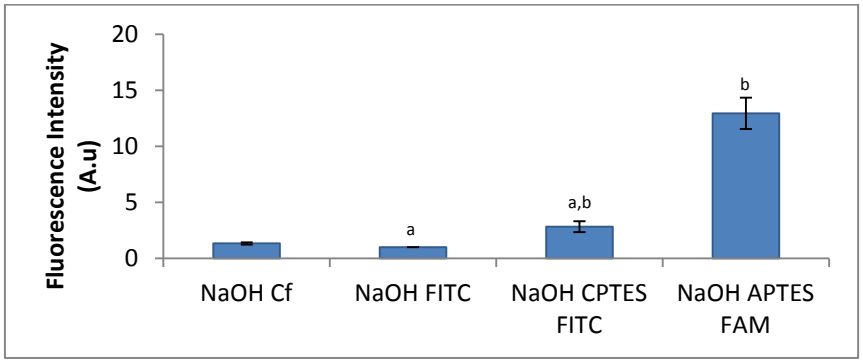


***Figure 2-30:*** *Fluorescence intensity of NaOH pre-activated Ti surfaces silanized with CPTES or APTES and loaded with FITC cadaverine and FAM-X, SE, respectively.* [a,b]*: statistical differences between the groups using the Mann-Whitney test.*

To compare the amount of peptides that can be effectively retained on the differently-silanized surfaces, those surfaces were exposed to FITC cadaverine and FAM-X, SE fluorescent probes as fluorescence surrogates for the oligopeptides. Both probes were selected because they can form covalent bonds with the terminal group of each of the silanes, in the same way that the surfaces would react and bond with oligopeptides. Figure 2-30 shows the fluorescence intensity of the images taken with the fluorescence microscope. APTES silanized surfaces showed a fluorescence intensity about four times higher than that of CPTES silanized surfaces.

### 2.5.2.2. Biological viability

To evaluate the biological viability of the titanium surfaces silanized with APTES and CPTES, a peptide containing the RGD sequence was immobilized on the different surfaces. Afterwards, cytotoxicity tests and cell adhesion tests were performed.

*2.5.2.2.1. Cytotoxicity*

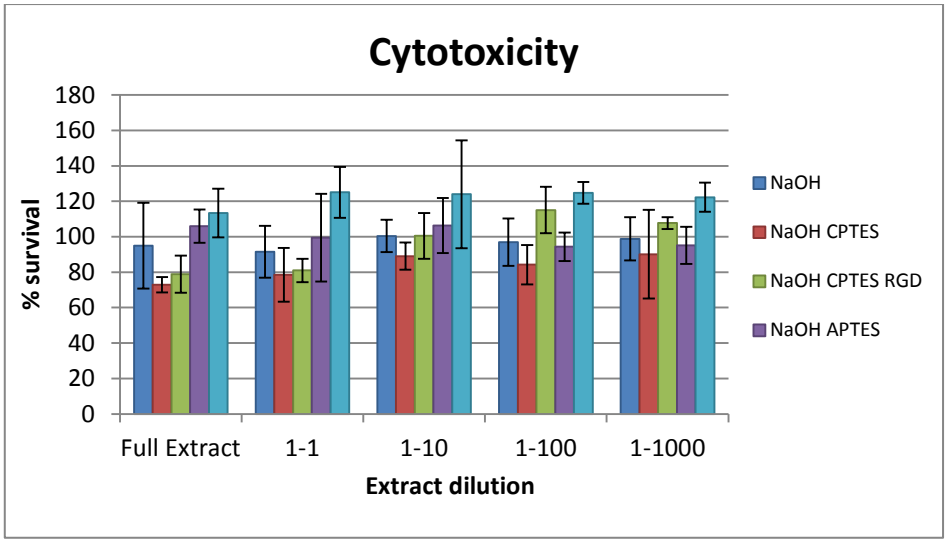


***Figure 2-31:*** *Indirect cytotoxicity results of the different silanized titanium surfaces with and without RGD peptide.*

Figure 2-31 shows the cytotoxicity results of MG63 cells exposed to the different extracts during 24 h. All of the groups tested surpassed the 64% mark of cell survival. APTES silanized surfaces remarkably showed null cytotoxicity. When RGD peptides are on the surfaces, the cell proliferation tended to increase with respect to NaOH treated surfaces. However, differences were not statistically significant.

### *2.5.2.2.2. Cell adhesion*

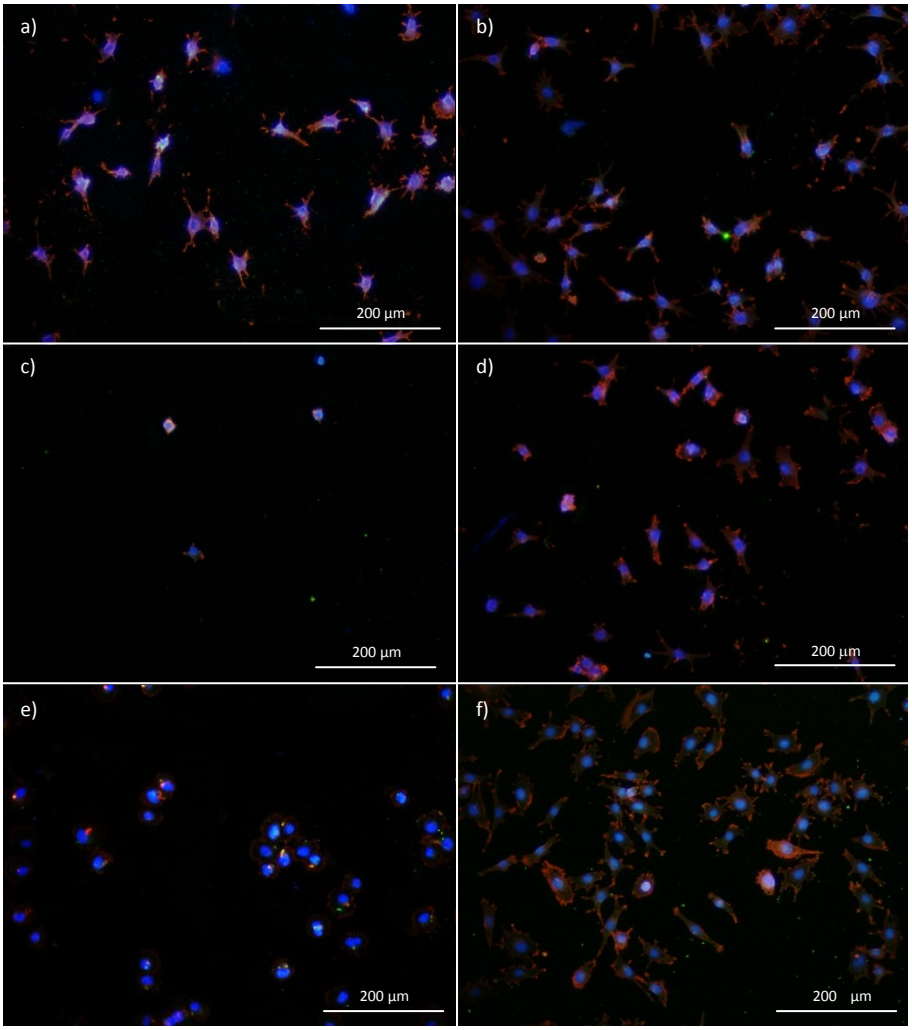


***Figure 2-32:*** *Immuno-fluorescence images of MG63 cells attached to the different titanium surfaces. a)Ti, b)Ti+RGD, c)CPTES, d)CPTES+RGD, e)APTES, f) APTES+RGD*

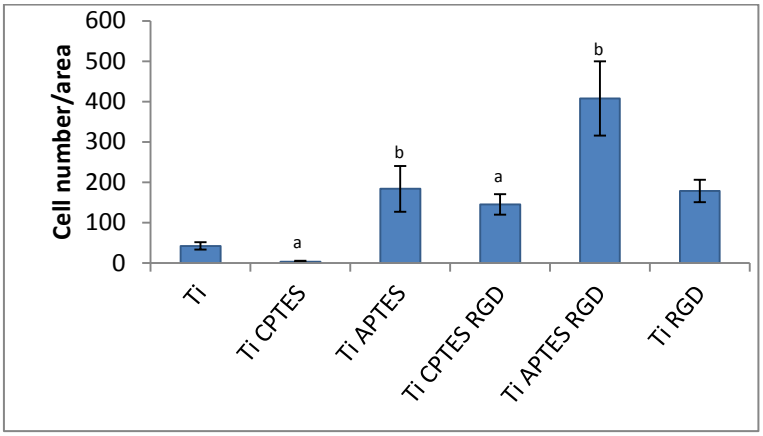


***Figure 2-33:*** *Cell number of MG63 cells attached to the different titanium surfaces. a and b indicate statistically significant differences (p=0.05) between groups with the same letter.*

Figure 2-32 and figure 2-33 show that APTES silanized surfaces promoted cell adhesion due to the presence of amino groups on the surface [117]. On the other hand, CPTES surfaces hindered cell adhesion. Surfaces coated with RGD peptides induced a substantial increase in cell adhesion. Also, the morphology of the cells attached to APTES+RGD surfaces was highly extended with long philopodia. This result demonstrates that the functionalization process was successful from biological point of view.

### 2.5.3. Discussion

Silanization is the most widely used method for the immobilization of biological molecules on model surfaces [130]. On titanium, a variety of methods have been applied in order to attach several types of biomolecules, such as peptides, proteins or polysaccharides, on the surface [3-5]. Anyway, silanization on titanium surfaces is still one of the preferred techniques when a covalent bond between Ti surface and biomolecule is desired [16,43,131-133]. Bibliography suggests that the silanization methods used on titanium surfaces have been directly derived from the methodologies used on model surfaces, which are highly known and less variable than titanium. Only one work about the optimization of the silanization of titanium surfaces has been found [78].

In this section pre-activated titanium surfaces were silanized using similar methodology but with two different silanes, APTES and CPTES. Apart from the samples used to characterize wettability, all the other samples were pre-activated with NaOH because this was the selected activation method taking into consideration the results of the detailed characterization shown in the previous section.

On the one hand, CPTES has the advantage of spontaneously linking primary amines and cysteine residues. This makes the complete silanization process simpler and faster than with APTES since there is no need of esterification of the carboxylates of the linking molecule or the use of a cross-linker. Another advantage of CPTES is that cell adhesion on CPTES surface is nearly null, and thus, facilitating the identification of the effects of the linked peptide on the functionalized surfaces.

On the other hand APTES showed a more homogeneous and dense surface coverage, a higher cell adhesion, and a much higher amount of immobilized peptide on the surface. The disadvantage of APTES is that conversion of the carboxylic acids of the peptide into esters is needed to react with the amine group of the APTES molecules. This methodology has two drawbacks: racemization of the peptides can occur during esterification; and more importantly, the peptides can polymerize due to the reaction between its carboxylic acids and primary amines, having no control over the length of the polymerized silane molecules.

APTES was selected for our protocol to biofunctionalize Ti surfaces with oligopeptides taking into consideration the quality of the chemically-obtained and biologically-effective silane layer. This selection was made despite the aforementioned methodological advantages associated to the use of CPTES. The use of APTES resulted in a more homogeneous silane covering of the metallic surface with higher amounts of immobilized peptides. Moreover, the model peptides used in this section, i.e., RGD peptides, retained their biological activity after being covalently-anchored to the APTES silanized surfaces.

## 2.6. Crosslinking with malonic, glutaric and diglycolic acids

As was discussed in section 2.5.3, when APTES is used for silanizing Ti surfaces prior to the functionalization with peptides a coupling reagent, such as a carbodiimide, should be used to activate the peptide to be covalently immobilized on the surface. The addition of a coupling reagent on the peptide solution would generate an uncontrolled polymerization and/or racemization of the peptide [90,92].

In an attempt to overcome those detrimental reactions during the functionalization process an innovative approach was investigated in this work. This new approach consisted of using a cross-linker molecule between the silane on the surfaces and the functional oligopeptide. The

cross-linker should then react first with the amines of the APTES molecules and further with the peptides to finalize the functionalization of the metallic surfaces.

To that purpose, three different candidate cross-linkers were evaluated here.

The molecular structure of the three selected cross-linkers; malonic acid, glutaric acid, and diglycolic acid, are shown in figure 2-34.

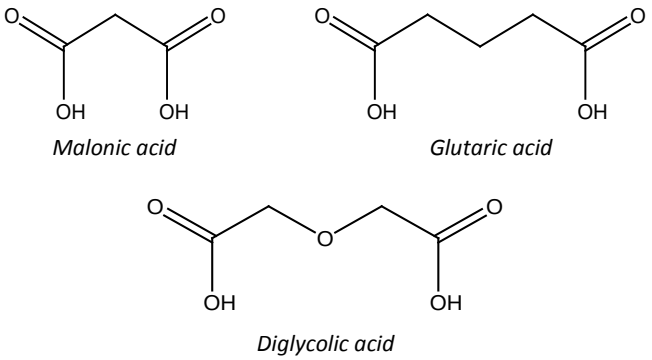


***Figure 2-34:*** *Chemical structures of the three cross-linkers evaluated in the study.*

All of the candidate crosslinkers have one carboxylic acid at each end. According to the proposed hypothesis, after esterification, one carboxylic acid interacts with the primary amines of the APTES molecules, and the other one interacts, in a posterior functionalization step, with the primary amines of the peptide, hence avoiding racemization and polymerization.

The cross-linkers are varied with respect to the length of the middle chain as after esterification of the two carboxylates, both of them might attach to an amine of APTES molecules in close proximity at the surface. If so, the amines of the APTES at the silanized surface would be significantly blocked and thus, subsequent linkage with the peptides might be seriously hindered. For this reason, cross-linkers of different lengths were selected in order to evaluate which length minimizes this detrimental effect. The structural similarity between diglycolic acid and polyethylene glycol [60,134] molecules was the key additional feature for its selection. Polyethylene glycol coatings are effective in preventing unspecific protein adsorption and thus, this additional property could also benefit the biological activity of the functionalized surfaces studied in this work.

## 2.6.1. Materials and Methods

### 2.6.1.1. Materials

In addition to the materials previously described in sections 2.4.1.1 and 2.5.1.1. we used the following cross-linkers: 99% malonic acid, 99% glutaric acid and 98% diglycolic acid (Aldrich, USA).

### 2.6.1.2. Crosslinking methods

Cross-linking was performed after surface activation and silanization with APTES. The three cross-linkers (malonic acid, glutaric acid and diglycolic acid) were bound to the surface using the same procedure, which started off by immersing the APTES silanized samples in a solution of DMF with 15 mmol/l of the cross-linker, 45 mmol/l of HBTU and 60 mmol/l of DIEA. This was carried out at room temperature for 2 hours with orbital agitation. After cross-linking, the samples were washed in DMF twice, rinsed in water, acetone and dried with nitrogen. The samples were then used or stored in vacuum for further experiments.

In some characterization techniques it was necessary to generate non silanized samples as controls. Those samples were exposed to the cross-linker in the same way as the silanized ones.

### 2.6.1.3. Characterization methods

#### *2.6.1.3.1. Wettability*

As with activation and silanization, to be able to measure the contact angles of the cross-linked samples it was necessary to pre-activate the titanium surfaces using plasma cleaning instead of

the NaOH treatment. The samples were measured and analyzed as described in section 2.4.1.4.2.

#### *2.6.1.3.2. Chemical composition*

##### 2.6.1.3.2.1. Fourier Transform Infrared Spectroscopy (FTIR)

Samples pre-activated with the NaOH treatment, silanized with APTES and treated with the three different crosslinkers were analyzed as described in section 2.5.1.3.2.3.

##### 2.6.1.3.2.2. X-Ray Photoelectron Spectroscopy (XPS)

Samples pre-activated with the NaOH treatment, silanized with APTES and treated with the three different crosslinkers were analyzed as described in section 2.4.1.4.3.1.

#### *2.6.1.3.3. Effectiveness of tethering biomolecules*

In order to evaluate which cross-linker shows best performance immobilizing primary amines on the surface, a fluorescent probe was used instead of an oligopeptide.

After cross-linking, the samples (except for the controls) were exposed overnight to a fluorescent probe solution at a concentration of 100 μmol/l of the fluorophore. The fluorescent molecule was FITC cadaverine which contains an amino group that can react with the esterified free carboxylic group of the cross-linker. The solvent was DMF.

The fluorescent microscopy analysis was performed as described in section 2.4.1.4.4.

#### *2.6.1.3.4. Biological viability*

##### 2.6.1.3.4.1. Cell adhesion

After pre-activation and silanization, the samples were cross-linked with the three different acids. The RGD peptide was then exposed on the surface and a cell adhesion test was performed using MG63 cells to assess the overall performance of the cross-linkers. The procedure of *in vitro* testing and analysis was the same as that described in section 2.5.1.3.4.2.

##### 2.6.1.3.4.2. Cytotoxicity of malonic acid

As it will be shown in the results section, malonic acid had the best performance of the three crosslinkers studied. For this reason, we evaluated the possibility of malonic acid being cytotoxic, a direct cytotoxicity test was performed. MG63 cells were cultured on a 48 polystyrene well plate for 24 hours. After this time, cells were washed twice with PBS, and different concentrations of malonic acid, ranging from 0.0015 to 15 mg/ml, were added to the culture medium. The cells were incubated with this medium for another 24 hours and then counted using the WST assay as described in section 2.5.1.3.4.1

### 2.6.1.4. Statistical analysis

The statistical analysis was conducted as previously described in section 2.4.1.5.

## 2.6.2. Results

### 2.6.2.1. Nomenclature

Like in the previous results, a nomenclature has been created in order to abbreviate the description of the different samples. Below, in addition to the abbreviations described in section 2.5.2.1, the abbreviation codes for the treatments used in the study of the crosslinkers are named and briefly described.

**Malonic a. or Mal:** Polished titanium previously treated with the indicated treatments and crosslinked with malonic acid as described in section 2.6.1.2.
**Glutaric a. or Glu:** Polished titanium previously treated with the indicated treatments and crosslinked with Glutaric acid as described in section 2.6.1.2.
**Diglycolic a. or Gly:** Polished titanium previously treated with the indicated treatments and crosslinked with Diglycolic acid as described in section 2.6.1.2.

### 2.6.2.2. Wettability

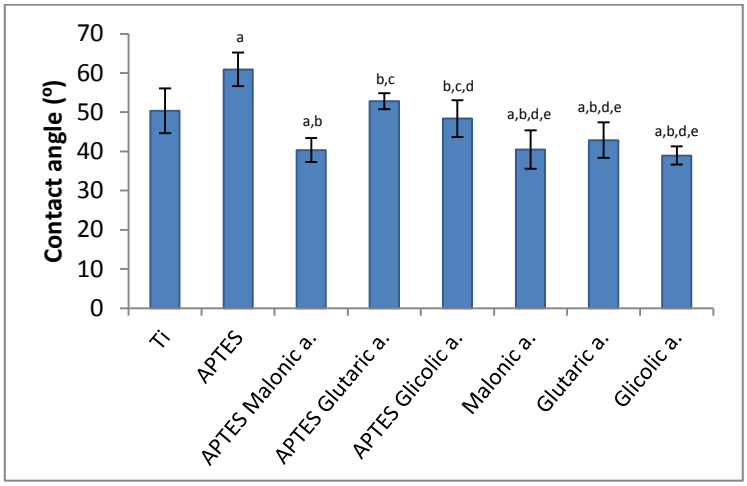


***Figure 2-35:*** *Contact angle values of the titanium surfaces activated by plasma cleaning, silanized with APTES and cross-linked with malonic, glutaric or diglycolic acid. [x]: Statistically different from a: Ti, b: Ti APTES c: Ti APTES Mal, d: Ti APTES Glu and e: Ti APTES Gli.*

Water contact angle, measured on titanium surfaces, previously attacked with NaOH, silanized with APTES and treated with the three different cross-linkers is presented in figure 2-35. As can be seen, the use of any cross-linker reduced the water contact angle. So the presence of the cross-linkers was revealed by the higher hydrophilicity of the surfaces than the surfaces before attaching the cross-linkers. The most hydrophilic of the surfaces were the ones treated with malonic acid.

### 2.6.2.3. Chemical composition

#### *2.6.2.3.1. Fourier Transform Infrared Spectroscopy (FTIR)*

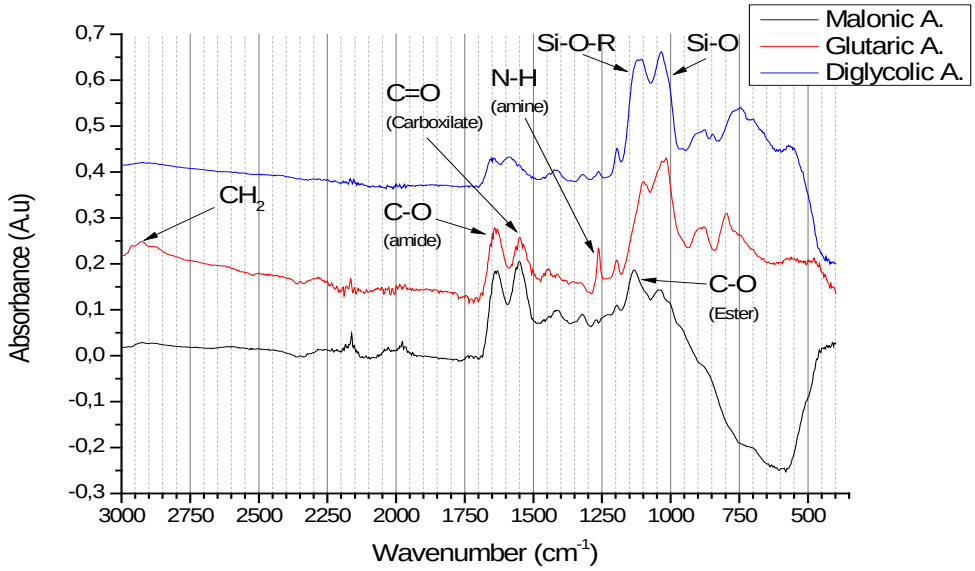


***Figure 2-36:*** *FTIR spectra of the different titanium samples cross-linked with malonic, glutaric and diglycolic acids.*

The results obtained by infrared spectroscopy show the presence of the crosslinkers on the three surfaces studied due to the detection of amide (1640 $cm^{-1}$) and carboxylate groups (1263 $cm^{-1}$) on the three spectra [135]. The ATR-FTIR spectra (Figure 2-36) showed that the sample treated with malonic acid provoked the lowest absorbance for the Si-O and Si-O-R peaks. This might reflect that the APTES layer was more homogenously covered by malonic acid molecules than by the other two cross-linkers. A high absorbance in amine peaks (1550 $cm^{-1}$)[135] could

mean that glutaric acid is present on the surface but has not reacted properly with APTES. The absorbance peak at 1640 $cm^{-1}$ is related to the presence of amides [135]. A high peak detected at this wavelength might be related to the fact that the cross-linker has properly reacted with APTES. The presence of this peak and the absence of the N-H peak would be an indicator that the totality of APTES molecules previously anchored on the metallic surface reacted with malonic acid. Finally, the absorbance peak at 1140 $cm^{-1}$ can be attributed to the C-O bond [135] of an ester which is further validation of the effective coupling between the malonic acid and the HOBt molecules. This would favor the surface treated with malonic acid to be well prepared for the further reaction with the peptide molecules.

#### *2.6.2.3.2. X-Ray photoelectron spectroscopy*

##### 2.6.2.3.2.1. Survey analysis

***Table 2-11*** *Chemical composition (%mol) of the titanium surfaces treated with the different crosslinking methods. Data extracted from XPS survey spectra.*

| | C1s | Cl2p | N1s | Na1s | O1s | S2p | Si2p | Ti2p | Total |
|---|---|---|---|---|---|---|---|---|---|
| **APTES** | 21.1 | 0.0 | 4.0 | 0.4 | 54.5 | 0.2 | 4.5 | 15.4 | 100.0 |
| **APTES Malonic a.** | 30.9 | 0.1 | 6.5 | 0.0 | 46.8 | 0.1 | 5.2 | 10.5 | 100.0 |
| **APTES Glutaric a.** | 34.6 | 0.0 | 6.3 | 0.7 | 43.2 | 0.4 | 5.9 | 8.9 | 100.0 |
| **APTES Diglycolic a.** | 30.5 | 0.1 | 5.8 | 0.0 | 49.3 | 0.0 | 4.8 | 9.7 | 100.0 |

Table 2-11 shows the chemical composition of the titanium surfaces treated with NaOH, silanized with APTES and treated with three different cross-linkers: malonic, glutaric and diglycolic acids. As can be observed, all cross-linkers increased the amount of nitrogen on the surface compared to an APTES silanized surface without cross-linkers. This increase in nitrogen is due to the HOBt molecule that is attached to one of the two carboxylic acids of the cross-linker, allowing it to react with the primary amines of the peptide in the following step of the functionalization process. It is important that the HOBt molecule be present, otherwise the carboxylic acids of the cross-linkers wouldn't react with the peptide and the covalent bond would not occur. There are no notable differences in chemical composition between the three surfaces.

2.6.2.3.2.2. Peak deconvolution

*Carbon C1s*

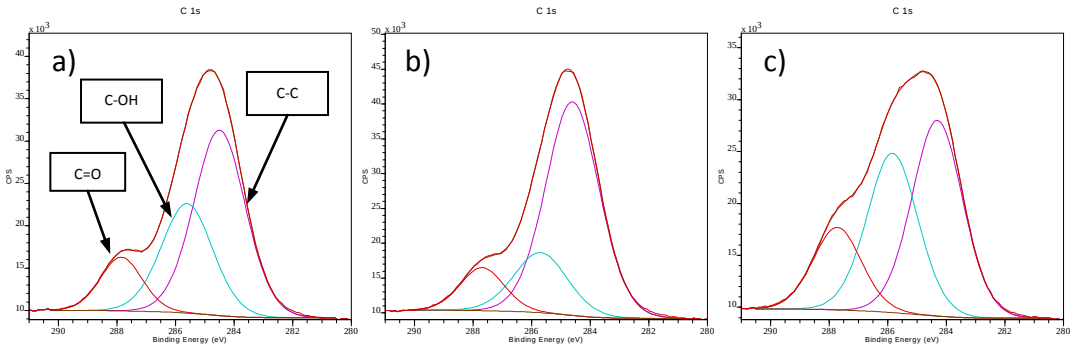


***Figure 2-37:*** *XPS Deconvolutions of the C1s peak of the titanium surfaces treated with the different crosslinking methods. a) malonic acid, b) glutaric acid and c) diglycolic acid.*

***Table 2-12*** *Deconvolution data of the carbon C1s for the titanium surfaces treated with the three cross-linkers*

| **Carbon C1s** | | | | |
|---|---|---|---|---|
| *Malonic a.* | | | | |
| **Chemical State** | **Position (eV)** | **Area (pixel)** | **Area (%)** | **References** |
| C-C | 284.49 | 13505.8 | 54.76 | [101-103] |
| C-OH, (CH2-CH2)n, C-N | 285.6 | 7966.33 | 32.3 | [102,104,122,123] |
| C=O, O=CN | 287.85 | 3192.84 | 12.94 | [99,102,104] |
| | | | | |
| *Glutaric a.* | | | | |
| **Chemical State** | **Position (eV)** | **Area (pixel)** | **Area (%)** | **References** |
| C-C | 284.6 | 19708.1 | 69.08 | [101-103] |
| C-OH, (CH2-CH2)n, C-N | 285.69 | 5555.32 | 19.47 | [102,104,122,123] |
| C=O, O=CN | 287.68 | 3267.68 | 11.45 | [99,102,104] |
| | | | | |
| *Diglycolic a.* | | | | |
| **Chemical State** | **Position (eV)** | **Area (pixel)** | **Area (%)** | **References** |
| C-C | 284.3 | 11496.2 | 45.14 | [101-103] |
| C-OH, (CH2-CH2)n, C-N | 285.83 | 9365.48 | 36.77 | [102,104,122,123] |
| C=O, O=CN | 287.72 | 4607.73 | 18.09 | [99,102,104] |

As can be seen from figure 2-37 the deconvolution of the carbon peak shows a sensibly different result than the one for the same peak on an APTES silanized surface (Figure 2-24). Also, there are important differences among the deconvoluted carbon peaks obtained for the titanium surfaces treated with each of the three cross-linkers. Nevertheless, the differences in area percentage among peaks are not significant, as shown on table 2-12. The analysis of these

results for the cross-linked surfaces is complex because of the mixture of species that contain rather similar C-groups. First, carbon contamination can be confused with the carbon chain of APTES silanes and with the aromatic ring of HOBt molecules. Second, the C-N group is present on APTES silanes and also on the amide bond generated when APTES and cross-linker molecules react. Also, the C-N group is present on the HOBt molecule that is coupled to the free carboxylate group of the cross-linker. Third, the C=O group is of the amide bond formed between APTES and the cross-linker, and/or of the free carboxylate groups of the cross-linkers.

Results shown on table 2-12 suggest that diglycolic acid had the highest attachment on the surface. Although possible mix-ups as to the origins of the species detected occur, higher percentage of the C=O, O=CN peak indicates higher amounts of cross-linker molecules on the surface. However, this is not the only requirement for a good functionalization process, since the cross-linker should be bonded to APTES on one side and attached to HOBt on the other side of the molecule.

*Oxygen O1s*

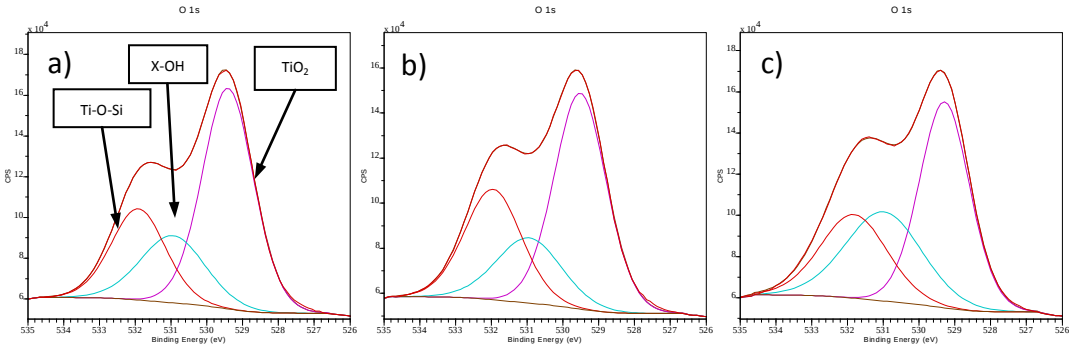


***Figure 2-38:*** *XPS Deconvolutions of the O1s peak of the titanium surfaces treated with the different cross-linkers. a) malonic acid, b) glutaric acid and c) diglycolic acid*

***Table 2-13*** *Deconvolution data of the oxygen O1s for the different titanium surfaces*

| **Oxygen O1s** | | | | |
|---|---|---|---|---|
| *Malonic a.* | | | | |
| **Chemical State** | **Position (eV)** | **Area (pixel)** | **Area (%)** | **References** |
| $TiO_2$ | 529.41 | 57686.1 | 54.92 | [99,104,106] |
| X-OH | 530.95 | 22116.6 | 21.06 | [99,107,108] |
| Ti-O-Si | 531.91 | 25226.5 | 24.02 | [99,108] |
| *Glutaric a.* | | | | |
| **Chemical State** | **Position (eV)** | **Area (pixel)** | **Area (%)** | **References** |
| $TiO_2$ | 529.51 | 52039.1 | 51.73 | [99,104,106] |
| X-OH | 530.95 | 19589.1 | 19.47 | [99,107,108] |
| Ti-O-Si | 531.95 | 28969.1 | 28.8 | [99,108] |
| *Diglycolic a.* | | | | |
| **Chemical State** | **Position (eV)** | **Area (pixel)** | **Area (%)** | **References** |
| $TiO_2$ | 529.29 | 52314.3 | 45.55 | [99,104,106] |
| X-OH | 530.98 | 34347.8 | 29.9 | [99,107,108] |
| Ti-O-Si | 531.82 | 28200.1 | 24.55 | [99,108] |

The $TiO_2$ and Ti-O-Si signals on the surfaces treated with cross-linkers were reduced compared to those on APTES surfaces (Table 2-9). Thus, the presence of the cross-linkers masked the original signal detected for this chemical group of the underneath silane layer. High percentage of the X-OH group indicates that most of the cross-linker either was not coupled with APTES molecules or did not attach to HOBt molecules, or both. Both possibilities are essential for the performance of a cross-linker and we can see that the highest X-OH values were reached on the diglycolic acid surfaces. Correlated with the results deduced from the carbon peak this could indicate that despite the amount of diglycolic acid present on the surface was higher than that of the other two crosslinkers, the crosslinker didn't reacted properly to reach a covalent bond with the silane and with the biomolecule on the subsequent step of the biofunctionalization process.

*Titanium Ti2p*

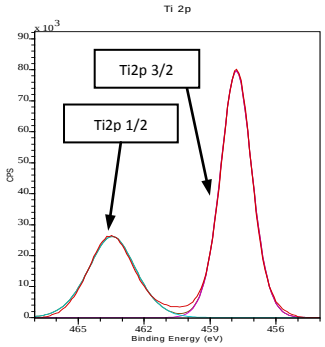


***Figure 2-39:*** *XPS Deconvolution of the Ti2p peak of a titanium surface treated with malonic acid. The peak deconvolutions from the other cross-linkers were similar.*

Once again, the percentage of titanium detected on the surfaces treated with cross-linkers varied with respect to the NaOH activated surface and APTES silanized surfaces, but the deconvolution of the titanium peak did not showed differences among those different surfaces.

*Nitrogen N1s*

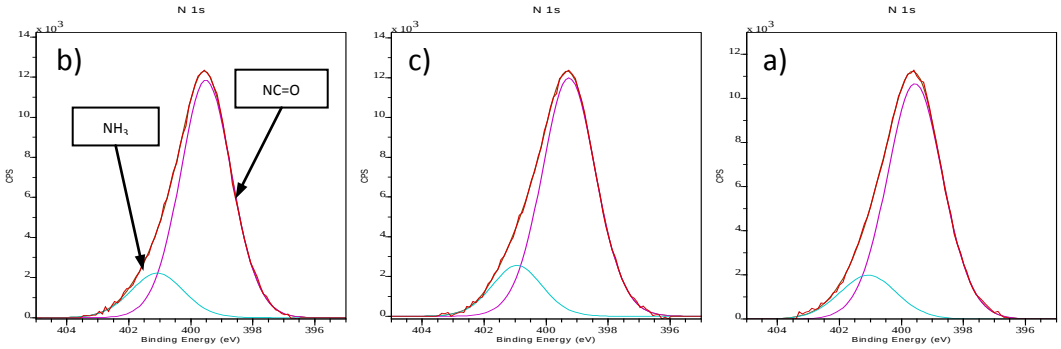


***Figure 2-40:*** *XPS Deconvolutions of N1s peak of the titanium surfaces treated with the different cross-linkers: a)malonic acid, b)glutaric acid, and c)diglycolic acid*

***Table 2-14*** *Deconvolution data of the nitrogen N1s and chlorine Cl2p for the different silanized surfaces*

| **Nitrogen N1s** | | | | |
|---|---|---|---|---|
| *Malonic a.* | | | | |
| **Chemical State** | **Position (eV)** | **Area (pixel)** | **Area (%)** | **References** |
| $NH_2$, N-C=O | 399.51 | 6.585 | 83.93 | [105,127] |
| $NH_3$ | 401.08 | 1.260 | 16.07 | [105,127] |
| | | | | |
| *Glutaric a.* | | | | |
| **Chemical State** | **Position (eV)** | **Area (pixel)** | **Area (%)** | **References** |
| $NH_2$, N-C=O | 399.26 | 6.948 | 83.47 | [105,127] |
| $NH_3$ | 400.94 | 1.376 | 16.53 | [105,127] |
| | | | | |
| *Diglycolic a.* | | | | |
| **Chemical State** | **Position (eV)** | **Area (pixel)** | **Area (%)** | **References** |
| $NH_2$, N-C=O | 399.56 | 6.429 | 84.07 | [105,127] |
| $NH_3$ | 401.07 | 1.218 | 15.93 | [105,127] |

The differences in the deconvoluted nitrogen peak after cross-linking with the three acids were not significant.

### 2.6.2.1. Effectiveness of tethering biomolecules

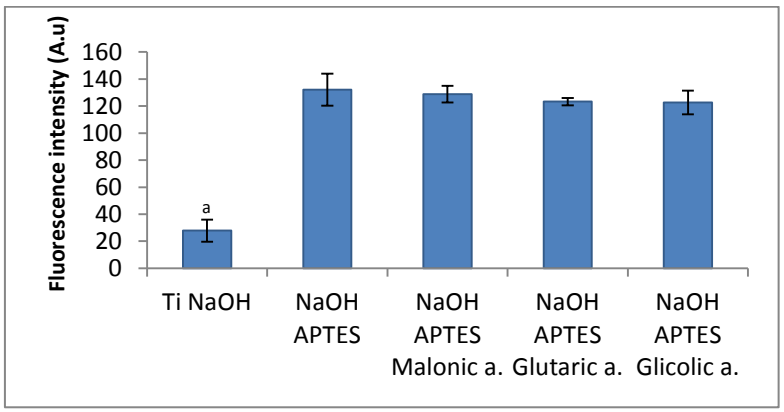


***Figure 2-41:*** *Fluorescence intensities of the titanium samples treated with different cross-linkers and labeled with FITC cadaverine.* [a] *means statistically significant differences with the rest of groups (p≤0.05).*

The difference on fluorescence intensities of the surfaces treated with the three different cross-linkers was not statistically significant. However, the surface with malonic acid was the one with highest fluorescent intensity, thus, it is potentially the most capable to immobilize peptides on the surface.

### 2.6.2.2. Biological viability

#### *2.6.2.2.1. Cell adhesion*

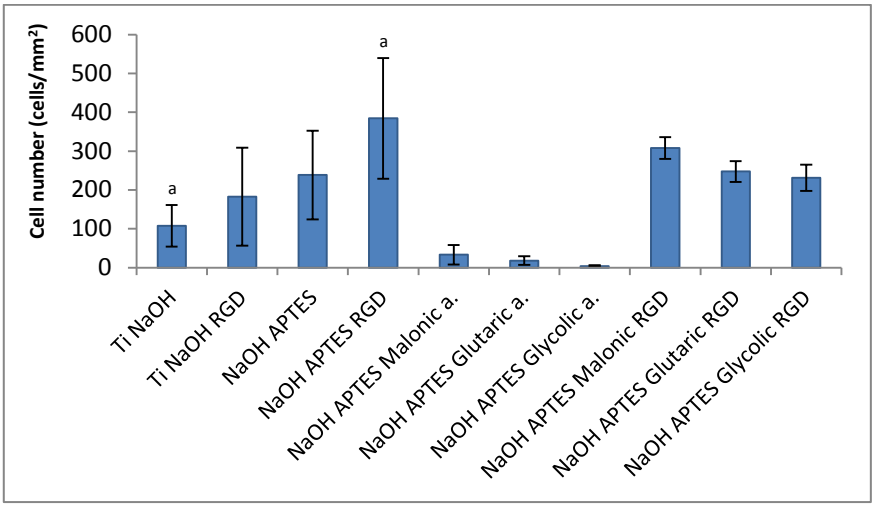


***Figure 2-42:*** *Cell number of MG63 cells on the titanium surfaces treated using the three different cross-linkers with or without RGD peptide.* [a] *means statistically significant differences between groups with the same letter.*

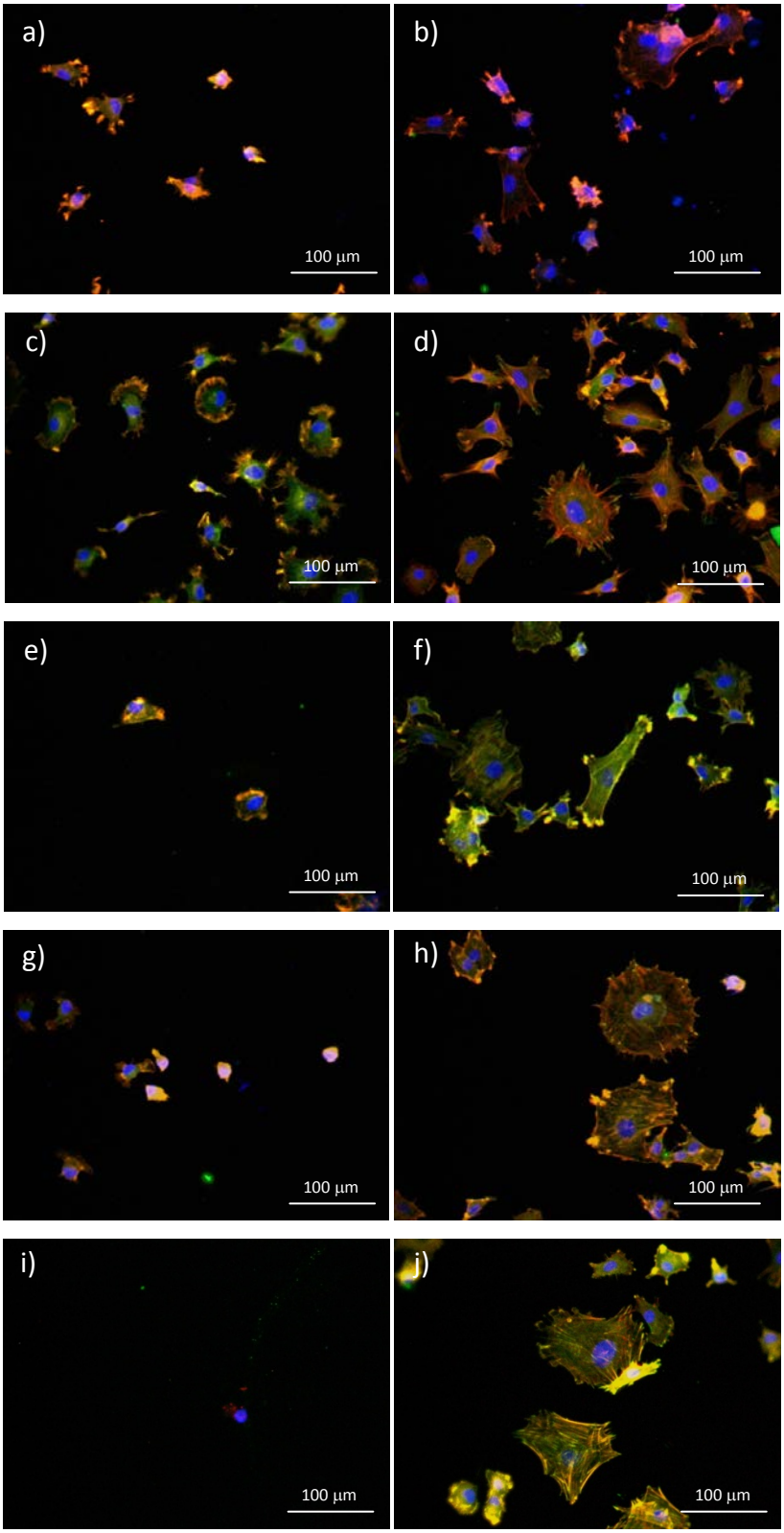


***Figure 2-43:*** *Immuno-fluorescence images of MG63 osteoblasts attached on the different Ti surfaces. a)Ti+NaOH, b)Ti+NaOH+RGD, c)Ti+NaOH+APTES d)Ti+NaOH+APTES+RGD e)Ti+NaOH+APTES+Malonic a. f)Ti+NaOH+APTES+Malonic a.+RGD, g)Ti+NaOH+APTES+Glutaric a., h)Ti+NaOH+APTES+Glutaric a.+RGD, i)Ti+NaOH+APTES+Diglycolic a. and j) Ti+NaOH+APTES+Diglycolic a.+RGD*

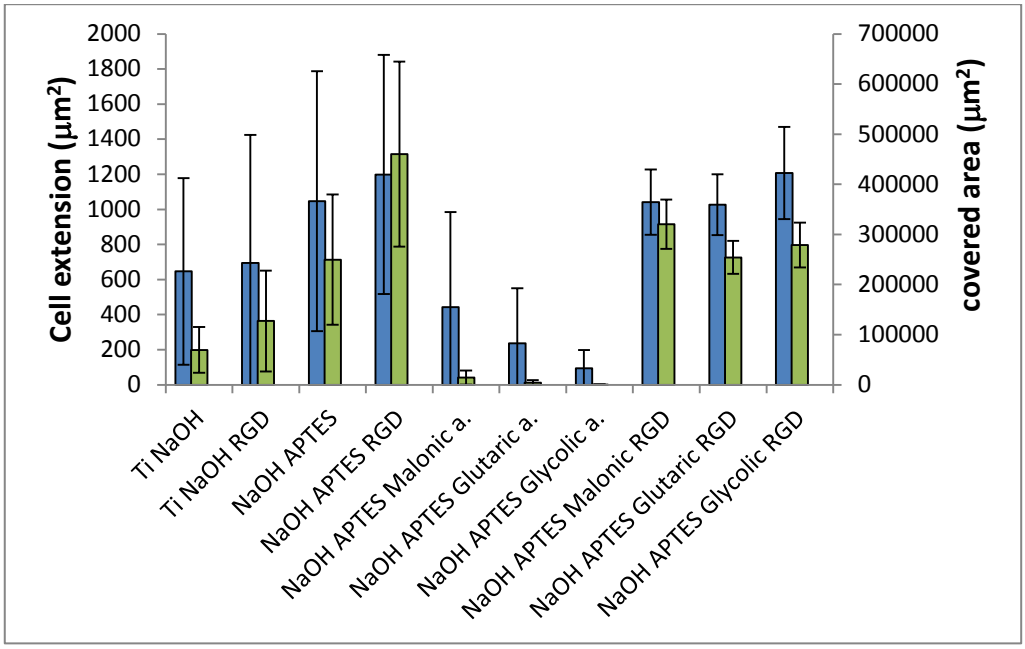


***Figure 2-44:*** *Cell extension and covered area of MG63 cells on the titanium surfaces treated using the three different cross-linkers with or without RGD peptide.*

As can be observed from the images of figure 2-43, and from the values in figures 2-42 and 2-44, there is no statistically significant differences in cell adhesion among the surfaces treated with the three different cross-linkers before RGD peptides were anchored. Few number of cells adhered on the surfaces treated with the cross-linkers due to the presence of carboxylates end HOBt molecules on the surface [136]. Nevertheless, the surface with malonic acid presented a slightly higher number of adhered cells. The almost null cell adhesion on the surfaces treated with diglycolic acid without RGD peptides suggests that the antifouling properties of the diglycolic acid are interfering with the appropriate cell interaction with those surfaces [137].

Once the RGD peptide is present on the surface the cell adhesion and extension is dramatically increased in all conditions and this effect is highly noted on the surfaces that were treated with any of the three crosslinkers. The high differences in cell adhesion and extension on these groups demonstrate that the RGD peptide is producing a high effect on the cells [7,10,12,15,58,138,139]. Therefore it can be assumed that the RGD peptides anchored on titanium surfaces trough the APTES+crosslinker route have biological effect *in vitro*. One interesting point is that, as it can be seen from the standard deviation bars on figure 2-42 and figure 2-44, the variability on cell adhesion and cell extension seems to be reduced when the RGD peptide is anchored to the surface through the APTES+crosslinker route. This effect is,

probably, due to a higher stability of the RGD peptide on these surfaces thank to a stable covalent bond between the surface and the peptide.

The differences among the three cross-linkers with RGD peptide with respect to cell adhesion and cell extension are also not statistically significant, indicating that the three crosslinkers had similar performance on anchoring the RGD peptides. From the images shown in figure 2-43 it can be seen that the presence of the RGD peptide affects the cell morphology intensely, making the cells more spreaded with clear actin filaments through the whole cell body and with longer philopodia. These differences are clearest on the images on the surfaces which were treated with any of the crosslinkers. Interestingly, though, an APTES surface without RGD has good cell adhesion due to the primary amines on the surface [136].

#### *2.6.2.2.2. Citotoxicity of malonic acid*

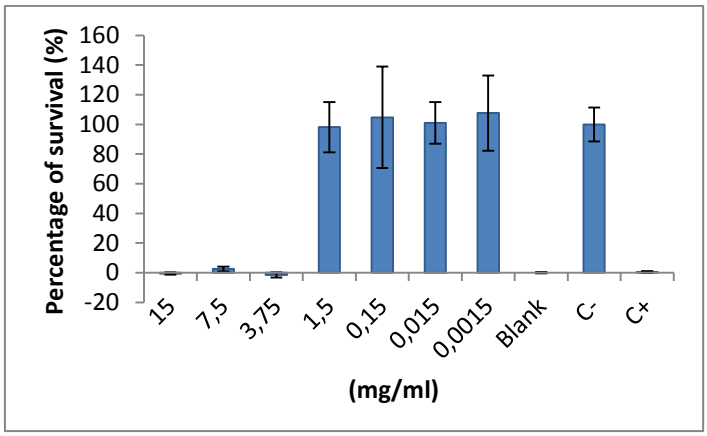


***Figure 2-45:*** *Citotoxicity results of MG63 cells exposed to different concentrations of malonic acid.*

Figure 2-45 shows the percentage of surviving cells depending on the dose of malonic acid administrated. There is a dose threshold between 1.5 and 3.75 mg/ml; above it, malonic acid is cytotoxic and kills the totality of the cells. Below this threshold, malonic acid is safe and innocuous to the cells. The concentration of malonic acid in the cross-linking solution was fixed at 1 mg/ml and, evidently, just a little proportion of the compound reacts and is adsorbed on the surface. Hence, we can ensure that the amount of malonic acid on the surface is much lower than the threshold value.

### 2.6.3. Discussion

The use of crosslinkers to covalently bind two organic molecules is a common procedure in biochemistry [140,141]. Molecules with two carboxylic acids, such as malonic acid, have been used as crosslinkers for several purposes in the medical a food fields [142,143], but, as far as authors know, they haven't been used as crosslinkers for functionalization purposes.

In general, we can say that the use of a new cross-linker based on two carboxylic acids was a success, independently of the cross-linker applied. The three cross-linkers worked similarly with few differences. Contact angle measurements showed a reduction of the hydrophobicity of the surfaces treated with the three crosslinkers. Fluorescence microscopy results shown that the surfaces treated with the three crosslinkers were able to adhere a similar amount of FITC cadaverine to the APTES silanized surface. Finally cell adhesion results demonstrated that, when any of the three crosslinkers is used, the RGD peptide is attached to the surface and is well presented to the cells so it can interact with them improving cell adhesion and extension. The results were approximately similar for the three crosslinkers although malonic acid showed a slightly better behavior than the others. These results combined ensure that surfaces with malonic acid attach or adsorb a higher amount of biomolecules on the surface.

FTIR and XPS results suggest that malonic acid has the best interaction with APTES and the HOBt molecule, both interactions necessary to have a covalent bond between the surface and the target oligopeptide. For all these reasons malonic acid was selected as the cross-linker for further experiments and as a part of the ultimate functionalization process. Moreover, cytotoxicity results have shown that the amount of malonic acid concentration used to prepare the functionalization samples was low enough to be completely safe for the cells.

# 2.7. Immobilization of the oligopeptides

Finally, the ultimate functionalization process was selected, being the following prodecure: 1.- activation with NaOH, 2.- silanization with APTES, 3.- crosslinking with malonic acid, and 4.- immobilization of the selected oligopeptide To confirm its effectiveness, a set of titanium samples were functionalized with the $NH_2$-KGGGGGGRGDS-OH peptide following the mentioned steps. The samples were then tested on a cell adhesion experiment using rat mesenchymal stem cells which are more sensitive to its environment than MG63 cell line.

## 2.7.1. Materials and Methods

### 2.7.1.1. Cell viability

To evaluate the effectiveness of the final step of the functionalization process, a cell adhesion assay was performed by exposing the samples to rat mesenchymal stem cells of pass 3, for a period of 3 hours.

Cells were exposed to samples with Advance MEM medium, supplemented with 1% penicillin/streptomycin and 2% sodium pyruvate and 1% L-glutamine (Gibco life technologies, UK), without serum to avoid the interference of serum proteins in the cell adhesion process and kept in an incubator at 37 $^{o}$C for 3 hours.

After exposure the samples were washed with 1x PBS (Gibco, UK) and proceeded to fluorescent triple --nuclei, cytoskeleton, focal adhesion points-- staining of cells. Cells were stained as described in section 2.5.1.3.4.2. Finally the samples were observed in a fluorescent lamp stereomicroscope SZX7 OLYMPUS (Japan).

## 2.7.2. Results

### 2.7.2.1. Cell Viability

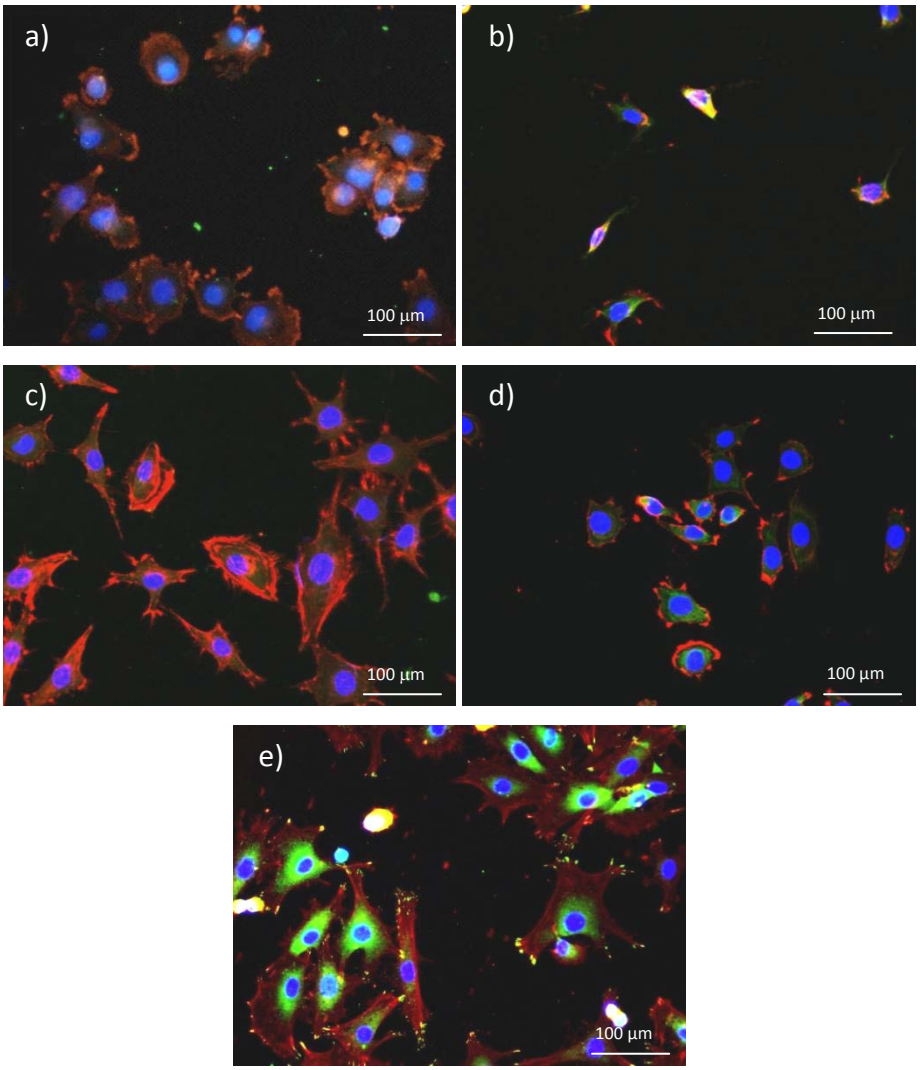


***Figure 2-46:*** *RMSC Cell adhesion immuno-fluorescence micrographs of a titanium surface after each step of the designed functionalization process. a) Ti, b)Ti+NaOH, c)Ti+NaOh+APTES, d)Ti+NaOH+APTES+Malonic a. and e)Ti+NaOH+APTES+Malonic a.+RGD*

To confirm that the design and development of the new functionalization process were conceived and carried out, the titanium surfaces were functionalized with a peptide containing the RGD sequence, and rat mesenchymal stem cells were exposed to titanium surfaces after each step of the functionalization process. As is observed in figure 2-46, the morphology of the cells attached to the surface after each step of the functionalization process changes dramatically. It is an indirect confirmation that each step was modifying the surface in some way. It is clear that APTES surfaces have a high adhesion potential due to the presence of amino groups on the surface [136], while after crosslinking, the cell adhesion is reduced due to the elimination of the free primary amines and the appearance of carboxylic groups [136].

Finally, when the RGD peptide is attached on the surface the cells show a high adhesion on the surface, and, more importantly, cells show focal adhesion points. β1 integrins are cell adhesion receptors belonging to the integrin supergene family that recognize multiple ligands, including fibronectin (FN), laminin, collagen, epiligrin, invasin, and vascular cell adhesion molecule-1. β1 integrins mediate cell-cell and cell-extracellular matrix interactions. The major integrin binding site is the RGD tripeptide, present in a variety of integrin ligands [144]. The green dots shown in figure 2-47e indicate integrin binding to the RGD sites present on the surface. Moreover, cells attached to RGD functionalized surfaces show high spreading as well as high number of attached cells. This is a proof of the excellent performance of the new developed functionalization process.

It can be seen that cell adhesion can be intensely modified by the chemical composition of the surface. This fact has helped us to confirm the presence of the chemical groups that we assumed to have on the titanium surface at each step according to our hypothesis since the results agreed with the found by other authors [117]. Additionally, it is clear that the functionalization process developed is able to retain a significant amount of RGD peptide provoking, therefore, an important increase in cell adhesion in comparison with the non-functionalized surfaces.

The excellent results obtained in attaching RGD peptides to titanium surfaces via the newly developed functionalization process has encouraged us on exploring the functionalization of our surfaces with other peptides which its effect on cell response is not as well-known as the

RGD sequence. The results obtained functionalizing titanium with newly developed peptides are shown on the following chapters of this thesis.

## 2.8. Conclusions

The sequential strategy of analysis and selection of each step of the functionalization process has been successfully applied. The comparison and selection among the different procedures and products in each step of the process has led to the final functionalization process shown in the scheme of figure 2-47:

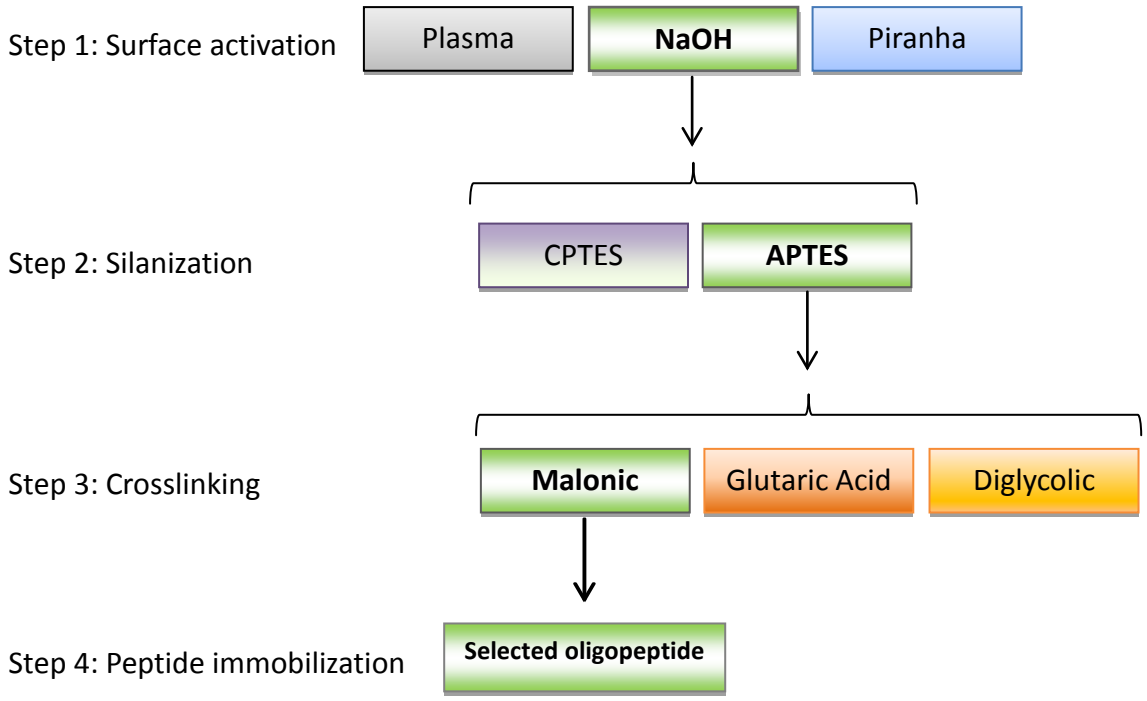


***Figure 2-47:*** *Selection sequence for each step of the functionalization process.*

Other conclusions drawn from the results obtained in this chapter are:

- A new functionalization process to covalently immobilize oligopeptides on titanium surfaces has been developed. The advantages of this new process are:
    - A high amount of biomolecules can be homogeneously immobilized on the titanium surface.
    - Prevention of polymerization or racemization of the peptides during the process of their immobilization on the titanium surface.
    - Selective bonding through the primary amines of the peptide as they react with the carboxylic terminal of the cross-linker molecules.

- The combination of surface activation with NaOH and silanization with APTES created a nano-roughened surface with very high surface area and thus, high reactivity and potential to retain large amount of molecules with carboxylates.

- RGD peptides have been successfully used as a model peptide to evaluate the biological effectiveness of the developed functionalization methodology. Their application for this purpose is a novel addition to their established applications which are the promotion of cell adhesion and integrin binding.

# 2.9. References

1. Pye AD, Lockhart DEA, Dawson MP, Murray CA, Smith AJ. A review of dental implants and infection. J Hosp Infect 2009;72:104-110.

2. Stadlinger B, Pilling E, Huhle M, Mai R, Bierbaum S, Scharnweber D, Kuhlisch E, Loukota R, Eckelt U. Evaluation of osseointegration of dental implants coated with collagen, chondroitin sulphate and BMP-4: an animal study. Int J Oral Maxillofac Surg 2008;37:54-59.

3. Bagno A, Piovan A, Dettin M, Chiarion A, Brun P, Gambaretto R, Fontana G, Di Bello C, Palù G, Castagliuolo I. Human osteoblast-like cell adhesion on titanium substrates covalently functionalized with synthetic peptides. Bone, 2007;40:693-699.

4. Porté-Durrieu MC, Guillemot F, Pallu S, Labrugère C, Brouillaud B, Bareille R, Amédée J, Barthe N, Dard M, Baquey C. Cyclo-(DfKRG) peptide grafting onto Ti–6Al–4V: physical characterization and interest towards human osteoprogenitor cells adhesion. Biomaterials 2004;25:4837-4846.

5. Tosatti S, Paul SMD, Askendal A, VandeVondele S, Hubbell JA, Tengvall P, Textor M. Peptide functionalized poly(-lysine)-g-poly(ethylene glycol) on titanium: resistance to protein adsorption in full heparinized human blood plasma. Biomaterials 2003;24:4949-4958.

6. Wang J, Wang Z, Guo S, Zhang J, Song Y, Dong X, Wang X, Yu J. Antibacterial and anti-adhesive zeolite coatings on titanium alloy surface. Microporous and Mesoporous Materials 2011;146:216-222.

7. Chua P, Neoh K, Kang E, Wang W. Surface functionalization of titanium with hyaluronic acid/chitosan polyelectrolyte multilayers and RGD for promoting osteoblast functions and inhibiting bacterial adhesion. Biomaterials 2008;29:1412-1421.

8. Pierschbacher MD, Hayman EG, Ruoslahti E. Location of the cell-attachment site in fibronectin with monoclonal antibodies and proteolytic fragments of the molecule. Cell 1981;26:259-267.

9. Mas-Moruno C, Rechenmacher F, Kessler H. Cilengitide: the first anti-angiogenic small molecule drug candidate design, synthesis and clinical evaluation. Anticancer Agents Med Chem 2010;10:753-768.

10. Feng Y, Mrksich M. The Synergy Peptide PHSRN and the Adhesion Peptide RGD Mediate Cell Adhesion through a Common Mechanism. Biochemistry 2004;43:15811-15821.

11. Park J, Kurashima K, Tustusmi Y, An C, Suh J, Doi H, Nomura N, Noda K, Hanawa T. Bone healing of commercial oral implants with RGD immobilization through electrodeposited poly(ethylene glycol) in rabbit cancellous bone. Acta Biomaterialia 2011;7:3222-3229.

12. Chollet C, Chanseau C, Remy M, Guignandon A, Bareille R, Labrugère C, Bordenave L, Durrieu M. The effect of RGD density on osteoblast and endothelial cell behavior on RGD-grafted polyethylene terephthalate surfaces. Biomaterials 2009;30:711-720.

13. Beuvelot J, Portet D, Lecollinet G, Moreau MF, Basle MF, Chappard D, Libouban H. In vitro kinetic study of growth and mineralization of osteoblast-like cells (Saos-2) on titanium surface coated with a RGD functionalized bisphosphonate. J Biomed Mater Res B Appl Biomater 2009;90:873-881.

14. Oya K, Tanaka Y, Saito H, Kurashima K, Nogi K, Tsutsumi H, Tsutsumi Y, Doi H, Nomura N, Hanawa T. Calcification by MC3T3-E1 cells on RGD peptide immobilized on titanium through electrodeposited PEG. Biomaterials 2009;30:1281-1286.

15. Pallu S, Fricain JC, Bareille R, Bourget C, Dard M, Sewing A, Amédée J. Cyclo-DfKRG peptide modulates in vitro and in vivo behavior of human osteoprogenitor cells on titanium alloys. Acta Biomaterialia 2009;5:3581-3592.

16. Rammelt S, Illert T, Bierbaum S, Scharnweber D, Zwipp H, Schneiders W. Coating of titanium implants with collagen, RGD peptide and chondroitin sulfate. Biomaterials 2006;27:5561-5571.

17. S. Tosatti, Z. Schwartz, C. Campbell, D. L. Cochran, S. VandeVondele, J. A. Hubbell, A. Denzer, J. Simpson, M. Wieland, C. H. Lohmann, M. Textor, B. D. Boyan. RGD-containing peptide GCRGYGRGDSPG reduces enhancement of osteoblast differentiation by polylysine)-graft-poly(ethylene glycol)-coated titanium surfaces. Journal of Biomedical Materials Research Part A 2004;68A:458-472.

18. Ryan CS, Kleinberg I. Bacteria in human mouths involved in the production and utilization of hydrogen peroxide. Arch Oral Biol 1995;40:753-763.

19. Guzman M, Dille J, Godet S. Synthesis and antibacterial activity of silver nanoparticles against gram-positive and gram-negative bacteria. Nanomedicine: Nanotechnology, Biology and Medicine 2012;8:37-45.

20. Lee SM, Lee BS, Byun TG, Song KC. Preparation and antibacterial activity of silver-doped organic–inorganic hybrid coatings on glass substrates. Colloids Surf Physicochem Eng Aspects 2010;355:167-171.

21. Lenton P, Rudney J, Chen R, Fok A, Aparicio C, Jones RS. Imaging in vivo secondary caries and ex vivo dental biofilms using cross-polarization optical coherence tomography. Dental Materials 2012;28:792-800.

22. Ito Y, Kajihara M, Imanishi Y. Materials for enhancing cell adhesion by immobilization of cell-adhesive peptide. J Biomed Mater Res 1991;25:1325-1337.

23. Pegueroles M, Aparicio C, Bosio M, Engel E, Gil FJ, Planell JA, Altankov G. Spatial organization of osteoblast fibronectin matrix on titanium surfaces: Effects of roughness, chemical heterogeneity and surface energy. Acta Biomaterialia 2010;6:291-301.

24. Velzenberger E, Kirat KE, Legeay G, Nagel M, Pezron I. Characterization of biomaterials polar interactions in physiological conditions using liquid–liquid contact angle measurements: Relation to fibronectin adsorption. Colloids and Surfaces B: Biointerfaces 2009;68:238-244.

25. Huang Y, Lü X, Jingwu M, Huang N. In vitro investigation of protein adsorption and platelet adhesion on inorganic biomaterial surfaces. Appl Surf Sci 2008;255:257-259.

26. Michiardi A, Aparicio C, Ratner BD, Planell JA, Gil J. The influence of surface energy on competitive protein adsorption on oxidized NiTi surfaces. Biomaterials 2007;28:586-594.

27. Puleo DA, Nanci A. Understanding and controlling the bone–implant interface. Biomaterials 1999;20:2311-2321.

28. Shen J, Wu T, Wang Q, Pan H. Molecular simulation of protein adsorption and desorption on hydroxyapatite surfaces. Biomaterials 2008;29:513-532.

29. Wennerberg A, Albrektsson T, Johansson C, Andersson B. Experimental study of turned and grit-blasted screw-shaped implants with special emphasis on effects of blasting material and surface topography. Biomaterials 1996;17:15-22.

30. Bai Z, Filiaggi MJ, Dahn JR. Fibrinogen adsorption onto 316L stainless steel, Nitinol and titanium. Surf Sci 2009;603:839-846.

31. Karimi S, Nickchi T, Alfantazi A. Effects of bovine serum albumin on the corrosion behaviour of AISI 316L, Co–28Cr–6Mo, and Ti–6Al–4V alloys in phosphate buffered saline solutions. Corros Sci 2011;53:3262-3272.

32. Bauer S, Schmuki P, von der Mark K, Park J. Engineering biocompatible implant surfaces: Part I: Materials and surfaces. Progress in Materials Science .

33. Ho D, Chang S, Montemagno CD. Fabrication of biofunctional nanomaterials via Escherichia coli OmpF protein air/water interface insertion/integration with copolymeric amphiphiles. Nanomedicine: Nanotechnology, Biology and Medicine 2006;2:103-112.

34. Cai K, Rechtenbach A, Hao J, Bossert J, Jandt KD. Polysaccharide-protein surface modification of titanium via a layer-by-layer technique: Characterization and cell behaviour aspects. Biomaterials 2005;26:5960-5971.

35. Schreiber F. Structure and growth of self-assembling monolayers. Prog Surf Sci 2000;65:151-257.

36. Tamura H, Tanaka A, Mita K, Furuichi R. Surface Hydroxyl Site Densities on Metal Oxides as a Measure for the Ion-Exchange Capacity. J Colloid Interface Sci 1999;209:225-231.

37. Morra M, Cassinelli C. Organic surface chemistry on titanium surfaces via thin film deposition. J Biomed Mater Res 1997;37:198-206.

38. Rezania A, Johnson R, Lefkow AR, Healy KE. Bioactivation of Metal Oxide Surfaces. 1. Surface Characterization and Cell Response. Langmuir 1999;15:6931-6939.

39. Hernández de Gatica NL, Jones GL, Gardella Jr. JA. Surface characterization of titanium alloys sterilized for biomedical applications. Appl Surf Sci 1993;68:107-121.

40. Puleo DA. Biochemical surface modification of CoCrMo. Biomaterials 1996;17:217-222.

41. Nanci A, Wuest JD, Peru L, Brunet P, Sharma V, Zalzal S, McKee MD. Chemical modification of titanium surfaces for covalent attachment of biological molecules. J Biomed Mater Res 1998;40:324-335.

42. Diamanti MV, Pedeferri MP. Effect of anodic oxidation parameters on the titanium oxides formation. Corros Sci 2007;49:939-948.

43. Puleo DA, Kissling RA, Sheu M-. A technique to immobilize bioactive proteins, including bone morphogenetic protein-4 (BMP-4), on titanium alloy. Biomaterials 2002;23:2079-2087.

44. Maoz R, Sagiv J, Degenhardt D, Möhwald H, Quint P. Hydrogen-bonded multilayers of self-assembling silanes: structure elucidation by combined Fourier transform infra-red spectroscopy and X-ray scattering techniques. Supramol Sci 1995;2:9-24.

45. Love JC, Wolfe DB, Haasch R, Chabinyc ML, Paul KE, Whitesides GM, Nuzzo RG. Formation and Structure of Self-Assembled Monolayers of Alkanethiolates on Palladium. J Am Chem Soc 2003;125:2597-2609.

46. Stevens MJ. Thoughts on the Structure of Alkylsilane Monolayers. Langmuir 1999;15:2773-2778.

47. Ferris DM, Moodie GD, Dimond PM, Giorani CWD, Ehrlich MG, Valentini RF. RGD-coated titanium implants stimulate increased bone formation in vivo. Biomaterials 1999;20:2323-2331.

48. Bell BF, Schuler M, Tosatti S, Textor M, Schwartz Z, Boyan BD. Osteoblast response to titanium surfaces functionalized with extracellular matrix peptide biomimetics. Clin Oral Implants Res 2011;22:865-872.

49. Costa F, Carvalho IF, Montelaro RC, Gomes P, Martins MCL. Covalent immobilization of antimicrobial peptides (AMPs) onto biomaterial surfaces. Acta Biomaterialia 2011;7:1431-1440.

50. Harris LG, Tosatti S, Wieland M, Textor M, Richards RG. Staphylococcus aureus adhesion to titanium oxide surfaces coated with non-functionalized and peptide-functionalized poly(l-lysine)-grafted-poly(ethylene glycol) copolymers. Biomaterials 2004;25:4135-4148.

51. Héquet A, Humblot V, Berjeaud J, Pradier C. Optimized grafting of antimicrobial peptides on stainless steel surface and biofilm resistance tests. Colloids and Surfaces B: Biointerfaces 2011;84:301-309.

52. Kazemzadeh-Narbat M, Kindrachuk J, Duan K, Jenssen H, Hancock REW, Wang R. Antimicrobial peptides on calcium phosphate-coated titanium for the prevention of implant-associated infections. Biomaterials 2010;31:9519-9526.

53. Onaizi SA, Leong SSJ. Tethering antimicrobial peptides: Current status and potential challenges. Biotechnol Adv 2011;29:67-74.

54. Rezania A, Healy KE. The effect of peptide surface density on mineralization of a matrix deposited by osteogenic cells. J Biomed Mater Res 2000;52:595-600.

55. Massia SP, Hubbell JA. An RGD spacing of 440 nm is sufficient for integrin alpha V beta 3-mediated fibroblast spreading and 140 nm for focal contact and stress fiber formation. The Journal of Cell Biology 1991;114:1089-1100.

56. DiMilla PA, Stone JA, Quinn JA, Albelda SM, Lauffenburger DA. Maximal migration of human smooth muscle cells on fibronectin and type IV collagen occurs at an intermediate attachment strength. J Cell Biol 1993;122:729-737.

57. Thid D, Bally M, Holm K, Chessari S, Tosatti S, Textor M, Gold J. Issues of Ligand Accessibility and Mobility in Initial Cell Attachment. Langmuir 2007;23:11693-11704.

58. Houseman BT, Mrksich M. The microenvironment of immobilized Arg-Gly-Asp peptides is an important determinant of cell adhesion. Biomaterials 2001;22:943-955.

59. Drumheller PD, Elbert DL, Hubbell JA. Multifunctional poly(ethylene glycol) semi-interpenetrating polymer networks as highly selective adhesive substrates for bioadhesive peptide grafting. Biotechnol Bioeng 1994;43:772-780.

60. Sharma S, Johnson RW, Desai TA. XPS and AFM analysis of antifouling PEG interfaces for microfabricated silicon biosensors. Biosensors and Bioelectronics 2004;20:227-239.

61. Andruzzi L, Nickel B, Schwake G, Rädler JO, Sohn KE, Mates TE, Kramer EJ. Bio-selective surfaces by chemically amplified constructive microlithography. Surf Sci 2007;601:4984-4992.

62. Awsiuk K, Psarouli A, Petrou P, Budkowski A, Kakabakos S, Bernasik A, Rysz J, Raptis I. Spectroscopic and microscopic examination of protein adsorption and blocking of non-specific binding to silicon surfaces modified with APTES and GOPS. Procedia Engineering 2011;25:334-337.

63. Schramm C, Rinderer B. Investigation of the hydrolysis of (3-triethoxysilylpropyl)succinic acid anhydride by means of FT-IR. J Mater Sci 2008;43:4215-4219.

64. Kim J, Seidler P, Fill C, Wan LS. Investigations of the effect of curing conditions on the structure and stability of amino-functionalized organic films on silicon substrates by Fourier transform infrared spectroscopy, ellipsometry, and fluorescence microscopy. Surf Sci 2008;602:3323-3330.

65. Tan G, Zhang L, Ning C, Liu X, Liao J. Preparation and characterization of APTES films on modification titanium by SAMs. Thin Solid Films 2011;519:4997-5001.

66. Dow Corning. A guide to silane solutions from Dow Corning. 2005.

67. Gelest. Silane coupling agents: Connecting across boundaries. 2006.

68. Takeda S, Fukawa M. Role of surface OH groups in surface chemical properties of metal oxide films. Materials Science and Engineering B 2005;119:265-267.

69. Chen Y, Zheng X, Ji H, Ding C. Effect of Ti–OH formation on bioactivity of vacuum plasma sprayed titanium coating after chemical treatment. Surface and Coatings Technology 2007;202:494-498.

70. Liu X, Chu PK, Ding C. Surface modification of titanium, titanium alloys, and related materials for biomedical applications. Materials Science and Engineering: R: Reports 2004;47:49-121.

71. Kominiak GJ, Mattox DM. Reactive plasma cleaning of metals. Thin Solid Films 1977;40:141-148.

72. Michiardi A, Hélary G, Nguyen P-T, Gamble LJ, Anagnostou F, Castner DG, Migonney V. Bioactive polymer grafting onto titanium alloy surfaces. Acta Biomaterialia 2010;6:667-675.

73. Lewandowska M, Roguska A, Pisarek M, Polak B, Janik-Czachor M, Kurzydłowski KJ. Morphology and chemical characterization of Ti surfaces modified for biomedical applications. Biomol Eng 2007;24:438-442.

74. Aparicio C, Rodriguez D, Gil FJ. Variation of roughness and adhesion strength of deposited apatite layers on titanium dental implants. Materials Science and Engineering: C 2011;31:320-324.

75. Nishiguchi S, Kato H, Fujita H, Oka M, Kim H, Kokubo T, Nakamura T. Titanium metals form direct bonding to bone after alkali and heat treatments. Biomaterials 2001;22:2525-2533.

76. Kim J, Seidler P, Wan LS, Fill C. Formation, structure, and reactivity of amino-terminated organic films on silicon substrates. J Colloid Interface Sci 2009;329:114-119.

77. Sargeant TD, Rao MS, Koh C, Stupp SI. Covalent functionalization of NiTi surfaces with bioactive peptide amphiphile nanofibers. Biomaterials 2008;29:1085-1098.

78. Song Y, Hildebrand H, Schmuki P. Optimized monolayer grafting of 3-aminopropyltriethoxysilane onto amorphous, anatase and rutile TiO2. Surf Sci 2010;604:346-353.

79. Vandenberg E, Elwing H, Askendal A, Lundström I. Protein immobilization of 3-aminopropyl triethoxy silane/glutaraldehyde surfaces: Characterization by detergent washing. J Colloid Interface Sci 1991;143:327-335.

80. Xiao SJ, Textor M, Sencer ND, Wieland M, Keller B, Sigrist H. Immobilization of the cell-adhesive peptide Arg–Gly–Asp–Cys (RGDC) on titanium surfaces by covalent chemical attachment. J Mater Sci Mater Med 1997;8:867-872.

81. Ege SN. Organic chemistry: Structure and reactivity. : Houghton Mifflin Company, 2004.

82. Pearson AJ, Roush WR. Handbook of Reagents for Organic Synthesis - Activating Agents and Protecting Groups. 1999.

83. Aldrich. Chemfiles, Peptide synthesis. http://www.sigmaaldrich.com/etc/medialib/docs/Aldrich/Brochure/al_chemfile_v7_n2.Par.0001.File.dat/al_chemfile_v7_n2.pdf. 2007.

84. Lloyd-Williams P, Albericio F, Giralt E. Chemical approaches to the synthesis of peptides and proteins (new directions in organic & biological chemistry). : CRC-Press, 1997.

85. Al-Warhi TI, Al-Hazimi HMA, El-Faham A. Recent development in peptide coupling reagents. Journal of Saudi Chemical Society 2012;16:97-116.

86. Naue N, Fedorov R, Pich A, Manstein DJ, Curth U. Site-directed mutagenesis of the χ subunit of DNA polymerase III and single-stranded DNA-binding protein of E. coli reveals key residues for their interaction. Nucleic Acids Research 2011;39:1398-1407.

87. Updegrove TB, Correia JJ, Chen Y, Terry C, Wartell RM. The stoichiometry of the Escherichia coli Hfq protein bound to RNA. RNA 2011;17:489-500.

88. Pierce. EDC, A water-soluble carbodiimide crosslinker for zero-length, carboxyl-to-amine conjugation.

89. Streitwieser A, Heathcock CH. Introduction to organic chemistry. : Maxwell MacMillan, 1985.

90. Tedeschi T, Corradini R, Marchelli R, Pushl A, Nielsen PE. Racemization of chiral PNAs during solid-phase synthesis: effect of the coupling conditions on enantiomeric purity. Tetrahedron: Asymmetry 2002;13:1629-1636.

91. Han S, Kim Y. Recent development of peptide coupling reagents in organic synthesis. Tetrahedron 2004;60:2447-2467.

92. Haver AC, David Smith D. Effect of solvent on racemization in carbodiimide mediated solid phase fragment condensations. Tetrahedron Lett 1993;34:2239-2242.

93. Miller R. Beyond ANOVA: Basics of applied statistics (texts in statistical science series). : Chapman & Hall/CRC, 1997.

94. Massey F. The Kolmogorov-Smirnov Test for Goodness of Fit. Journal of the American Statistical Association 1951;46:68-78.

95. Wasserman L. All of nonparametric statistics (springer texts in statistics). : Springer, 2007.

96. Katz B, Mcsweeney M. A Multivariate Kruskal-Wallis Test With Post Hoc Procedures. Multivariate Behavioral Research 1980;15:281-297.

97. Yan L, Dodier R, Mozer M, Wolniewicz R. Optimizing Classifier Performance Via the Wilcoxon-Mann-Whitney Statistics. 2003.

98. Iucci G, Dettin M, Battocchio C, Gambaretto R, Bello CD, Polzonetti G. Novel immobilizations of an adhesion peptide on the TiO2 surface: An XPS investigation. Materials Science and Engineering: C 2007;27:1201-1206.

99. Mekhalif Z, Cossement D, Hevesi L, Delhalle J. Electropolymerization of pyrrole on silanized polycrystalline titanium substrates. Appl Surf Sci 2008;254:4056-4062.

100. Gil FJ, Padrós A, Manero JM, Aparicio C, Nilsson M, Planell JA. Growth of bioactive surfaces on titanium and its alloys for orthopaedic and dental implants. Materials Science and Engineering: C 2002;22:53-60.

101. Bondarenka V, Tvardauskas H, Grebinskij S, Senulis M, Pa?i?kevi?ius A, Volkov V, Zakharova G. - Sol-gel synthesis and XPS study of vanadium-hydroquinone oxide bronze films. - physica status solidi (c) - 2009;- 6:- 2807--2809.

102. Moulder JF, Stickle WF, Sobol PE, Bomben KD. Handbook of X-ray photoelectron spectroscopy. : Physical Electronics Inc., 1992.

103. National Institute of Standards and Technology, NIST. NIST X-ray Photoelectron Spectroscopy Database. http://srdata.nist.gov/xps/. 2007.

104. Kang B, Sul Y, Oh S, Lee H, Albrektsson T. XPS, AES and SEM analysis of recent dental implants. Acta Biomaterialia 2009;5:2222-2229.

105. Polzonetti G, Battocchio C, Iucci G, Dettin M, Gambaretto R, Di Bello C, Carravetta V. Thin films of a self-assembling peptide on TiO2 and Au studied by NEXAFS, XPS and IR spectroscopies. Materials Science and Engineering: C 2006;26:929-934.

106. F Werfel and OB. Corundum Structure Oxides Studied by XPS. Phys Scripta 1983;28:92.

107. Bertóti I, Mohai M, Sullivan JL, Saied SO. Surface characterisation of plasma-nitrided titanium: an XPS study. Appl Surf Sci 1995;84:357-371.

108. Sargeant TD, Rao MS, Koh C, Stupp SI. Covalent functionalization of NiTi surfaces with bioactive peptide amphiphile nanofibers. Biomaterials, 2008;29:1085-1098.

109. Tanaka Y, Nakai M, Akahori T, Niinomi M, Tsutsumi Y, Doi H, Hanawa T. Characterization of air-formed surface oxide film on Ti–29Nb–13Ta–4.6Zr alloy surface using XPS and AES. Corros Sci 2008;50:2111-2116.

110. Meng X, Wang D, Liu J, Zhang S. Preparation and characterization of sodium titanate nanowires from brookite nanocrystallites. Mater Res Bull 2004;39:2163-2170.

111. Mekhalif Z, Cossement D, Hevesi L, Delhalle J. Electropolymerization of pyrrole on silanized polycrystalline titanium substrates. Appl Surf Sci 2008;254:4056-4062.

112. Matinlinna JP, Lassila LVJ, Kangasniemi I, Yli-Urpo A, Vallittu PK. Shear bond strength of Bis-GMA resin and methacrylated dendrimer resins on silanized titanium substrate. Dental Materials 2005;21:287-296.

113. Matinlinna JP, Özcan M, Lassila LVJ, Vallittu PK. The effect of a 3-methacryloxypropyltrimethoxysilane and vinyltriisopropoxysilane blend and tris(3-trimethoxysilylpropyl)isocyanurate on the shear bond strength of composite resin to titanium metal. Dental Materials 2004;20:804-813.

114. Bagno A, Piovan A, Dettin M, Brun P, Gambaretto R, Palù G, Di Bello C, Castagliuolo I. Improvement of Anselme's adhesion model for evaluating human osteoblast response to peptide-grafted titanium surfaces. Bone 2007;41:704-712.

115. Müller R, Abke J, Schnell E, Scharnweber D, Kujat R, Englert C, Taheri D, Nerlich M, Angele P. Influence of surface pretreatment of titanium- and cobalt-based biomaterials on covalent immobilization of fibrillar collagen. Biomaterials 2006;27:4059-4068.

116. Isackson D, McGill LD, Bachus KN. Percutaneous implants with porous titanium dermal barriers: An in vivo evaluation of infection risk. Med Eng Phys 2011;33:418-426.

117. Lee MH, Brass DA, Morris R, Composto RJ, Ducheyne P. The effect of non-specific interactions on cellular adhesion using model surfaces. Biomaterials 2005;26:1721-1730.

118. Wang J, Zhu T, Song J, Liu Z. Gold nanoparticulate film bound to silicon surface with self-assembled monolayers. Thin Solid Films 1998;327–329:591-594.

119. Cras JJ, Rowe-Taitt CA, Nivens DA, Ligler FS. Comparison of chemical cleaning methods of glass in preparation for silanization. Biosensors and Bioelectronics 1999;14:683-688.

120. ISO. ISO 10993-12:2007, Biological evaluation of medical devices -- Part 12: Sample preparation and reference materials. 2007.

121. Santacruz Biotechnology. Inmunofluorescence staining protocol. http://www.scbt.com/protocol_immunofluorescence_cell_staining.html.

122. Beamson G, Briggs D. High resolution XPS of organic polymers: The scienta ESCA 300 database. Chichester: John Wiley & Sons Ltd., 1993.

123. Awsiuk K, Bernasik A, Kitsara M, Budkowski A, Rysz J, Haberko J, Petrou P, Beltsios K, Raczkowska J. Protein coverage on silicon surfaces modified with amino-organic films: A study by AFM and angle-resolved XPS. Colloids and Surfaces B: Biointerfaces 2010;80:63-71.

124. Iucci G, Battocchio C, Dettin M, Ghezzo F, Polzonetti G. An XPS study on the covalent immobilization of adhesion peptides on a glass surface. Solid State Sciences 2010;12:1861-1865.

125. Bierbaum K, Kinzler M, Woell C, Grunze M, Haehner G, Heid S, Effenberger F. A Near Edge X-ray Absorption Fine Structure Spectroscopy and X-ray Photoelectron Spectroscopy Study of the Film Properties of Self-Assembled Monolayers of Organosilanes on Oxidized Si(100). Langmuir 1995;11:512-518.

126. Gu Q, Cheng X. Tribological behaviors of lanthanum-based phosphonate 3-aminopropyltriethoxysilane self-assembled films. Appl Surf Sci 2007;253:6800-6806.

127. Xue A, Zhou S, Zhao Y, Lu X, Han P. Effective NH2-grafting on attapulgite surfaces for adsorption of reactive dyes. J Hazard Mater 2011;194:7-14.

128. Vargo TG, Gardella JA. Development of Ti K a Radiation for ESCA Analysis of Polymer Surfaces. Journal of vacuum science & technology 1989;A7:1733-1741.

129. Izquierdo ML. Absorciones de grupo características de moléculas orgánicas. http://es.scribd.com/doc/37601411/Espectroscopia-Infrarrojo-Absorciones-de-Grupo-Caracteristicas. 2012.

130. Guha Thakurta S, Subramanian A. Fabrication of dense, uniform aminosilane monolayers: A platform for protein or ligand immobilization. Colloids Surf Physicochem Eng Aspects 2012;414:384-392.

131. Hélary G, Noirclère F, Mayingi J, Migonney V. A new approach to graft bioactive polymer on titanium implants: Improvement of MG 63 cell differentiation onto this coating. Acta Biomaterialia 2009;5:124-133.

132. Sevilla P, Godoy M, Salvagni E, Gil FJ. Biofunctionalization of titanium surfaces for osseintegration process improvement. Journal of Physics: Conference Series 2010;252:012009.

133. Eisenbarth E, Velten D, Breme J. Biomimetic implant coatings. Biomol Eng 2007;24:27-32.

134. Dalsin JL, Messersmith PB. Bioinspired antifouling polymers. Materials Today 2005;8:38-46.

135. Glagovich N. Infrared Spectroscopy, IR Absorptions for Representative Functional Groups. 2012.

136. Lee MH, Brass DA, Morris R, Composto RJ, Ducheyne P. The effect of non-specific interactions on cellular adhesion using model surfaces. Biomaterials 2005;26:1721-1730.

137. Tu Q, Wang J, Liu R, He J, Zhang Y, Shen S, Xu J, Liu J, Yuan M, Wang J. Antifouling properties of poly(dimethylsiloxane) surfaces modified with quaternized poly(dimethylaminoethyl methacrylate). Colloids and Surfaces B: Biointerfaces 2013;102:361-370.

138. Larsen CC, Kligman F, Kottke-Marchant K, Marchant RE. The effect of RGD fluorosurfactant polymer modification of ePTFE on endothelial cell adhesion, growth, and function. Biomaterials 2006;27:4846-4855.

139. Dettin M, Conconi MT, Gambaretto R, Pasquato A, Folin M, Di Bello C, Parnigotto PP. Novel osteoblast-adhesive peptides for dental/orthopedic biomaterials. J Biomed Mater Res 2002;60.

140. Chapter 3 basic technologies developed for tissue engineering. Interface Science and Technology: Elsevier. p. 235-421.

141. Shriver-Lake LC, Donner B, Edelstein R, Kristen Breslin, Bhatia SK, Ligler FS. Antibody immobilization using heterobifunctional crosslinkers. Biosensors and Bioelectronics 1997;12:1101-1106.

142. Ghosh Dastidar T, Netravali AN. 'Green' crosslinking of native starches with malonic acid and their properties. Carbohydr Polym 2012;90:1620-1628.

143. Trochimczuk AW. Chelating resins with N-substituted diamides of malonic acid as ligands. European Polymer Journal 1998;34:1657-1662.

144. Yamada KM. Adhesive recognition sequences. Journal of Biological Chemistry 1991;266:12809-12812.

# 3. Analysis of interactions between surfaces and oligopeptides for functionalization purposes

## CONTENTS

# 3.1. Introduction

## 3.1.1. Scope

Protein adsorption on biomaterials surfaces is an interesting topic which relates to many novel applications in implantology, regenerative medicine and biotechnology in general. The processes involved in protein adsorption on a surface are not yet fully understood. Nevertheless, certain parameters seem to play an important role in the amount of proteins adsorbed, in their stability, and in the conformations they adopt on the surface. Such parameters are listed below:

- Environmental pH [1,2]
- Basicity and acidity of the amino acid side chains that compose the protein [3-5]
- Surface topography [6,7]
- Primary, secondary, tertiary and quaternary structure of proteins [2,8,9]
- Self-protein interactions [10-12]
- Surface hydrophilicity/hydrophobicity [13-16]
- Surface charge [1,3,17]

Protein adsorption is a complex phenomenon. When a synthetic device comes into contact with body fluids, hundreds of different proteins interact at the same time with the surface [18]. Additionally there is a wide range of different materials with many different surface treatments which can be inserted in the body. This makes protein adsorption unpredictable in the majority of cases, despite the tremendous progress made in this field.

Oligo-peptide adsorption on biomaterial surfaces may be less complex than protein adsorption due to the fact that peptides don't adopt secondary, tertiary and quaternary structures. Unfortunately, bibliography on peptide adsorption is very limited due to the fact that whereas materials surfaces will always interact with proteins in the body, they're only exposed to oligopeptides in lab situations [4,5,9,16].

Regarding biofunctionalization of surfaces with short peptides, it is important to bear in mind that material surfaces need to interact with oligopeptides in order to immobilize them on the surface. Thus, the study of oligopeptide adsorption on biomaterial surfaces could be useful to improve peptide immobilization methodology.

So far, the general trend for achieving immobilization of oligopeptides on biomaterial surfaces has been to involve a chemical reaction that establishes a covalent bond between the peptide and the surface. The most common approach used for this purpose is the generation of amide bonds between primary amines and carboxylates using a coupling reagent to activate the carboxylate and catalyze the reaction [19-21]. Other techniques consist of generating disulfide bonds using glutaraldehyde as a cross-linker [22,23] or performing nucleophilic-electrophilic substitutions involving a halogen atom [24,25].

There is often a lack of knowledge and rigor in the methodology employed to immobilize biomolecules on surfaces in the field of biofunctionalization. In general, researchers don't focus on the immobilization process but rather on aspects relevant to the materials generated The results obtained in the second chapter suggested that both surface charge and peptide surface charge are key properties for a successful immobilization of the biomolecules on the synthetic substrates. These two properties and its interconnected effect on the effective biofunctionalization have not been fully considered in the research in the field so far.

Thus, this chapter studies the adsorption behavior of oligopeptides on titanium surfaces focusing on understanding the effects of these two main parameters. Understanding the effect of surface charge and peptide net charge on peptide adsorption could help us improve and develop better strategies for the efficient immobilization of oligopeptides on biomaterial surfaces.

### 3.1.2. Surface charge

Surface charge is the electric charge present at an interface. There are many different processes which can lead to a surface being charged, including adsorption of ions,

protonation/deprotonation, and the application of an external electric field. Surface charge causes a particle to emit an electric field, which causes particle repulsions and attractions [26] .

When a surface is immersed in a solution containing electrolytes, it develops a net surface charge. This is often because of ionic adsorption. Aqueous solutions universally contain positive and negative ions (cations and anions, respectively), which interact with partial charges on the surface, adsorbing to and thus ionizing the surface and creating a net surface charge [27]. This net charge results in a surface potential, which causes the surface to be surrounded by a cloud of counter-ions, which extends from the surface into the solution, and also generally results in repulsion between species. The larger the partial charges in the material, the more ions are adsorbed to the surface, and the larger the cloud of counter-ions. A solution with a higher concentration of electrolytes also increases the size of the counter-ion cloud. This ion/counter ion layer is known as the electric double layer [28,29].

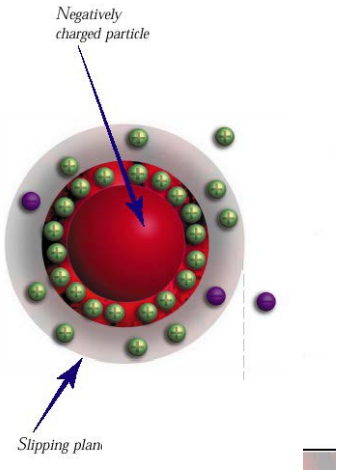


***Figure 3-1**: Electric double layer surrounding an electronegatively charge particle [28].*

A solution's pH can also greatly affect surface charge because functional groups present on the surface of materials can often contain nitrogen or oxygen, two atoms which can be protonated or deprotonated to become charged. Thus, as the concentration of hydrogen ions changes, so does the surface charge. At a given pH, the average surface charge will be equal to zero; this is known as the point of zero charge (PCZ), when referred to surfaces, or isoelectric point, when referred to proteins [29,30].

The measurement of the surface charge is often performed by means of the ζ potential measurement. Surface ζ potential is further explained in section 3.4.2.4.1 and Annex A of this thesis in electronic format.

### 3.1.3. Net charge of a biomolecule

Polypeptides and proteins are ampholytes. Ampholytes contain positive and negative charges. Moreover, a trait common to all ampholytes is that their net charge is pH dependent. They have a positive charge at low pH values, and negative charge at high pH values. For each ampholyte there is a pH value having a net zero charge. This pH value is called the isoelectric point of the molecule. In this isoelectric point, the ampholyte will not move if it is subjected to an electric field and will not be attracted or repelled by other electrically charged molecules [31].

To determine the net charge of a protein it is necessary to know the amino acid sequence and understand the charges on each amino acid residue in the amino acid sequence. To do this, we need to know the charge on each weak acid of the protein before and after dissociation. We must also know the pH of the solution and the pKa of each weak acid on the protein [32].

The strength of molecules to dissociate (the negative logarithm of the acid dissociation constant of a weak acid) is known as pKa.

$$pK_a = -\log K_a \qquad \textbf{Equation 3-1}$$

A convenient way of expressing the relative strength of an acid is by its pKa value, which presents a simple way to see small changes in pKa associated with large variations in Ka. Small values of pKa equal large values of Ka (dissociation constant) and, as the pKa decreases, the acid strength increases. An acid will be stronger the lower its pKa; and the reverse applies to base-- the stronger the base, the higher its value of pKa. These dissociation constants nevertheless depend on other variables. For example, the dissociation constant changes at different temperatures. However, it maintains its value at the same temperature, despite changes in the concentration of any species or even in front of the action of a catalyst [32].

In defining the pH-dependent characteristics of a protein, pKa values of amino acid side chains play an important role. The pH-dependence of the activity displayed by enzymes and the pH-dependence of protein stability, for example, are properties that are determined by the pKa values of amino acid side chains. The pKa values of an amino acid side chain in solution is typically inferred from the pKa values of model compounds (compounds that are similar to the side chains of amino acids). The $pK_a$ values of all amino acid side chains are calculated and available [33].

When a protein folds, the titratable amino acids in the protein are transferred from a solution-like environment to an environment determined by the 3-dimensional structure of the protein. For example, in an unfolded protein an aspartic acid typically is in an environment which exposes the titratable side chain to water. When the protein folds the aspartic acid could find itself buried deep in the protein interior with no exposure to solvent. Furthermore, in the folded protein the aspartic acid will be closer to other titratable groups in the protein and will also interact with permanent charges (e.g. ions) and dipoles in the protein. All of these effects alter the $pK_a$ value of the amino acid side chain, and $pK_a$ calculation methods generally calculate the effect of the protein environment on the model $pK_a$ value of an amino acid side chain [34-37].

Due to the fact that short peptides lack secondary and tertiary structures, they don't have the ability to fold, so all the amino acid side chains are exposed to the environment. Therefore, the calculation of the $pK_a$ of an oligopeptide can be done directly using the tabulated values as is shown in section 3.3.2.1.

### 3.1.4. Adsorption of biomolecules on biomaterial surfaces

Adsorption is a process by which atoms, ions or molecules are trapped or retained on the surface of an adsorbent [38]. Adsorption can be classified into two types:

- Physisorption: Physisorption is the simplest form of adsorption, and is due to weak attractive forces, generally Van der Waals forces. Since these forces are ubiquitous, any clean surface exposed to the atmosphere quickly acquires a layer of physisorbed material.
- Chemisorption: Chemisorption occurs when a chemical bond, defined here as an exchange of electrons, is formed. The degree of exchange and its symmetry depend on the materials involved.

Moreover, protein adsorption is the first step in the acute biological response to artificial materials. Furthermore, it is widely held that adsorbed protein catalyzes, mediates, or moderates subsequent biochemical reactions having an effect on biocompatibility [39-41]. From this assumption, one can deduce the paramount importance of understanding protein adsorption phenomena concerning prospective biomaterials design for advanced medical devices. As a matter of fact, there is a vast ocean of literature on the subject of protein adsorption [2,8,10-15,18,42,43]. On the other hand, there is almost no available literature regarding the adsorption of short peptides on biomaterials surfaces [1,3-5,9,16]. In fact, to our knowledge the protein adsorption phenomena on peptide-biofunctionalized surfaces has been studied yet.

### 3.1.5. Covalent interactions between a surface and a biomolecule

In the previous section the term adsorption was defined, and it was classified into physisorption and chemisorption. When chemisorption occurs, a chemical bond between the surface and the target biomolecule is generated. In most cases the chemical bond is covalent. As mentioned in section 3.1.1, a covalent bond is the preferred strategy to immobilize biomolecules on biomaterials surfaces due to the strength and long-term stability of the bond. Several covalent immobilization techniques have been developed in order to obtain peptide functionalized surfaces [19,20,22-24,44,45].

To reach a covalent bond between a surface and a biomolecule it is necessary that both surface and biomolecule contain functional groups able to react with each other in order to generate a

covalent bond. Figure 3-2 shows some examples of covalent interaction between surfaces and biomolecules.

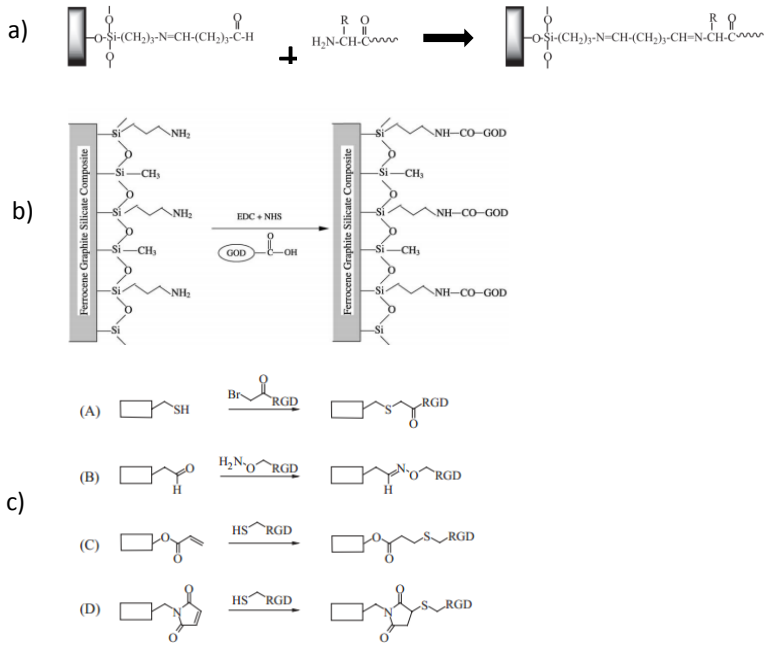


***Figure 3-2**: Some examples of covalent immobilization approaches of oligopeptides on surfaces. a) Covalent immobilization of adhesion peptides on a glass surface [46] b) Reaction scheme for the fabrication of the carbon sol–gel silicate composite electrode/biosensor [47] c) Chemoselective ligation of selected pairs of functional groups.(A) Thiol and bromoacetyl-RGD. (B) Aldehyde and aminooxy-RGD. (C) Acrylate and thiol-RGD. (D) Maleinimide and thiol-RGD [48].*

## 3.2. Objectives

The aim of this chapter is to test the following hypothesis:

Regarding biofunctionalization of titanium surfaces, when the surface charge is opposite to the peptide net charge the amount of immobilized molecule is higher and more homogeneously distributed than when the difference between both charges null or when the charge have the same sign.

Additionally, we wanted to know whether the differences in net charge between surface and peptide could affect the possibility of generating a covalent bond between the surface and the peptide.

To accomplish the primary objectives of this chapter it was necessary to design and produce fluorescent peptides to be tested. Therefore, a secondary objective of this work was to develop and set up a methodology to synthesize peptides by solid phase peptide synthesis and label them with fluorescent probes. These procedures were never performed in our laboratory before, so it was a challenging activity.

# 3.3. Experimental design

To accomplish the primary objective of this work we decided to generate titanium surfaces with different surface electric charges on the one hand, and peptides with different net charge on the other. Once this was achieved, the next goal was to expose the different peptides to the different surfaces in order to measure their level of interaction.

## 3.3.1. Titanium surfaces

The design of the different titanium surfaces was not a trivial matter since, in addition to the accomplishment of a different charge on each surface, we wanted to evaluate the possibility of a covalent interaction between surface and peptide. Therefore, we decided to make use of the knowledge obtained about silanization from the work developed and set out in chapter 2 of this thesis, and thus create 4 different titanium surfaces in which 2 of them would be able to covalently interact with primary amines and 2 of them would not.

- Polished titanium treated with NaOH at 60 $^{o}$C for 24 hours
- Polished titanium treated with NaOH and silanized with 3-aminopropyltriethoxysilane (APTES)
- Polished titanium treated with NaOH and silanized with 3-chloropropyltriethoxysilane (CPTES)
- Polished titanium treated with NaOH and silanized with APTES and crosslinked with malonic acid.

The two first surfaces mentioned are not able to covalently interact with primary amines while the two last surfaces are.

### 3.3.2. Peptides

Due to the necessities of the study, the testing peptides would need to meet several requirements:

- The peptides would need to be manufacturable
- The different peptides would need to have remarkably different net charges
- The amount of peptide on the surface would need to be measurable
- The peptides would require having a free amino group to be able to covalently interact with the surfaces that had this possibility.

To fulfil the first requirement it was decided to generate 2 different short peptides containing less than 10 amino acids and to produce them by solid phase peptide synthesis (SPPS).

The second requirement would be fulfilled generating peptides which would have opposite net charge and, therefore, containing different amino acids with polar side chains.

The third requirement would be solved by attaching a fluorescent probe to the amino-terminus of the peptide. This would let to study the titanium surfaces by fluorescent microscopy and measure the amount of attached peptide by spectrofluorophotometry. To avoid the possibility that the charge of the fluorescent probe would affect to the overall charge of the peptide it was decided to use dansyl [49], which has a null net charge at mild pH values and emits light when it is excited with ultraviolet light.

Since the designed peptide hadn't N-terminus due to the fluorescent molecule attached to it, it was decided to add a lysine in both peptides in order to have a free amino group which could covalently interact with the different surfaces.

Finally, the two different peptides designed are presented next:

- Positive peptide containing the next amino acid sequence: $NH_2$-RRRRRK-OH with a dansyl molecule attached to its N-terminus.
- Negative peptide containing the next amino acid sequence: $NH_2$-DDDDDK-OH with a dansyl molecule attached to its N-terminus.

#### 3.3.2.1. Peptide net charge

To calculate the net charge of the synthesized peptides, the Henderson–Hasselbalch equation (equation 3-2) was used [50,51]:

$$Z = \sum_i N_i \frac{10^{pKa_i}}{10^{pH}+10^{pKa_i}} - \sum_j N_j \frac{10^{pH}}{10^{pH}+10^{pKaj}} \qquad \textbf{Equation 3-2}$$

where Z is the net charge at a certain pH, $N_i$ and $pK_{ai}$ are the number and pKa value of the each side chains of arginines and lysines as well as the N-terminus in the peptide. $N_j$ and $pK_{aj}$ are the number and pKa value of the each side chains of aspartic acid amino acids as well as the C-terminus in the peptide. The $pK_a$ values for the C and N terminus and the amino acid side chains where the following:

***Table 3-1:*** *$pK_a$ values used in equation 3-5 [52]*

| | **$pK_a$** |
|---|---|
| **N-Terminus** | 9.69 |
| **Lysine** | 10.5 |
| **Arginine** | 12.4 |
| **C-Terminus** | 2.34 |
| **Aspartic acid** | 3.86 |

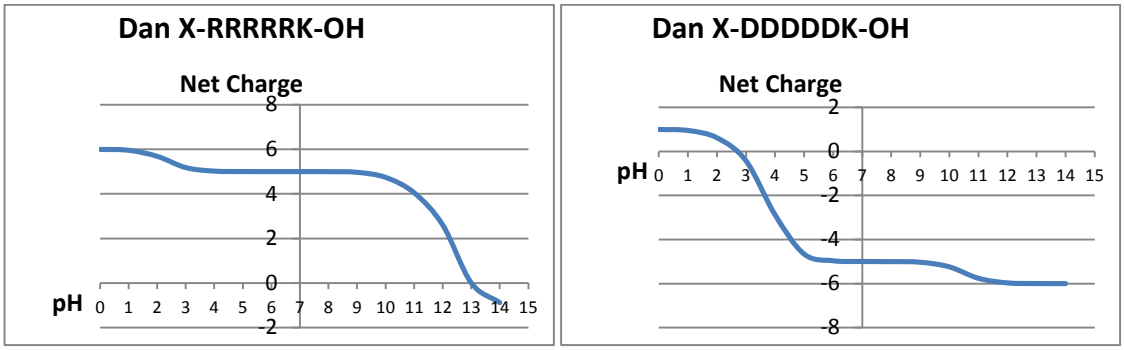


***Figure 3-3**: Titration curves of the net charge of the fabricated peptides*

Figure 3-3 shows the net charge of the two peptides at different pHs. As designed, at pH 7.4 the two peptides have opposite charge, being +5 for the Dan X-RRRRRK peptide and -5 for the Dan X-DDDDDK peptide. Table 3-2 summarizes the charges of the peptides at pH 7.4 and their isoelectric points. Dansyl X fluorescent label was selected to label the peptide because it doesn´t modify the charge of the peptides since it doesn't have any polar group in its molecular structure.

***Table 3-2:** Peptide properties of the fabricated peptides.*

| Peptide | Molecular Weight (g/mol) | Isoelectric point (pH) | Charge at pH 7.4 |
|---|---|---|---|
| **Dan X-RRRRRK** | 1273.6 | 13 | +5 |
| **Dan X-DDDDDK** | 1068.1 | 2.68 | -5 |

A last experiment to evaluate the competitive behaviour of both peptides for the different surfaces would consist on mixing both peptides and make them interact with the four different titanium surfaces. In order to evaluate both peptides separately it would be needed to label each of the two peptides with a different fluorescent probe which would make them to emit light at different wavelengths of the visible spectrum. Therefore it was decided to prepare another batch of the $NH_2$-DDDDDK-OH peptide and label it with rhodamine which emits light when it is exposed to wavelengths around 575 nm.

# 3.4. Materials and Methods

## 3.4.1. Materials

### 3.4.1.1. Base material

The base material for the experiments was c.p. grade 2 titanium bars from Daido Steel Co. (Japan). The chemical compounds to perform the NaOH treatment on the titanium surfaces was sodium hydroxide in the form of pellets from Sigma-Aldrich (USA). To wash the titanium samples we used 96%ethanol, acetone PAI-ACS, Panreac (Spain), Milli-Q Water, Millipore (USA), 99% 2-propanol and 99.5% cyclohexane anhydrous from Sigma-Aldrich (USA).

### 3.4.1.2. Solid phase peptide synthesis

The synthesis of the two peptides used in this study was a complex process in which many chemical compounds were involved in order to accomplish all the steps of the synthesis. A list of the materials used to fabricate the peptides is shown below. The description of the solid phase synthesis process can be found in section 3.4.2.2.1.

- Resin support
    - Wang Resin (100-200 mesh) 0.9 mmol/g, NovaBioChem, EMD group (USA)
- Coupling reagents
    - 2-(1H-Benzotriazole-1-yl)-1,1,3,3-tetramethyluronium hexafluorophosphate (HBTU), NovaBioChem, EMD group (USA)
    - *N,N'*-Diisopropylcarbodiimide (DIC), Sigma-Aldrich (USA)
    - 1-Hydroxybenzotriazole hydrate (HOBt), Sigma-Aldrich (USA)
- Acylating Reagent
    - 4-(Dimethylamino)pyridine (DMAP), Sigma-Aldrich (USA)

- Bases
    - *N*,*N*-Diisopropylethylamine (DIEA), Sigma-Aldrich (USA)
    - Piperidine, Sigma-Aldrich (USA)
    - Pyridine, Sigma-aldrich (USA)
- Acids
    - Acetic anhydride, Sigma-Aldrich (USA)
- Solvent
    - *N,N*-Dimethylformamide, Sigma-Aldrich (USA)
- Swelling solution
    - Dichloromethane (DCM), Merck-Millipore (USA)
- Aminoacid building blocks
    - N-α-Fmoc-N-ε-4-methyltrityl-L-*lysine* or Fmoc-Lys(Mtt)-OH, NovaBioChem, EMD Group (USA)
    - N-α-Fmoc-$N^G$-(2,2,4,6,7-pentamethyldihydrobenzofuran-5-sulfonyl)-L-arginine or Fmoc-Arg(Pbf)-OH, NovaBioChem, EMD Group (USA)
    - N-α-*Fmoc*-L-*aspartic acid* β-t.-butyl ester or Fmoc-Asp(OtBu)-OH, NovaBioChrm, EMD group (USA)
- Cleavage reagents
    - Trifluoroacetic acid (TFA) Sigma-Aldrich (USA)
    - Milli-Q water
    - Phenol, Sigma-Aldrich (USA)
    - Triisopropylsilane (TIPS), Sigma-Aldrich (USA)
- Separation reagent
    - Diethyl ether, Sigma-Aldrich (USA)
- Dialysis material
    - Cellulose acetate membrane, MWCO 1000 Da, Sigma-Aldrich (USA)
    - Biodialyser®, Sigma-Aldrich (USA)
- Fluorescent probes
    - Dansyl X-acid, Anaspec (USA)
    - 5 (and -6) Carboxy X rhodamine (ROX), Anaspec (USA)

## 3.4.2. Methods

### 3.4.2.1. Base material preparation

The titanium samples were cut from a titanium bar, grinded, polished and washed as is explained in section 2.4.1.2.

### 3.4.2.2. Solid phase peptide synthesis

Solid phase peptide synthesis (SPPS) is a chemical procedure that consists of producing peptides using a solid support, usually a polymeric resin [53,54]. The solid support contains functional groups on its surface able to react with the first amino acid of the peptide chain. The subsequent amino acids of the peptide chain are then linked, one by one, by amide bonds, also referred to as peptide bonds [32].

SPPS was developed by Merrifield in 1963 [55] and is currently the main method for synthesizing short peptide sequences for research and pharmaceutical industry. This method has overtaken the classical liquid phase synthesis due to its simplicity and effectiveness in separating the peptide under construction from the residual compounds after each chemical reaction. Moreover, SPPS can be performed manually or automatized using peptide synthesizers programmed to carry out the repetitive steps in the synthesis of a peptide [56], allowing syntheses to be performed in a matter of hours under favorable circumstances.

The development of the chemistry involved in SPPS has been intense. Most of the reactions take place repetitively and the use of the newest developed chemicals generates reaction yields very close to 100% with minimal undesirable side effects such as racemization or amino acid deprotection. Nowadays, a myriad of coupling reagents, amino acid blocks and pretreated resin supports can be purchased at a reasonable cost [57].

#### *3.4.2.2.1. Solid-Phase peptide synthesis procedure*

In SPPS the synthesis of a peptide starts with a polymeric resin which acts as support for the peptide under construction. These supports are insoluble resins that swell in the solvents used, forming open gel systems in which peptide synthesis takes place.

The amino acids used to construct the peptide need to be protected at its $N^{\alpha}$-terminus and at its side chain if necessary. The protection of the $N^{\alpha}$-terminus prevents the polymerization of the peptide in solution, away from the resin. The protection of the side chain prevents undesired reactions between the amino acid reactive residues and other compounds involved in the synthesis. Usually, non-reactive side chains don't need to be protected.

- In the first step of the synthesis, the first (C-terminus) amino acid of the peptide to be synthesized is anchored chemically, either by the formation of an ester or an amide bond, to the resin, typically a copolymer of styrene and 1% divinylbenzene.

- Once the coupling of the first amino acid is completed, the resin is washed, eliminating the excess amino acids and the other chemicals used to catalyze the coupling reaction.

- Then, the $N^{\alpha}$-terminus of the coupled amino acid is deprotected. The deprotection will permit, in the subsequent step, the reaction between the $N^{\alpha}$-terminus of the first amino acid and the carboxylate of the second amino acid, creating an amide bond.

- After washing the resin again to eliminate the deprotection solution and by-products, the resin is swelled in a new solution containing the second amino acid, protected at its $N^{\alpha}$-terminus and its side chain if necessary. Then, the reaction between the first and the second amino acids takes place until it is completed.

- Subsequently, the deprotection and coupling reactions are repeated for each amino acid of the chain in the desired order.

In this way, the desired peptide chain is built up on the support in a linear fashion, almost always from the C-terminus to the N-terminus. Since the resin is washed in each step of the process, thereby eliminating excess reagents and by-products, large excesses of the soluble $N^{\alpha}$-urethane-protected amino acids can be used in order to drive the coupling reaction to completion with very high coupling yields and short times.

After each deprotection and coupling step it is recommendable to check whether the deprotection or the coupling reaction has been completed. There are some tests to discern this. The most popular is the Kaiser's test or Ninhydrin test [58], a simple, fast and inexpensive colorimetric test that reveals whether free amino groups exist in the solution or on a surface.

When the peptide chain has been synthesized, the peptide must be separated from the solid support. Cleavage of the peptide from the resin is usually brought about by acidolysis with a strong acid, often trifluoroacetic acid. This also removes all the amino acid-protecting groups at the same time, affording the crude free peptide that is subsequently purified. A scheme of the SPPS process is shown in figure 3-4.

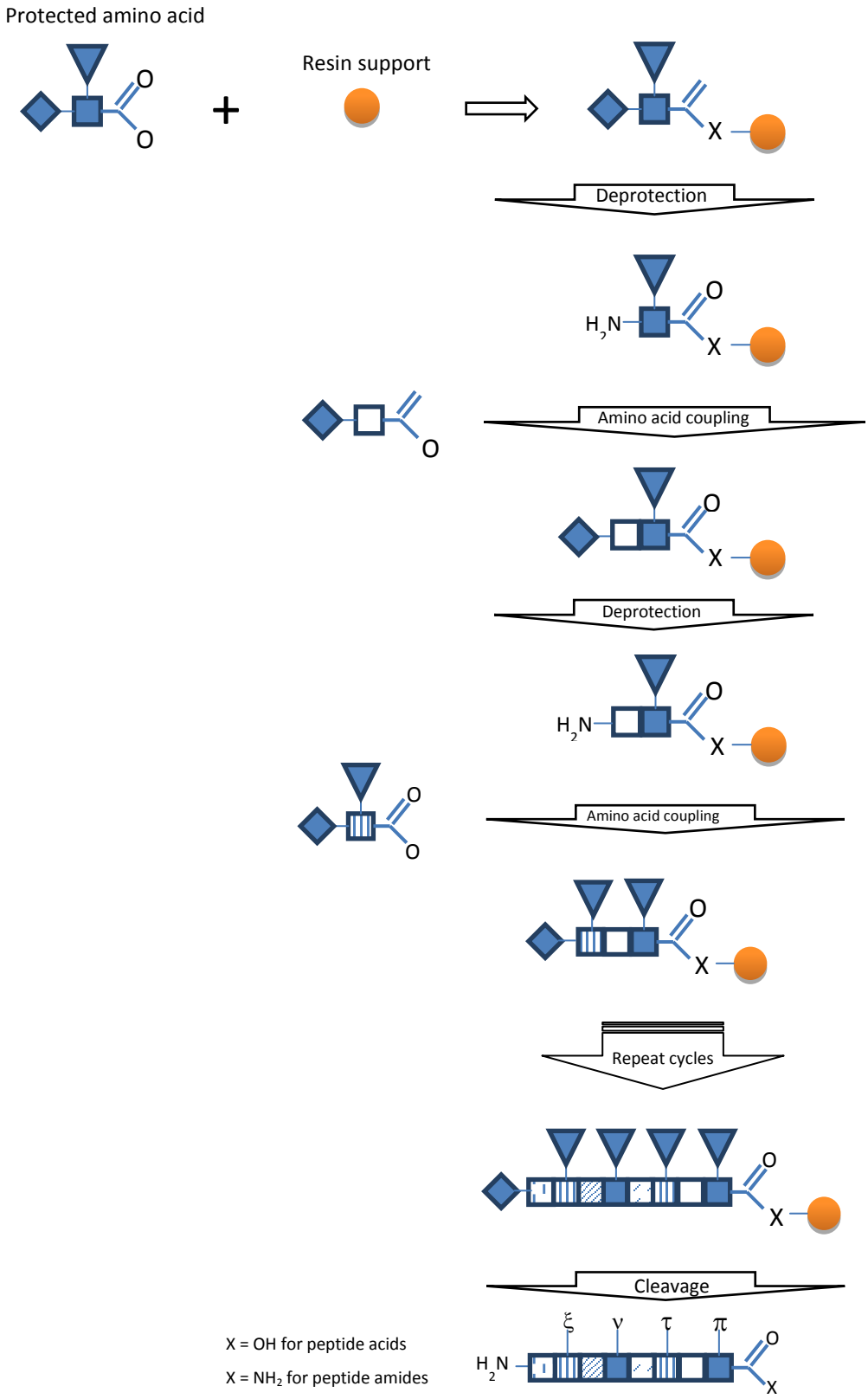


***Figure 3-4**: Linear SPPS. Amino acids are represented by squares, the protected α-amino group by a diamond, and the protected side chains functional groups by triangles and the deprotected ones by Greek characters. The C-terminus of the peptide is bound to a solid support. Scheme based on [54].*

#### *3.4.2.2.2. Fmoc synthesis*

In SPPS, $N^{\alpha}$ protection is almost always either the Boc [59] group or the Fmoc [60] group (figure 3-5). The main difference of Boc and Fmoc protecting groups is its lability; i.e., deprotecting a Boc-protected amino acid requires the use of a strong acid, such as 33% trifluoroacetic acid in dichloromethane, while Fmoc-protected amino acids can be deprotected in milder conditions, using 20% piperidine in dimethylformamide.

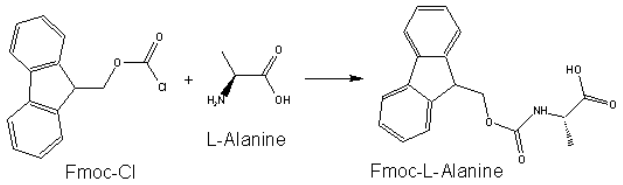


*Figure 3-5: Reaction between the Fmoc-Cl and L-Alanine to protect the $N^{\alpha}$ group of the amino acid. Drawings performed with Chemdraw ®.*

The use of hazardous trifluoroacetic acid in the synthesis of peptides requires greater care in carrying out the process both when it is manually performed and machine-assisted, and it also calls for the use of acid resistant materials. For this reason, Fmoc-protected amino acids were selected for the synthesis of the peptides in this thesis. Figure 3-6 illustrates the reaction involved in the removal of the Fmoc group with piperidine.

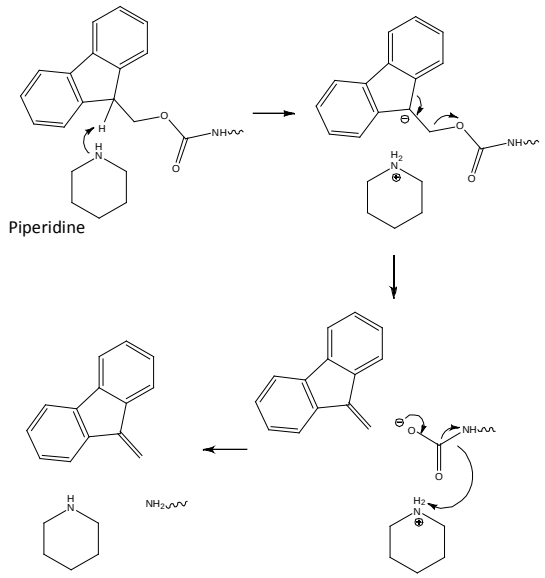


*Figure 3-6: Fmoc group deprotection with piperidine.*

*3.4.2.2.3. Methodology for the synthesis of Dansyl X-DDDDDK-OH and Dansyl X-RRRRRK-OH peptides*

The synthetized peptides were the following:

- Dansyl X-DDDDDK-OH
- Dansyl X-RRRRRK-OH
- ROX-DDDDDK-OH

The peptides were synthetized by SPPS Fmoc Synthesis. Below, a detailed description of the synthesis of the two peptides is shown:

The synthesis of the two peptides was done simultaneously using an Endeavor 90 peptide synthesizer, aapptec (USA). The endeavor 90 disposes of two separate reaction vessels to prepare two peptides at the same time, both of which are controlled by the SPPS aapptec software.

Step 1.- The resin used as solid support was the Wang resin [61] (figure 3-7). The Wang resin grants the securing of peptide acids with a free carboxylate at the C-terminus of the peptide after cleavage, ensuring the predesigned peptides are achieved. 50 mg of Wang Resin were introduced in each reaction vessel and were swelled with 10 ml of DCM/DMF 9:1 v/v for 10 minutes, twice.

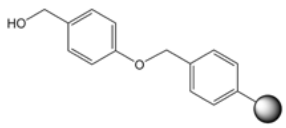


*Figure 3-7: Chemical scheme for Wang resin support.*

Step 2.- The first amino acid, Fmoc-Lys(Mtt)-OH, of each peptide was coupled using a DIC/HOBt/DMAP mixture. 2.5 equivalents of the Fmoc amino acid, (relative to the resin), were dissolved in 2 ml of DMF. Then, the same equivalency of HOBt was added to the mixture. When HOBt dissolved, the mixture was added to the resin. Next, 0.1 equivalents of DMAP (relative to the resin) were dissolved in 1 ml of DMF. 2.5 equivalents of DIC (relative to the resin) were added to the resin and the DMAP mixture was then also added. The mixture was mechanically stirred for 3 hours at room temperature. Subsequently 2 equivalents of acetic anhydride and

pyridine (relative to the resin) were added to the mixture to cap any unreacted hydroxyl group on the resin and stirred for 45 additional minutes. Finally, the resin was filtered and washed 3 times in 6 ml of DMF, 3 times in 6 ml of DCM, 3 times in 6 ml of methanol and dried with nitrogen.

Step 3.- The de-protection of the $N^{\alpha}$-terminus of the Fmoc amino acid was performed adding 20% piperidine in DMF to the resin and agitating the vessel for 15 minutes, three times. After de-protection, the resin was washed thrice with DMF, twice with DCM and again thrice with DMF.

Step 4.- The second Fmoc amino acid (Fmoc-Arg(Pbf)-OH for the Dansyl X-RRRRRK-OH peptide and Fmoc-Asp(OtBu)-OH for the Dansyl X-DDDDDK-OH peptide) was dissolved in 4 ml of DMF at a concentration of 4 equivalents (relative to the resin). The same equivalency of HBTU was added to the Fmoc amino acid solution and when HBTU was dissolved, 400 μl of DIEA were added to the mixture and stirred until a homogeneous solution was achieved. Then, the mixture was added to the resin and mechanically stirred for 1 hour. After this time, the resin was filtered and a similar new mixture was added to the resin and stirred for 1 more hour. Then the resin was filtered and washed thrice with 6 ml of DMF.

For the coupling of the subsequent Fmoc amino acids, steps 3 and 4 were repeated until completion of the two peptides. When all the Fmoc couplings were completed, a part of the resin from the fmoc-DDDDDK-Wang peptide was extracted from the vessel and stored for the future coupling of ROX fluorophore to the peptide.

After each coupling, Kaiser tests were performed, transferring few resin beads from the reaction vessel to a small glass test tube and adding 3 drops of 80%phenol in ethanol, 3 drops of KCN in $H_2O$/pyridine and 3 drops of 6%ninhydrin in ethanol. The test tube was heated to 120$^{o}$C for 5 minutes. If the Kaiser test revealed remaining free amino groups, the coupling step was repeated. The synthesis of Dansyl X-RRRRRK was especially difficult due to esteric effects provoked by the fact that the Pbf group, in charge of protecting each of the arginine side chains, is big and rigid. For this reason the coupling of the 3 last Fmoc-arginines needed up to 16 h to be completed.

Finally, Dansyl-X acid was attached to the last amino acid of the peptide in the same fashion, using 2 equivalencies (relative to the resin) of the fluorophore on each peptide during 16 hours. Due to the coupling of the Dansyl fluorophore at the N-terminus of the peptide, the developed peptides don´t have a free amino group at the N-terminus. The only free amino group in the two peptides belongs to the Lysine residue of the last amino acid. To generate the ROX-DDDDDK-OH peptide, the previously stored resin was treated in the same fashion substituting Dansyl X, acid for the ROX fluorophore.

Cleavage and side chain deprotection of the peptide was performed using 50%TFA/10%$H_2O$/5%phenol/5%TIPS in DCM for 3 hours with gentle agitation.

The peptides were precipitated using ice-cold Diethyl ether and dried overnight. Subsequently, the peptides were dissolved in 1 ml of $H_2O$ and dialyzed, using a 1000 Da cellulose acetate membrane at 4 $^oC$ overnight. After dialysis, the peptides were lyophilized, weighed and reconstituted in $H_2O$.

#### 3.4.2.3. Surface treatments

##### *3.4.2.3.1. Surface activation*

Titanium samples were treated with 5 M NaOH to maximize the surface index and the presence of OH groups on the surface. The activation of the samples was performed as described in section 2.4.1.3.3.

##### *3.4.2.3.2. Silanization*

After NaOH treatment some of the titanium samples were silanized with APTES in order to generate surfaces with the presence of amino groups. The silanization procedure is described in section 2.5.1.2.1.

#### *3.4.2.3.3. Cross-linking*

To generate surface with the presence of carboxylate groups, some of the APTES silanized surfaces were treated with malonic acid as described in section 2.6.1.2.

#### *3.4.2.3.4. Peptide adsorption*

The different titanium surfaces were immersed in a solution of the Dansyl X-DDDDDK-OH, Dansyl X-RRRRRK-OH or ROX-DDDDDK-OH peptide of 100 μmol/ml of peptide in PBS at a pH of 7.4. The samples were left in the peptide solution overnight with gentle agitation. After peptide adsorption, the titanium samples were washed with ethanol, isopropanol, water, acetone and dried with nitrogen.

### 3.4.2.4. Characterization techniques

#### *3.4.2.4.1. Surface charge*

The surface charge of the different titanium surfaces was determined by means of ζ potential measurements. A description of the ζ potential technique can be found in Annex A of this thesis in electronic format.

A commercial streaming potential instrument is available which has been used for all the measurements reported (SurPASS Electrokinetic Analyzer for solid surface analysis, Anton Paar, Austria). This apparatus includes an integrated titration unit which gives automated measurement series of varied solution compositions.

The ζ potential measurements were carried out with 1mM KCl-solution as the electrolyte and 0,1 M HCl as the titration liquid. The pressure ramp was run to a maximum pressure of 400 mbar. The electrolyte solution was adjusted to pH 3.0 with 0,1 M HCl followed by automatic titration to pH 9.5 with 0,1 M KOH. All electrolyte solutions (potassium chloride, potassium hydroxide and hydrochloric acid) were prepared using deionized water.

To obtain the ζ potential for our surfaces, a symmetric clamping cell has been used. A photographic representation of the symmetric adjustable gap cell is shown in figure 3-8-a. The adjustable gap cell has two cavities to place two samples holders in opposing positions. On each of the two sample holders (Figure 3-8-b), a rectangular titanium sample was adhered. Then, the two sample holders were fixed in the adjustable gap cell with two nuts for the adjustment of the gap between the two samples (figure 3-8-c). Once the adjustable gap cell was assembled, it was mounted on the SurPASS analyzer (figure 3-8-d) and the experiment started.

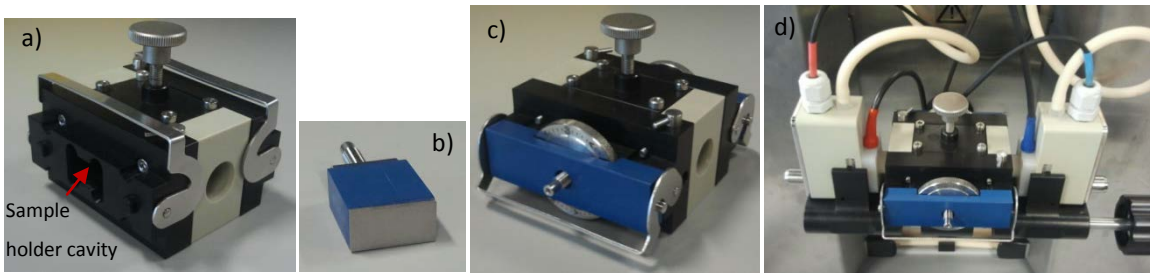


***Figure 3-8**: a) SurPASS adjustable gap cell. b)Sample holder with a titanium sample. c) assembled adjustable gap cell. d) adjustable gap cell mounted on the SurPASS.*

Streaming potential measurements with the symmetric cell were taken eight times at each pH, with alternating flow direction of the solution (i.e., 4 measurements in each direction).

After loading the sample in the symmetric cell, the entire system was flushed thoroughly with deionized water for 20 min. Following the deionized water rinse, the streaming potential analyzer system and measuring cell were flushed with the electrolyte solution (1mM KCl) for 30 min. This time was sufficient to completely displace deionized water in the system tubing. Once thoroughly flushed, the electrolyte solution was recirculated through the cell for 4 h. The system was equilibrated and the pH adjustment prior to the subsequent streaming potential measurement was done. All electrokinetic experiments were performed at room temperature.

3.4.2.4.1.1. Streaming Potential

Streaming potential occurs when counter-ion displacement caused by hydrodynamic flow along a charged surface is balanced by the reverse conduction current developed due to the potential difference appearing along the liquid stream. In fact, the solid sample is mounted between two electrodes for detection of the potential difference. The liquid phase, which is an aqueous electrolyte solution, is pumped through this measuring cell, thereby generating a pressure difference across the sample plug. The differential pressure causes a relative movement of the charges in the electrochemical double layer, and the streaming potential can be obtained by measuring the resulting electrical potential with electrodes in the bulk electrolyte solution [62].

The relation between streaming potential and ζ potential was first derived by Smoluchowski [63,64]:

$$\zeta = \frac{dU}{dp} \times \frac{\eta}{\varepsilon \times \varepsilon_0} \times \frac{L}{Q \times R} \qquad \textbf{Equation 3-3}$$

where dU/dp is the slope of streaming potential versus pressure, $\eta$ is the viscosity of the electrolyte solution, $\varepsilon$ is the dielectric constant of the electrolyte solution, $\varepsilon_0$ is the vacuum permittivity, L and Q are dimensions of the fluid flow and R is the cell resistance.

Thus, ζ potential is not only determined by the nature and charge of the solid surface but also by the properties of the electrolyte solution. Since it is impossible to determine the geometry of the fluid flow at the solid interface, the Smoluchowski equation needs some modification to be applicable in practice. Fairbrother and Mastin [65] developed an approach in 1924, the surface conductivity correction, which is still accepted [66] . By introducing the conductivity of the electrolyte solution, the geometric factor of the sample may be eliminated. The electrical conductivity is then experimentally accessible.

3.4.2.4.1.2. Surface conductivity correction

At high electrolyte concentration the contribution of surface conductivity to the overall conductivity decreases until it becomes negligible. In our work a dilute solution has been used for the measurements, and then a surface conductivity correction has been performed.

The surface conductivity is the excess electrical conductivity tangential to a charged surface compared to the conductivity of the bulk electrolyte. The influence of surface conduction on the zeta potential should be considered for samples with sufficiently high conductive surfaces or samples that exhibit a strong swelling of the surface. To obtain the surface conductivity correction, the electrolyte solution used for the measurement of the streaming potential is replaced by a 0,1 M KCl solution. Due to the high electrical conductivity of such a concentrated solution, the surface conductivity may be neglected. The conductivity of the 0,1 M KCl solution is available from the literature data.

With this method of surface conductivity correction, zeta potential is determined from streaming potential measurement by introducing this term in the Smoluchowski equation:

$$\zeta = \frac{dU}{dp} \times \frac{\eta}{\varepsilon \times \varepsilon_0} \times k_{corr} \qquad \textbf{Equation 3-4}$$

$$k_{corr} = \frac{R_{0.1M\ KCl} \times K_{0.1M\ KCl}}{R_{0.001M\ KCl}} \qquad \textbf{Equation 3-5}$$

where $K_{0.1M\ KCl}$ and $R_{0.1M\ KCl}$ are the specific electrical conductivity and cell resistance using 0.1 M KCl solution.

#### *3.4.2.4.2. Quantification of peptides on a surface*

##### 3.4.2.4.2.1. Fluorescence microscopy

The quantification of the fluorescence intensity of the different titanium surfaces covered by fluorescent peptides was performed in the same fashion as explained in section 2.4.1.4.3. In this case, the micrographs were taken exposing the samples to ultraviolet light (wavelengths between 300 and 400 nm) since dansyl X probe has an excitation wavelength of 333 nm.

##### 3.4.2.4.2.2. Spectrofluorophotometry

To quantify the amount of peptide present on the different titanium surfaces it was previously necessary to extract the totality of the peptides from the surfaces. It was done by immersing the samples in a solution of NaOH 0.1 mol/l and leaving them to sonicate for a minimum of 3 hours. To check if the peptides were totally released from the surface, the titanium samples were analyzed by fluorescence microscopy. If the samples emitted fluorescence, it meant that an amount of peptide remained on the surface. Then, the surfaces were sonicated for a longer time in the same NaOH solution until no fluorescence was detected by fluorescence microscopy [67-70].

Following the sonication, the NaOH solutions of each sample, now with the fluorescence peptide, were collected and analyzed by spectrofluorophotometry [68,69] using an Infinite® 200 pro NanoQuant Microplate reader (Tecan, Switzerland). The excitation and emission wavelengths were set at 333 and 518 nm respectively according to the excitation and emission wavelengths of the dansyl X probe.

#### *3.4.2.4.3. Adsorption and chemical bond*

##### 3.4.2.4.3.1. Mechanical stability test

Sonication is often used to accelerate the washing processes of surfaces [70,71]. In the functionalization field, many immobilization processes end with a sonication procedure to remove from the surface loosened molecules that haven't reacted properly or have been weakly adsorbed onto the surface [72,73]. If the peptide release from the surface during sonication could be screened, we would have information about the difference between the molecules that are strongly adhered to the surface and the ones that are just weakly adsorbed on it.

To screen the release of the peptide from the different titanium surfaces, an experiment was set up. First the different titanium samples covered with the two fluorescent peptides were immersed in deionized water and sonicated for 1 hour. After sonication, fluorescence micrographs were taken and the fluorescence intensity measured as described in section 2.4.1.4.4. Then, the samples were immersed again in deionized water and sonicated for another hour. Then, micrographs of the same samples were taken again using exactly the same microscopy parameters in order to make the micrographs comparable. This process was repeated for a total amount of 5 hours of sonication.

##### 3.4.2.4.3.2. X-Ray photoelectron spectroscopy

The different titanium samples covered with both peptides separately were analyzed by XPS as described in section 2.4.1.4.3.1. The samples were prepared and analyzed at the same time as the samples analyzed in chapter 2. This makes the comparative work between surfaces with and without peptide on the surface more reliable.

Since the XPS analysis was meant to determine whether a covalent bond was developed between the peptides and titanium surfaces, prior to analysis the samples were sonicated in deionized water for 2 hours in order to release loosly attached peptides from the surface.

#### *3.4.2.4.1. Competitive adsorption*

The different titanium surfaces where immersed in a mixture of 1:1 molar of Dansyl X-RRRRRK-OH and ROX-DDDDDK-OH peptides overnight, washed with ethanol, isopropanol, water, acetone and dried with nitrogen. For the characterization of competitive adsorption fluorescence micrographs were taken, after the mentioned treatment. The fluorescence micrographs were obtained as described in section 2.4.1.4.4.

#### *3.4.2.4.2. Statistical analysis*

The statistical treatment of the data was performed as that described in section 2.4.1.5.

## 3.5. Results

In this section, the results about the interactions between the two oppositely charged peptides and the different titanium surfaces are shown. Apart from the samples shown in the results, plain titanium surfaces without any other treatment apart from cleaning procedures have also been tested as a control. The following graphs and tables do not show the plain titanium control samples because the results would be confusing due to surface roughness and surface indexes being significantly different from the treated samples.

### 3.5.1. Nomenclature

In order to make the results understandable and easy to follow, a nomenclature has been created. As the studied surfaces and samples are always titanium with one or more treatment on its surface, the nomenclature code is additional. That is to say, to describe a surface with various treatments, an abbreviation of all treatments performed on the surface has been added to the word Ti (Titanium) in the same order as the treatments which have been applied. Below, the abbreviation codes for every treatment are listed.

**Ti:** *Titanium.* Polished and clean titanium as described in section 3.4.2.1.

**NaOH or N:** *NaOH treatment.* Ti etched with 5M sodium hydroxide as described in section 3.4.2.3.1.

**APTES or APT:** *APTES silanized surface.* As described in section 3.4.2.3.2.

**CPTES:** *CPTES silanized surface.* As described in section 3.4.2.3.2.

**Malonic a. or Mal:** Surface treated with malonic acid as described in section 3.4.2.3.3.

**Dan X-RRRRRK (+) or RK:** *Peptide $H_2N$-RRRRRK-OH labeled with the fluorescent molecule Dansyl X, acid* at its $N^{\alpha}$-terminus *a*s described in section 3.4.2.2.3. When the peptide is present on a surface the conditions for the obtaining the coating of the peptide on the different surfaces are the ones described in section 3.4.2.3.4.

**Dan X-DDDDDK (-) or DK:** *Peptide $H_2N$-DDDDDK-OH labeled with the fluorescent molecule Dansyl X, acid* at its $N^{\alpha}$-terminus as described in section 3.4.2.2.3. When the peptide is present on a surface the coating conditions are the ones described in section 3.4.2.3.4

**ROX-DDDDDK (-):** *Peptide $H_2N$-DDDDDK-OH labeled with the fluorescent molecule -5 (and -6) Carboxy X rhodamine (ROX),* as described in section 3.4.2.2.3. When the peptide is present on a surface the coating conditions are the ones described in section 3.4.2.3.4

## 3.5.2. Surface charge

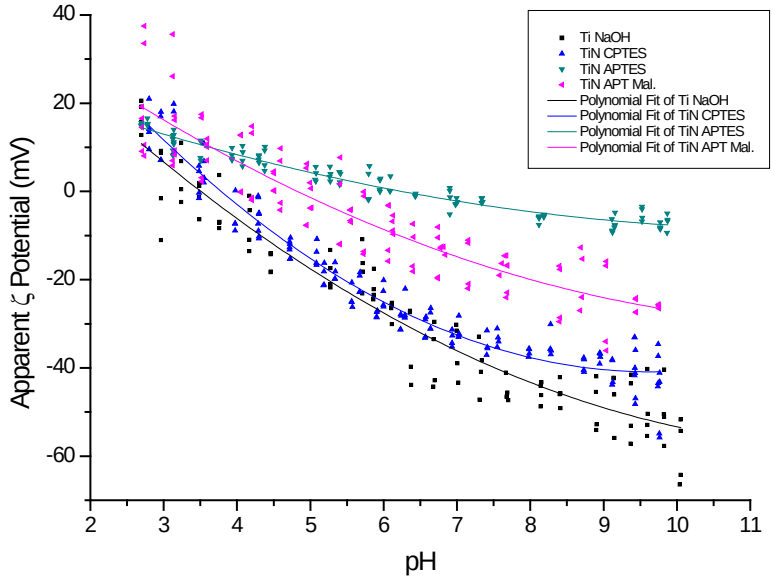


***Figure 3-9**: Titration graph of the apparent ζ potential of the 4 different surfaces studied.*

***Table 3-3** Characteristic values extracted from the ζ potential assay.*

| Surface treatment | ζ Potential at pH 7.4 | Isoelectric Point |
|---|---|---|
| TiN APTES | -3.05±1.14 | 6.24 |
| TiN APT Mal. | -10.87±9.93 | 4.82 |
| TiN CPTES | -33.81±1.43 | 3.78 |
| Ti NaOH | -38.36±3.71 | 3.51 |

Figure 3-9 shows the titration curves for the different studied surfaces. The points are the individual measured values of two replicas of each type of sample, while the lines are the polynomial fits for the values of the two replicates of each surface, fitting the two replicas together. The graph shows the apparent ζ potential depending on the pH value. The apparent ζ potential instead of the real ζ potential are shown to better compare the results obtained for the different tested surfaces.

As can be seen in table 3-3, at pH 7.4, which is the pH where the peptides were adsorbed on the different surfaces as well as the biological pH, the most electronegative sample is the surface etched with sodium hydroxide (Ti NAOH). CPTES silanized surfaces show a very

electronegative behavior too, while the least electronegative sample was the APTES silanized surface. APTES-malonic acid surfaces showed an intermediate behavior among them. The point of zero charge of the four surfaces was also different too, but the tendencies followed the ζ potential at pH 7.4, being TiN APTES surfaces the ones with the highest point of zero charge and Ti NaOH the ones with the lowest point of zero charge. It is interesting to remark that all surfaces, at pH 3, had a similar ζ potential, while the differences in ζ potential increased with pH value.

## 3.5.3. Quantification of adsorbed peptides

### 3.5.3.1. Fluorescence microscopy

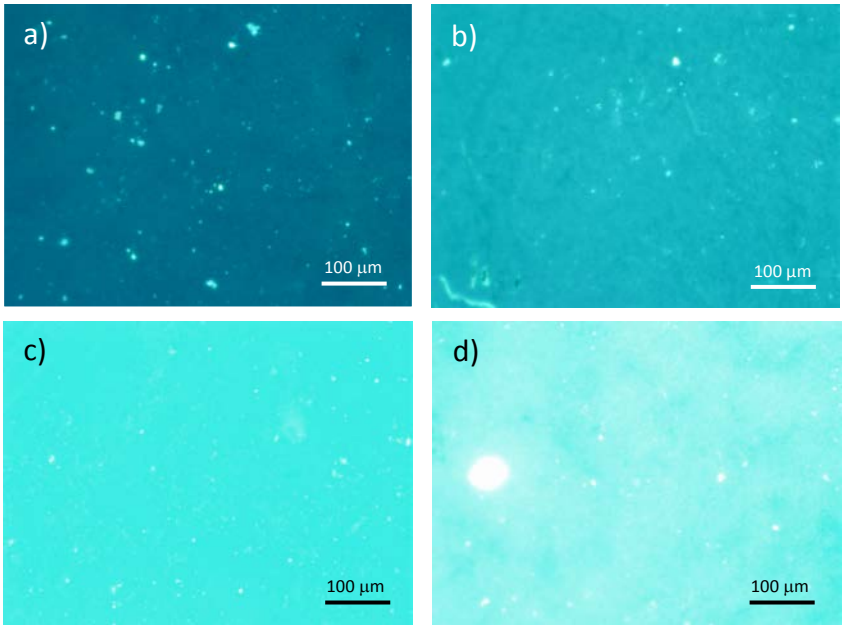


***Figure 3-10**: Fluorescence micrographs of the different surfaces coated with Dan X-RRRRRK peptide. a) TiN APTES, b) TiN APT Mal, c) TiN CPTES and d) Ti NaOH.*

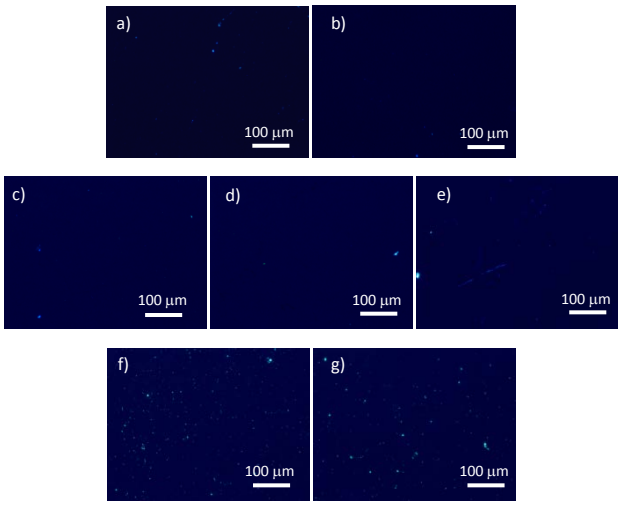


***Figure 3-11**: Fluorescence micrographs of all the control samples performed. a)Ti, b)Ti NaOH, c)TiN APTES, d)TiN CPTES, e) TiN APTES Mal, f)Ti + Dan X-DDDDDK-OH and g)Ti + Dan X-RRRRRK-OH*

Fluorescence microscopy is a qualitative technique which provides quick and useful information when surfaces have fluorescent properties. Results shown in figure 3-10 prove that a) the fluorescence intensity is significantly different between differently treated surfaces and the controls shown in figure 3-11, which validates the methodology as to compare the efficiency in peptide coatings of the surfaces; and b) a non-homogeneous adsorption of the Dan X-RRRRRK peptide was detected on all surfaces, showing some bright clusters where the intensity is higher than in the rest of the image. It is apparent that the heterogeneity increased with the amount of peptide adsorbed on the surface.

Comparing the four images shown in figure 3-10, it can be seen that there is a trend regarding the fluorescence intensity and the electronegativity of the surface. The surface with less brightness corresponds to TiN APTES which is the least electronegative of the four. Brightness on the images increases following an order corresponding to a growing electronegativity on the surfaces, being the brightest surface the most electronegative, the Ti NaOH surface.

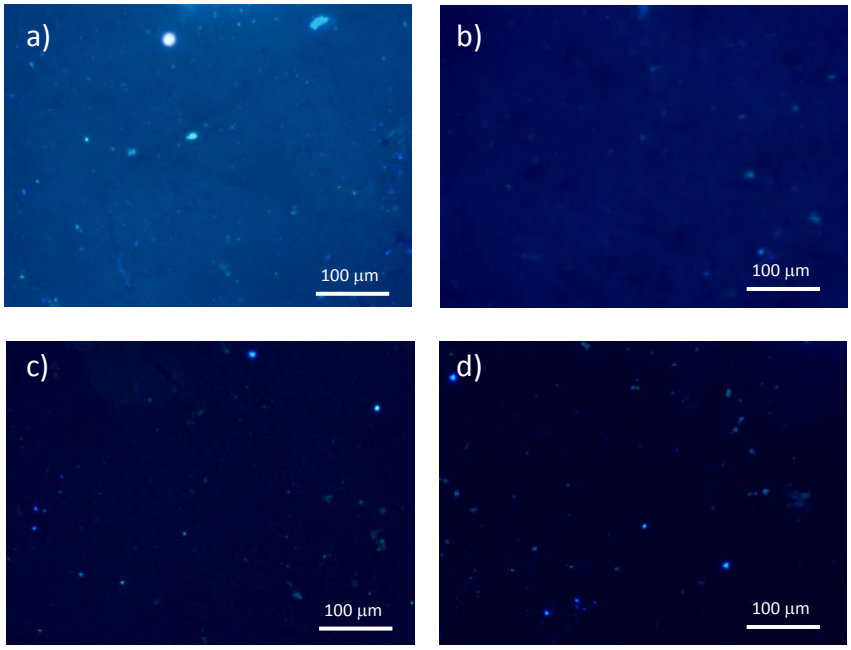


***Figure 3-12**: Fluorescence micrographs of the different surfaces coated with Dan X-DDDDDK peptide. a) TiN APTES, b) TiN APT Mal, c) TiN CPTES and d) Ti NaOH.*

The surfaces covered with Dan X-DDDDDK peptide (figure 3-12) show the opposite tendency with respect to the surfaces covered with Dan X-RRRRRK peptide in terms of fluorescence intensity. The surface with the highest fluorescence signal and thus, with the highest peptide amount was, in this case the TiN APTES surface, which is the least electro negatively charged. In general, the intensities of fluorescence of the surfaces covered with the electronegatively charged peptide were lower than the surfaces covered with the positively charged Dan X-RRRRRK peptide. Similarly to surfaces covered with Dan X-RRRRRK peptide, the surfaces with negatively charged Dan X-DDDDDK peptide showed a more heterogeneous surface coverage when the amount of peptide on the surface was increased.

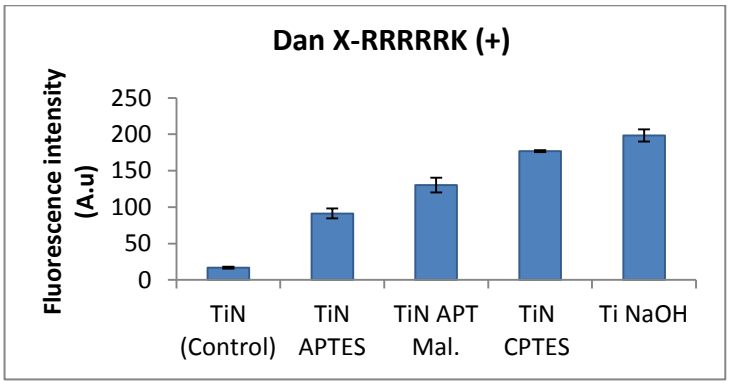


***Figure 3-13**: Fluorescence intensity values of the different surfaces treated with Dan X-RRRRRK peptide. All samples are statistically different ($\alpha$=95%).*

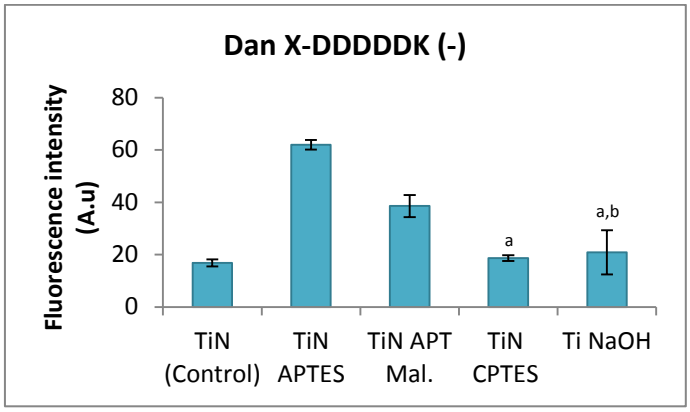


***Figure 3-14**: Fluorescence intensity values of the different surfaces treated with Dan X-DDDDDK peptide. Groups marked with same letters (a or b) were not statistically different.*

The two graphs above show the fluorescence intensity of the images taken by fluorescence microscopy. In general, the values obtained with the Dan X-RRRRRK peptide were higher than the values obtained with the Dan X-DDDDDK peptide. It is important to remark that the immobilization of the peptides was performed at pH 7.4 where all the titanium surfaces, even APTES silanized titanium, had a negative ζ potential. However, the tendency of the results with both peptides is reversed, showing the important effect that has the difference between peptide net charge and surface charge on the interaction between them.

### 3.5.3.2. Spectrofluorophotometry

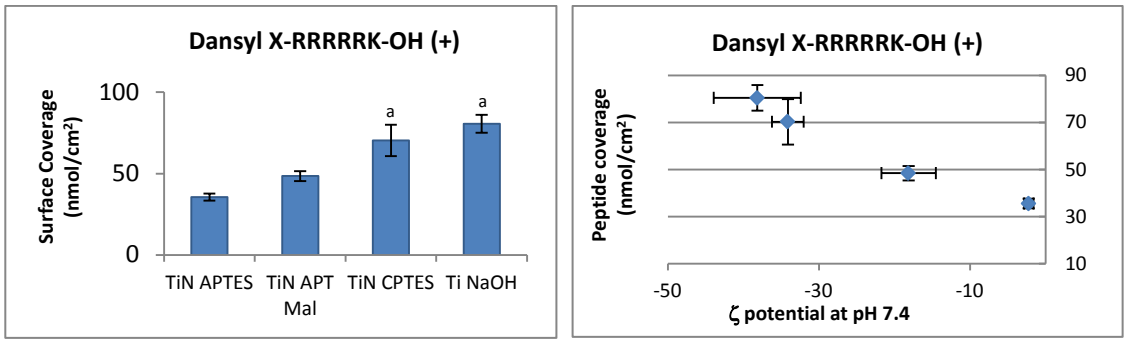


***Figure 3-15**: Left: Amount of Dan X-RRRRRK peptide present on the different titanium surfaces. Ti NaOH samples without peptides were used as background. Groups marked with same letter (a) were not statistically different. Right: Correlation between peptide coverage and ζ potential at working pH.*

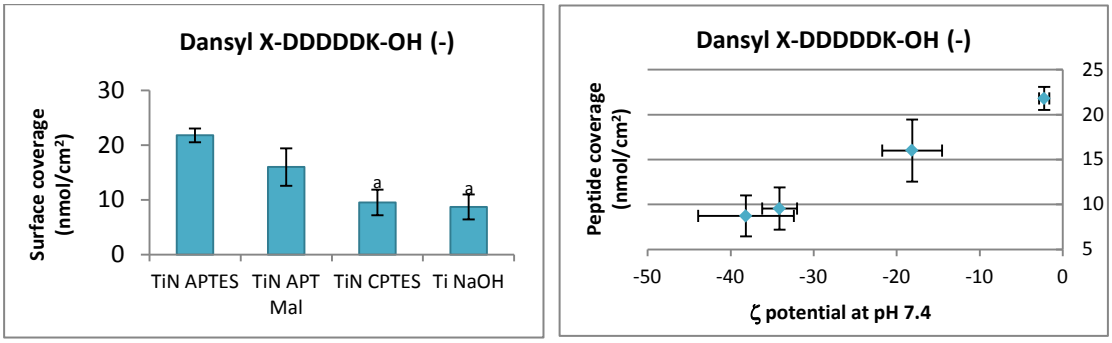


***Figure 3-16**: Left: Amount of Dan X-RRRRRK peptide present on the different titanium surfaces. Ti NaOH samples without peptides were used as background. Groups marked with same letter (a) were not statistically different. Right: Correlation between peptide coverage and ζ potential at working pH.*

The quantification of the peptide adsorbed on each studied surface and a correlation between the ζ potential of the surfaces at pH 7.4 and the amount of peptide present on each surface is shown in figure 3-15 and figure 3-16. As could be expected, the tendency was similar to the results obtained by fluorescence microscopy, although the values were not proportional between the two methodologies. This result suggests that the fluorescence intensity measured on a sample doesn´t follow a linear correlation with the peptide surface density. The surface density varied from 5 to 80 nmol/cm$^2$ among the different surfaces studied. It is worth remarking that the amount of peptide detected on all surfaces was considerably higher than the amounts of peptide reported on the literature related to biofunctionalized surfaces [74-77]. This fact is due to the high increase in surface index; i.e. real surface area generated by the etching with NaOH during the activation process, as was discussed in section 2.4.1.4.1.2. Additionally, the correlation between peptide coverage and ζ potential shows an approximately linear trend which demonstrates a dependency between both parameters.

### 3.5.4. Adsorption and chemical bonding

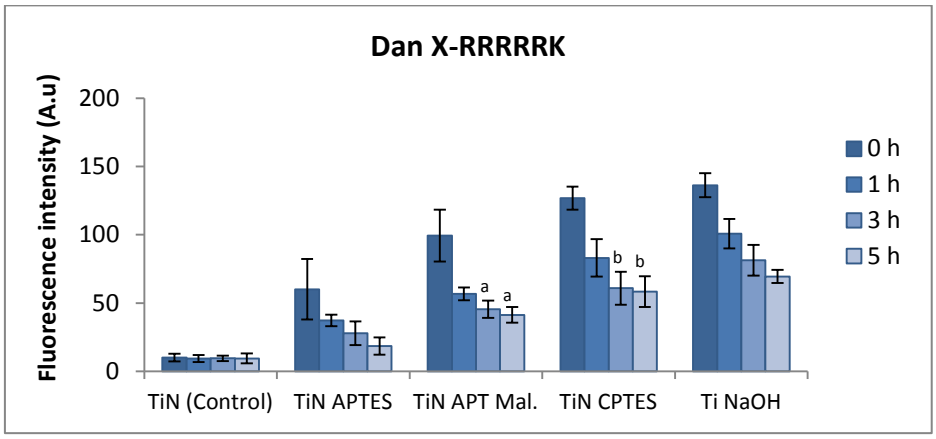


***Figure 3-17**: Mechanical stability results of the titanium samples treated with the Dan X-RRRRRK peptide. Groups marked with the same letter (a or b) were not statiscally different.*

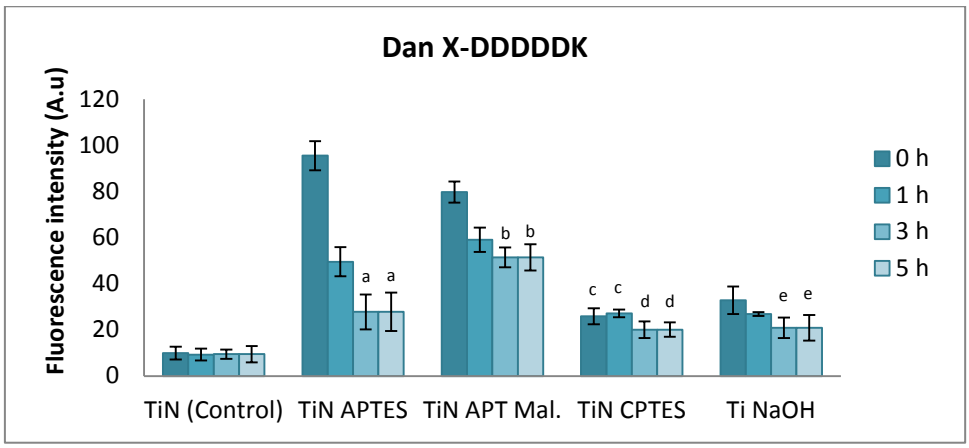


***Figure 3-18**: Mechanical stability results of the titanium samples treated with the Dan X-DDDDDK peptide. Groups marked with the same letter (a, b,c d or e) were not statiscally different.*

Figure 3-17 and figure 3-18 show the fluorescence intensities given by the titanium samples treated with Dan X-RRRRRK or Dan X-DDDDDK peptides and submitted to different sonication times in water. All the samples reduced their fluorescence intensity over sonication time. One interesting point is that, after 3h of sonication, TiN APT Mal and TiN CPTES surfaces reached a plateau of fluorescence intensity when both peptides interacted with those surfaces; i.e., those surfaces did not continue releasing peptide. This plateau is confirmed by the statistical analysis. Thus, TiN APT Mal and TiN CPTES surfaces showed themselves more mechanically stable. In the case of figure 3-18 TiN APTES and Ti NAOH surfaces showed a stable plateau. Although, this plateau was reached at very low values of fluorescence intensity near to the values observed in

the controls without peptide. Therefore, results obtained performing the interaction between the differents surfaces and the Dan X-DDDDDK peptide are inconclusive. Despite the fact that the fluorescence intensity values are not proportional to the amount of peptide present on the surface, we can see that the higher the amount of peptide initially present on each surface, the higher the amount of peptide that is released during sonication.

Despite the fact that the Ti NaOH surface can't develop a covalent bond to stabilize the peptide, it is nevertheless the sample with the highest amount of Dan X-RRRRRK peptide on its surface after 5 hours of sonication. This suggests that the electrostatic interactions might play a big role in the adsorption and retention of peptides on the treated surfaces, particularly when the difference of electrical charge between peptide and surface is very high. The significant amount of available charges in the surfaces etched with NaOH due to the high increase in surface area also might play a significant role in the big amount of peptide attracted to these surfaces.

Another point that can be observed on figure 3-18 is that the TiN CPTES and Ti NaOH surfaces, compared to the control sample without peptide, are both able to stabilize a certain amount of peptide which remains after 5 hours of sonication. This means that, regardless of whether there is a covalent interaction or not between the peptide and the surface, the electrostatic interaction can be sufficiently important so as to stabilize low amounts of peptide on a surface.

### 3.5.4.1. X-Ray photoelectron spectroscopy (XPS)

#### *3.5.4.1.1. Survey quantification*

***Table 3-4:*** *Survey quantifications of the titanium surfaces covered with the different fluorescent peptides.*

| Dan-RRRRRK-OH (+) | C1s | N1s | O1s | Ti2p | N/Ti |
|---|---|---|---|---|---|
| TiN APTES | 20.9 | 3.9 | 65.6 | 7.4 | 0.5 |
| TiN APT Mal | 21.0 | 4.2 | 66.8 | 5.8 | 0.7 |
| TiN CPTES | 23.9 | 4.9 | 62.0 | 7.1 | 0.7 |

| Dan-DDDDDK-OH (-) | C1s | N1s | O1s | Ti2p | N/Ti |
|---|---|---|---|---|---|
| TiN APTES | 20.1 | 2.0 | 67.3 | 7.8 | 0.3 |
| TiN APT Mal | 18.4 | 1.8 | 73.0 | 4.7 | 0.4 |
| TiN CPTES | 15.0 | 0.9 | 77.6 | 5.5 | 0.2 |

It is worth bearing in mind that the samples analyzed by XPS were previously sonicated in water for 3 hours in order to reduce the amount of physisorbed peptide on the surface, once that amount is stable for most of the surfaces analyzed according to the results shown in figures 3-17 and 3-18. The molar percentages of carbon, nitrogen, oxygen and titanium have been taken from the survey analysis. Traces of sodium, calcium, chlorine, sulfur and zinc have also been detected (data not shown). The study of these surfaces is complex as there is not any signature element that can be used to unambiguously identify the presence the peptides on the surface. For instance, TiN APTES and TiN APT Mal surfaces contain nitrogen in varying amounts, making it impossible to differentiate between the signal of nitrogen from APTES and the tone from the peptide. Also, TiN APT Mal surfaces contain malonic acid that could mask the nitrogen signal from the APTES underneath. Titanium also shows a variable signal depending on the surface analyzed, being lowest in TiN APT Mal surfaces regardless of the type of peptide on the surface.

The N/Ti ratio is the most valuable result to efficiently compare the results of peptide retention on the tested surfaces. On the surfaces covered with the Dan X-RRRRRK peptide, the N/Ti ratio was the lowest on TiN APTES surfaces, which is expected as this was the surface which retained the least amount of positive peptide according to the fluorescence signals reported in figure 3-17. The N/Ti ratio of TiN APT Mal and TiN CPTES surfaces covered with Dan X-RRRRRK peptide show similar values. We have to bear in mind that CPTES surfaces don't contain nitrogen, so, although the N/Ti ratio is similar in both surfaces it is safe to assume that a higher amount of Dan X-RRRRRK peptide was retained on the TiN CPTES surfaces than on the TiN APT Mal ones. This result also correlates well with results of fluorescence signals shown in figure 3-17.

The surfaces covered with Dan X-DDDDDK peptide showed an N/Ti ratio proportional to the amount of peptide expected after 3 hours of sonication, showing the highest value on the TiN APT Mal surface and the lowest value on the TiN CPTES surface. Again, this values support the results obtained for the mechanical stability tests shown in figure 3-18. These results also validate the formulated hypothesis as the expected covalent bond formed between the linker, malonic acid, and the peptides favored the mechanical retention of the peptides on the treated

surfaces in contrast to the most likely weakly-adsorbed peptides retained on the TiN APTES surfaces.

The TiN APTES and TiN APT Mal surfaces covered with the Dan X-DDDDDK peptide showed a much lower amount of nitrogen and titanium than the same surfaces but without being covered with peptides, as presented in section 2.5.2.3.1. This fact demonstrates that a significant amount of peptides were retained on top of the treated titanium surfaces because there was a high X-ray masking effect on the Ti signal and a much increased N signal. This proves once more that our chemical route for anchoring peptides through a silanization process was successful.

#### *3.5.4.1.2. Peak deconvolution*

##### 3.5.4.1.2.1. Carbon C1s

*Peptide Dan X-RRRRRK (+):*

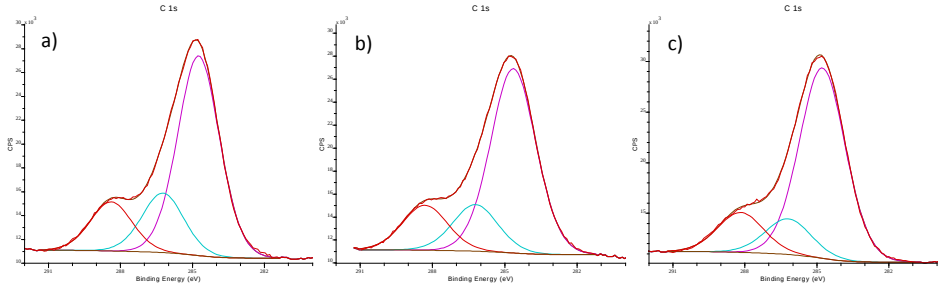


***Figure 3-19**: Deconvolutions of the carbon C1s peak on the different titanium samples covered with Dan X-RRRRRK peptide. a) TiN APTES, b) TiN APTES Mal, c) TiN CPTES.*

***Table 3-5:*** *Composition of the C1s peak of the different surfaces covered with Dan X-RRRRRK peptide*

| **Carbon C1s** | | | | | |
|---|---|---|---|---|---|
| *TiN APTES RK* | | | | | |
| **Chemical State** | **Position (eV)** | **Area (pixel)** | **Area (%)** | **References** | **(C-OH, C-N / C=O, O=CN) ratio** |
| **C-C** | 284.74 | 10240.2 | 64.74 | [78-80] | 1.21 |
| **C-OH, C-N** | 286.23 | 3055.66 | 19.32 | [78,79,81] | |
| **C=O, O=CN** | 288.39 | 2521.93 | 15.94 | [80,82] | |
| *TiN APT Mal RK* | | | | | |
| **Chemical State** | **Position (eV)** | **Area (pixel)** | **Area (%)** | **References** | **(C-OH, C-N / C=O, O=CN) ratio** |
| **C-C** | 284.75 | 9406.26 | 69.26 | [78-80] | 1.09 |
| **C-OH, C-N** | 286.36 | 2185.42 | 16.09 | [78,79,81] | |
| **C=O, O=CN** | 288.64 | 1988.84 | 14.64 | [80,82] | |
| *TiN CPTES RK* | | | | | |
| **Chemical State** | **Position (eV)** | **Area (pixel)** | **Area (%)** | **References** | **(C-OH, C-N / C=O, O=CN) ratio** |
| **C-C** | 284.77 | 12669.1 | 71.59 | [78-80] | 0.89 |
| **C-OH, C-N** | 286.20 | 2370.53 | 13.40 | [78,79,81] | |
| **C=O, O=C-N** | 288.18 | 2657.11 | 15.01 | [80,82] | |

A progressive increase of the C-C peak from the APTES surface covered with Dan X-RRRRRK (around 65%) peptide to the CPTES surface covered with the same peptide (around 72%) was detected (Table 3-5). The values of the C-OH, C-N peak and C=O, O=C-N peak did not show a clear tendency due to the different chemical compositions under the peptide layer. Nevertheless, the O-C/O=C relation shows a downward trend linked with the increase of peptides on the surface.

*Peptide Dan X-DDDDDK (-):*

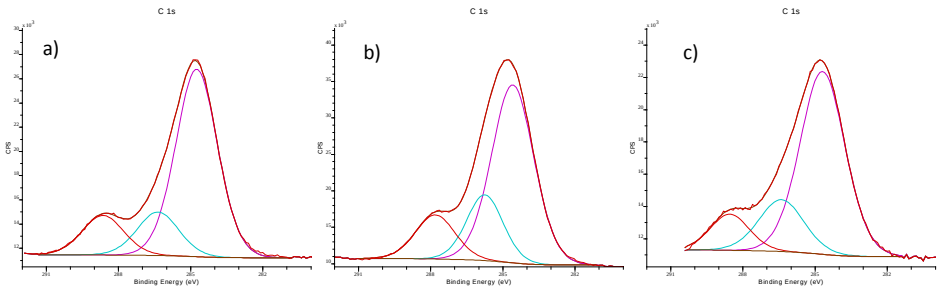


***Figure 3-20****: Deconvolutions of the carbon C1s peak on the different titanium samples covered with Dan X-RRRRRK peptide. a) TiN APTES, b) TiN APTES Mal, c) TiN CPTES.*

***Table 3-6:*** *Composition of the C1s peak of the different surfaces covered with Dan X-DDDDDK peptide*

| **Carbon C1s** | | | | | |
|---|---|---|---|---|---|
| *TiN APT DK* | | | | | |
| **Chemical State** | **Position (eV)** | **Area (pixel)** | **Area (%)** | **References** | **(C-OH, C-N / C=O, O=CN) ratio** |
| **C-C** | 284.75 | 9406.26 | 69.26 | [78-80] | 1.09 |
| **C-O, C-N** | 286.36 | 2185.42 | 16.09 | [78,79,81] | |
| **C=O, O=CN** | 288.64 | 1988.84 | 14.64 | [80,82] | |
| *TiN APTES Mal DK* | | | | | |
| **Chemical State** | **Position (eV)** | **Area (pixel)** | **Area (%)** | **References** | **(C-OH, C-N / C=O, O=CN) ratio** |
| **C-C** | 284.59 | 15051.6 | 64.43 | [78-80] | 1.36 |
| **C-O, C-N** | 285.75 | 4800.79 | 20.55 | [78,79,81] | |
| **C=O, O=CN** | 287.81 | 3510.25 | 15.03 | [80,82] | |
| *TiN CPTES DK* | | | | | |
| **Chemical State** | **Position (eV)** | **Area (pixel)** | **Area (%)** | **References** | **(C-OH, C-N / C=O, O=CN) ratio** |
| **C-C** | 284.65 | 6979.43 | 74.04 | [78-80] | 1.39 |
| **C-O, C-N** | 286.34 | 1423.61 | 15.10 | [78,79,81] | |
| **C=O, O=CN** | 288.49 | 1023.25 | 10.86 | [80,82] | |

There appears to be a tendency of the O-C/O=C relation to be the lowest on APTES surfaces and the highest on CPTES surfaces, which there might be related to a higher amount of carboxylic groups (relative to the total amount of carbon) from the high amount of aspartic acid-containing peptides on APTES surfaces. The C=O,O=CN and C-O,C-N peaks showed their highest values on TiN APT Mal surfaces which had the greatest amount of peptide after 3 hours of sonication.

3.5.4.1.2.2. Oxygen O1s

*Dan X-RRRRRK Peptide (+):*

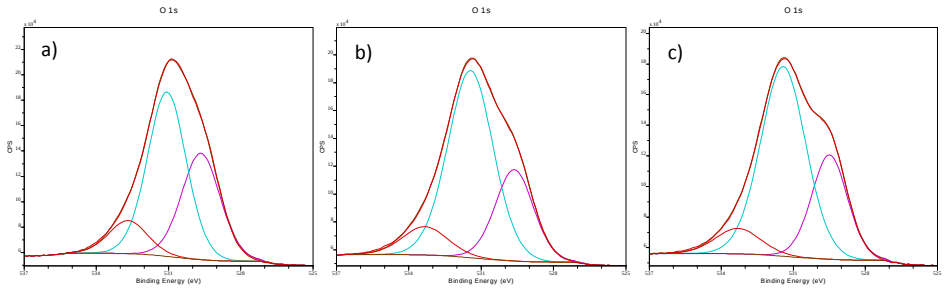


***Figure 3-21****: Deconvolutions of the Oxygen O1s peak on the different titanium samples covered with Dan X-RRRRRK peptide. a) TiN APTES, b) TiN APTES Mal, c) TiN CPTES.*

***Table 3-7:*** *Composition of the O1s peak of the different surfaces covered with Dan X-RRRRRK peptide*

| **Oxygen O1s** | | | | | |
|---|---|---|---|---|---|
| *TiN APTES RK* | | | | | |
| **Chemical State** | **Position (eV)** | **Area (pixel)** | **Area (%)** | **References** | **(O=C-N/$TiO_2$) ratio** |
| **$TiO_2$** | 529.7 | 52119.2 | 36.46 | [83-85] | |
| **O=C-N** | 531.11 | 77202.6 | 54.01 | [78,79,81] | 1.48 |
| **$H_2O$** | 532.8 | 13611.4 | 9.52 | [80,82] | |
| *TiN APT Mal RK* | | | | | |
| **Chemical State** | **Position (eV)** | **Area (pixel)** | **Area (%)** | **References** | **(O=C-N/$TiO_2$) ratio** |
| **$TiO_2$** | 529.74 | 46739.7 | 33.02 | [88,93,95] | |
| **O=C-N** | 531.46 | 78663.9 | 55.58 | [78,79,81] | 1.68 |
| **$H_2O$** | 532.99 | 16127.8 | 11.4 | [80,82] | |
| *TiN CPTES RK* | | | | | |
| **Chemical State** | **Position (eV)** | **Area (pixel)** | **Area (%)** | **References** | **(O=C-N/$TiO_2$) ratio** |
| **$TiO_2$** | 529.7 | 51060.5 | 37.21 | [88,93,95] | |
| **O=C-N** | 531.56 | 75593.1 | 55.09 | [78,79,81] | 1.48 |
| **$H_2O$** | 533.41 | 10555.7 | 7.69 | [80,82] | |

The oxygen peak can be deconvoluted into three peaks. $TiO_2$ peak is located at 529,7 eV. The highest peak is located at 531,3 eV corresponding to the O=C-N groups from the peptide bonds of the peptides on the surface. Compared with the surfaces without peptide (presented in section 2.5.2.3.1 and 2.6.2.3.2) where the highest peak was always the $TiO_2$, these surfaces experimented a notable growth of the O=C-N peak, making evident the presence of a significant amount of Dan X-RRRRRK peptide on the surface as the quantitative results in section 3.5.4.1.1 revealed. Finally, the third peak is located at around 533 eV and corresponds to the physisorbed water on the surface. It is interesting to remark that while the shape of the peaks (Figure 3-21) was clearly different, the calculated composition of the O1s peak did not show significant differences.

*Peptide Dan X-DDDDDK (-):*

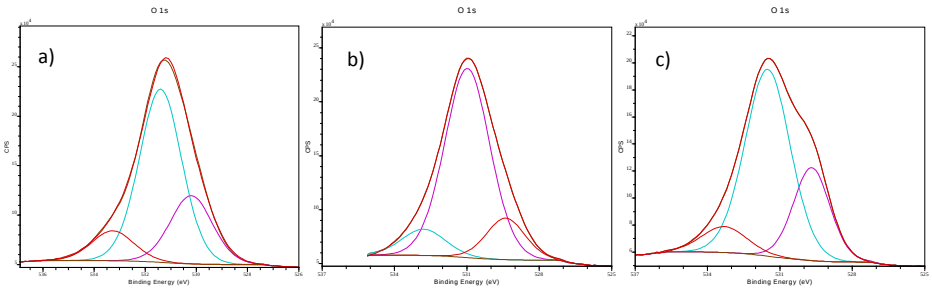


***Figure 3-22****: Deconvolutions of the oxygen O1s peak on the different titanium samples covered with Dan X-DDDDDK peptide. a) TiN APTES, b) TiN APTES Mal, c) TiN CPTES.*

***Table 3-8:*** *Composition of the O1s peak of the different surfaces covered with Dan X-DDDDDK peptide*

| **Oxygen O1s** | | | | | |
|---|---|---|---|---|---|
| *TiN APTES DK* | | | | | |
| **Chemical State** | **Position (eV)** | **Area (pixel)** | **Area (%)** | **References** | **(O=C-N/$TiO_2$) ratio** |
| **$TiO_2$** | 530.2 | 42308.7 | 25.15 | [83-85] | |
| **O=C-N** | 531.4 | 107334 | 63.81 | [78,79,81] | 2.53 |
| **$H_2O$** | 533.27 | 18571.6 | 11.04 | [80,82] | |
| *TiN APT Mal DK* | | | | | |
| **Chemical State** | **Position (eV)** | **Area (pixel)** | **Area (%)** | **References** | **(O=C-N/$TiO_2$) ratio** |
| **$TiO_2$** | 529.83 | 33098.2 | 20.96 | [83-85] | |
| **O=C-N** | 531.1 | 106711 | 67.58 | [78,79,81] | 3.22 |
| **$H_2O$** | 532.94 | 18089.4 | 11.46 | [80,82] | |
| *TiN CPTES DK* | | | | | |
| **Chemical State** | **Position (eV)** | **Area (pixel)** | **Area (%)** | **References** | **(O=C-N/$TiO_2$) ratio** |
| **$TiO_2$** | 529.82 | 49352 | 34.02 | [83-85] | |
| **O=C-N** | 531.55 | 79445.7 | 54.77 | [78,79,81] | 1.61 |
| **$H_2O$** | 533.06 | 16266.4 | 11.21 | [80,82] | |

In contrast to Dan-RRRRRK-OH surfaces, surfaces covered with Dan-DDDDDK-OH peptide evidenced a clear trend on the $TiO_2$ peak to have the lowest intensity on the TiN APT Mal silanized surfaces, and to have the highest intensity on the CPTES silanized surfaces. When more amount of peptide is covering the surface, the $TiO_2$ peak becomes lower because of the masking effect of the peptide components. It has to be taken in account that the TiN APT-Mal surface was the one which reached the highest amount of Dan X-DDDDDK peptide after 3 hours of sonication due to its low electronegativity and its ability to generate a covalent bond between the surface and the peptide, while CPTES surface was the one which reached the lowest amount of peptide due to its high electronegativity. The opposite tendency was shown by the O=C-N, where the highest value was for the TiN APT Mal surface, due to a higher amount of peptide on the surface.

Regarding physisorbed water amounts, there were no significant differences among surfaces and the water content did not vary, regardless of the type of peptide on the surface.

3.5.4.1.2.3. Nitrogen N1s

*Peptide Dan X-RRRRRK (+):*

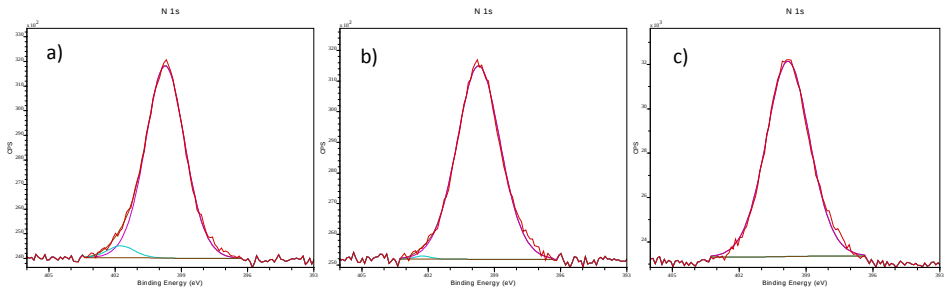


***Figure 3-23**: Deconvolutions of the Nitrogen N1s peak on the different titanium samples covered with Dan X-RRRRRK peptide. a) TiN APTES, b) TiN APTES Mal, c) TiN CPTES.*

***Table 3-9:** Composition of the N1s peak of the different surfaces covered with Dan X-DDDDDK peptide*

| **Nitrogen N1s** | | | | | |
|---|---|---|---|---|---|
| *TiN APTES RK* | | | | | |
| **Chemical State** | **Position (eV)** | **Area (pixel)** | **Area (%)** | **References** | **($NH_2/NH_3$) ratio** |
| **-NH-, $NH_2$** | 399.72 | 4630.89 | 95.88 | [86-88] | 23,27 |
| **$NH_3^+$** | 401.73 | 198.783 | 4.12 | [86-88] | |
| | | | | | |
| *TiN APT Mal RK* | | | | | |
| **Chemical State** | **Position (eV)** | **Area (pixel)** | **Area (%)** | **References** | **($NH_2/NH_3$) ratio** |
| **-NH-, $NH_2$** | 399.71 | 4146.19 | 99.41 | [86-88] | 168,49 |
| **$NH_3^+$** | 402.24 | 24.5338 | 0.59 | [86-88] | |
| | | | | | |
| *TiN CPTES RK* | | | | | |
| **Chemical State** | **Position (eV)** | **Area (pixel)** | **Area (%)** | **References** | **($NH_2/NH_3$) ratio** |
| **-NH-, $NH_2$** | 399.81 | 5744.66 | 100 | [86-88] | ∞ |
| **$NH_3^+$** | 402.8 | 0.00026243 | 0 | | |

The results show that surfaces silanized with CPTES revealed only one nitrogen peak in their deconvolution corresponding to the NH and $NH_2$ groups from the arginine residues and the N-C=O species, which are mainly peptide bonds. Additionally, APTES and APTES Mal surfaces showed a weak $NH_3^+$ peak from the protonated form of the amino group of APTES silane. Again, an upward trend is shown in the $NH_2/NH_3$ ratio which increases from APTES surface to CPTES surface. The fact that the value of $NH_2/NH_3$ was slightly higher on APTES Mal surfaces than on APTES surfaces could be explained by the fact that APTES Mal surface has the potential to develop a covalent bond between the APTES and the malonic acid, and between malonic acid and the lysine residue of the peptide. APTES surfaces cannot form those bonds, exposing therefore a higher amount of protonated amino groups.

*Peptide Dan X-DDDDDK (-):*

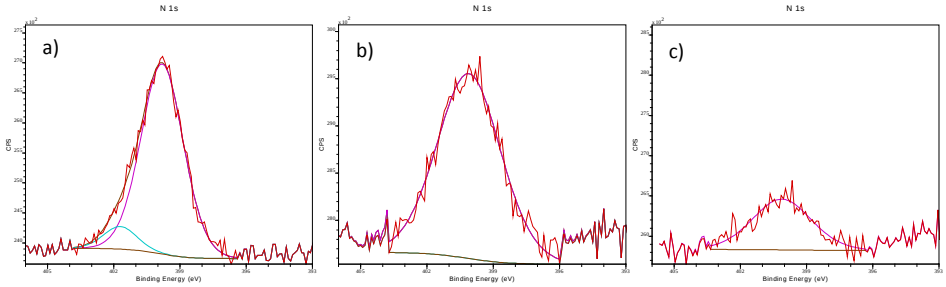


***Figure 3-24**: Deconvolutions of the nitrogen N1s peak from the different titanium samples covered with Dan X-RRRRRK peptide. a) TiN APTES, b) TiN APTES Mal, c) TiN CPTES.*

***Table 3-10:** Composition of the N1s peak of the different surfaces covered with Dan X-DDDDDK peptide*

| **Nitrogen N1s** | | | | | |
|---|---|---|---|---|---|
| *TiN APTES DK* | | | | | |
| **Chemical State** | **Position** | **Area (pixel)** | **Area (%)** | **References** | **($NH_2$/$NH_3$) ratio** |
| **-NH-, $NH_2$** | 399.8 | 2034.98 | 91.42 | [86-88] | 10.65 |
| **$NH_3^+$** | 401.7 | 190.875 | 8.58 | [86-88] | |
| | | | | | |
| *TiN APT Mal DK* | | | | | |
| **Chemical State** | **Position** | **Area (pixel)** | **Area (%)** | **References** | |
| **-NH-, $NH_2$** | 400.09 | 1886.59 | 100 | [86-88] | |
| | | | | [86-88] | |
| *TiN CPTES DK* | | | | | |
| **Chemical State** | **Position** | **Area (pixel)** | **Area (%)** | **References** | |
| **-NH-, $NH_2$** | 400.12 | 562.129 | 100 | [86-88] | |

In general, the nitrogen peaks on the surfaces covered with Dan-DDDDDK-OH peptide had low intensity due to the fact that the amount of peptide attached to the three surfaces was low because the three surfaces compared are negatively charged at pH 7.4 and so is the Dan X-DDDDDK peptide. Also, to the low amount of nitrogen present on the Dan X-DDDDDK-OH peptide was lower than on the Dan X-RRRRRK peptide. In fact, the N1s peaks for TiN APT Mal and TiN CPTES surfaces are too weak and too noisy as to obtain reliable deconvolutions. On all these surfaces the $NH_3^+$ peak corresponded to the presence of the protonated form of a free amino group of the APTES silane or from the free amino group of the unreacted lysine residues. The fact that TiN APTES Mal and TiN CPTES surfaces did not show the $NH_3^+$ might be an indirect evidence for the formation of covalent bonds between the peptide and the molecules on the metallic surface. Unfortunately, these peaks had high noise due to their low intensity.

### 3.5.5. Competitive adsorption

Prior to the competitive adsorption experiment, the retention of the fluorescently red ROX-labeled DDDDK peptide on the titanium surfaces was tested and compared to the already-reported retention obtained with the same peptide but labeled with the fluorescently blue Dansyl-X molecules. Figure 3-25 shows representative fluorescence micrographs of the different surfaces functionalized solely with ROX-DDDDDK-OH peptide. The fluorescence, now in red, presents the same tendency as the fluorescence on the surfaces functionalized with blue Dansyl-X-DDDDDK-OH (Figure 3-25).

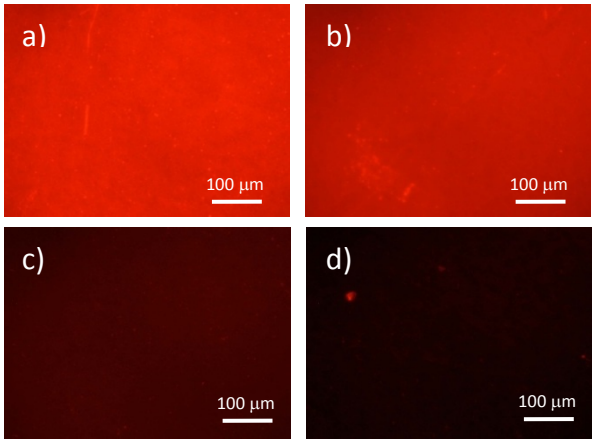


***Figure 3-25**: Fluorescence micrographs of the different surfaces treated with ROX-RDDDDDK peptide. a) TiN APTES, b) TiN APT Mal, c) TiN CPTES and d) Ti NaOH.*

It is worth noticing that ROX has higher fluorescence intensity than Dansyl-X. Thus, the competitive adsorption images with both peptides showed a general trend to be with red hues than to be with blue ones. That fact led to an analysis that was restricted to a qualitative comparison between the tested surfaces.

Once the good functionality of the ROX-DDDDDK peptide was confirmed, the competitive adsorption experiment was performed in 1:1 molar Dansyl X-RRRRRK:ROX-DDDDDK peptide solutions.

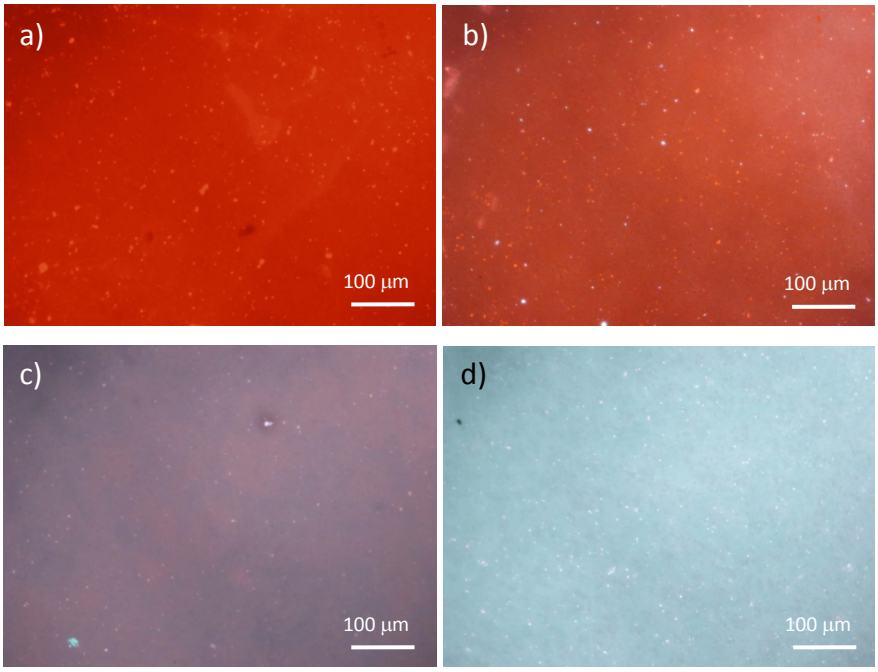


***Figure 3-26**: Fluorescence micrographs of the different surfaces treated with 1:1 Dan X-RRRRRK and ROX-DDDDDK mix. a) TiN APTES, b) TiN APT Mal, c) TiN CPTES and d) Ti NaOH.*

Results in figure 3-26 confirmed that the electrostatic interactions play a paramount role in the adsorption of short peptides on titanium surfaces. The tendencies are very clear in the fluorescent images where the least electronegative surface (TiN APTES) retained higher amounts of the negatively charged peptide (ROX-DDDDDK), while the most electronegative surface (Ti NaOH) retained almost solely the positively charged peptide (Dan X-RRRRRK).

## 3.6. Discussion

All results have shown a clear pattern which establishes a correlation between the amount of deposited peptide on the surface and the difference between surface and peptide electrical charge. Although all the surfaces developed for this study have shown a negative $\zeta$ potential at pH 7.4, they have also evidenced significant differences regarding peptide adsorption.

Although the peptides used in this study have a relatively low charge for a biological molecule, the specific charge (charge in relation to its molecular weight) is very high. Also, if compared to proteins, these peptides don't have secondary, tertiary or quaternary structures that could

diminish the calculated value of charge. The use of short peptides with an opposite specific charge has been a proved adequate to test our hypothesis on the charge-dependent behavior in the peptide adsorption process.

Regarding the differences between adsorption of proteins and peptides, we can say that the differences in adsorption behavior are based on the complex structures that proteins are able to develop and that peptides lack. According to the bibliography consulted, it seems that, in general, proteins have a higher adsorption potential than short peptides [5,9]. Nevertheless, this work demonstrates that short peptides have a high adsorption potential when the charge of the surface and the charge of the peptide are opposite.

The study of functionalized surfaces is challenging because of the intrinsic limitations of the analysis techniques. Most techniques for quantification of organic molecules are exclusively for quantification in solution but not for surface quantification. Also, the deposited molecules on the surface have a nanometer-scale size. This means that the topographical changes are too small to be detected by most topographical techniques of analysis, thereby forcing researchers to test the samples with several complementary techniques in order to gather enough and reliable data to support sound conclusions. We have seen that even though fluorescence microscopy is a semi-quantitative technique with a low-resolution degree, it is a very useful technique due to its economy, versatility, sensitivity and speed. Also, it was very convenient for carrying out preliminary tests to optimize processes and methodologies. However, to study the coverage of the surfaces and the stability of the immobilized peptides, other techniques such as spectrofluorophotometry and XPS have been successfully used, achieving reasonably well-correlated results.

The use of surfaces with different treatments in this study is supported by the fact that we needed titanium surfaces with similar topographical properties but different chemical properties in order to have different $\zeta$ potential at pH 7.4. Additionally, two of the four different surfaces used in this study (TiN APTES Mal. and TiN CPTES) had the potential to develop a covalent bond between the surface and the immobilized peptides through an electrophilic substitution as was described in section 2.3.3. In the case of TiN APTES Mal. surface, the covalent interaction would be produced between the free carboxylate of malonic

acid the primary amine of the lysine residue of the peptide while in the case of CPTES surfaces the nucleophilic substitution would be produced between the organofunctional group of CPTES and the amine of the lysine side chain. The other two surfaces (Ti NaOH and TiN APTES) weren't able to generate covalent bonds due to the absence of functional groups that could react with any group of the peptide. Therefore, the mechanical stability of the peptide on the surface would have been lower than on the ones with potential for covalent immobilization. This experimental setup has led us to detect differences in the amounts of peptide present after sonication in water. The surfaces in which the covalent bond was possible presented a higher mechanical stability, suggesting that the covalent bond was generated. This statement is supported by the XPS results confirming a higher amount of peptide species on the surfaces with covalent potential.

Mechanical stability results gave information about several points of the functionalization of surfaces with short peptides. 1- Independently of the capability of a surface to develop a covalent bond with the peptide, all surfaces retained a loosen amount of peptide which was released from the surface by means of sonication. 2- The surfaces which were capable to generate a covalent bond with the peptide reached a plateau on the fluorescence signal and stopped loosening peptide after 3 hours of sonication. The surfaces which were not able to generate a covalent bond with the peptide didn't reach this plateau. 3- On surfaces treated with Dan X-RRRRRK peptide, after 5 hours of sonication the amount of peptide retained on the surface was proportional to the initial amount of peptide present on each surface and, therefore, also proportional to the electronegativity of each surface. On surfaces treated with Dan X-DDDDDK peptide the trend was similar with the exception of the TiN APT Mal. surface which had the highest amount of retained peptide after 5 hours of sonication.

These results suggests the following ideas: from the point 1 we can extract that on a functionalization process there is always an amount of physisorbed peptide that can be easily released from the surface. Even when a covalent bond is developed between the surface and the peptide, there will be a certain amount of peptide which will not be covalently bound but attached by weak bonds. From point 2 we can say that, since physisorbed peptide is more weakly bound to the surface than the peptide attached by covalent bonds it is possible to release the physisorbed peptide from the surface by sonication and therefore obtain surfaces

with only covalently bound peptide. Point 3 revealed that the amount of covalently bound peptide is dependent on the overall amount of peptide attached on the surface. Therefore, when surface and peptide have highly opposite charges it is possible to retain more covalently bound peptide on the surface than when the charges of both elements are similar. Although, results obtained on Ti NaOH surface treated with the Dan X-RRRRRK peptide suggest that when the charges of peptide and surface are highly opposite the electrostatic forces between them play an important role on the retention of peptide on the surface.

The competitive adsorption test had some disadvantages with regards to evaluating the results given that: a quantification of the amount of both peptides was not possible; the ROX molecule could modify the charge of the DDDDDK peptide; and the mechanical stability didn't reveal any differences. However, qualitative analysis of the fluorescence of the surfaces showed a clear trend suggesting that the surface charge is a crucial parameter to control the adsorption of short peptides on the surface. On the surfaces with the highest and lowest ζ potential we could see that one peptide dominated the surface, impeding the other one from adsorbing onto it. Knowing this fact can be a useful in future investigations when developing new surfaces with different peptides co-immobilized on a surface to achieve multifunctional biomaterials. The relationship between surface charge and peptide net charge can be used to control the proportion of each peptide on the surface.

As has been evidenced in this chapter, many different modifications can be carried out in order to control surface ζ potential [89], a matter that is especially relevant with regards to biofunctionalization purposes. Additionally some modifications of the peptide design that do not affect the biological role of the bioactive motive can also be performed in order to optimize the presence of a peptide on a surface and hence increase its bioactive effect.

The selection of the silane to achieve a covalent immobilization of the peptide on the surface is also important to achieve a successful functionalization. As it has been shown, silanes can modify dramatically the surface ζ potential. Fortunately, there are a myriad of silanes with different functional groups that can be used for this purpose [90] providing many possibilities to achieve a desired surface functionalization.

Additionally, the design and modification of the peptide sequence can be a useful resource in the design of new surfaces. For instance, it is possible to add, to the peptide, several amino acids with charged side chains that provoke the modification of the surface charge when the peptide is present on the surface, or add amino acids with hydrophilic or hydrophobic side chains to modify the surface wettability.

Another parameter to take in account on the functionalization of surfaces with short peptides is the pH at which the peptide immobilization is performed [1,2]. As it has been seen in this chapter the charge, as much of the surface as of peptide, is affected by the pH. The control upon the pH gives the capability to narrow or widen the differences between peptide and surface in terms of charge and therefore obtain a better control on the amount and the type of peptide adsorbed on a surface.

This chapter has revealed two important facts. The first one is that it is possible to modify the amount of peptide present on a surface and achieve, with the adequate conditions an important amount of peptide on a surface. This point has a paramount importance on the biological response of cells and tissues to functionalized surfaces since increasing the surface density of a bioactive biomolecule improves the biological response to the substrate [48,91]. The second fact is that a covalent bond between the surface and the peptide can be achieved providing a high stability to the system.

The stability of a biomolecule on a surface is a crucial factor for the success of biomaterial since a high stability helps to sustain the bioactive effect of a surface in a biological environment over time and to avoid the undesired release of the biomolecule when the surface is immersed into a biological fluid [92]. Moreover, a strong anchorage of the biomolecule to a surface is desirable when a biomaterial (i.e. a dental implant) is surgically inserted in bone since it helps the system to bear the shear stresses produced by the body tissues.

# 3.7. Conclusions

This study has led us to better understand the phenomenon of short peptide adsorption onto a surface so as to apply this knowledge to the development of new biofunctionalization processes in order to immobilize oligopeptides on titanium surfaces.

The following conclusions have been drawn from the study:

- The amount of oligopeptide adsorbed on a surface is strongly dependent on its net charge compared to the surface charge where the peptide is deposited. The greater the difference, the higher the amount of peptide on the surface.

- Peptide charge and the amount of adsorbed peptide do not seem to affect the possibility of generating a covalent bond between the surface and the peptide whenever possible.

- It is possible to control the amount of peptide deposited on a surface by modifying the surface $\zeta$ potential and/or the peptide net charge.

# 3.8. References

1. Barrias CC, Martins MCL, Miranda MCS, Barbosa MA. Adsorption of a therapeutic enzyme to self-assembled monolayers: effect of surface chemistry and solution pH on the amount and activity of adsorbed enzyme. Biomaterials 2005;26:2695-2704.

2. Nakanishi K, Sakiyama T, Imamura K. On the adsorption of proteins on solid surfaces, a common but very complicated phenomenon. Journal of Bioscience and Bioengineering 2001;91:233-244.

3. Burns NL, Holmberg K, Brink C. Influence of Surface Charge on Protein Adsorption at an Amphoteric Surface: Effects of Varying Acid to Base Ratio. J Colloid Interface Sci 1996;178:116-122.

4. Imamura K, Kawasaki Y, Awadzu T, Sakiyama T, Nakanishi K. Contribution of acidic amino residues to the adsorption of peptides onto a stainless steel surface. J Colloid Interface Sci 2003;267:294-301.

5. Imamura K, Kawasaki Y, Nagayasu T, Sakiyama T, Nakanishi K. Adsorption characteristics of oligopeptides composed of acidic and basic amino acids on titanium surface. Journal of Bioscience and Bioengineering 2007;103:7-12.

6. Ekblad T, Liedberg B. Protein adsorption and surface patterning. Current Opinion in Colloid & Interface Science 2010;15:499-509.

7. Pegueroles M, Aparicio C, Bosio M, Engel E, Gil FJ, Planell JA, Altankov G. Spatial organization of osteoblast fibronectin matrix on titanium surfaces: Effects of roughness, chemical heterogeneity and surface energy. Acta Biomaterialia 2010;6:291-301.

8. Kao P, Parhi P, Krishnan A, Noh H, Haider W, Tadigadapa S, Allara DL, Vogler EA. Volumetric interpretation of protein adsorption: Interfacial packing of protein adsorbed to hydrophobic surfaces from surface-saturating solution concentrations. Biomaterials 2011;32:969-978.

9. Sakiyama T, Tomura J, Imamura K, Nakanishi K. Adsorption characteristics of bovine serum albumin and its peptide fragments on a stainless steel surface. Colloids and Surfaces B: Biointerfaces 2004;33:77-84.

10. Barnthip N, Parhi P, Golas A, Vogler EA. Volumetric interpretation of protein adsorption: Kinetics of protein-adsorption competition from binary solution. Biomaterials 2009;30:6495-6513.

11. Noh H, Vogler EA. Volumetric interpretation of protein adsorption: Competition from mixtures and the Vroman effect. Biomaterials 2007;28:405-422.

12. Noh H, Yohe ST, Vogler EA. Volumetric interpretation of protein adsorption: Ion-exchange adsorbent capacity, protein pI, and interaction energetics. Biomaterials 2008;29:2033-2048.

13. Noh H, Vogler EA. Volumetric interpretation of protein adsorption: Mass and energy balance for albumin adsorption to particulate adsorbents with incrementally increasing hydrophilicity. Biomaterials 2006;27:5801-5812.

14. Noh H, Vogler EA. Volumetric interpretation of protein adsorption: Partition coefficients, interphase volumes, and free energies of adsorption to hydrophobic surfaces. Biomaterials 2006;27:5780-5793.

15. Parhi P, Golas A, Barnthip N, Noh H, Vogler EA. Volumetric interpretation of protein adsorption: Capacity scaling with adsorbate molecular weight and adsorbent surface energy. Biomaterials 2009;30:6814-6824.

16. Sheng Y, Wang W, Chen P. Peptide adsorption on the hydrophobic surface: A free energy perspective. J Mol Struct 2011;995:142-147.

17. Rapuano BE, MacDonald DE. Surface oxide net charge of a titanium alloy: Modulation of fibronectin-activated attachment and spreading of osteogenic cells. Colloids and Surfaces B: Biointerfaces 2011;82:95-103.

18. Vogler EA. Protein adsorption in three dimensions. Biomaterials 2012;33:1201-1237.

19. Bell BF, Schuler M, Tosatti S, Textor M, Schwartz Z, Boyan BD. Osteoblast response to titanium surfaces functionalized with extracellular matrix peptide biomimetics. Clin Oral Implants Res 2011;22:865-872.

20. Chollet C, Chanseau C, Remy M, Guignandon A, Bareille R, Labrugère C, Bordenave L, Durrieu M. The effect of RGD density on osteoblast and endothelial cell behavior on RGD-grafted polyethylene terephthalate surfaces. Biomaterials 2009;30:711-720.

21. Porté-Durrieu MC, Guillemot F, Pallu S, Labrugère C, Brouillaud B, Bareille R, Amédée J, Barthe N, Dard M, Baquey C. Cyclo-(DfKRG) peptide grafting onto Ti–6Al–4V: physical characterization and interest towards human osteoprogenitor cells adhesion. Biomaterials 2004;25:4837-4846.

22. Bagno A, Piovan A, Dettin M, Chiarion A, Brun P, Gambaretto R, Fontana G, Di Bello C, Palù G, Castagliuolo I. Human osteoblast-like cell adhesion on titanium substrates covalently functionalized with synthetic peptides. Bone, 2007;40:693-699.

23. Dettin M, Bagno A, Gambaretto R, Iucci G, Conconi MT, Tuccitto N, Menti AM, Grandi C, Bello CD, Licciardello A, Polzonetti G. Covalent surface modification of titanium oxide with different adhesive peptides: Surface characterization and osteoblast-like cell adhesion. Journal of Biomedical Materials Research Part A 2009;90A.

24. Sevilla P, Godoy M, Salvagni E, Gil FJ. Biofunctionalization of titanium surfaces for osseintegration process improvement. Journal of Physics: Conference Series 2010;252:012009.

25. Barthélémy B, Devillers S, Minet I, Delhalle J, Mekhalif Z. Surface-initiated ATRP of 2-(methacryloyloxy)ethyl 2-(trimethylammonio)ethyl phosphate on Phynox. Appl Surf Sci 2011;258:466-473.

26. Butt H, Graf K, Kappl M. Physics and chemistry of interfaces. : Wiley-VCH, 2003.

27. Gibbs R. Silver Colloids, http://www.silver-colloids.com/Tutorials/Intro/pcs13.html. 2012.

28. Gibbs R. The electric double layer, Silver Colloids, http://www.silver-colloids.com/Tutorials/Intro/pcs17A.html. 2012.

29. Wittstock G. Fundamentals of Electrochemistry. Electrochmical Society Series, 2nd Edition. Edited by Vladimir S. Bagotsky. ChemPhysChem 2006;7:2022-2023.

30. Kosmulski M. Chemical properties of material surfaces. : Marcel Dekker, 2001.

31. Paselk RA. Physical biochemistry, applications to biochemistry and molecular biology, second edition (Freifelder, David). J Chem Educ 1983;60:A321.

32. Ege S. Organic chemistry. : Reverte, 1998.

33. Gorga F. Proteins, peptides and amino acids. 2011.

34. Bashford D. Macroscopic electrostatic models for protonation states in proteins. Frontiers in Bioscience 2004;9:1082-1099.

35. Gunner MR, Mao J, Song Y, Kim J. Factors influencing the energetics of electron and proton transfers in proteins. What can be learned from calculations. Biochimica et Biophysica Acta (BBA) - Bioenergetics 2006;1757:942-968.

36. Ullmann G, Kloppmann E, Essigke T, Krammer E, Klingen A, Becker T, Bombarda E. Investigating the mechanisms of photosynthetic proteins using continuum electrostatics. Photosynthesis Res 2008;97:33-53.

37. Antosiewicz JM, Shugar D. Poisson-Boltzmann continuum-solvation models: applications to pH-dependent properties of biomolecules. Mol BioSyst 2011;7:2923-2949.

38. Helfferich FG. Principles of adsorption & adsorption processes, by D. M. Ruthven, John Wiley & Sons, 1984, xxiv + 433 pp. AIChE J 1985;31:523-524.

39. Ratner B, Hoffman A, Schoen F, Lemons J. Biomaterials science, third edition: An introduction to materials in medicine. : Academic Press, 2012.

40. Horbett TA. Protein adsorption on biomaterials. Biomaterials: Interfacial Phenomena and Applications: American Chemical Society, 1982. p. 233-244.

41. Hlady V, Buijs J. Protein adsorption on solid surfaces. Curr Opin Biotechnol 1996;7:72-77.

42. Barnthip N, Noh H, Leibner E, Vogler EA. Volumetric interpretation of protein adsorption: Kinetic consequences of a slowly-concentrating interphase. Biomaterials 2008;29:3062-3074.

43. Pegueroles Neyra M. Interactions between titanium surfaces and biological components.

44. Sargeant TD, Rao MS, Koh C, Stupp SI. Covalent functionalization of NiTi surfaces with bioactive peptide amphiphile nanofibers. Biomaterials, 2008;29:1085-1098.

45. Beuvelot J, Portet D, Lecollinet G, Moreau MF, Basle MF, Chappard D, Libouban H. In vitro kinetic study of growth and mineralization of osteoblast-like cells (Saos-2) on titanium surface coated with a RGD functionalized bisphosphonate. J Biomed Mater Res B Appl Biomater 2009;90:873-881.

46. Iucci G, Battocchio C, Dettin M, Ghezzo F, Polzonetti G. An XPS study on the covalent immobilization of adhesion peptides on a glass surface. Solid State Sciences 2010;12:1861-1865.

47. Yang X, Hua L, Gong H, Tan SN. Covalent immobilization of an enzyme (glucose oxidase) onto a carbon sol–gel silicate composite surface as a biosensing platform. Anal Chim Acta 2003;478:67-75.

48. Hersel U, Dahmen C, Kessler H. RGD modified polymers: biomaterials for stimulated cell adhesion and beyond. Biomaterials 2003;24:4385-4415.

49. Holmes-Farley S, Whitesides GM. Fluorescence properties of dansyl groups covalently bonded to the surface of oxidatively functionalized low-density polyethylene film. Langmuir 1986;2:266-281.

50. Henderson LJ. Concerning the Relationship Between the Strength of Acids and Their Capacity to Preserve Neutrality. Surv Anesthesiol 1964;8:504.

51. Po HN, Senozan NM. The Henderson-Hasselbalch Equation: Its History and Limitations. J Chem Educ 2001;78:1499.

52. Lehninger A, Nelson D, Cox M. Lehninger principles of biochemistry. : W. H. Freeman, 2008.

53. Andreu D, Rivas L. Péptidos en biología y biomedicina. Madrid, Spain: Raycar S.A., 1997.

54. Lloyd-Williams P, Albericio F, Giralt E. Chemical approaches to the synthesis of peptides and proteins (new directions in organic & biological chemistry). : CRC-Press, 1997.

55. Merrifield RB. Solid Phase Peptide Synthesis. I. The Synthesis of a Tetrapeptide. J Am Chem Soc 1963;85:2149-2154.

56. Merrifield RB. Automated Synthesis of Peptides. Science 1965;150:178-185.

57. Aldrich. Chemfiles, Peptide synthesis. http://www.sigmaaldrich.com/etc/medialib/docs/Aldrich/Brochure/al_chemfile_v7_n2.Par.0001.File.dat/al_chemfile_v7_n2.pdf. 2007.

58. Kaiser E, Colescott RL, Bossinger CD, Cook PI. Color test for detection of free terminal amino groups in the solid-phase synthesis of peptides. Anal Biochem 1970;34:595-598.

59. Carpino L. Oxidative Reactions of Hydrazines .4. Elimination of Nitrogen from 1,1-Disubstituted-2-Arenesulfonhydrazides. J Am Chem Soc 1957;79:4427-4431.

60. Carpino L, Han G. 9-Fluorenylmethoxycarbonyl Amino-Protecting Group. J Org Chem 1972;37:3404-&.

61. Wang S. Para-Alkoxybenzyl Alcohol Resin and Para-Alkoxybenzyloxycarbonylhydrazide Resin for Solid-Phase Synthesis of Protected Peptide Fragments. J Am Chem Soc 1973;95:1328-1333.

62. Christoforou CC, Westermann-Clark GB, Anderson JL. The streaming potential and inadequacies of the Helmholtz equation. J Colloid Interface Sci 1985;106:1-11.

63. Zembala M. Electrokinetics of heterogeneous interfaces. Adv Colloid Interface Sci 2004;112:59-92.

64. Werner C, König U, Augsburg A, Arnhold C, Körber H, Zimmermann R, Jacobasch H. Electrokinetic surface characterization of biomedical polymers — a survey. Colloids Surf Physicochem Eng Aspects 1999;159:519-529.

65. Fairbrother F, Mastin H. CCCXII.-Studies in electro-endosmosis. Part I. J Chem Soc , Trans 1924;125:2319-2330.

66. Fievet P, Sbaï M, Szymczyk A, Vidonne A. Determining the ζ-potential of plane membranes from tangential streaming potential measurements: effect of the membrane body conductance. J Membr Sci 2003;226:227-236.

67. Xing Y, Borguet E. Specificity and Sensitivity of Fluorescence Labeling of Surface Species. Langmuir 2007;23:684-688.

68. Xing Y, Dementev N, Borguet E. Chemical labeling for quantitative characterization of surface chemistry. Current Opinion in Solid State and Materials Science 2007;11:86-91.

69. McArthur EA, Ye T, Cross JP, Petoud S, Borguet E. Fluorescence Detection of Surface-Bound Intermediates Produced from UV Photoreactivity of Alkylsiloxane SAMs. J Am Chem Soc 2004;126:2260-2261.

70. Fykse EM, Olsen JS, Skogan G. Application of sonication to release DNA from Bacillus cereus for quantitative detection by real-time PCR. J Microbiol Methods 2003;55:1-10.

71. Ma Y, Lin J. Effect of pre-sonication on removal of organic matters resulting from chlorinated humic acids. Water Science and Technology 1998;38:253-260.

72. Toworfe GK, Composto RJ, Shapiro IM, Ducheyne P. Nucleation and growth of calcium phosphate on amine-, carboxyl- and hydroxyl-silane self-assembled monolayers. Biomaterials 2006;27:631-642.

73. Lee MH, Brass DA, Morris R, Composto RJ, Ducheyne P. The effect of non-specific interactions on cellular adhesion using model surfaces. Biomaterials 2005;26:1721-1730.

74. Chollet C, Chanseau C, Remy M, Guignandon A, Bareille R, Labrugère C, Bordenave L, Durrieu M. The effect of RGD density on osteoblast and endothelial cell behavior on RGD-grafted polyethylene terephthalate surfaces. Biomaterials 2009;30:711-720.

75. Chua P, Neoh K, Kang E, Wang W. Surface functionalization of titanium with hyaluronic acid/chitosan polyelectrolyte multilayers and RGD for promoting osteoblast functions and inhibiting bacterial adhesion. Biomaterials 2008;29:1412-1421.

76. Houseman BT, Mrksich M. The microenvironment of immobilized Arg-Gly-Asp peptides is an important determinant of cell adhesion. Biomaterials 2001;22:943-955.

77. Rezania A, Healy KE. The effect of peptide surface density on mineralization of a matrix deposited by osteogenic cells. J Biomed Mater Res 2000;52:595-600.

78. Bondarenka V, Tvardauskas H, Grebinskij S, Senulis M, Pa?i?kevi?ius A, Volkov V, Zakharova G. - Sol-gel synthesis and XPS study of vanadium-hydroquinone oxide bronze films. - physica status solidi (c) - 2009;- 6:- 2807--2809.

79. National Institute of Standards and Technology, NIST. NIST X-ray Photoelectron Spectroscopy Database. http://srdata.nist.gov/xps/. 2007.

80. Moulder JF, Stickle WF, Sobol PE, Bomben KD. Handbook of X-ray photoelectron spectroscopy. : Physical Electronics Inc., 1992.

81. Awsiuk K, Bernasik A, Kitsara M, Budkowski A, Rysz J, Haberko J, Petrou P, Beltsios K, Raczkowska J. Protein coverage on silicon surfaces modified with amino-organic films: A study by AFM and angle-resolved XPS. Colloids and Surfaces B: Biointerfaces 2010;80:63-71.

82. Polzonetti G, Battocchio C, Iucci G, Dettin M, Gambaretto R, Di Bello C, Carravetta V. Thin films of a self-assembling peptide on TiO2 and Au studied by NEXAFS, XPS and IR spectroscopies. Materials Science and Engineering: C 2006;26:929-934.

83. F Werfel and OB. Corundum Structure Oxides Studied by XPS. Phys Scripta 1983;28:92.

84. Kang B, Sul Y, Oh S, Lee H, Albrektsson T. XPS, AES and SEM analysis of recent dental implants. Acta Biomaterialia 2009;5:2222-2229.

85. Mekhalif Z, Cossement D, Hevesi L, Delhalle J. Electropolymerization of pyrrole on silanized polycrystalline titanium substrates. Appl Surf Sci 2008;254:4056-4062.

86. Bierbaum K, Kinzler M, Woell C, Grunze M, Haehner G, Heid S, Effenberger F. A Near Edge X-ray Absorption Fine Structure Spectroscopy and X-ray Photoelectron Spectroscopy Study of the Film Properties of Self-Assembled Monolayers of Organosilanes on Oxidized Si(100). Langmuir 1995;11:512-518.

87. Gu Q, Cheng X. Tribological behaviors of lanthanum-based phosphonate 3-aminopropyltriethoxysilane self-assembled films. Appl Surf Sci 2007;253:6800-6806.

88. Xue A, Zhou S, Zhao Y, Lu X, Han P. Effective NH2-grafting on attapulgite surfaces for adsorption of reactive dyes. J Hazard Mater 2011;194:7-14.

89. Cai K, Frant M, Bossert J, Hildebrand G, Liefeith K, Jandt KD. Surface functionalized titanium thin films: Zeta-potential, protein adsorption and cell proliferation. Colloids and Surfaces B: Biointerfaces 2006;50:1-8.

90. Gelest. Silane coupling agents: Connecting across boundaries. 2006.

91. Jeanene Willcox P, Reinhart-King CA, Lahr SJ, DeGrado WF, Hammer DA. Dynamic heterodimer-functionalized surfaces for endothelial cell adhesion. Biomaterials 2005;26:4757-4766.

92. Kim YH, Baek NS, Han YH, Chung M, Jung S. Enhancement of neuronal cell adhesion by covalent binding of poly-d-lysine. J Neurosci Methods 2011;202:38-44.

# 4. Biofunctionalization of titanium surface with the TGF-β inhibitor peptide P17

## CONTENTS

# 4.1. Introduction

## 4.1.1. Scope

The experimental work included in this chapter of the thesis was performed, in its entirety, in the Minnesota Dental Research Center for Biomaterials and Biomechanics in the School of Dentistry of the University of Minnesota. The techniques for characterization and generation of the surfaces are quite similar to the ones used in the previous chapters of the thesis, but the equipment and the lab material used was different.

After having developed an effective method to immobilize peptides on titanium surfaces we wanted to generate a new TGF-β-inhibiting titanium surface in order to study what repercussions the inhibition of this cytokine has on fibroblastic and osteoblastic cells. To generate such a surface, we collaborated with Dr. Francisco Borrás-Cuesta and Dr. Javier Dotor from the Centro de Investigación Médica Avanzada in the University of Navarra. Dr. Dotor kindly provided us with two short peptides, P17 and P144 (Digna Biotech, Spain) [1,2], developed by the Borrás-Cuesta group, that have the potential to inhibit the effect of TGF-β in a biological environment. The Borrás-Cuesta group also fabricated peptides with some modifications that we designed and incorporated to properly anchor the peptides on the titanium surfaces.

The biological aspects of the TGF-β inhibitor peptides and the titanium surface biofunctionalized with these peptides are treated in chapter 6. This chapter includes the study of the physico-chemical properties of the titanium surfaces biofunctionalized with the TGF-β inhibitor peptide (P17).

Although Dr. Dotor contributed two different TGF-β inhibitor sequences (P17 and P144), in this chapter we decided to work only with the P17 peptide to set reproducible and reliable immobilization conditions. Chapter 5 includes further studies done with P144 peptide to confirm the proper immobilization of the two peptides through the developed immobilization route.

### 4.1.2. TGF-β

The transforming growth factor β (TGF-β) is a cytokine family that regulates the balance between cell mass and extracellular matrix. Three components of this family (TGF-β1, TGF-β2 and TGF-β3) are present in the extracellular matrix and are expressed by stem cells.

TGF-β increases deposition of collagen and other proteins directly stimulating the expression of the corresponding genes and inhibiting the synthesis of collagenase [3,4]. In chronic viral hepatitis, the secretion of TGF-β in the liver is closely related to fibro genesis [5]. In bone, the most abundant form of TGF-β is TGF-β1.

As for the regeneration of bone, there is considerable controversy regarding the TGF-β. TGF-β1 has been shown to promote osteoblast proliferation, but also to be an inhibitor of alkaline phosphatase and osteoblast mineralization [6].

Although the effectiveness of TGF-β1 for bone repair has been demonstrated in several animal studies employing both large-quantity applications (10-335 mg) [7-9] and in small amounts (0.3-1.0 μg) [10,11], certain other studies have shown results that point to the other extreme, affirming that administration of TGF-β1 is either ineffective, at best, or even harmful for bone regeneration [12-15]. Aspenberg et al. [12] placed titanium implants in rat tibiae that had been treated with 1.33 or 1000 ng of TGF-β1 and compared them with untreated controls, obtaining a negative correlation between the amount of TGF-β1 administered and bone formation. Nikolidakis et al. [15] conducted a similar study inserting implants loaded with 0.5 or 1 mg of TGF-β1 in goat femurs, and obtained similar results. The authors maintain that TGF-β1 can stimulate the fibrotic reaction in the bone just as it does in the liver. Similarly Tielinen et al. [13] inserted bio-absorbable implants containing 50 μg of TGF-β1 in rat distal femurs. After 3 weeks of implantation, histological analysis showed a fibroblast-rich mesenchymal tissue within the defects treated with TGF-β1. Finally, Ueda et al. [14] demonstrated that a single dose of 0.1 micrograms of TGF-β1 was ineffective in promoting bone formation in rabbit cranial defects after 6 weeks (rapid diffusion of the growth factor was suggested as a possible explanation).

More information about TGF-β signalling pathway and interactions with the biological environment can be found in chapter 6.

### 4.1.3. TGF-β inhibitor peptides: P17 and P144

Borrás-Cuesta and his group in CIMA (University of Navarra) have developed a series of peptides capable of inhibiting TGF-β activity [5,16,17]. These peptides bind to TGF-β1, blocking the interaction with the cellular receptors, thereby preventing their interaction with cells. These peptides have demonstrated their beneficial effect by inhibiting fibro genesis in cirrhotic rat livers [5] and inhibiting angiogenesis [17]. They have not yet been evaluated in bone *in vitro* or *in vivo*, although unpublished studies suggest beneficial effects on cartilage regeneration.

Among several different TGF-β inhibitor peptides developed by Borrás-Cuesta's group, there are two that excel in the inhibition of the TGF-β1 activity on cells. These two peptides are named P17 and P144. Below, their amino acid sequences are shown:

- P17: $NH_2$-KRIWFIPRSSWYERA-OH
- P144: $NH_2$-TSLDASIIWAMMQN-OH

P144 is a peptide derived from the TGF-β type III receptor found at the cytoskeleton of multiple cell types. P144 interacts with TGF-β1 in the region where the cytokine connects with the cell receptor and blocks the cell signaling pathway [5,17,18]. On the other hand, P17 was identified as peptide inhibitor using a 15-mer phage-display random peptide library. P17 demonstrated it had a high binding affinity for TGF-β1 and had the highest efficacy in blocking TGF-β1 signaling pathway *in vivo* and *in vitro* [16,17,19].

# 4.2. Objectives

The main objective of this chapter is to characterize the physicochemical properties of titanium surfaces biofunctionalized with the TGF-β inhibitor peptide MP17 through the immobilization procedure developed in chapter 1, and evaluate whether the peptide is properly immobilized on the titanium surface.

To maximize the chances of success in blocking the TGF-β activity in a biological environment, the P17 inhibitor peptide developed by Borrás-Cuesta et al. has been modified as described next:

The P17 TGF-β inhibitor peptide has the following amino acid sequence:

- P17: $NH_2$-KRIWFIPRSSWYERA-OH

This sequence is biologically active in a liquid environment and can interact with TGF-β inhibiting its interaction with cells [16,17,19]. In order to immobilize the peptide on a surface without hindering its biological effect it was decided that 2 modifications be made:

- Adding a chain of 5 glycines at the N-terminus
- After the addition of the 5 glycines, adding a lysine at the N-terminus

After the modification, the new peptide developed has the following amino acid sequence:

- MP17: $NH_2$-KGGGGGKRIWFIPRSSWYERA-OH

The reason for adding 5 glycines at the N-terminus of the peptide was to generate a spacer that separates the biological sequence of the P17 from the surface so the peptide can likely interact with TGF-β. On the other hand, the lysine at the N-terminus was added to benefit covalent anchoring between the peptide and the surface through the N-terminus since lysine contains a

primary amine as a side chain that could react covalently through a nucleophilic interaction using the malonic acid/HBTU route.

# 4.3. Materials and Methods

## 4.3.1. Materials

### 4.3.1.1. Titanium samples

The base material for the experiments was c.p. grade 2 titanium bars from Daido Steel Co. (Japan).

To perform the spectroscopic ellipsometry experiments it was necessary to purchase silicon wafers covered with a thin layer of $TiO_2$ using focused ion beam lithography [20,21]. The wafers were purchased from the Plataforma de Nanotecnología of the Barcelona Science Park (Spain).

### 4.3.1.2. Chemicals

The chemical compound employed to perform the NaOH treatment on the titanium surfaces was sodium hydroxide in pellet form from Sigma-Aldrich (USA). To wash the titanium samples we used 96% ethanol, 99%acetone, Chemsolv Inc. (USA), deionized water, 99% 2-propanol and 99.5% anhydrous cyclohexane from Sigma-Aldrich (USA).

To silanize the different surfaces, 98% 3-aminopropyltriethoxysilane (APTES) and anhydrous toluene from Sigma-Aldrich (USA) were used.

In the cross-linking step, N,N-Dimethylformamide (DMF), *O*-(Benzotriazol-1-yl)-*N,N,N',N'*-tetramethyluronium hexafluorophosphate (HBTU), *N*,*N*-Diisopropylethylamine (DIEA) and malonic acid from Sigma-Aldrich (USA) were used.

The fluorophores used to characterize the surfaces were 6 - (Fluorescein - 5 - carboxamido) hexanoic acid, succinimidyl ester; 5 - FAM - X, NHS ester or 5-FAM-X, SE and [5 - ((5 - Aminopentyl)thioureidyl)fluorescein] or FITC cadaverine from Anaspec (USA).

#### 4.3.1.3. Peptides

The MP17 peptide with the $NH_2$-KGGGGGKRIWFIPRSSWYERA-OH sequence was kindly provided by Dr. Javier Dotor, from Digna Biotech (Spain). The peptide was delivered as a trifluoroacetic salt.

## 4.3.2. Methods

#### 4.3.2.1. Base material preparation

The initial material was grade 2 commercially pure titanium discs of 10 mm diameter and 1 mm thickness. The disks were ground with silicon carbide disks and polished with alumina suspension until achieving a mirror surface with a Ra of less than 50 nm. After polishing, the samples were subsequently washed with cyclohexane, isopropanol, distilled water and acetone during 5 minutes, with sonication in each of the aforementioned solvents.

MP17 trifluoroacetic salt peptide was dialyzed in order to eliminate the trifluoroacetic acid that could interfere in the covalent immobilization processes. To do so, the MP17 peptide was dissolved in 1 ml of Milli-Q water and poured into a Biodialyser®, equipped with 1000 Da cellulose acetate membrane, Sigma-Aldrich (USA). The Biodialyser® was then immersed in deionized water with agitation for 2 hours, the water was subsequently changed and dialysis run for 2 more hours. Finally, the dialyzed MP17 peptide was lyophilized using a LD53 freeze dryer, Millrock Technology (USA), weighed and stored at -20 $^{o}$C.

#### 4.3.2.2. Surface treatments

##### *4.3.2.2.1. Surface activation*

In order to obtain effective silanization, the titanium surfaces were activated using two different methods in order to produce a high amount of OH groups on the surface that will react with APTES in the silanization process. The two different activation methods are described hereafter:

###### 4.3.2.2.1.1. Plasma cleaning:

The polished titanium samples were plasma cleaned [22] in oxygen plasma during 5 minutes in a PDC-32G plasma cleaner (Harrick Plasma, USA) following the manufacturer's protocol.

###### 4.3.2.2.1.2. Alkaline etching:

The clean and polished titanium samples were immersed in NaOH 5 mol/l at 60 $^{o}$C for 24 h [23,24]. After etching, the samples were immersed three times in deionized water for 30 minutes, washed with acetone and dried with nitrogen.

##### *4.3.2.2.2. Silanization*

Immediately after activation, the silanization process was performed. For silanization, the activated titanium samples were immersed in a solution of 30 mM of 3-aminopropyltriethoxysilane (APTES) in anhydrous toluene at 70 $^{o}$C during 1h with agitation and in a nitrogen atmosphere. After silanization, the samples were sonicated in anhydrous toluene for 15 minutes to detach any loose APTES molecules. Subsequently, the silanized samples were washed with ethanol, isopropanol, distilled water and acetone and dried with nitrogen.

#### *4.3.2.2.3. Cross-linking*

In the third step, the silanized samples were treated by immersing them into a dimethylformamide (DMF) solution containing the following reagents:

- 10 mM malonic acid
- 25 mM O-Benzotriazole-N,N,N',N'-tetramethyl-uronium-hexafluoro-phosphate (HBTU)
- 100 mM Di-isopropylethylamine (DIEA)

The cross-linking treatment was performed for 2h at room temperature with agitation. After this, the titanium samples were washed, twice immersing them in pure DMF.

#### *4.3.2.2.4. Peptide immobilization*

After the cross-linking step, the titanium samples were immediately immersed in a DMF solution containing 0,2 mM of the MP17 peptide or, failing that, 0,2 mM of the fluorescent molecules used for the fluorescence tests: the 5-FAM-X,SE or the FITC cadaverine.

The samples were immersed in the aforementioned solution overnight at room temperature with agitation. Thereafter, the samples were washed with ethanol, isopropanol, water, and acetone, dried with nitrogen and stored in vacuum until the selected characterization test was to be performed.

### 4.3.2.3. Surface characterization

Below is a description of the characterization methods used in this study. Depending on the method chosen, some modifications of the biofunctionalization procedure were necessary. These modifications are detailed in the description of each experiment.

#### *4.3.2.3.1. Surface chemical composition*

##### 4.3.2.3.1.1. X-Ray photoelectron spectroscopy (XPS):

Prior to the XPS analysis, the titanium samples, treated with the different steps of the biofunctionalization process, were sonicated for 2 hours in water in order to eliminate or diminish sufficient amount of physisorbed molecules from the surface. The XPS analyses were performed with a Quantum 2000 spectrometer (Physical Instruments, USA) using monochromated Al Kα: 1.487 KeV, at a take-off angle of 45$^{o}$ and a pass energy of 23.5 eV.

##### 4.3.2.3.1.2. Fourier Transform Infrared spectroscopy (FTIR):

As in the XPS experiment, the samples were sonicated for 2 hours prior to the FTIR analysis in order to eliminate the loosened molecules from the surface. The titanium samples were characterized with diffuse reflectance Infrared Fourier Transform Spectroscopy (DRIFTS) [25,26] with a Nicolet 6700 FTIR spectrometer (Thermo Scientific, USA).

#### *4.3.2.3.2. Evaluation of the coatings*

##### 4.3.2.3.2.1. Water contact angle:

Water contact angle measurements were performed using a DM-CE1 goniometer (Kyowa, Japan) injecting a 3 µl drop of distilled water on the samples and measuring the water contact angle after 30 s with the FAMAS software (Kyowa, Japan).

The activation method for this set of samples was plasma cleaning and the treatment was similar to the treatments applied on the fluorescence microscopy samples for mechanical and chemical stability respectively.

4.3.2.3.2.2. Thickness of the coatings:

To evaluate the thickness of the different coatings on the titanium surfaces the spectroscopic ellipsometry technique was used [27-38]. A description of spectroscopic ellipsometry can be found in Annex A of this thesis in electronic format.

To be able to study the presence of very thin organic layers on the surface of titanium by ellipsometry, a roughness lower than the thickness of the layers is necessary [39]. For this reason, the titanium disks were substituted by silicon wafers covered with a homogeneous titanium oxide layer. The activation method was plasma cleaning to maintain the smooth roughness of the samples. The spectroscopic ellipsometry tests were performed with a VASE spectroscopic ellipsometer (J.A. Wollam Co., USA). The angles of incidence of the beam were $60^{o}$ and $75^{o}$ and spectra was collected with a wavelength from 500 nm to 1100 nm with a pass of 15 nm.

The data was modeled using the WVASE software from the same company. The WVase software contains a database of the values of refractive index (n) and extinction coefficient (k) depending on the wavelength for the majority of known materials. The WVASE software calculates the thickness and optical properties automatically using an iterative algorithm. Equations used by the software to calculate the film thickness can be found in Annex A of this thesis in electronic format. Following there is a description of the data treatment performed to obtain the film thickness values on the different samples.

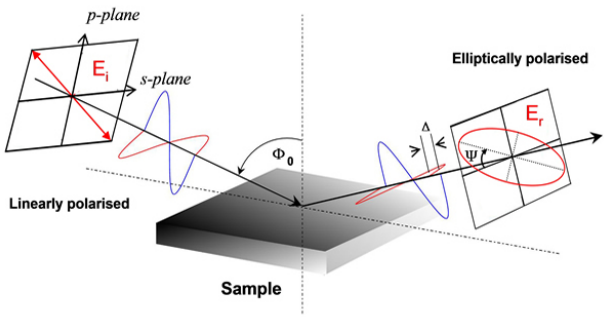


***Figure 4-1:*** *Linearly polarised light is generally elliptical polarised upon reflection with asymmetric intensity difference (tan Ψ) and phase difference (Δ) [40].*

Ellipsometry is a specular optical technique (the angle of incidence equals the angle of reflection). Ellipsometry detects changes in p- and s- components of the polarized light beam (Figure 4-1) upon reflection or transmission in relation to each other. In this manner, the reference beam is part of the experiment. A known polarization is reflected or transmitted from the sample and the output polarization is measured. The change in polarization is the ellipsometry measurement, commonly written as:

$$\rho = \frac{r_p}{r_s} = \tan(\Psi)e^{i\Delta} \qquad \textbf{Equation 4-1}$$

where $\rho$ is the complex ratio, $r_p$ and $r_s$ are the amount of light reflected at the parallel and perpendicular planes of the surfaces, respectively, as described by Fresnel [41,42]. $\Psi$ is the amplitude ratio and $\Delta$ is the phase shift of the light beam (Figure 4-1).

When a sample is analyzed, the raw data obtained with the spectroscopic ellipsometer are the amplitude ratio $\Psi$ and the phase shift $\Delta$ at all wavelengths in a given range as shown in figure 4-2:

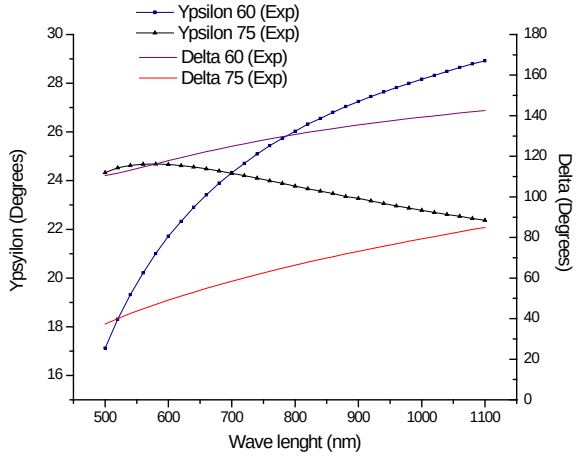


***Figure 4-2:*** *Spectroscopic ellipsometry data obtained on a $TiO_2$ covered silicon wafer for two different angles of light incidence.*

When n and k of the silicon substrate and the $TiO_2$ layer are known, it is possible to obtain the thickness of the $TiO_2$ layer by fitting the theoretical values with the experimental values as is shown in figure 4-3, additionally the Mean Square Error (MSE) of the fitting is shown.

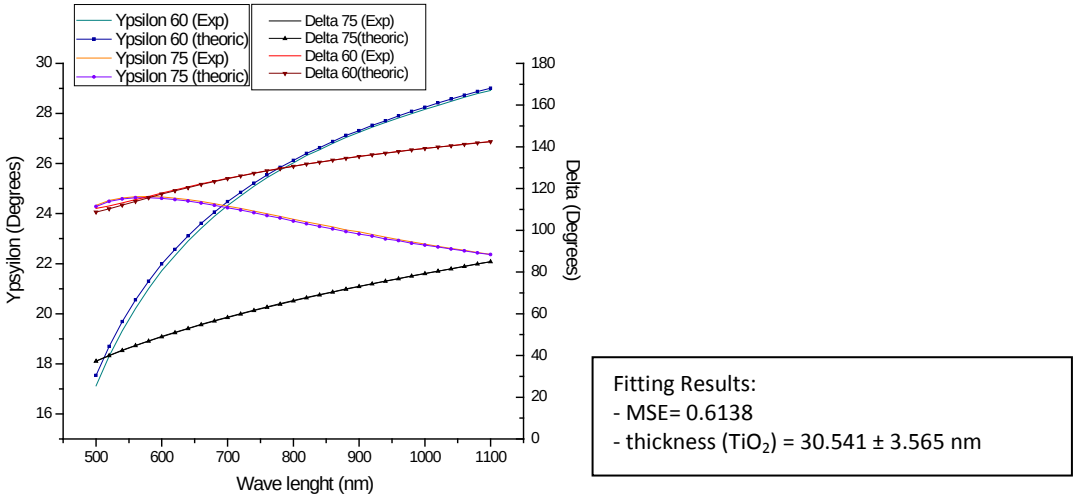


***Figure 4-3:*** *Spectroscopic ellipsometry fit data for a $TiO_2$ covered silicon wafer for two different angles of light incidence.*

Once the thickness of the $TiO_2$ layer of each silicon wafer was measured, the samples were treated with the different surface treatments of each step of the biofunctionalization process. Subsequently, spectroscopic analysis was performed again and a three layer model was set on the WVASE software to calculate the thickness of the different layers deposited on the wafers.

***Table 4-1:*** *Layer scheme of the model for ellipsometry study.*

| |
|---|
| **Cauchy layer** n,k (fixed), Thickness = 1 nm (fit), An=1.5 (fit), Bn=0.1 (fit), Cn=-0.5 (fit) |
| **$TiO_2$** n,k (fixed), Thickness = X nm (fixed) |
| **Silicon** n,k (fixed), Thickness = 1 mm (fixed) |

When n and k of one of the layers are unknown, it is possible to use a mathematic model to obtain the thickness and their optical parameters. The most useful model for organic layers is the Cauchy dispersion model (equation 4-2) [43-45].

$$n(\lambda) = A + \frac{B}{\lambda^2} + \frac{C}{\lambda^4} \qquad \textbf{Equation 4-2}$$

where A, B and C are coefficients obtained by fitting the data.

Once the samples were analysed and the layer model was set, the fitting algorithm was run to obtain the thickness and the Cauchy layer coefficients as is shown in figure 4-4.

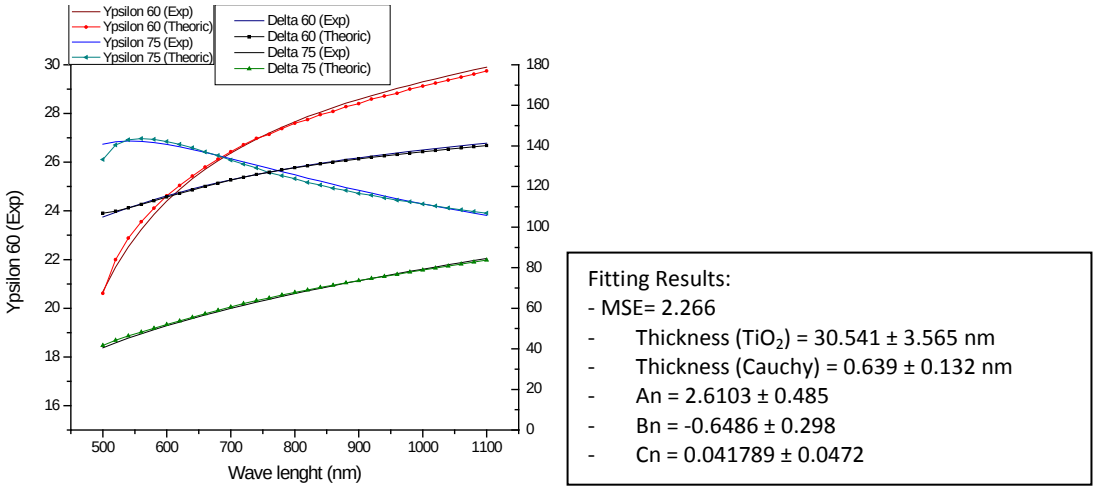


***Figure 4-4:*** *Spectroscopic ellipsometry fit data for an APTES silanized $TiO_2$ covered silicon wafer for two different angles of light incidence.*

To evaluate the values obtained by spectroscopic ellipsometry theoretical thicknesses of the layers were calculated by means of Chemdraw 3D Pro (Cambridgesoft, UK). The different molecules where drawn in 3 dimensions, respecting the theoretical distances and angles of the different atomic bonds present in the molecules and the distances between the atoms located on the opposite sides of the molecules were measured.

#### *4.3.2.3.3. Mechanical stability*

##### 4.3.2.3.3.1. Water contact angle:

For the mechanical stability tests, water contact angle measurements were measured after functionalization and, subsequently, the samples were sonicated in water at room temperature and the water contact angle measured after different sonication times to study the mechanical stability of the immobilized molecules.

4.3.2.3.3.2. Fluorescence:

For the fluorescence microscopy the samples were treated with the same protocol than the one used for the samples tested for water contact angle measurements.
The fluorescence microscopy analysis was performed by means of a BX51 microscope (Olympus, USA). The microscope was equipped with a fluorescent lamp and an Olympus DP 25 digital camera. The exposure time for each taken picture was 2 s and all parameters were fixed to get comparable intensities. After all the pictures were taken, the fluorescence intensity was evaluated extracting the mean value from the histogram of each micrography, using Image J ver. 1.45s.

Instead of the MP17 peptide, the samples were functionalized using the 5-FAM-X,SE or the FITC cadaverine in order to be able to characterize the effectiveness of the functionalization method. The reason to use these fluorophores to characterize the immobilization process is that they are surrogates for the peptide in the immobilization process. They are used to visualize the quality and homogeneity of the 'peptide' coatings before and after being both mechanically and thermal-chemically challenged. They can be used as surrogates of the peptides for this purpose as they reproduce the type of chemical reactions that the peptide will undergo with the processed titanium surface and, of course, provide fluorescent signaling.

It is worth noting that the samples used for water contact angle measurements were activated with plasma cleaning and the MP17 peptide was deposited on the surface in the last step of the biofunctionalization process. In the case of the fluorescence microscopy characterization, the samples were activated using NaOH, and the molecule deposited on the surface in the last step of the biofunctionalization process was FITC cadaverine or FAM-X, SE.

*4.3.2.3.4. Chemical stability*

For the chemical stability tests the samples followed similar treatment to the mechanical stability test but instead of being sonicated, samples were immersed in water at 37 $^{o}$C for different periods of time.

#### *4.3.2.3.5. Statistical analysis*

The statistical treatment of the data was similar to that described in section 2.4.1.5. In this chapter the software used to analyse the data was the IBM SPSS ver. 20.0 statistics software, IBM (USA).

# 4.4. Results

## 4.4.1. Nomenclature

Following the same nomenclature code used in chapter 3, abbreviations of the different samples have been created to facilitate monitoring of the results. In addition to the nomenclature code shown in section 3.4.1, the specific nomenclature for the materials or processes used in this chapter is presented as follows:

**TiO:** Refers to the silicon wafers covered with titanium dioxide used in the spectroscopic ellipsometry experiment.

**Plasma or P:** *Plasma cleaning.* Ti treated with plasma cleaning as described in section 2.4.1.3.1.

**FITC:** *FITC cadaverine.* Surface treated with [5 - ((5 - Aminopentyl)thioureidyl)fluorescein] or FITC cadaverine*,* as described in section 4.3.2.2.4

**FAM:** *FAM-X, SE.* Surface treated with 6 - (Fluorescein - 5 - carboxamido)hexanoic acid, succinimidyl ester; 5 - FAM - X, NHS ester or 5-FAM-X, SE as described in section 4.3.2.2.4.

**MP17:** Modified P17 peptide as described in section 4.3.2.2.4.

**Step1 or St1:** Refers to a polished titanium sample with the first step of the functionalization process which is the NaOH activation as described in section 4.3.2.2.1.2.

**Step2 or St2:** Refers to a polished titanium sample with the first (alkaline etching) and second (silanization) steps of the functionalization process as described in section 4.3.2.2.2.

**Step3 or St3:** Refers to a polished titanium sample with the first (alkaline etching), second (silanization) and third (crosslinking) steps of the functionalization process as described in section 4.3.2.2.3.

**Step4 or St4:** Refers to a polished titanium sample with the first (alkaline etching), second (silanization), third (crosslinking) and fourth (peptide immobilization) steps of the functionalization process as described in section 4.3.2.2.4.

## 4.4.2. Chemical composition of the biofunctionalized surfaces

### 4.4.2.1. X-Ray photoelectron spectroscopy

***Table 4-2:*** *XPS survey results in atomic percentage (NA: Not Assessed).*

| (%) At. | Ti | Ti NaOH (St. 1) | TiN APTES (St. 2) | TiNAPT Malonic A. (St. 3) | TiN APT Mal. MP17 (St. 4) |
|---|---|---|---|---|---|
| **O 1s** | 46.9 | 51.6 | 49.6 | 49.1 | 41.5 |
| **Ti 2p** | 8.3 | 16.2 | 14.5 | 13.1 | 10.9 |
| **Ca 2p** | 0.6 | 1.0 | 1.3 | 0.8 | 1.4 |
| **C 1s** | 37.3 | 24.6 | 22.4 | 24.9 | 32.9 |
| **Al 2p** | 7.0 | NA | NA | NA | NA |
| **Na 2p** | NA | 6.6 | 3.4 | 3.3 | 2.1 |
| **N 1s** | NA | NA | 3.7 | 5.0 | 7.8 |
| **Si 2p** | NA | NA | 4.2 | 3.9 | 3.5 |
| **Cl 2p** | NA | NA | 0.9 | NA | NA |

Table 4-2 shows the chemical composition of the titanium surfaces in each step of the functionalization process. It can be seen that polished titanium tended to adsorb higher quantities of carbon than the etched titanium, resulting in a lower titanium signal in these polished samples due to the masking effect of the carbon molecules. A masking effect on titanium was also shown throughout the whole functionalization process every time more layers were placed on the surface, and this was also observed in the progressively decreasing sodium and silicon signals.

The increase in nitrogen from step 2 to step 3 is due to the presence of the HOBt molecule attached to the malonic acid (see section 2.3.4), suggesting that the free carboxylate in the malonic acid remained activated after washing the samples. The high increases in nitrogen and carbon from step 3 to step 4 revealed the presence of peptide on the surface.

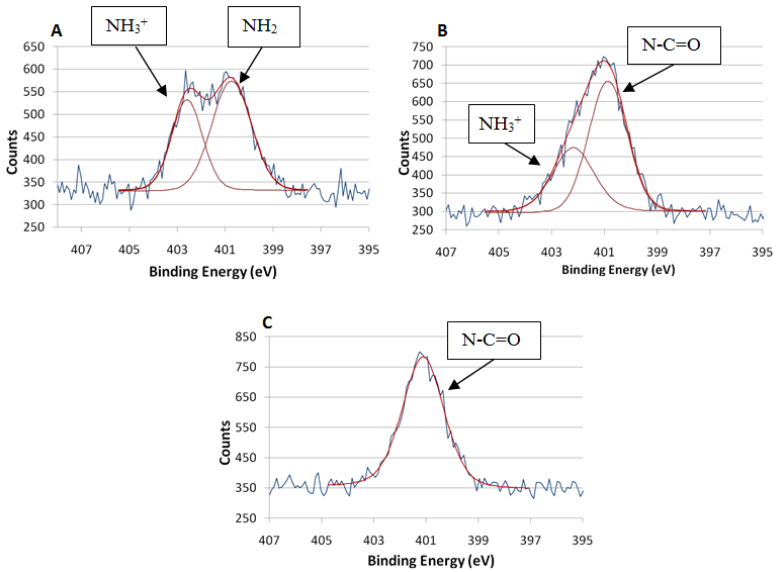


***Figure 4-5:*** *XPS deconvolutions of nitrogen peaks on the different titanium samples. A: TiN APTES. B: TiN APT Malonic a.. C: TiN APT Mal. MP17.*

One can observe, from figure 4-5, that the shape of the nitrogen peak changes in every step of the process. On APTES silanized samples, the amine from APTES silane is present in its protonated and unprotonated forms [38,46]. Once the malonic acid is coupled to the APTES silane, the presence of the amide bond at 400.7 eV [47,48] is highly evident together with an important reduction of the protonated amines from APTES, probably due to the presence of the HOBt molecule attached to the free carboxylates of the malonic acid. Finally, when the MP17 peptide is exposed to the surface, only one nitrogen peak is present on the spectra due to the APTES-malonic acid and malonic acid-MP17 amide bonds and the peptide bonds from the MP17 peptide [49,50]. These results demonstrate that the MP17 is attached covalently to the surface through the APTES+malonic acid route.

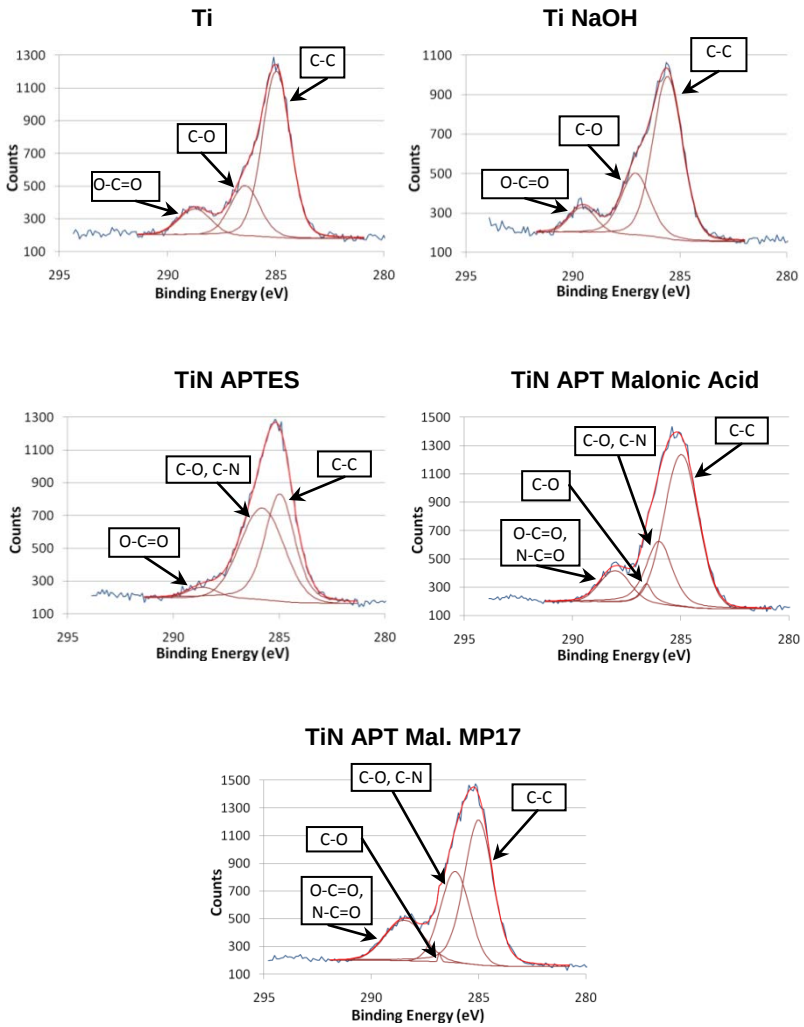


***Figure 4-6:*** *XPS deconvolutions of carbon peaks on the different titanium samples.*

***Table 4-3:*** *XPS atomic ratios between the different species detected in the C1s peak.*

| ***Ratio*** | **C-C/(C-N.C-O)** | **C-C/(O-C=O.N-C=O)** |
|---|---|---|
| **Ti** | 3.12 | 5.85 |
| **Ti NaOH (St. 1)** | 2.55 | 7.34 |
| **TiN APTES (St. 2)** | 0.89 | 11.66 |
| **TiN APT Malonic a. (St.3)** | 2.34 | 5.46 |
| **TiN APT Mal. MP17 (St. 4)** | 1.67 | 2.87 |

The deconvolution of the carbon peaks in every step of the functionalization process mainly revealed the presence of 3 carbon species: the C-C bond [51-53], the N-C bond [52,54,55] and the N-C=O bond [52,54,56]. Given that O-C, and O-C=O species are indistinguishable from the N-C and N-C=O species respectively [57,58], all the possible species present are labeled in figure 4-5. Nevertheless, the differences between peak ratios revealed substantial changes on the surface chemistry in every step of the process. The most remarkable change was detected after

the silanization step where a high increase of the C-N peak was observed, suggesting a successful silanization. When the malonic acid was added to the surface, the N-C=O peak increased due to the presence of a covalent bond between the malonic acid and APTES. The C-C/C-N ratio was also increased compared to the silanized samples, probably due to the presence of the aromatic ring on the HOBt molecule, activating the carboxylate of the malonic acid. In the last step, when the MP17 peptide was present on the surface, the N-C=O peak increased again due to the presence of the peptide bonds from the MP17.

### 4.4.2.2. Fourier Transform Infrared Spectroscopy (FTIR)

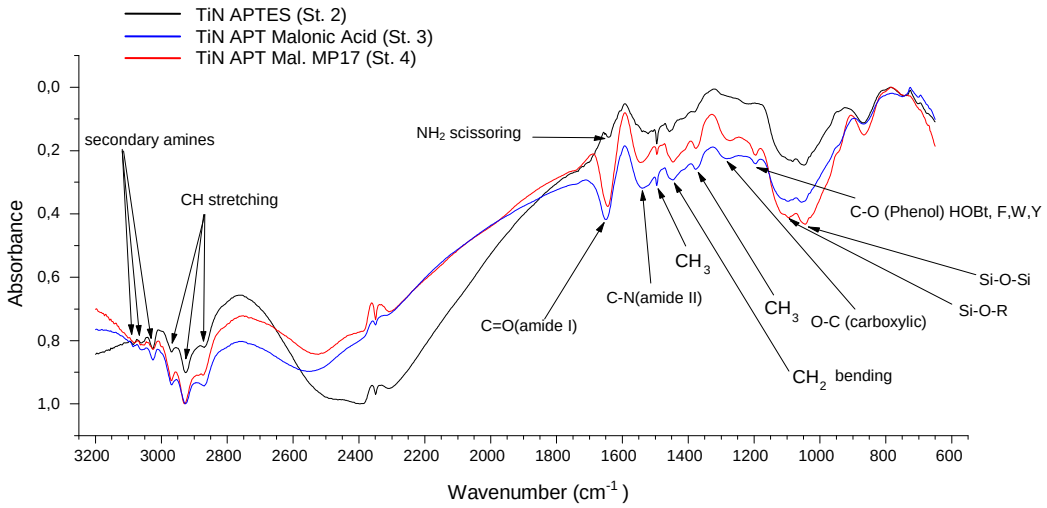


***Figure 4-7:****FTIR spectra of the different titanium surfaces obtained with DRIFTS.*

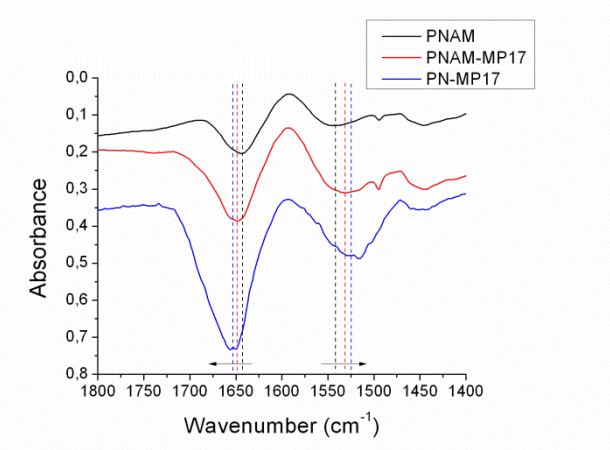


***Figure 4-8:*** *Detail of the amide bonds from the FTIR spectra of the titanium surfaces of interest. The dashed lines show the centre of the peaks for every sample.*

The FTIR spectra of the different titanium surfaces are shown in figure 4-7. The presence of APTES silane was well detected by this technique, showing the Si-O-Si [28,59] and Si-O-R [28] bonds at 1050 and 1097 cm-1 respectively. The silane backbone was clearly detected at 1444 and 2925 cm-1 [60] corresponding to $CH_2$ bending and CH stretching respectively. The band detected at 1641 $cm^{-1}$ [61] on the APTES silanized sample is attributed to the primary amines of the silane. This band was substituted by amide peaks (1544 and 1643 $cm^{-1}$ [62,63]) on the silanized and cross-linked sample, demonstrating the existence of a covalent bond between the APTES and malonic acid. When adding the MP17 peptide to the surface, the amide bands were shifted from 1542 to 1529 $cm^{-1}$ and from 1643 to 1648 $cm^{-1}$ (Figure 4-8). On a plain titanium sample with the MP17 peptide simply physisorbed on its surface, the amide peaks were located at 1525 and 1653 $cm^{-1}$ suggesting that the signal for the amide bonds on the biofunctionalized sample was significantly affected by the presence of the MP17 peptide.

## 4.4.3. Physical-chemical properties of the biofunctionalized surfaces

### 4.4.3.1. Surface wettability

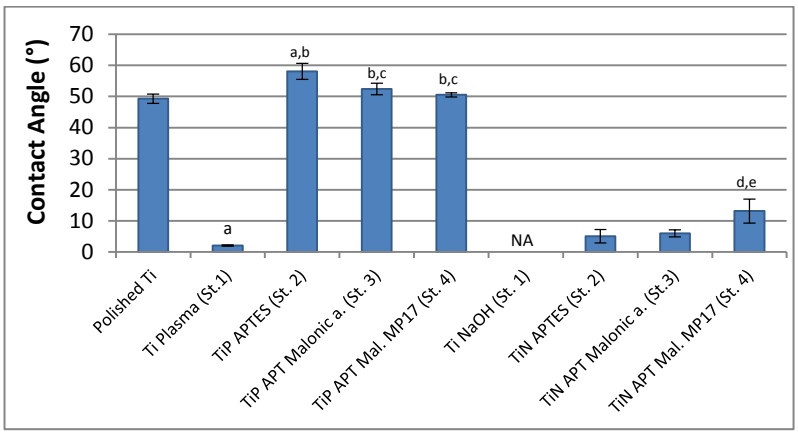


***Figure 4-9:*** *Water contact angle measurement of the different titanium surfaces (NA: Not assessed). Statistically significant differences with respect to a) Polished Ti, b) Ti Plasma and c) TiP APTES, d) TiN APTES and e) TiN APT Malonic a ($p<0,08$).*

The water contact angles measured in every step of the biofunctionalization process are reported in figure 4-9. The plasma cleaning treatment caused a dramatic reduction in the values of water contact angle due to the generation of $OH^-$ groups on the surface [64]. NaOH treatment was even more effective producing a highly polar surface as the Ti NaOH surfaces were superhydrophilic, which make the measurement of the water contact angle an impossible task. After silanization with APTES, the plasma-treated surfaces notably increased their water contact angle; however, only moderate increase of water contact angle on NaOH treated surfaces after silanization was assessed. The difference is probably due to the higher roughness of the NaOH treated samples which increased the hydrophilicity of the titanium surface. This fact made the evaluation of water contact angles on the NaOH treated samples a challenging task in general. After silanization, the water contact angle on plasma surfaces increased significantly due to presence of the hydrophobic alkyl chain in APTES [65]. After cross-linking, the water contact angle decreased slightly, and after peptide immobilization the water contact angle decreased again, due to the hydrophilic properties of malonic acid and MP17. On the surfaces treated with NaOH the contact angle increased slightly after silanization, remained similar after crosslinking and increased slightly again after MP17 immobilization. This result suggests that the NaOH surfaces have so high hydrophilic character that even after silanization and crosslinking there are still many hydrophilic sites on the surface, mainly due to its porosity, which are conditioning the general wettability of the surface. The fact that the contact angle increases after MP17 immobilization on the NaOH treated surfaces contrarily to the tendency on the plasma treated surfaces can be explained because of the contact angle on the NaOH treated surfaces were the MP17 is present tend to reach a value similar to the one obtained on the plasma treated surface but still is very influenced by the hydrophilicity provoked by the NaOH treatment. In other words, if there weren't the porosity and the hydrophilic character superimposed by the NaOH treatment, the samples with peptide, treated with plasma or NaOH would reach the same contact angle. Therefore, this is why both surfaces tend to reach a similar contact angle.

### 4.4.3.2. Thickness of the coatings

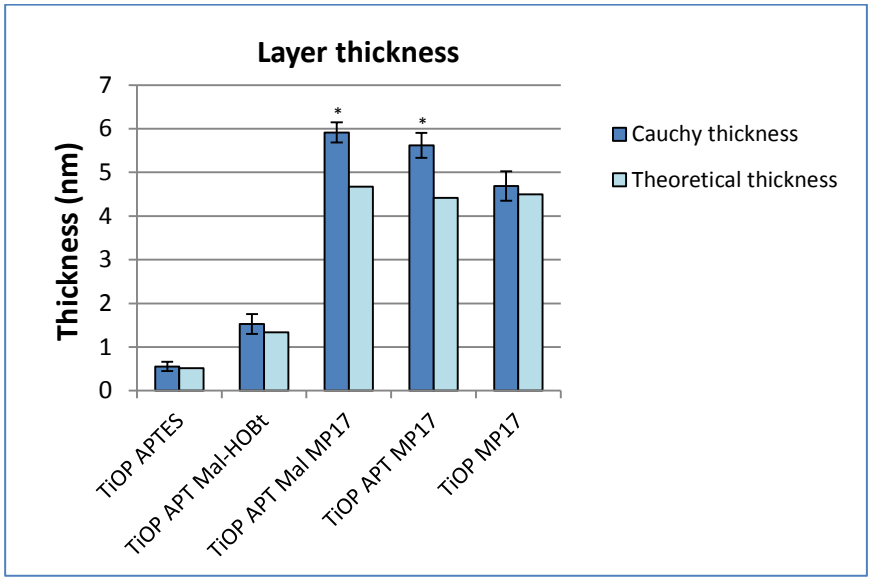


***Figure 4-10:*** *Thickness of the different coatings during the process of fabrication of the biofunctionalized surfaces calculated as Cauchy thickness of the coatings from ellipsometry tests (blue) and theoretical values obtained with Chemdraw 3D Pro (Cyan). * means that the differences are not statiscally significant between groups (p≥0,05).*

The analysis of the thickness of the Cauchy layers obtained by spectroscopic ellipsometry revealed the successful building up of the coatings during the biofunctionalization process. The calculated thickness of the APTES layer (about 0.52 nm) suggests that, after 2 h of sonication in water, a silane monolayer remained on the surface [28,29,34,37].

To validate the results, molecular drawings were performed using Chemdraw 3D Pro software. The software is capable to draw molecules in 3 dimensions respecting the theoretical distances and angles of atomic bonds. The software doesn't perform any molecular folding. Therefore, the atomic distances measured through this methodology are approximate to the real atomic distances when the molecules are small or don't have any folded geometry. In our case, we can assume that the theoretical distances obtained for the APTES molecule and APTES + Malonic acid coupling can be approximate to the real ones since little or no folding is expected. The theoretical atomic distances obtained for the MP17 peptide are not reliable because some folding is expected due to the interactions between amino acid side chains. After cross-linking with malonic acid, the coating grew about 1 nm in thickness. This result correlates well with the

theoretical dimensions, measured through the theoretical atomic distances of the molecules present on the surface, of a monolayer of APTES+ malonic acid + HOBt molecule figure 4-10. After linking the MP17 peptide, the thickness of the coating significantly increased due to the presence of the more bulky peptide molecules that remained attached after 2 h of sonication in water. It can be seen, in figure 4-10, that the theoretical thickness of the layers, where the MP17 peptide was present, was lower than the obtained through the ellipsometry measurements, even when the theoretical results didn't take in account molecular foldings which would decrease the value of the theoretical thickness. These result suggests thata multilayer of peptide was deposited on the surface, meaning that a physisorbtion process is always generated between the peptide and the surface, independently of whether a covalent reaction is taking place or not.

## 4.4.4. Stability of the coatings

### 4.4.4.1. Mechanical stability

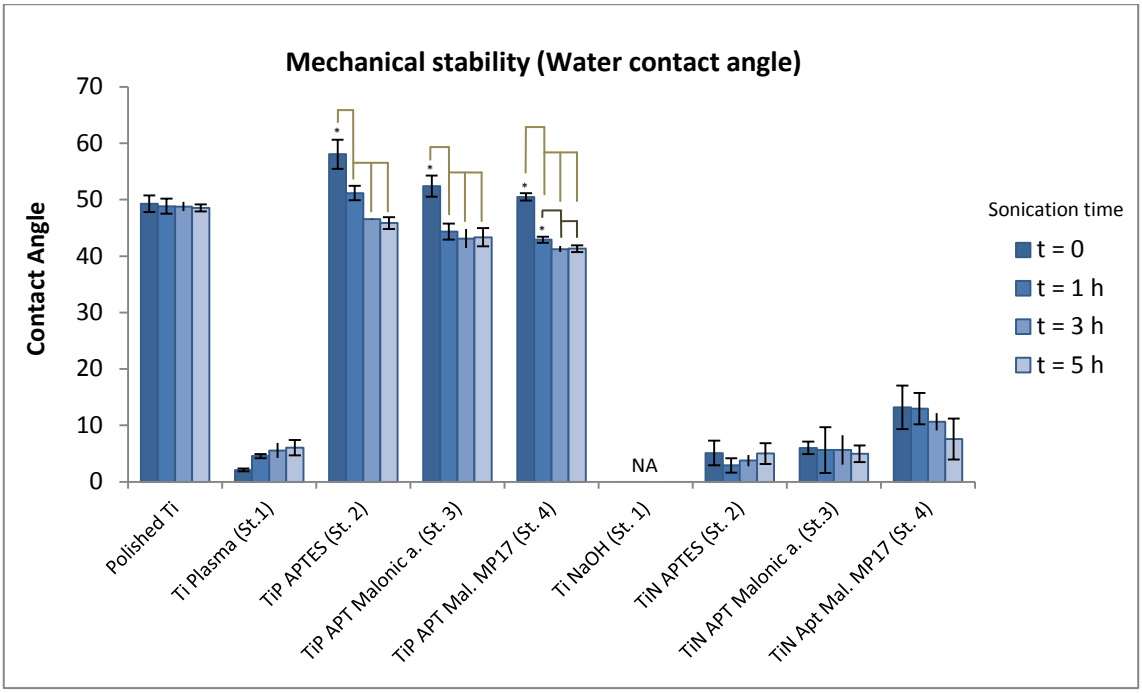


***Figure 4-11:*** *Water contact angle measurement of the different titanium surfaces after different sonication times in water (ND: Notassessed). * means that the differences are statiscally significant between the group marked with * and the groups pointed with a vertical line (p<0.08).*

In figure 4-11 one can observe that the water contact angle on the plasma activated samples increased with the sonication time but was still notably lower than clean titanium after 5 h of sonication in water. After steps 2, 3 and 4 of the preparation of the coatings the plasma-treated surfaces diminished their water contact angles during sonication. These results show that during sonication the loose APTES that was not strongly bonded to the surface was detached, decreasing the water contact angle. Physisorbed malonic acid and peptide can also be released from the surface during sonication, but the results suggest that it was loose APTES which was the weakest point of the coating. It is important to remark that after 3 h of sonication all surfaces were stable during sonication time. The data on NaOH treated surfaces did not show statistically significant differences; moreover, the measured water contact angles were very low and its reproducibility was too bad to get reliable results. This is due to the high hydrophilic character of the surfaces produced by the NaOH treatment as was explained in section 4.4.3.1.

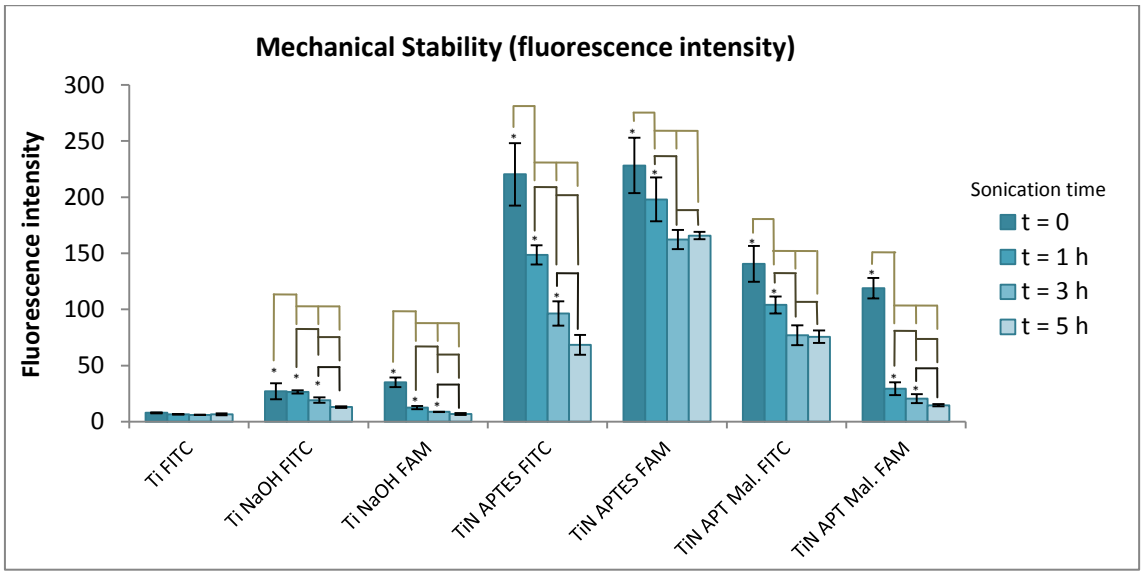


***Figure 4-12:*** *Fluorescence intensities of the different titanium surfaces coated with fluorescent molecules as surrogates of MP17 peptides: 5-FAM-X,SE and FITC cadaverine.* means that the differences are statiscally significant between the group marked with * and the groups pointed with a vertical line ($p<0.08$).*

In figure 4-12 is possible to observe that the silanized samples labeled with 5-FAM-X, SE and the silanized and cross-linked samples labeled with FITC cadaverine reached a stable intensity after 3 hours of sonication in water. Since APTES contains a primary amine and 5-FAM-X, SE has an active ester; a covalent bond should form between the two molecules. Also, the active ester of the malonic acid and the amine of FITC cadaverine should react to form covalent bonds

between these two molecules on the silanized and cross-linked samples. Covalent bonds were not expected to occur in the rest of the samples and thus, they did not produce stable coatings that were progressively detached during sonication in water.

FITC cadaverine contains a free primary amine. Thus, it can act as surrogate for the MP17 peptide since it is expected that the peptide would perform a reaction between the active ester of the malonic acid and the primary amines of the peptide at its N-terminus or at the lysine side chains, similar to the reaction between malonic acid and FITC cadaverine.

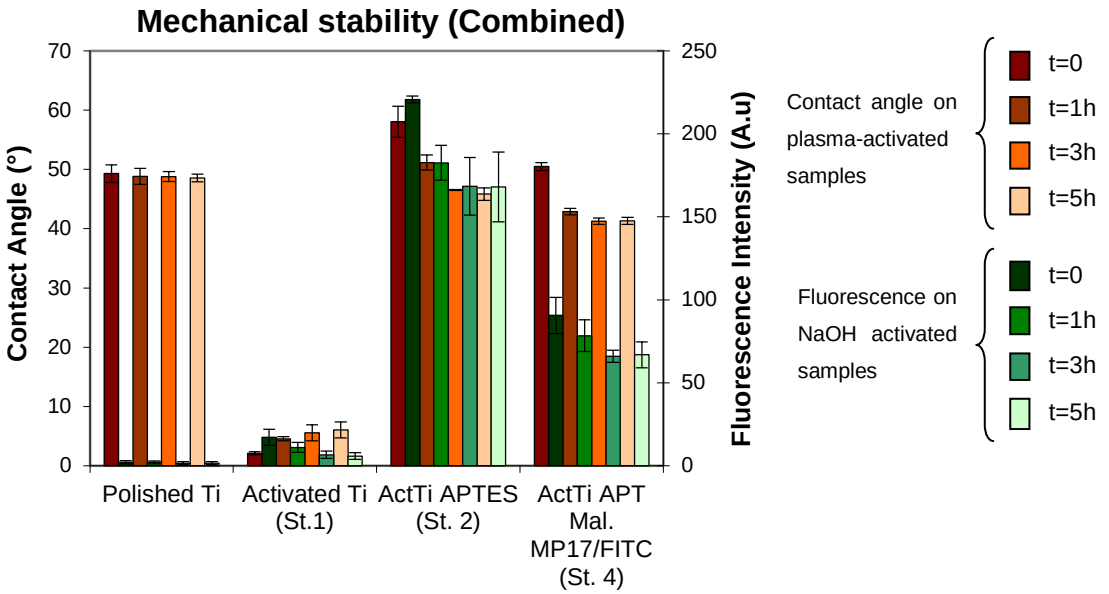


***Figure 4-13:*** *Combination of the results obtained in the fluorescence test and the results obtained in the water contact angle test for different times of sonication in water.*

The results of fluorescence intensity and water contact angle for different sonication times are combined and compared in figure 4-13. Even though the samples for water contact angle were activated by plasma cleaning and the samples used for assessing fluorescent intensity were activated by alkaline etching the correlation between the two techniques was very good. As the water contact angles in step 4 were obtained by linking the MP17 peptide, and the fluorescence results for the same step were obtained by labeling the surface with FITC cadaverine the good correlation between both results also validated the use of the fluorescent molecules as surrogates for the peptides under these bonding conditions. Most importantly, this result also confirmed that both the NaOH treatment and plasma cleaning are valid treatments for

activating the titanium surface to facilitate and obtain a successful anchoring of APTES molecules. It is worth noting to add that NaOH treatment generates a higher surface index; i.e., a much rougher surface and thus, it provides with a higher potential for activation and subsequent bonding of silane molecules.

#### 4.4.4.2. Chemical stability

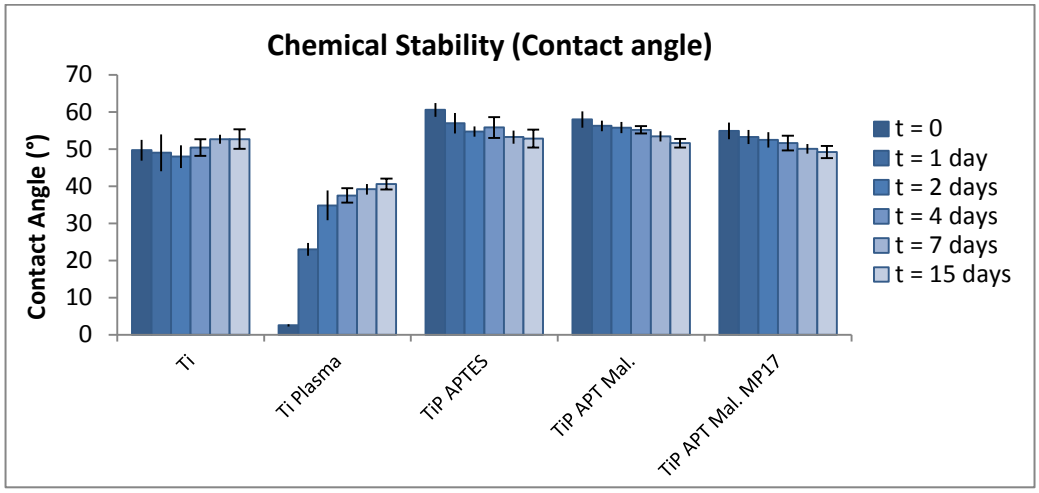


***Figure 4-14:*** *Water contact angle measurement of the different titanium surfaces after different immersion times in water at 37 °C.*

As can be observed in figure 4-14, the response of all samples correlates to the behavior shown in the mechanical stability from figure 4-11 except that here the treated surfaces did not stabilize over time. These results suggested that on top of the release of not covalently bonded APTES molecules, hydrolysis of APTES took place during the immersion of the coatings in water [66], releasing silane molecules and all the other molecules covalently-attached to the surface through the silane linker. A curing treatment after silanization, consisting on heating the silanized samples at 100 $^{o}$C for 24 h, could reduce this effect. This procedure provokes the siloxane condensation creating a stable and dense silane layer on the surface [29]. Nevertheless, the hydrolysis of APTES seems to be slow enough for our purposes, since the inhibition of TGF-β by the MP17 present on the surface is expected to last few days due to the surface remodelation that cells perform, *in vitro,* when cells are seeded on a surface or *in vivo*, when a biomaterial is implanted in bone[67].

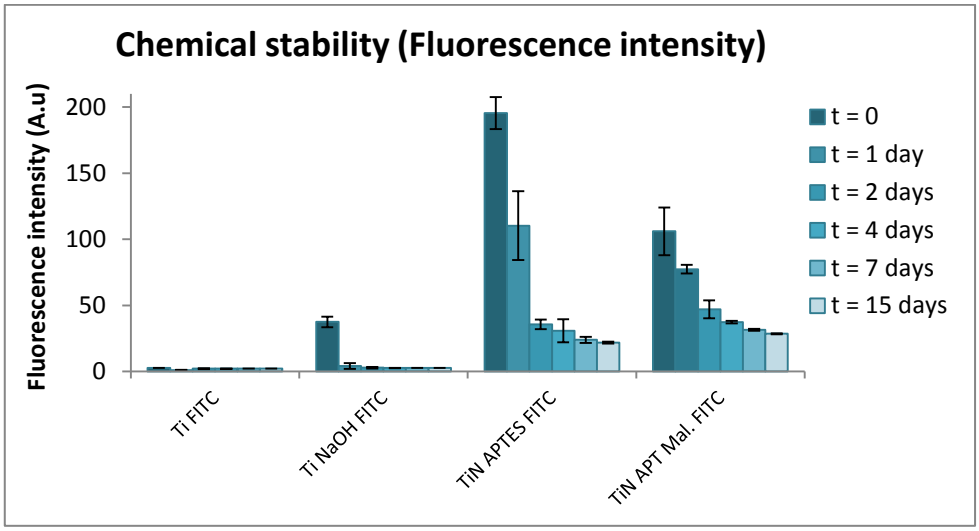


***Figure 4-15:*** *Fluorescence intensities of the different titanium surfaces, labelled with FITC cadaverine, during different immersion times in water at 37 °C.*

The results in figure 4-15 correlate with the results of water contact angle for chemical stability as hydrolysis of APTES occurred and thus, other molecules linked to it to the silane were partially released from the surface. The covalent bond between malonic acid and FITC cadaverine hindered the release of the fluorescent label during the first days of immersion compared to the non-covalently physisorbed FITC-label on the silanized samples.

## 4.5. Discussion

A peptide, P17, developed by Borrás-Cuesta et. al. has demonstrated its effect on inhibiting the TGF-β1 signaling pathway and reducing fibrosis in liver injury in rats [5]. The TGF-β1 antagonistic peptide, P17, binds TGF-β1 blocking the interaction between TGF-β1 and the cell receptors and, therefore, reducing the production of type I collagen and fibrotic reaction [16,19].

So far, titanium surfaces have been modified with peptides or proteins that act directly with the cells to control their behavior. The most common modification is the immobilization of peptides with RGD sequences to promote cell adhesion [68-73]. We have developed a 4-step process to covalently immobilize TGF-β1 antagonistic peptides to titanium surfaces in order to inhibit the

interaction between TGF-β1 and cell receptors, and therefore, reduce the expression of fibrous tissue. This process generates a high and homogeneous surface coverage that generates a selective covalent bond to the primary amines of the peptide without polymerization and/or racemization.

To evaluate the performance of every step of the functionalization process, XPS analysis was carried out. The increase in nitrogen and carbon on the surfaces treated with the MP17 peptide demonstrated the presence of the peptide on the surface. Deconvolution of nitrogen peaks in the samples where nitrogen was present revealed the existence of amide bonds between the surface and the other components deposited on it. Therefore, a covalent bond was achieved between the surface and the MP17 peptide.

The different molecular species present on the surfaces were analyzed by DRIFTS. DRIFTS results confirmed XPS results and the shift of amide peaks between the silanized surfaces treated with malonic acid and the ones with the MP17 peptide suggested that a covalent bond was formed. In general XPS is a powerful technique that allows to get a high amount of chemical information of the surface of a sample. Although, it is an expensive and time consuming technique. DRIFTS, on the other side, is a non-destructive technique that can be performed in few seconds by a user without a high knowledge on the technique. Therefore, DRIFTS can be an excellent choice for a rapid evaluation of the quality of a functionalized surface.

Despite the fact that diverse activation techniques, such plasma cleaning and NaOH etching, were used to analyze the titanium surfaces by employing different characterization methods (contact angle and fluorescent intensity), the results obtained presented similar tendencies. This fact boosts our confidence concerning the interpretation of the results and the existence of a covalent bond between the surface and the MP17 peptide.

Ellipsometry results showed that the silanized titanium oxide wafers produced a silane monolayer according to the thickness obtained by other authors [28,29,34,37]. Also it has been reported that the MP17 peptide forms a multilayer of peptide on the surface, confirming the results obtained with other peptides in the previous chapters of this thesis.

On a fully functionalized surface (i.e. Activated, silanized, crosslinked and peptide immobilized) the fact of having a multilayer of peptide on the surface would mean that the amount of peptide that one can obtain on the surface is greatly increased in comparison with a monolayer of peptide. A high amount of MP17 peptide on the surface is desirable, since the more amount of peptide on the surface, the higher would be the TGF-β inhibition effect. Additionally, a multilayer of peptide on the surface implies that not all the peptide would be covalently bound to the surface. The not covalently bound peptide will be physisorbed on the surface and, therefore, it will detach more easily than the covalently bound peptide from the surface. The covalently attached peptide will remain on the surface when all the physisorbed multilayer of peptide is gone, allowing the surface to be bioactive for longer times than a surface with only physisorbed peptide on it.

## 4.6. Conclusions

Through the APTES+malonic acid/HBTU route, the biofunctionalization of pre-activated titanium surfaces with the TGF-β inhibitor peptide MP17 has been accomplished.

The developed surfaces presented a multilayer of MP17 peptide on the surface. A certain part of the peptide was covalently bound to the surface and the rest physisorbed.

A covalent bond between the titanium surface and the MP17 peptide has been achieved, ensuring a high stability of the surfaces in the presence of mechanical and thermal-chemical challenges.

# 4.7. References

1. Digna Biotech. Digna Biotech - P17. http://www.dignabiotech.com/r_d.Products_p17.asp. 2012.

2. Digna Biotech. Digna Biotech - P144. http://www.dignabiotech.com/r_d.Products_p114.asp. 2012.

3. Sporn MB, Roberts AB. Introduction: What is TGF-beta? Ciba foundation Symposium 1991;157:1-6.

4. Massague J. The Transforming Growth Factor-beta Family. Annu Rev Cell Biol 1990;6:597-641.

5. Ezquerro I, Lasarte J, Dotor J, Castilla-Cortázar I, Bustos M, Peñuelas I, Blanco G, Rodríguez C, Lechuga MdCG, Greenwel P, Rojkind M, Prieto J, Borrás-Cuesta F. A synthetic peptide from transforming growth factor β type III receptor inhibits liver fibrogenesis in rats with carbon tetrachloride liver injury. Cytokine 2003;22:12-20.

6. Bosetti M, Boccafoschi F, Leigheb M, Cannas MF. Effect of different growth factors on human osteoblasts activities: A possible application in bone regeneration for tissue engineering. Biomol Eng 2007;24:613-618.

7. Sumner DR, Turner TM, Purchio AF, Gombotz WR, Urban RM, Galante JO. Enhancement of bone ingrowth by transforming growth factor-beta. The Journal of Bone & Joint Surgery 1995;77:1135-1147.

8. Clokie CML, Bell RC. Recombinant Human Transforming Growth Factor [beta]-1 and Its Effects on Osseointegration. J Craniofac Surg 2003;14:268-277.

9. Schmidmaier G, Lucke M, Schwabe P, Raschke M, Haas NP, Wildemann B. Collective review: bioactive implants coated with poly(D,L-lactide) and growth factors IGF-I, TGF-beta1, or BMP-2 for stimulation of fracture healing. Journal of Long-Term Effects of Medical Implants 2006;16:61-69.

10. Lind M, Overgaard S, Søballe K, Nguyen T, Ongpipattanakul B, Bünger C. Transforming growth factor-?1 enhances bone healing to unloaded tricalcium phosphate coated implants: An experimental study in dogs. Journal of Orthopaedic Research 1996;14:343-350.

11. Lind M, Overgaard S, Glerup H, Søballe K, Bünger C. Transforming growth factor-β1 adsorbed to tricalciumphosphate coated implants increases peri-implant bone remodeling. Biomaterials 2001;22:189-193.

12. Aspenberg P, Jeppsson C, Wang J-, Boström M. Transforming growth factor beta and bone morphogenetic protein 2 for bone ingrowth: A comparison using bone chambers in rats. Bone 1996;19:499-503.

13. Tielinen L, Puolakkainen P, Pohjonen T, Rautavuori J, Törmälä P, Rokkanen P. The effect of transforming growth factor-β1, released from a bioabsorbable self-reinforced polylactide pin, on a bone defect. Biomaterials 2002;23:3817-3823.

14. Ueda H, Hong L, Yamamoto M, Shigeno K, Inoue M, Toba T, Yoshitani M, Nakamura T, Tabata Y, Shimizu Y. Use of collagen sponge incorporating transforming growth factor-β1 to promote bone repair in skull defects in rabbits. Biomaterials 2002;23:1003-1010.

15. Nikolidakis D, Meijer GJ, Oortgiesen DAW, Walboomers XF, Jansen JA. The effect of a low dose of transforming growth factor β1 (TGF-β1) on the early bone-healing around oral implants inserted in trabecular bone. Biomaterials 2009;30:94-99.

16. Vicent S, Luis-Ravelo D, Antón I, García-Tuñón I, Borrás-Cuesta F, Dotor J, De Las Rivas J, Lecanda F. A novel lung cancer signature mediates metastatic bone colonization by a dual mechanism. Cancer Res 2008;68:2275-2285.

17. Serrati S, Margheri F, Pucci M, Cantelmo AR, Cammarota R, Dotor J, Borràs-Cuesta F, Fibbi G, Albini.A, Del Rosso M. TGFb1 antagonistic peptides inhibit TGFb1-dependent angiogenesis. Biochemical Pharmacology 2009;77:812-825.

18. Hermida N, López B, González A, Dotor J, Lasarte JJ, Sarobe P, Borrás-Cuesta F, Díez J. A synthetic peptide from transforming growth factor-β1 type III receptor prevents myocardial fibrosis in spontaneously hypertensive rats. Cardiovascular Research 2009;81:601-609.

19. Dotor J, López-Vázquez AB, Lasarte JJ, Sarobe P, García-Granero M, Riezu-Boj J, Martínez A, Feijoó E, López-Sagaseta J, Hermida J, Prieto J, Borrás-Cuesta F. Identification of peptide inhibitors of transforming growth factor beta 1 using a phage-displayed peptide library. Cytokine 2007;39:106-115.

20. Morimoto H, Sasaki Y, Saitoh K, Watakabe Y, Kato T. Focused ion beam lithography and its application to submicron devices. Microelectronic Engineering 1986;4:163-179.

21. Luttge R. Chapter 4 - nanotechnology. Microfabrication for Industrial ApplicationsBoston: William Andrew Publishing, 2011. p. 91-146.

22. Kominiak GJ, Mattox DM. Reactive plasma cleaning of metals. Thin Solid Films 1977;40:141-148.

23. Aparicio C, Rodriguez D, Gil FJ. Variation of roughness and adhesion strength of deposited apatite layers on titanium dental implants. Materials Science and Engineering: C 2011;31:320-324.

24. Gil FJ, Padrós A, Manero JM, Aparicio C, Nilsson M, Planell JA. Growth of bioactive surfaces on titanium and its alloys for orthopaedic and dental implants. Materials Science and Engineering: C 2002;22:53-60.

25. Workman Jr. J. 12 - review of near-infrared and infrared spectroscopy. The Handbook of Organic CompoundsBurlington: Academic Press, 2001. p. 79-129.

26. Warner WS, Tenge BJ, Hungerford JM, Honigs DE. Diffuse reflectance infrared Fourier transform spectroscopic characterization of a silica-immobilized N-hydroxysuccinimide active ester crosslinking agent and its precursors. Anal Biochem 1989;176:137-149.

27. Höök F, Vörös J, Rodahl M, Kurrat R, Böni P, Ramsden JJ, Textor M, Spencer ND, Tengvall P, Gold J, Kasemo B. A comparative study of protein adsorption on titanium oxide surfaces using in situ ellipsometry, optical waveguide lightmode spectroscopy, and quartz crystal microbalance/dissipation. Colloids and Surfaces B: Biointerfaces 2002;24:155-170.

28. Kim J, Seidler P, Wan LS, Fill C. Formation, structure, and reactivity of amino-terminated organic films on silicon substrates. J Colloid Interface Sci 2009;329:114-119.

29. Kim J, Seidler P, Fill C, Wan LS. Investigations of the effect of curing conditions on the structure and stability of amino-functionalized organic films on silicon substrates by Fourier transform infrared spectroscopy, ellipsometry, and fluorescence microscopy. Surf Sci 2008;602:3323-3330.

30. Kurrat R, Wälivaara B, Marti A, Textor M, Tengvall P, Ramsden JJ, Spencer ND. Plasma protein adsorption on titanium: comparative in situ studies using optical waveguide lightmode spectroscopy and ellipsometry. Colloids and Surfaces B: Biointerfaces 1998;11:187-201.

31. Lee MH, Brass DA, Morris R, Composto RJ, Ducheyne P. The effect of non-specific interactions on cellular adhesion using model surfaces. Biomaterials 2005;26:1721-1730.

32. Love JC, Wolfe DB, Haasch R, Chabinyc ML, Paul KE, Whitesides GM, Nuzzo RG. Formation and Structure of Self-Assembled Monolayers of Alkanethiolates on Palladium. J Am Chem Soc 2003;125:2597-2609.

33. Rezania A, Johnson R, Lefkow AR, Healy KE. Bioactivation of Metal Oxide Surfaces. 1. Surface Characterization and Cell Response. Langmuir 1999;15:6931-6939.

34. Tosatti S, Paul SMD, Askendal A, VandeVondele S, Hubbell JA, Tengvall P, Textor M. Peptide functionalized poly(-lysine)-g-poly(ethylene glycol) on titanium: resistance to protein adsorption in full heparinized human blood plasma. Biomaterials 2003;24:4949-4958.

35. Toworfe GK, Composto RJ, Shapiro IM, Ducheyne P. Nucleation and growth of calcium phosphate on amine-, carboxyl- and hydroxyl-silane self-assembled monolayers. Biomaterials 2006;27:631-642.

36. Vandenberg E, Elwing H, Askendal A, Lundström I. Protein immobilization of 3-aminopropyl triethoxy silane/glutaraldehyde surfaces: Characterization by detergent washing. J Colloid Interface Sci 1991;143:327-335.

37. Vandenberg ET, Bertilsson L, Liedberg B, Uvdal K, Erlandsson R, Elwing H, Lundström I. Structure of 3-aminopropyl triethoxy silane on silicon oxide. J Colloid Interface Sci 1991;147:103-118.

38. Xiao SJ, Textor M, Sencer ND, Wieland M, Keller B, Sigrist H. Immobilization of the cell-adhesive peptide Arg–Gly–Asp–Cys (RGDC) on titanium surfaces by covalent chemical attachment. J Mater Sci Mater Med 1997;8:867-872.

39. Wollam JA. Ellipsometry tutorial. http://www.jawoollam.com/tutorial_1.html. 2012.

40. McGilp JF, McGovern IT, McGuinness C. Surface and Interfase Physics - Ellipsometry. 2012.

41. Azzam RMA. The intertwined history of polarimetry and ellipsometry. Thin Solid Films 2011;519:2584-2588.

42. Azzam,R.,M.,A., Bashara N,M. Ellipsometry and Polarized Light. 1986.

43. Suzuki I, Ejima M, Watanabe K, Xiong Y, Saitoh T. Spectroscopic ellipsometry characterization of Ba0.7Sr0.3TiO3 thin films prepared by the sol-gel method. Thin Solid Films 1998;313–314:214-217.

44. Eiamchai P, Chindaudom P, Pokaipisit A, Limsuwan P. A spectroscopic ellipsometry study of TiO2 thin films prepared by ion-assisted electron-beam evaporation. Current Applied Physics 2009;9:707-712.

45. Gao G, Lange D, Hilpert K, Kindrachuk J, Zou Y, Cheng JTJ, Kazemzadeh-Narbat M, Yu K, Wang R, Straus SK, Brooks DE, Chew BH, Hancock REW, Kizhakkedathu JN. The biocompatibility and biofilm resistance of implant coatings based on hydrophilic polymer brushes conjugated with antimicrobial peptides. Biomaterials 2011;32:3899-3909.

46. Kallury KMR, Macdonald PM, Thompson M. Effect of Surface Water and Base Catalysis on the Silanization of Silica by (Aminopropyl)alkoxysilanes Studied by X-ray Photoelectron Spectroscopy and 13C Cross-Polarization/Magic Angle Spinning Nuclear Magnetic Resonance. Langmuir 1994;10:492-499.

47. Polzonetti G, Battocchio C, Iucci G, Dettin M, Gambaretto R, Di Bello C, Carravetta V. Thin films of a self-assembling peptide on TiO2 and Au studied by NEXAFS, XPS and IR spectroscopies. Materials Science and Engineering: C 2006;26:929-934.

48. Xue A, Zhou S, Zhao Y, Lu X, Han P. Effective NH2-grafting on attapulgite surfaces for adsorption of reactive dyes. J Hazard Mater 2011;194:7-14.

49. Deligianni DD, Katsala N, Ladas S, Sotiropoulou D, Amedee J, Missirlis YF. Effect of surface roughness of the titanium alloy Ti–6Al–4V on human bone marrow cell response and on protein adsorption. Biomaterials 2001;22:1241-1251.

50. Serro AP, Gispert MP, Martins MCL, Brogueira P, Colaço R, Saramago B. Adsorption of albumin on prosthetic materials: Implication for tribological behavior. Journal of Biomedical Materials Research Part A 2006;78A:581-589.

51. Bondarenka V, Tvardauskas H, Grebinskij S, Senulis M, Pasiskevicius A, Volkov V, Zakharova G. - Sol-gel synthesis and XPS study of vanadium-hydroquinone oxide bronze films. - physica status solidi (c) - 2009;- 6:- 2807--2809.

52. Moulder JF, Stickle WF, Sobol PE, Bomben KD. Handbook of X-ray photoelectron spectroscopy. : Physical Electronics Inc., 1992.

53. National Institute of Standards and Technology, NIST. NIST X-ray Photoelectron Spectroscopy Database. http://srdata.nist.gov/xps/. 2007.

54. Kang B, Sul Y, Oh S, Lee H, Albrektsson T. XPS, AES and SEM analysis of recent dental implants. Acta Biomaterialia 2009;5:2222-2229.

55. Awsiuk K, Bernasik A, Kitsara M, Budkowski A, Rysz J, Haberko J, Petrou P, Beltsios K, Raczkowska J. Protein coverage on silicon surfaces modified with amino-organic films: A study by AFM and angle-resolved XPS. Colloids and Surfaces B: Biointerfaces 2010;80:63-71.

56. Mekhalif Z, Cossement D, Hevesi L, Delhalle J. Electropolymerization of pyrrole on silanized polycrystalline titanium substrates. Appl Surf Sci 2008;254:4056-4062.

57. Feng B, Weng J, Yang BC, Chen JY, Zhao JZ, He L, Qi SK, Zhang XD. Surface characterization of titanium and adsorption of bovine serum albumin. Mater Charact 2002;49:129-137.

58. Iucci G, Dettin M, Battocchio C, Gambaretto R, Bello CD, Polzonetti G. Novel immobilizations of an adhesion peptide on the TiO2 surface: An XPS investigation. Materials Science and Engineering: C 2007;27:1201-1206.

59. Meng X, Wang D, Liu J, Zhang S. Preparation and characterization of sodium titanate nanowires from brookite nanocrystallites. Mater Res Bull 2004;39:2163-2170.

60. Maoz R, Sagiv J, Degenhardt D, Möhwald H, Quint P. Hydrogen-bonded multilayers of self-assembling silanes: structure elucidation by combined Fourier transform infra-red spectroscopy and X-ray scattering techniques. Supramol Sci 1995;2:9-24.

61. R.J. Martín-Palma, M. Manso, J.M. Martínez-Duart, J. Pérez-Rigueiro, J.P. García-Ruiz. Surface biofunctionalization of materials by amine groups.

62. Xie J, Riley C, Kumar M, Chittur K. FTIR/ATR study of protein adsorption and brushite transformation to hydroxyapatite. Biomaterials 2002;23:3609-3616.

63. Cheng S, Chittur KK, Sukenik CN, Culp LA, Lewandowska K. The Conformation of Fibronectin on Self-Assembled Monolayers with Different Surface Composition: An FTIR/ATR Study. J Colloid Interface Sci 1994;162:135-143.

64. Takeda S, Fukawa M. Role of surface OH groups in surface chemical properties of metal oxide films. Materials Science and Engineering B 2005;119:265-267.

65. Tan G, Zhang L, Ning C, Liu X, Liao J. Preparation and characterization of APTES films on modification titanium by SAMs. Thin Solid Films 2011;519:4997-5001.

66. Schramm C, Rinderer B. Investigation of the hydrolysis of (3-triethoxysilylpropyl)succinic acid anhydride by means of FT-IR. J Mater Sci 2008;43:4215-4219.

67. Aparicio C, Padrós A, Gil F. In vivo evaluation of micro-rough and bioactive titanium dental implants using histometry and pull-out tests. Journal of the Mechanical Behavior of Biomedical Materials ;In Press, Corrected Proof.

68. Sevilla P, Godoy M, Salvagni E, Gil FJ. Biofunctionalization of titanium surfaces for osseintegration process improvement. Journal of Physics: Conference Series 2010;252:012009.

69. Raynor JE, Petrie TA, García AJ, Collard DM. Controlling Cell Adhesion to Titanium: Functionalization of Poly[oligo(ethylene glycol)methacrylate] Brushes with Cell-Adhesive Peptides. Adv Mater 2007;19:1724-1728.

70. Dettin M, Conconi MT, Gambaretto R, Bagno A, Di Bello C, Menti AM, Grandi C, Parnigotto PP. Effect of synthetic peptides on osteoblast adhesion. Biomaterials, 2005;26:4507-4515.

71. Porté-Durrieu MC, Guillemot F, Pallu S, Labrugère C, Brouillaud B, Bareille R, Amédée J, Barthe N, Dard M, Baquey C. Cyclo-(DfKRG) peptide grafting onto Ti–6Al–4V: physical characterization and interest towards human osteoprogenitor cells adhesion. Biomaterials 2004;25:4837-4846.

72. Sargeant TD, Rao MS, Koh C, Stupp SI. Covalent functionalization of NiTi surfaces with bioactive peptide amphiphile nanofibers. Biomaterials 2008;29:1085-1098.

73. Chollet C, Chanseau C, Remy M, Guignandon A, Bareille R, Labrugère C, Bordenave L, Durrieu M. The effect of RGD density on osteoblast and endothelial cell behavior on RGD-grafted polyethylene terephthalate surfaces. Biomaterials 2009;30:711-720.

# 5. Biofunctionalization of titanium surface with TGF-β inhibitor peptide P144

## CONTENTS

# 5.1. Introduction

## 5.1.1. Scope

This chapter is an extension of the research presented in chapter 4 as it is the natural continuation of all the experiments that were performed at the MDRCBB of the University of Minnesota School of Dentistry. Here we set out all the results obtained from surfaces biofunctionalized with MP144 peptide and thus, we complete the work carried out on the physicochemical properties of the titanium surfaces biofunctionalized with TGF-β inhibitor peptides.

This chapter presents the experiments performed and the results obtained from titanium surfaces biofunctionalized with MP144 peptide in comparison with surfaces biofunctionalized with MP17, so as to corroborate the good biofunctionalization achieved by MP144 surfaces and also to reveal new information about these biofunctionalized titanium surfaces.

# 5.2. Objectives

The main objective of this chapter is to confirm that the titanium surfaces biofunctionalized with MP144 peptides attain similar functionalization properties to those of the MP17 surfaces presented in chapter 4.

As in the case of P17 peptides, we modified the P144 peptide sequence of amino acids in order to increase the changes for a successful coating process by favoring covalent anchoring of the peptides and thus, potentially improving the inhibitory effect of the surfaces on TGF-β activity. The original sequence of P144 peptides is the following:

- P144: $NH_2$-TSLDASIIWAMMQN-OH

The sequence was modified adding 6 glycines and a lysine to the N-terminus of the P144 sequence. The modified sequence, called MP144, is the following:

- MP144: $NH_2$-KGGGGGGTSLDASIIWAMMQN-OH

# 5.3. Materials and Methods

## 5.3.1. Materials

### 5.3.1.1. Titanium samples

The base material for the experiments was c.p. grade 2 titanium bars from Daido Steel Co. (Japan).

### 5.3.1.2. Chemicals

The chemicals used to treat the titanium samples and to functionalize the surfaces were those described in section 4.3.1.2.

In order to generate fluorescence surfaces functionalized with the TGF-β inhibitor peptides, streptavidin-FITC was purchased from Anaspec (USA).

### *5.3.1.3. Peptides*

MP17 peptide, with the $NH_2$-KGGGGGKRIWFIPRSSWYERA-OH sequence and MP144 peptide, with the $NH_2$-KGGGGGGTSLDASIIWAMMQN-OH sequence were kindly furnished by Dr. Javier Dotor, from Digna Biotech (Spain). The peptides were delivered as a trifluoroacetic salt.

P17 and P144 peptides biotinylated on their C-terminus were also provided by Dr. Javier Dotor, from Digna Biotech (Spain). Biotin has a very high affinity for streptavidin, therefore, biotinylated peptides will easily react with streptavidin-FITC to label them with a fluorescent probe.

## 5.3.2. Methods

### 5.3.2.1. Base material preparation and surface treatments

The preparation of the titanium samples was similar to that described in section 4.3.2.1. The functionalization was performed as set forth in section 4.3.2.2.

### 5.3.2.2. Surface chemical composition

The titanium surfaces were functionalized through the APTES + Malonic acid route with the MP17 and MP144 peptides. The XPS analyses were performed as described in section 2.4.1.4.3.1.

### 5.3.2.3. Peptide quantification

In order to quantify the amount of peptide present on the titanium surfaces, the surfaces were treated following the different steps of the biofunctionalization treatment, but in this case the peptides used were the biotinylated peptides P17 and P144. These peptides contain the previously shown amino acid sequences with a biotin molecule attached to their C-terminus.

Biotin binds very tightly to the tetrameric protein avidin (and also to streptavidin and neutravidin), with a dissociation constant $K_d$ in the range of $10^{-15}$ M, which is one of the strongest known protein-ligand interactions [1,2]. This is often used in different

biotechnological applications. Until 2005, very harsh conditions were thought to be required to break the biotin-streptavidin bond [3,4].

To label the samples 5 mg/ml of streptavidin-FITC conjugate were dissolved in 10 mM phosphate buffer (PBS), 150 mM NaCl, pH 7.2, with 2 % BSA and 2 mM of sodium azide. The samples were immersed in this solution overnight and washed with ethanol, isopropanol, water and acetone.

Once the titanium surfaces were labeled with streptavidin-FITC conjugate, the samples were immersed in a solution of NaOH 0.1 M and sonicated until none fluorescence signal was detected on the surface. The NaOH solution, now with FITC conjugate dissolved in it, was quantified by spectrofluorophotometry using an Infinite 200 Pro spectrofluorophotometer (Tecan, Switzerland) setting the excitation wavelength at 495 nm and emission wavelength at 520 nm.

#### 5.3.2.4. Stability of the surfaces

To determine the mechanical stability of the surfaces, the titanium samples were treated as described previously in the 5.3.2.1 section, but the streptavidin-FITC conjugate was not released from the surface with NaOH. Instead, the fluorescence intensity of the samples was measured using an Olympus E600 upright microscope, equipped with a digital Olympus DP 25 camera (Olympus, Japan). After the first measurement, the samples were sonicated in water and the fluorescence intensity was measured after different sonication times.

# 5.4. Results

## 5.4.1. Surface chemical composition

### 5.4.1.1. X-Ray Photoelectron Spectroscopy (XPS)

#### *5.4.1.1.1. Survey analysis*

***Table 5-1:*** *Atomic percentage on functionalized surfaces calculated from the XPS survey spectra.*

| | C1s | N1s | O1s | Si2p | Ti2p |
|---|---|---|---|---|---|
| **TiN APT Mal MP144** | 36.1 | 7.1 | 42.8 | 6.1 | 7.8 |
| **TiN APT Mal MP17** | 38.8 | 7.6 | 40.3 | 6.5 | 6.8 |

Table 5-1 shows the atomic composition of the titanium surfaces biofunctionalized with the TGF-β inhibitor MP144 and MP17 peptides. As can be seen, the chemical composition was very similar for both peptides. The high amounts of carbon and nitrogen detected revealed the presence of the peptides on the surfaces.

#### *5.4.1.1.2. Peak deconvolution*

##### 5.4.1.1.2.1. Carbon C1s

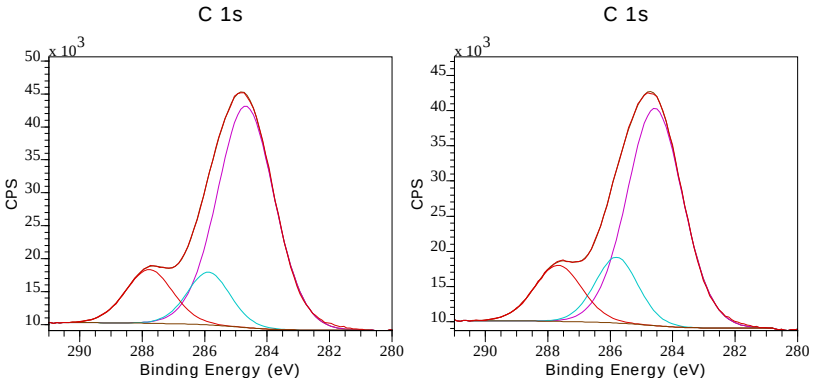


***Figure 5-1****: Deconvolutions of the carbon C1s peak on the different titanium samples biofunctionalized with MP144 (left) and MP17 (right).*

***Table 5-2:*** *Composition of the C1s peak in the different surfaces biofunctionalized with TGF-β inhibitor peptides.*

| ***TiN APT Mal. MP144*** | | | | | |
|---|---|---|---|---|---|
| **ChemState** | **Binding energy (eV)** | **Area (Pixels)** | **Area (%)** | **References** | **O-C/O=C** |
| **C-C** | 284.68 | 111.605 | 72.41 | [5-7] | 0.89 |
| **C-OH, C-N** | 285.87 | 200.857 | 13.03 | [5,6,8] | |
| **C=O, O=CN** | 287.77 | 224.474 | 14.56 | [7,9] | |
| | | | | | |
| ***TiN APT Mal. MP17*** | | | | | |
| **ChemState** | **Binding energy (eV)** | **Area (Pixels)** | **Area (%)** | **References** | **O-C/O=C** |
| **C-C** | 284.57 | 100.72 | 68.77 | [5-7] | 1.06 |
| **C-OH, C-N** | 285.8 | 235.258 | 16.06 | [5,6,8] | |
| **C=O, O=CN** | 287.67 | 222.154 | 15.17 | [7,9] | |

There were no relevant differences in the composition of the carbon peak between the MP17 and MP144 functionalized surfaces. The minimal differences in the O-C/O=C ratio were attributed to the different compositions of the amino acid side chains of the two peptides which their theoretical ratios are 1.06 for MP144 and 1.41 for MP17.

5.4.1.1.2.2. Oxygen O1s

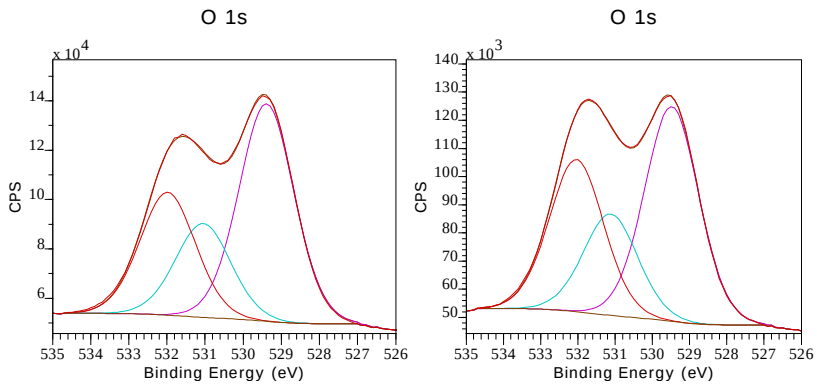


***Figure 5-2****: Deconvolutions of the oxygen O1s peak on the different titanium samples biofunctionalized with MP144 (left) and MP17 (right).*

***Table 5-3:*** *Composition of the O1s peak of the different surfaces biofunctionalized with TGF-β inhibitor peptides.*

| ***TiN APT Mal. MP144*** | | | | | |
|---|---|---|---|---|---|
| **ChemState** | **Binding energy (eV)** | **Area (Pixels)** | **Area (%)** | **References** | **O=C/$TiO_2$** |
| **$TiO_2$** | 529.39 | 47,285 | 50.07 | [5-7] | 0.43 |
| **O=C-N** | 531.05 | 20,404 | 21.61 | [5,6,8] | |
| **$H_2O$** | 531.98 | 26,750 | 28.33 | [7,9] | |
| | | | | | |
| ***TiN APT Mal. MP17*** | | | | | |
| **ChemState** | **Binding energy (eV)** | **Area (Pixels)** | **Area (%)** | **References** | **O=C/$TiO_2$** |
| **$TiO_2$** | 529.48 | 41,186 | 45.84 | [5-7] | 0.47 |
| **O=C-N** | 531.12 | 19,447 | 21.65 | [5,6,8] | |
| **$H_2O$** | 532.04 | 29,204 | 32.51 | [7,9] | |

The higher amount of $TiO_2$ on the MP144 surfaces suggested that the titanium surfaces functionalized through the APTES + Malonic acid route were able to retain a higher amount of MP17 peptide than of MP144 peptide. MP17 surfaces had a slightly higher amount of water adsorbed compared to MP144 surfaces.

5.4.1.1.2.3. Nitrogen N1s

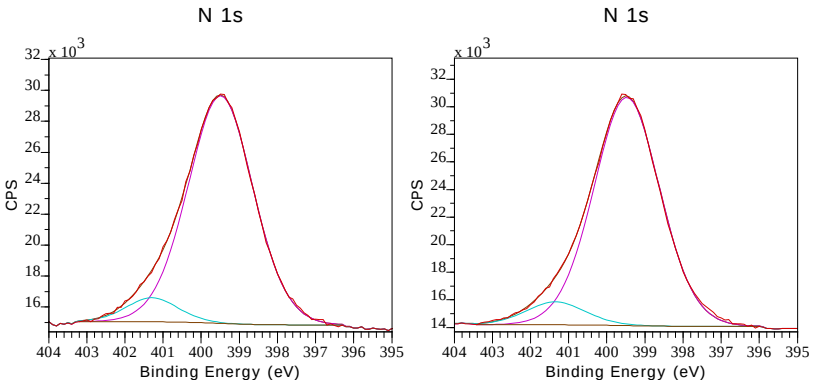


***Figure 5-3****: Deconvolutions of the nitrogen N1s peak of the different titanium samples biofunctionalized with MP144 (left) and MP17 (right).*

***Table 5-4:*** *Composition of the N1s peak of the different surfaces biofunctionalized with TGF-β inhibitor peptides.*

| ***TiN APT Mal. MP144*** | | | | |
|---|---|---|---|---|
| **ChemState** | **Binding energy (eV)** | **Area (Pixels)** | **Area (%)** | **References** |
| **-NH-, $NH_2$** | 399.49 | 8,359 | 92.27 | [5-7] |
| **$NH_3^+$** | 401.29 | 700,499 | 7.73 | [5,6,8] |
| ***TiN APT Mal. MP17*** | | | | |
| **ChemState** | **Binding energy (eV)** | **Area (Pixels)** | **Area (%)** | **References** |
| **-NH-, $NH_2$** | 399.47 | 9552,91 | 91.71 | [5-7] |
| **$NH_3^+$** | 401.34 | 863,926 | 8.29 | [5,6,8] |

The nitrogen peak had similar composition on both surfaces with MP17 and MP144 peptides. The low amount of $NH_3^+$ present could be due to the presence of non-reacted APTES. The similar percentage of $NH_3^+$ groups on both surfaces suggested that the ratio of covalently bound peptide compared to the adsorbed peptide on the surfaces was similar.

### 5.4.1.2. Peptide quantification

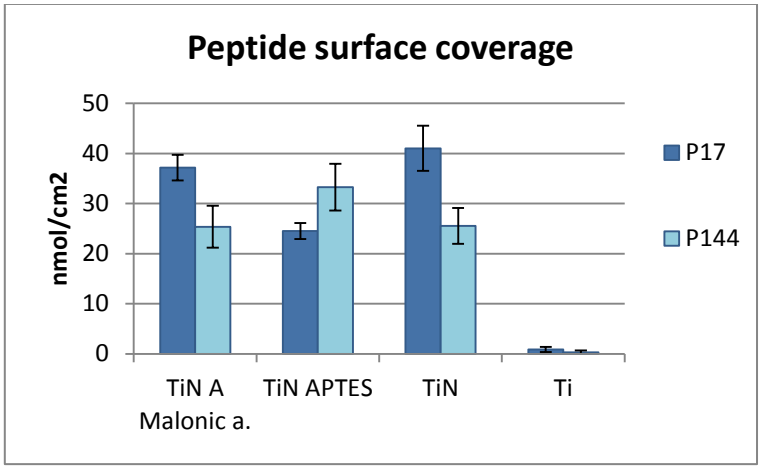


***Figure 5-4****: Quantification of the amount of peptide retained on the different functionalized titanium surfaces.*

Fluorimetry results revealed that the amount of P17 adsorbed on the surface was higher than the amount of P144 peptide Based on the conclusions of Chapter 3 we attributed this result to the higher net charge of the P17 peptide than the one of P144 peptide. The significant adsorption of P17 peptide on NaOH surfaces was also attributed to the higher net charge of P17 peptide. The amount of peptide covering TiN APT mal. surfaces was approximately 36 nmol/cm$^2$ for P17 peptide and 25 nmol/cm$^2$ for P144 peptide.

#### 5.4.1.1. Coatings stability

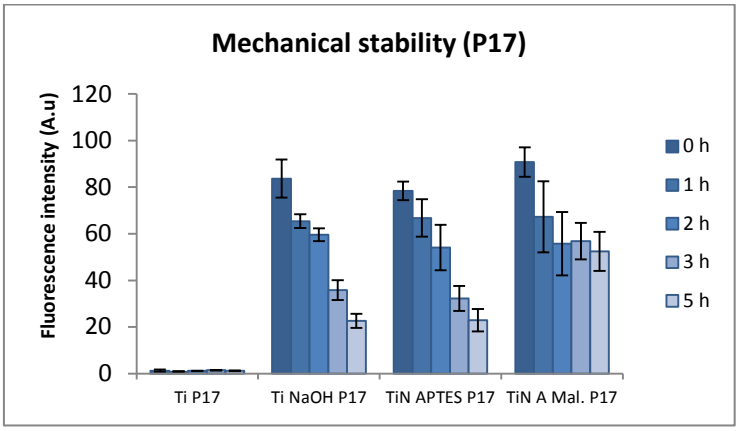


***Figure 5-5**: Fluorescence intensities of the different titanium surfaces functionalized with biotinylated TGF-β inhibitor P17 peptide and labelled with streptavidin-FITC*

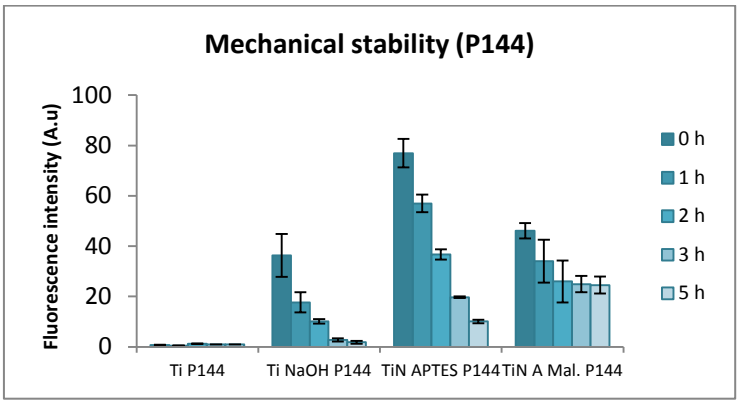


***Figure 5-6**: Fluorescence intensities of the different titanium surfaces functionalized with biotinylated TGF-β inhibitor P144 peptide and labelled with streptavidin-FITC*

Results on mechanical stability for titanium surfaces biofunctionalized with the two biotinylated peptides show similar trends. The fact that the TiN APT Mal surfaces reached a stable fluorescence signal after 3 hours of sonication revealed that the peptides were covalently bound to the surface in both cases.

## 5.5. Discussion

The differences in the amount of peptide adsorbed on the titanium surfaces could be attributed to the net charge of P17 and P144 peptides. The net charge of MP144 peptide at pH 7 is 0, while MP17 has a charge of +4. In accordance with the results presented in chapter 3, a positive peptide adsorbs in higher amount on Ti APTES Malonic acid surfaces than a negative or neutral peptide.

MP17-coated surfaces presented a slightly higher amount of adsorbed water than the MP144-caoted surfaces. This fact is due to the higher hydrophilicity of the MP17 peptide compared to the MP144 peptide. MP17 contains 6 polar amino acid residues and 7 hydrophobic amino acid side chains, being the 29% of the total chain hydrophilic and the 33% hydrophobic, while MP144 contains 2 polar aminoacid side chains and 7 hydrophobic residues, being the 10% of the total chain hydrophilic and 35% hydrophobic.

The new developed surfaces functionalized using APTES and malonic acid are able to retain near 30 nmol/cm$^2$ of peptide. This amount is much higher than the amounts of adsorbed peptide reported by other authors [10-13]. This increase in the amount of peptide adsorbed on the surface is mainly due to the increased surface index accomplished with the NaOH treatment which generates an important nano-roughness on the titanium surface and also generates a high amount of OH groups that notable increases the amount of APTES silane initially anchored to the surface.

# 5.6. Conclusions

Coatings of covalently-bonded MP144 and MP17 peptides were developed and obtained using the same APTES+malonic cid/HBTU route. This efficient and reliable chemical route produced coatings with high coverage percentage of those two peptides that were mechanical and thermal-chemical stable.

Thus, these coatings are promising candidates for being further studied *in vitro* as to assess their inhibitory effect on TGF-β activity and related effects on differentiation of fibroblasts, osteoblasts, and mesenchymal stem cells.

# 5.7. References

1. Laitinen OH, Hytonen VP, Nordlund HR, Kulomaa MS. Genetically engineered avidins and streptavidins. Cell Mol Life Sci 2006;63:2992-3017.

2. Tanaka T, Masunari S, Ishii J, Wakamura K, Segawa M, Fukuda H, Kondo A. Displaying non-natural, functional molecules on yeast surfaces via biotin–streptavidin interaction. J Biotechnol 2010;145:79-83.

3. Bitsch R. BIOTIN | properties and determination. In: Editor-in-Chief: Benjamin Caballero, editor. Encyclopedia of Food Sciences and Nutrition (Second Edition)Oxford: Academic Press, 2003. p. 506-516.

4. Holmberg A, Blomstergren A, Nord O, Lukacs M, Lundeberg J, Uhlen M. The biotin-streptavidin interaction can be reversibly broken using water at elevated temperatures. Electrophoresis 2005;26:501-510.

5. Bondarenka V, Tvardauskas H, Grebinskij S, Senulis M, Pa?i?kevi?ius A, Volkov V, Zakharova G. - Sol-gel synthesis and XPS study of vanadium-hydroquinone oxide bronze films. - physica status solidi (c) - 2009;- 6:- 2807-- 2809.

6. National Institute of Standards and Technology, NIST. NIST X-ray Photoelectron Spectroscopy Database. http://srdata.nist.gov/xps/. 2007.

7. Moulder JF, Stickle WF, Sobol PE, Bomben KD. Handbook of X-ray photoelectron spectroscopy. : Physical Electronics Inc., 1992.

8. Awsiuk K, Bernasik A, Kitsara M, Budkowski A, Rysz J, Haberko J, Petrou P, Beltsios K, Raczkowska J. Protein coverage on silicon surfaces modified with amino-organic films: A study by AFM and angle-resolved XPS. Colloids and Surfaces B: Biointerfaces 2010;80:63-71.

9. Polzonetti G, Battocchio C, Iucci G, Dettin M, Gambaretto R, Di Bello C, Carravetta V. Thin films of a self-assembling peptide on TiO2 and Au studied by NEXAFS, XPS and IR spectroscopies. Materials Science and Engineering: C 2006;26:929-934.

10. Bell BF, Schuler M, Tosatti S, Textor M, Schwartz Z, Boyan BD. Osteoblast response to titanium surfaces functionalized with extracellular matrix peptide biomimetics. Clin Oral Implants Res 2011;22:865-872.

11. Kazemzadeh-Narbat M, Kindrachuk J, Duan K, Jenssen H, Hancock REW, Wang R. Antimicrobial peptides on calcium phosphate-coated titanium for the prevention of implant-associated infections. Biomaterials 2010;31:9519-9526.

12. Imamura K, Kawasaki Y, Nagayasu T, Sakiyama T, Nakanishi K. Adsorption characteristics of oligopeptides composed of acidic and basic amino acids on titanium surface. Journal of Bioscience and Bioengineering 2007;103:7-12.

13. Raynor JE, Petrie TA, García AJ, Collard DM. Controlling Cell Adhesion to Titanium: Functionalization of Poly[oligo(ethylene glycol)methacrylate] Brushes with Cell-Adhesive Peptides. Adv Mater 2007;19:1724-1728.

# 6. Titanium surfaces biofunctionalized with TGF-β inhibitor peptides: Biological response

## CONTENTS

# 6.1. Introduction

## 6.1.1. Scope

Once the biofunctionalization of Ti surfaces with TGF-β inhibitor peptides had been accomplished successfully, the next step was to evaluate the biological response of the biofunctionalized surfaces *in vitro,* given that their performance in this context is a determining factor to be able to consider them as candidates for improving osseointegration processes.

TGF-β plays an important role in many cellular processes, but mainly in extracellular matrix (ECM) production [1]. It is believed to control the production of collagen and the fibrogenic response in many diseases [2]. It is also believed to promote osteoblastic differentiation, although there are many divergent opinions regarding these statements [3,4].

Since TGF-β1 can modify fibrogenic response and osteoblastic behavior, we decided to study the effect that titanium surfaces biofunctionalized with TGF-β inhibitor peptides has on fibroblasts and osteoblasts. This approach would let us evaluate which metabolic processes were modified by obtained coatings.

## 6.1.2. Biological behaviour of TGF-β1

Transforming growth factor beta 1, known as TGF-β1 or TGFB1, is a protein belonging to the superfamily of beta transforming growth factors of cytokines. It is a secreted protein that performs various functions in the cell, such as control of cell growth, cell proliferation, differentiation and apoptosis. In humans, TGF-β1 is encoded by the tgfb1 gene [5].

TGF-β1 plays an important role in controlling the immune system and carries out different activities in different cell types or at different stages of cell development. Most immune cells (or leukocytes) secrete TGF-β1 [6].

TGF-β1 acts synergistically with TGF-α in the induction of tumorigenesis. It also acts as a negative autocrine growth factor. The deregulation of the TGF-β1 signalling pathway can trigger apoptosis. Many cells synthesize TGF-β and almost all of them have specific receptors that recognize it [7].

TGF-β isoforms 1, 2 and 3 share a high amino acid sequence homology, have different expression patterns, and their functions are mediated by the same receptors [8,9]. TGF-β1 is the most extensively studied member of the family and can act as a mitogen for mesenchymal cells, or indirectly as a stimulator for the synthesis of extracellular matrix proteins. However, it is also a potent inhibitor of the proliferation of epithelial cells, endothelial cells, and lymphoid and myeloid cells.

TGF-β1 can be considered the prototype of a multifunctional cytokine due to the effects it has on different cellular targets. It is the most potent inhibitor of the proliferation of myeloid cells, mesenchymal cells, epithelial cells, lymphoid cells, endothelial cells and various types of malignant cells. However, it can stimulate the proliferation of normal fibroblasts, and of epithelial cells from certain mesenchymal cell types [9]. It is a strong stimulator of protein synthesis and deposition of extracellular matrix (ECM) by fibroblasts, osteoblasts and endothelial cells, and it also increases the expression of integrins and receptors that mediate cellular interactions with ECM proteins [10].

Streuli et al [11] have shown that the expression of the TGF-β1 gene is affected by the presence or absence of ECM proteins, which suggests a possible negative regulation *in vivo* [11]. The decrease in cellular interactions with ECM proteins induces the expression of TGF-β1, which leads to the synthesis of various ECM proteins and suggests a self-regulatory mechanism [11].

As TGF-β1 induces fibroblasts to synthesize and contract ECM, this cytokine has long been believed to be a central mediator of the fibrotic response [12]. Upon cutaneous injury, TGF-β1 is rapidly induced [13]. This release reinforces the attraction of neutrophils, macrophages, and fibroblasts, which in turn release more TGF-β1; accordingly, TGF-β1 is consistently present in wound fluid throughout the repair process. Expression of TGF-β1 and TGF-β1 receptors are

elevated in fibroblasts of human postburn hypertrophic scars, in keloids (benign, limited fibrotic skin lesions occurring from an excessive wound healing response), and in keloid-derived fibroblasts [14]. In dermal fibrotic lesions of scleroderma patients, high TGF-β1 levels are found at the leading edge of the forming scar tissue but not in the established lesions [15]. These results suggest that TGF-β1 is involved in the initiation of the fibrotic response *in vivo*. This idea has moved us to develop the surfaces described in chapters 4 and 5 of this thesis and to study the biological response of the developed surfaces in order to evaluate whether the inhibition of TGF-β1 activity could entail beneficial effects on the integration of metallic implants in bone.

TGF-β1 induces excess matrix synthesis when injected subcutaneously in mice or into metal chambers implanted in the back of rats [16]. Incisional rat wounds, if treated with anti-TGF- antibodies or antisense oligonucleotides, suppress ECM synthesis and scarring [17].

Collectively, the above results stress the potential challenges regarding the use of TGF- as an antifibrotic target. The use of TGF-β as a target for antifibrotic intervention may be limited to acute situations, such as immediately after surgery [18], which would require application of the antifibrotic agent for a limited period [19].

#### 6.1.2.1. TGF-β signalling pathway

The signalling mechanism of TGF-β is a very complex process that involves many proteins and can be modified in many ways by several regulatory processes. Below is presented a brief explanation of the TGF-β signalling pathway.

TGF-β superfamily ligands bind to a type II receptor, which recruits and phosphorylates a type I receptor. The type I receptor then phosphorylates receptor-regulated SMADs (R-SMADs) which can now bind the coSMAD SMAD4. R-SMAD/coSMAD complexes accumulate in the nucleus where they act as transcription factors and participate in the regulation of target gene expression. Figure 6-1 schematizes the process, which is next described.

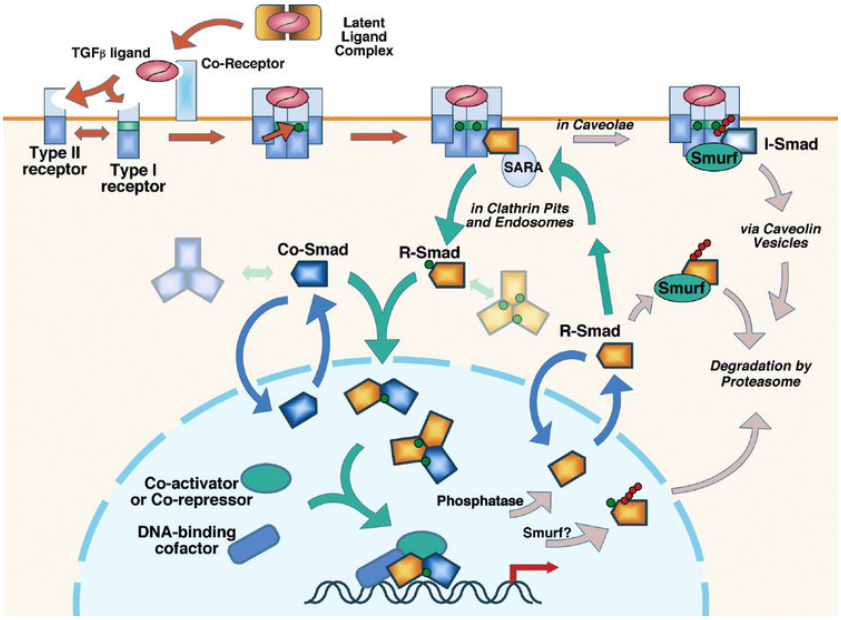


***Figure 6-1:*** *Schematic diagram of TGF-β superfamily signalling pathway. TGF-β is produced as a latent protein that is activated by various factors including plasmin, MMPs, and Tsp-1. The active form of TGF-β binds to its receptors and induces Smad2/3 phosphorylation, and BMPs induce Smad1/5/8 phosphorylation. Activated R-Smads form heteromeric complexes with Smad4 and regulate the expression of TGF-β target genes such as fibronectin, collagen type I, PAI-1 and MMP-2 in the nucleus. TGF-β: transforming growth factor-β, SARA: SMAD anchor for receptor activation, MMPs: metalloproteinases, Tsp-1: thrombospondin-1 and BMP: bone morphogenetic protein [20].*

#### 6.1.2.1.1. *Ligand binding*

As it was mentioned in section 1.5.2, the TGF-β superfamily of ligands include: bone morphogenetic proteins (BMPs), growth and differentiation factors (GDFs), activin, nodal and TGF-βs [21]. Signaling begins with the interaction of a TGF-β superfamily ligand with a TGF-β type II receptor. The type II receptor is a serine/threonine receptor kinase, which triggers the phosphorylation of the Type I receptor. Each class of ligand binds to a specific type II receptor. In mammals there are seven known type I receptors and five type II receptors [22]. Additionally, in some cases, a type III receptor is involved in the process presenting the cytokine to the receptor type II [23].

#### 6.1.2.1.2. *Receptor recruitment and phosphorylation*

In a first step, The TGF-β ligand binds to a type II receptor dimer, which engages a type I receptor dimer forming a hetero-tetrameric complex with the ligand. These two receptors have a cysteine rich extracellular domain to accomplish the interaction between them. Also, they contain a cytoplasmic serine/threonine rich domain which phosphorylates the serine OH group when it is exposed. The binding of a TGF-β family ligand causes the rotation of the receptors so that their cytoplasmic kinase domains are arranged in a catalytically favorable orientation. The Type II receptor phosphorylates serine residues of the Type I receptor, provoking a series of reactions in the cell [22].

#### 6.1.2.1.3. *SMAD phosphorylation*

Five receptor regulated SMADs (also called R-SMADs) are involved in the TGF-β signaling pathway. These are SMAD1, SMAD2, SMAD3, SMAD5, and SMAD8. Essentially, there are two intracellular pathways regarding these R-SMADs. TGF-βs, Activins, Nodals and some GDFs are mediated by SMAD2 and SMAD3, while BMPs, AMH and a few GDFs are mediated by SMAD1, SMAD5 and SMAD8. When the type I receptor is phosphorylated, then binds the corresponding R-SMAD. These binding is mediated by the SARA (The SMAD anchor for receptor activation) [16].

SARA recruits an R-SMAD and permits the binding of the R-SMAD to the type I receptor. SARA orients the R-SMAD so that the serine residue on its C-terminus faces the catalytic region of the Type I receptor. The Type I receptor phosphorylates the serine residue of the R-SMAD. Phosphorylation induces a conformational change of the R-SMAD and its subsequent dissociation from the receptor complex and SARA [24].

#### 6.1.2.1.4. *CoSMAD binding*

The phosphorylated R-SMAD has a high affinity for a coSMAD (SMAD4) and uses the phosphate group attached to it in order to form a R-SMAD/coSMAD complex. Nevertheless one must keep in mind that the phosphate group does not act as a docking site for coSMAD, but rather opens up an amino acid stretch allowing interaction.

#### 6.1.2.1.5. *Transcription*

Finally, the phosphorylated R-SMAD/coSMAD complex enters the cell nucleus where it binds transcription promoters/cofactors and causes the transcription of DNA.

### 6.1.3. TGF-β and bone

TGF-β has been reported to exhibit both positive and negative effects on bone. Exogenously injected TGF-β induced bone formation on periosteum [25,26], whereas transgenic mice overexpressing TGF-β2 in bone exhibited an osteoporotic phenotype characterized by increased activities of osteoblasts and osteoclasts and impaired matrix mineralization by osteoblasts [27]. Alliston et al reported that TGF-β inhibits osteoblast differentiation through modulation of the expression and transcriptional activity of Runx2 [28]. However, the roles of TGF-β in bone formation have not been fully elucidated [29].

Apparently, there are important differences between TGF-β types. Although exogenous BMP-2, BMP-3 and IGF-I seem to consistently promote osteoblastic differentiation [3,4,29], TGF-β1 seems to have an ambiguous behaviour showing negative results in many cases [29-31]. Kahai et al demonstrated that TGF-β1 regulates collagen type V,$\alpha$1 production in MC3T3-E1 cells [32]. TGF-β1, 2 and 3 have been shown to promote osteoblast proliferation but inhibit its differentiation on human primary osteoblasts [33].

When TGF-β1 is loaded on titanium, it seems to have a negative effect on osteoblastic differentiation while on the other hand promoting the production of collagen and fibrous tissue. In an excellent work, Fischer et al immobilized TGF-β1 on Ti6Al4V collagen coated

implants and found a significant decrease in the activity of the osteoblastic marker but a slight enhancement of the collagen synthesis [34]. Nikolidakis et al inserted TGF-β1 loaded titanium implants in goat condyles and they found that a thick fibrous tissue layer had grown around the implant surface [35]. On the other hand, Clokie et al found a higher osseointegration of implants inserted in minipig mandibles when treated with recombinant TGF-β1 [36].

### 6.1.4. Effects of TGF-β inhibition

The inhibition of TGF-β is a wide field that has influence over a vast number of biochemical processes and medical diseases such as corneal regeneration, neuro-degenerative injury, tissue healing, and many types of cancer, among others [37-40]. However, recent researches have focused their on the TGF-β inhibition of cancer, and it is believed that carcinogenic cell growth is highly influenced by TGF-β and some mutations of this cytokine [41-44].

Inhibition of TGF-β reduces fibrosis in many tissues [12,43,45-47]. Other beneficial effects of TGF-β are the inhibition of tumoral cell growth, and the control of the up-regulation of TGF-β [48,49].

The effect of TGF-β inhibition on bone has not yet been fully studied. Nevertheless, some authors are shedding light in this field. Zhong-Jian et al showed that the knockdown of TGF-β1 pathway enhanced osteoblastic differentiation in SAOS-2 cells via the enhancement of BMP-2 interaction [50]. Takeuchi et al demonstrated, in stromal cells as well as in MC3T3-E1 cells that TGF-β1 supressed osteoblast differentiation and its inhibition restored its differentiation capacity. Also, TGF-β1 inhibition suppressed myeloma cell growth [51]. Mohammad et al shown that the inhibition of TGF-β type 1 receptor resulted in increased bone mass and multiple aspects of bone quality, including trabecular bone architecture and macro-mechanical behavior of vertebral bone while reducing osteoclast differentiation and bone resorption. Furthermore, inhibition induced the expression of Runx2 and EphB4, which promote osteoblast differentiation, and ephrinB2, which antagonizes osteoclast differentiation [52].

Since there are no studies on the inhibition of TGF-β on titanium surfaces or metallic implants, the previously mentioned results encourage us to study the effect of our newly developed surfaces *in vitro*.

# 6.2. Objectives

The main objective of this chapter is to evaluate, *in vitro*, the biological response of the new developed titanium surfaces biofunctionalized with TGF-β inhibitor peptides.

The main objective of this chapter can be divided into the following secondary objectives:

- To evaluate the efficiency of the biofunctionalized surfaces in inhibiting TGF-β1 and its signaling pathway.
- To confirm that the biofunctionalized titanium surfaces do not compromise the health and overall response of the cells.
- To assess the fibrogenic response of fibroblasts adhered to the biofunctionalized surfaces.
- To study the osteoblastic response and osteoblast inductive properties of the biofunctionalized surfaces on both osteoblasts and human mesenchymal stem cells.

# 6.3. Materials and Methods

## 6.3.1. Materials

### 6.3.1.1. Titanium samples

The base material for the majority of experiments was c.p. grade 2 titanium bars of 10 mm of diameter from Daido Steel Co. (Japan).

For the experiment of TGF-β1 inhibition through Western Blot it was necessary to have large titanium surfaces in order to seed a high amount of cells so as to be able to extract enough protein for the assay. For this experiment, 50 mm diameter and 1 mm thick titanium disks (Goodfellow, UK) were used.

#### 6.3.1.2. Chemicals and bio-chemicals

The number of chemical and biochemical products used for the *in vitro* experiments is elevated. To facilitate the reading of the methodology procedures we preferred to create a list of the products used in each experiment separately and use abbreviators of the products on the description of the methods. A list of the chemical and biochemical products used in each experiment is shown below:

##### 6.3.1.2.1. *Cleaning and washing of the titanium samples*

- Milli-Q Water (Millipore, USA)
- Ethanol 96%, PAI (Panreac, Spain)
- 2-Propanol anhydrous, 99.5% (Sigma-Aldrich, USA)
- Cyclohexane anhydrous, 99.5% (Sigma-Aldrich, USA)
- Acetone PAI-ACS (Panreac, Spain)

##### 6.3.1.2.2. *Surface treatments*

###### 6.3.1.2.2.1. NaOH Treatment

- Milli-Q Water (Millipore, USA)
- Sodium Hydroxide pellets (Sigma-Aldrich, USA)

###### 6.3.1.2.2.2. Silanization

- Toluene anhydrous 99,8% (Sigma-Aldrich, USA)
- (3-Aminopropyl) triethoxysilane ≥98% (Sigma-Aldrich, USA)

6.3.1.2.2.3. Cross-linking

- *N,N*-Dimethylformamide anhydrous, 99.8% (Sigma-Aldrich, USA)
- Malonic acid (Sigma-Aldrich, USA)
- *N*,*N*-Diisopropylethylamine, 99.5% (Sigma-Aldrich, USA)
- *O*-(Benzotriazol-1-yl)-*N,N,N',N'*-tetramethyluronium hexafluorophosphate (*NovaBioChem, EMD Group,USA)*

6.3.1.2.2.4. Peptide immobilization

- MP17 peptide (Digna biotech, Spain)
- MP144 peptide (Digna biotech, Spain)
- *N,N*-Dimethylformamide anhydrous, 99.8% (Sigma-Aldrich, USA)

#### 6.3.1.2.3. *Cell culture*

Except for the culture media, the chemical products used in culturing the cells were similar for all the cell types used in the study.

- Penicillin-streptomycin, liquid (Gibco, Life Technologies, USA)
- L-Glutamine-200 mM (100X), Liquid (Gibco, Life Technologies, USA)
- Fetal Bovine Serum, Certified, US Origin (Gibco, Life Technologies, USA)
- Phosphate-Buffered Saline, PBS (Gibco, Life Technologies, USA)
- 0.05% Trypsin-EDTA (1X), Phenol Red (Gibco, Life Technologies, USA)
- β-glycerol phosphate salt hydrate (Sigma-Aldrich, USA)
- L-ascorbic acid (Sigma-Aldrich, USA)
- Dexamethasone (Sigma-Aldrich, USA)
- TGF-β1 Human Recombinant, (Prospec, Israel)

The culture media used for each cell type was different, depending on the requirements of the cell type. The culture media used for the different cell types was the following:

##### 6.3.1.2.3.1. MC3T3-E1 cells

- MEM α (Gibco, Life Technologies, USA)

##### 6.3.1.2.3.2. NIH/3T3 cells

- DMEM (Gibco, Life Technologies, USA)

##### 6.3.1.2.3.3. Human mesenchymal stem cells

- Mesenchymal Stem Cell Expansion Medium (Millipore, USA)
- Advanced DMEM (Gibco, Life Technologies, USA)

#### 6.3.1.2.4. *Western Blot*

Western Blot assay requires a high amount of chemical products. To speed up the assay several buffers and mixtures can be prepared and stored. Below are shown the recipes for all the compounds used in the Western Blot assay:

##### 6.3.1.2.4.1. Modified RIPA buffer

- 50 mM Trizma® base pH 7.4 (Sigma-Aldrich, USA)
- 150 mM NaCl (Sigma-Aldrich, USA)
- 1 mM Ethylenediaminetetraacetic acid, EDTA (Sigma-Aldrich, USA)
- 1% Tergitol type-NP40 (Sigma-Aldrich, USA)
- 0.25% Sodium Deoxycholate (Sigma-Aldrich, USA)
- Protease Inhibitor Cocktail (100X) concentration 1:100 (Cell signaling, USA)

##### 6.3.1.2.4.2. 4x lower (resolving or separating) buffer:

- 1.5M Trizma® hydrochloride, pH 8.8 + 0.4% SDS (Sigma-Aldrich, USA)
- 181.7 g Trizma base (Sigma-Aldrich, USA)
- 4 g Sodium dodecyl sulfate, SDS (Sigma-Aldrich, USA)
- Add Milli-Q water to 800 mL
- pH to 8.8 with HCl
- Add Milli-Q water to 1000 mL

##### 6.3.1.2.4.3. 4x upper (stacking) buffer:

- 0.5M Trizma® hydrochloride, pH 6.8 + 0.4% SDS (Sigma-Aldrich, USA)
- 30.3 g Trizma® base (Sigma-Aldrich, USA)
- 2 g Sodium dodecyl sulfate, SDS (Sigma-Aldrich, USA)
- Add Milli-Q water to 350 mL
- pH to 6.8 with HCl
- Add Milli-Q water to 500 mL

6.3.1.2.4.4. 10% resolving acrylamide gel:

- 4.1 Milli-Q water
- 3.3 ml 30% acrylamide:Bis (29:1) (Bio Rad, USA)
- 2.5 ml 4x Lower buffer
- 50 µL 10% Ammonium persulfate (APS) in water (Sigma-Aldrich, USA)
- 5 µL TEMED (Bio Rad, USA)

6.3.1.2.4.5. 4% stacking acrylamide gel:

- 6.1 Milli-Q water
- 1.3 ml 30% acrylamide: Bis (29:1) (Bio Rad, USA)
- 2.5 ml 4x upper buffer
- 50 µL 10% Ammonium persulfate (APS) in water (Sigma-Aldrich, USA)
- 15 µL TEMED (Bio Rad, USA)

6.3.1.2.4.6. 4x SDS loading buffer:

- 2 mL 1M trizma base pH 6.8 (Sigma-Aldrich, USA)
- 0.8 g SDS (Sigma-Aldrich, USA)
- 4 mL glycerol (Sigma-Aldrich, USA)
- 6 mg bromophenol blue (Bio Rad, USA)
- 1/4 volume 2M Dithiothreitol, DTT (Immediately before use) (Bio Rad, USA)

6.3.1.2.4.7. 10x SDS running buffer:

- 30.3 g Trizma base (Sigma-Aldrich, USA)
- 144 g glycine (Sigma-Aldrich, USA)
- 10 g SDS (Sigma-Aldrich, USA)
- Milli-Q water to 1 liter
- Dilute to 1x in water before use

6.3.1.2.4.8. 10x Lemmli transfer buffer:

- 30.3 g trizma base (Sigma-Aldrich, USA)
- 144 g glycine (Sigma-Aldrich, USA)
- 10% methanol (Sigma-Aldrich, USA)
- 0.01% SDS (Sigma-Aldrich, USA)
- Milli-Q Water to 1 liter
- Dilute to 1x in water before use

6.3.1.2.5. *Cell proliferation assay*

Cell proliferation assays performed on MV-1-Lu and MC3T3-E1 cells were similar. Therefore, the products used in both experiments were the same:

- AlamarBlue®, Molecular Probes®, (Life Technologies, USA)

6.3.1.2.6. *Cell adhesion*

The cell staining to reveal the cells adhered to the titanium surfaces followed a protocol which is described in section 6.3.2.3.4. To perform all the steps of the protocol, a set of mixtures was prepared prior to the cell staining. Next, the recipes of all these mixtures are presented:

6.3.1.2.6.1. 3%Paraformaldehyde (PFA )

- 760µl of 16% Paraformaldehyde (DAC) PRS-CODEX, (Panreac, Spain)
- 240µl de sucrose 1M, 0.3423g of sucrose in 10ml of Milli-Q water. (Sucrose, SigmaUltra, pH 5.5-7.5, >99.5% (Sigma-Aldrich, USA)
- 2ml of PB buffer (sodium phosphate buffer) 0.2M. Two solution to be prepared:
    - A: $NaH_2PO4xH_2O$, 0.2M
    - B: $Na_2HPO4xH_2O$, 0.2M

      Mix in equal parts
- 1ml of Milli-Q water.

6.3.1.2.6.2. PBS-gly

- Glycine, BioUltra, for molecular biology, >99.0% (Fluka, Sigma-Aldrich, USA). Dissolve 0.15g of glycine in 100ml of PBS.

6.3.1.2.6.3. 6%PBS-gly-BSA

- (Albumin from Bovine Serum, BSA, Cohn Fraction V (Sigma-Aldrich, USA). Dissolve 6 g of BSA in 100 ml of PBS-gly.

6.3.1.2.6.4. 0.25%Triton

- Triton X-100, (Sigma-Aldrich, USA). Dissolve 0.25% of Triton in PBS-gly

6.3.1.2.7. *Real Time quantitative PCR (qPCR Cell adhesion*

Although real time qPCR was performed using the kits purchased from Qiagen, it was necessary to select and purchase primers to amplify the target genes in the studied cells. The DNA primers were purchased from Invitrogen, Life technologies (USA). The list of primers from 5’ to 3’ is shown as follows:

***Table 6-1:*** *Primer DNA sequences used in the qPCR assay;*

| | |
|---|---|
| **Alpha-SMA Mouse Forward** | 5'-cccacccagagtggagaa-3' |
| **Alpha-SMA Mouse Reverse** | 5'-acatagctggagcagcgtct-3' |
| | |
| **Beta-actin Mouse Forward** | 5'-ctaaggccaaccgtgaaaag-3' |
| **Beta-actin Mouse Reverse** | 5'-accagaggcatacagggaca-3' |
| | |
| **ALP Mouse Forward** | 5'-cggatcctgaccaaaaacc-3' |
| **ALP Mouse Reverse** | 5'-tcatgatgtccgtggtcaat-3' |
| | |
| **Osteocalcin Mouse Forward** | 5'-agactccggcgctacctt-3' |
| **Osteocalcin Mouse Reverse** | 5'-ctcgtcacaagcagggttaag-3' |
| | |
| **RUNX2 Mouse Forward** | 5'-gcccaggcgtatttcaga-3' |
| **RUNX2 Mouse Reverse** | 5'-tgcctggctcttcttactgag-3' |
| | |
| **Col1alpha1 Mouse Forward** | 5'-catgttcagctttgtggacct-3' |
| **Col1alpha1 Mouse Reverse** | 5'-gcagctgacttcagggatgt-3' |
| | |
| **MMP2 Mouse Forward** | 5'-taacctggatgccgtcgt-3' |
| **MMP2 Mouse Reverse** | 5'-ttcaggtaataagcacccttgaa-3' |
| | |
| **MMP3 Mouse Forward** | 5'-ttgttctttgatgcagtcagc-3' |
| **MMP3 Mouse Reverse** | 5'-gatttgcgccaaaagtgc-3' |
| | |
| **MMP9 Mouse Forward** | 5'-acgacatagacggcatcca-3' |
| **MMP9 Mouse Reverse** | 5'-gctgtggttcagttgtggtg-3' |
| | |
| **Fibronectin Mouse Forward** | 5'-cggagagagtgcccctacta-3' |
| **Fibronectin Mouse Reverse** | 5'-cgatattggtgaatcgcaga-3' |

#### 6.3.1.3. Peptides

MP17 peptide, with sequence $NH_2$-KGGGGGKRIWFIPRSSWYERA-OH and MP144, with sequence $NH_2$-KGGGGGGTSLDASIIWAMMQN-OH were kindly contributed by Dr. Javier Dotor, from Digna Biotech (Spain). The peptides were delivered as a trifluoroacetic salt.

#### 6.3.1.4. Cells

4 different types of cells were used in the different experiments of this study. A description of the 4 cell types is given as follows:

##### 6.3.1.4.1. *MC3T3-E1 pre-osteoblasts*

The MC3T3-E1 osteoblastic cell line has been established from C57BL/6 mouse calvaria and selected on the basis of high alkaline phosphatase (ALP) activity in the resting state. Cells have the capacity to differentiate into osteoblasts and osteocytes and have been demonstrated to form calcified bone tissue *in vitro*. Mineral deposits have been identified as hydroxyapatite. Expression of basic fibroblast growth factor (bFGF) mRNA and protein has been shown to be regulated by treatment with TGF beta and bFGF. Prostaglandin F2a has been reported to stimulate DNA synthesis and proliferation by upregulation of insulin-like growth factor I receptors [53]. MC3T3-E1 secrete collagen and express murine leukemia inhibitory factor (mLIF) in RNA. Additionally, MC3T3-E1 cells have been shown to be very sensitive to TGF-β1 and its inhibition [51].

1 vial of 1 million cells of the MC3T3-E1 sub clone 14 strand was purchased from ATCC®, USA.

##### 6.3.1.4.2. *NIH/3T3 fibroblasts*

NIH 3T3 mouse embryonic fibroblast cells come from a cell line isolated and initiated in 1962 at the Department of Pathology of the New York University School of Medicine. 3T3 refers to the cell transfer and inoculation protocol for the line, and means "3-day transfer, inoculum 3 x 10^5 cells." Using this protocol, the immortal cell line begins to thrive and stabilize in cell culture after about 20-30 generations of *in vitro* growth.

George Todaro and Howard Green, the scientists who first cultured this cell line, obtained the cells from desegregated NIH Swiss mouse embryo fibroblasts. The cell line has since become a standard fibroblast cell line [54].

Established from a NIH Swiss mouse embryo, these cells are sensitive to sarcoma virus focus formation and leukemia virus propagation. Cells have now lost their contact inhibition [55].

NIH/3T3 is the most widely used fibroblast cell line in studies related to TGF-β and its inhibition [56].

1 vial of 1 million cells of the NIH/3T3 strand was purchased from ATCC®, USA.

#### 6.3.1.4.3. *MV-1-Lu mink lung epithelial cells*

MV-1-Lu cell line is especially sensitive to TGF-β. TGF-β significantly suppresses its proliferation capacity via the saturation of SMAD2 signaling [57]. Therefore, this cell line has been widely used to evaluate the effects of TGF-β in many different conditions, and also to evaluate the efficiency of TGF-β inhibitors.

A vial of 1 million MV1Lu cells was kindly provided by Dr. Javier Dotor from Digna Biotech.

#### 6.3.1.4.4. *Human mesenchymal stem cells*

Mesenchymal stem cells, or MSCs, are multipotent stromal cells that can differentiate into a variety of cell types, including osteoblasts, chondrocytes and adipocytes. This phenomenon has been documented in specific cells and tissues in living animals and in their counterparts growing in tissue culture [58].

It was decided that a human type cell be used to corroborate the results obtained in the mice cell lines in order to ensure the effectiveness of the new developed titanium surfaces in humans.

1 vial of 1 million human mesenchymal stem cells (derived from bone marrow) was purchased from Millipore (USA).

## 6.3.2. Methods

### 6.3.2.1. Base material preparation

The preparation of the titanium surfaces and the MP17 and MP144 peptides was similar to that explained in section 4.3.2.1.

### 6.3.2.2. Surface treatments

All the surface treatments performed on the titanium surfaces are the same as the ones described in section 4.3.2.2. A summary of the surface treatments performed on the titanium samples is presented below:

#### 6.3.2.2.1. *Titanium surface activation*

The titanium surfaces were all activated using NaOH treatment as described in section 4.3.2.2.1.2.

#### 6.3.2.2.2. *Silanization*

The activated titanium surfaces were silanized with APTES as described in section 4.3.2.2.2.

#### 6.3.2.2.3. *Cross-linking*

The previously silanized surfaces were cross-linked with malonic acid as described in section 4.3.2.2.3.

#### 6.3.2.2.4. *Peptide Immobilization:*

The activated, silanized and cross-linked surfaces were treated with MP17 or MP144 peptide as described in section 4.3.2.2.4.

### 6.3.2.3. *In vitro* characterization of titanium surfaces

#### 6.3.2.3.1. *Sample Surfaces*

10 mm diameter titanium disks were used for this study. 3 titanium disks were employed for every condition and time. The previously treated titanium disks were allocated on wells of 48 well plates. The different conditions are described as follows:

- PS: Polystyrene well without titanium samples (control)
- Ti: Plain titanium
- N: Activated plain titanium by etching with NaOH
- NAM: Activated and silanized titanium with NaOH+APTES+malonic acid
- NAMMP17: Functionalized titanium with NaOH+APTES+malonic acid and MP17 peptide
- NAMMP144: Functionalized titanium with NaOH+APTES+malonic acid and MP144 peptide

Prior to the cell culture, the titanium samples were disinfected immersing them in 96% ethanol for 10 minutes and were then rinsed twice in PBS.

#### 6.3.2.3.2. *Inhibition of TGF-β1 activity*

##### 6.3.2.3.2.1. Phospho-SMAD2 activity by Western Blot

The protocol to determine the expression of phosphorylated-SMAD2 protein by Western Blot is described as follows:

###### *6.3.2.3.2.1.1. Cell exposition to the different titanium surfaces:*

MC3T3-E1 pre-osteoblasts were cultured and proliferated using Alpha-MEM supplemented with 1% penicillin/streptomycin, 1% L-glutamine, and 5% of fetal bovine serum (SBF), until reaching the necessary amount of cells.

The titanium samples with the different surface treatments were sterilized immersing them in 96% ethanol for 10 minutes. After sterilization the samples were washed and rinsed with sterile PBS. The samples were allocated in polystyrene petri dishes of the same diameter as the titanium samples to ensure that cells would attach to the titanium surface rather than to the polystyrene.

Cells were trypsinized using 2 ml of trypsin and incubating the cells for 5 minutes. After trypsinization, the cells were centrifuged at 1000 rpm for 5 minutes in order to eliminate the trypsin, and were then re-suspended in serum-free Alpha-MEM. Subsequently, the cells were counted and 300,000 cells were seeded on each titanium sample with 3 ml of serum-free Alpha-MEM.

The MC3T3-E1 cells were cultured on the different titanium surfaces for 24 hours. After this time, the medium was extracted and the Ti samples were rinsed with sterile PBS twice in order to eliminate the dead and non-attached cells.

Then, the cells were treated with 0.7 ng/ml of recombinant TGF-β1 dissolved in serum-free Alpha-MEM for 1 hour. Some non-treated samples, as is indicated in the results, were used as controls and 200 μg/ml of MP17 or MP144 were added to the medium in order to determine the capacity of the peptides to inhibit TGF-β1 in solution.

After 1 hour of exposition, the samples were rinsed twice with PBS and the cells were lysed with 300 µl of RIPA buffer on ice for 5 minutes, supplemented with the protease inhibition cocktail, collected with a rubber scraper, and this lysate was then stored in 1.5 ml eppendorfs at -80 $^{o}$C for further treatment.

The experiment was performed twice and the results were combined in order to obtain statistical results.

#### *6.3.2.3.2.1.2. Western Blot*

A description of the Real Time qPCR technique can be found in Annex A of this thesis in electronic format.

The cell lysates were thawed and centrifuged at 12,000 rpm for 12 minutes. After centrifugation the supernatant was collected and the protein concentration of the samples was quantified by bis-bicinchinonic acid (BCA) assay using Pierce® BCA Protein Assay Kit (Thermo Scientific, USA).

After protein quantification, 60 µg of protein were extracted from each sample and mixed with SDS-PAGE loading buffer + reducing agent to 1x final concentration. The mixtures were stirred and heated at 96 $^{o}$C for 5 minutes to open the protein.

SDS-PAGE resolving gel was prepared and poured between the protean glass plates (Bio Rad, USA). Once the resolving gel was polymerized the stacking gel was prepared and poured onto the resolving gel using the Mini-Protean comb to form the different tracks on the gel. The gel was left to polymerize for 20 minutes.

40 µl of each sample was loaded on the SDS-PAGE gel and 5 µl of the Dual Color Recombinant Precision Plus Protein Standard (Bio-Rad, USA) were loaded in the first track of the gel. Once the gels were loaded, they were immersed in the electrophoresis buffer and the

electrophoresis was run at 120 V using the Mini-Protean Tetracell apparatus (Bio-Rad, USA) until the samples had traveled the whole track.

In a parallel time frame, PVDF membrane (Immobilon-P, Millipore, USA) was immersed briefly in methanol, and then in transfer buffer for 5-10 minutes. After this, the gel and the PVDF membrane were assembled in the cassette of the Tetracell apparatus and immersed in transfer buffer. The protein transfer run at 60 V overnight at 4 $^{o}$C.

Membranes were blocked for 1 hour with 5%BSA in TBS containing 0.1% Tween 20 (TBST), incubated for 3 hours with the anti-alpha-smooth muscle actin antibody (1:2000) (Santa Cruz Biotechnology, USA) to create a protein loading control, and then subsequently incubated with anti-phospho-SMAD2 antibody (1:1500) (Cell Signaling Technology, USA). Afterwards they were washed three times in TBST, and incubated for 1 h with a mouse-anti-rabbit peroxidase-coupled secondary antibody (1:20,000). After final washing with TBST (3 times for 5 min each) blots were developed by using a chemiluminiscence detection system (Lumi Light Plus, Roche GmbH, Mannheim, Germany) and a luminescent image analyzer (Fujifilm LAS1000 Pro). A densitometric analysis of the blots was performed using the AIDA image analyzer software. During the analysis, the luminometric signal of interest (phosphorylated SMAD2) was normalized to the luminescence signal of actin.

#### 6.3.2.3.3. *Proliferation of MV-1-Lu cells*

4 titanium samples (10 mm of diameter) of each condition were disinfected immersing them in 96% ethanol for 10 minutes and rinsed twice in PBS. Subsequently, the samples were inserted in a Corning® CellBIND® 48 Well Multiple Well Plate. MV-1-Lu mink lung epithelial cells were cultured using DMEM supplemented with 1% penicillin/streptomycin, 1% of L-glutamine and 5% FBS, trypsinized with 3 ml of trypsin and incubated for 5 minutes in a 5% $CO_2$ atmosphere at 37 $^{o}$C. The cells were next centrifuged and the trypsin discarded. Then the cells were re-suspended in DMEM with the mentioned additives and 20,000 cells per well were seeded in the well plate.

After 24 hours of adhesion, 50 µl of AlamarBlue® was added to each well and after 4 hours of incubation at 37 ºC, 5% $CO_2$, the medium was collected and its fluorescence analysed with an Infinite 200 Pro (Tecan, Switzerland) setting the fluorescence excitation and emission at 560 and 590 nm respectively. On another side, the extracted medium was substituted by fresh medium, adding 0,5 ng/ml of recombinant TGF-β1. Additionally, 200 µg/ml of MP17 or MP144 were added to some wells as controls. This procedure was repeated every day until a week was completed in order to measure the cell growth over time.

#### 6.3.2.3.4. *Cell adhesion of MC3T3-E1 pre-osteoblasts*

20,000 MC3T3-E1 cells were seeded on each of the 3 samples of each condition inserted in a Corning® CellBIND® 48 Well Multiple Well Plate. The medium used was serum-free Alpha-MEM supplemented with 1% penicillin/streptomycin and 1% L-glutamine. After 3 hours of adhesion, the medium was extracted and cells were washed with PBS-gly fixed with 3% PFA for 20 minutes at 4 ºC. Subsequently, cells were washed thrice with cold PBS-gly for 5 minutes each wash.

After fixation, cells were permeabilized for 10 minutes using 0.25% triton in PBS-gly and washed again thrice with PBS-Gly for 5 minutes.

Then the blocking of the non-specific linking sites was performed incubating the cells in 6% BSA in PBS-gly for 40 minutes. Afterwards, the cells were washed thrice with PBS-gly.

Subsequently, the cells were incubated, with 0.1 µg/ml Hoetsch and rhodamine phalloidin (1:500) in 3%BSA/PBS-gly, for 1 hour at room temperature. Finally the samples were washed thrice with PBS-gly and visualized using fluorescence microscopy.

Finally, the samples were observed in an OLYMPUS SZX7 fluorescent lamp stereomicroscope (Japan), and micrographs were recorded on a computer. The cell number measurements were performed counting the cell nuclei in the micrographs using Image J ver. 1.45s from the images taken at the microscope. Cell extension measurements were performed measuring the area

covered by cell F-Actin over the total area scanned. This ratio was then divided by the cell number in each image analyzed using Equation 6-1 (shown below). At least four images of each condition were analyzed to obtain statistical results.

$$\text{Cell ext} = \frac{\text{Total Area} - \text{Area covered by cells}}{\text{Cell number}} \qquad \textbf{Equation 6-1}$$

#### 6.3.2.3.5. *Cell proliferation of MC3T3-E1 pre-osteoblasts*

The cell proliferation assay was performed using MC3T3-E1 mice pre-osteoblasts. The cell proliferation was determined by means of the AlamarBlue® fluorimetry as described in section 6.3.2.3.3. In this case, the medium used with the MC3T3-E1 was Alpha-MEM supplemented with 1% penicillin/streptomycin, 1% L-glutamine and 5% FBS.

#### 6.3.2.3.6. *Cell differentiation*

##### 6.3.2.3.6.1. Gene expression by fibroblasts

The times selected for harvesting the cells were 1, 3 and 7 days. Therefore, a total of 9 polystyrene wells were left without titanium samples and 45 titanium samples with different treatments were allocated on well plates.

NIH/3T3 cells from the fifth passage were used for this study. 40,000 cells were seeded on every polystyrene or titanium sample using serum free DMEM supplemented with 0.5 ng/ml of TGF-β1, 1% penicillin/streptomicyn and 1% L-glutamine. After 1 day, the cells from 3 samples of each condition were lysed with RLT buffer and the mRNA was collected and purified using RNEasy Plus Minikit (Qiagen, Germany), following kit protocol. In the RNA extraction step the 3 samples of each condition were joined and mixed, thus obtaining one sample from each condition, which is the compendium of the 3 replicas. The samples were stored in 1,5 ml eppendorfs at -80 $^{o}$C.

After the first day of culture, the free DMEM serum + 0.5 ng/ml of TGF-β1 was substituted by DMEM complemented with 5% FBS and 0,5 ng/ml of TGF-β1. This medium was changed every two days until the end of the experiment.

On days 3 and 7 the cells were lysed and the mRNA was extracted with the same protocol as the one used for day 1.

The target genes selected for the evaluation of fibroblastic differentiation were collagen 1 alpha 1, alpha-smooth muscle actin (α-SMA), fibronectin (FN), matrix metallopeptidase 2 (MMP-2), matrix metallopeptidase 3 (MMP-3), and matrix metallopeptidase 9 (MMP-9). In the case of collagen, fibronectin and α-SMA a high gene expression is indicative of fibroblastic activity related with the production of fibrous extracellular matrix [59]. Matrix metallopeptidases are involved in the breackdown of extracellular matrix processes and tissue remodeling. Also, these enzymes play a role in the regulation of vascularization and inflammatory response [60]. A high expression of theses enzymes is related with fibroblastic activity and remodelation of the extracellular matrix. More information of each gene can be found in the results section.

#### 6.3.2.3.6.2. Gene expression by pre-osteoblasts

The times selected for harvesting the cells were 2, 7, 14 and 21 days. Therefore, a total of 12 polystyrene wells were left without titanium samples and 60 titanium samples with different treatments were allocated on well plates.

MC3T3-E1 cells from the third passage were used for this study. 40,000 cells were seeded on every polystyrene or titanium sample using free Alpha-MEM serum supplemented with 10 mM β-glycerol phosphate, 50 μg/m ascorbic acid and 50 μM dexamethasone. After 2 days, the cells from 3 samples of each condition were lysed with RLT buffer and the RNA was collected in the same fashion as with the NIH/3T3 fibroblasts.

After the second day of culture the free Alpha-MEM serum with the osteogenic complement was substituted by Alpha-MEM complemented with 5% bovine serum and the osteogenic complement previously described. This medium was changed every two days until the end of the experiment.

On days 7, 14 and 21, the cells were lysed and the mRNA was extracted in the same fashion as on the first day.

The target genes evaluated for the osteoblastic differentiation were Collagen Type 1 alpha 1, Runt related transcription factor 2 (RUNX2), alkaline phosphatase (ALP) and osteocalcin (OC). Collagen is one the main components of the bone extracellular matrix, RUNX2 is essential for osteoblastic differentiation and skeletal morphogenesis and acts as a scaffold for nucleic acids and regulatory factors involved in skeletal gene expression [61]. Alkaline phosphatase is an enzyme responsible of dephosphorylate many types of proteins. Alkaline phosphatase is particularly concentrated in bone and it is secreted by many types of cells including osteoblasts [62]. Osteocalcin is only secreted by osteoblasts, binds bone extracellular matrix and plays a role in bone mineralization [63]. A high expression of all these genes indicates osteoblastic differentiation and production of extracellular matrix.

#### 6.3.2.3.6.3. Real Time qPCR

A description of the Real Time qPCR technique can be found in Annex A of this thesis in electronic format.

In this study, the following protocol was performed: (1) mRNA extraction; (2) spectrophotometric quantification of RNA; (3) reverse transcription, RT; and (4) polymerase chain reaction, PCR. The mRNA extraction has been described in section 6.3.2.3.2.1.1. The subsequent steps of the protocol are described as follows:

##### *6.3.2.3.6.3.1. Spectrophotometric quantification of RNA*

RNA quantification was carried out by measuring absorbance with the Infinite® 200 PRO NanoQuant (Tecan, Switzerland) using Tecan's Nanoquant Plate and the i-control™ – Microplate Reader Software of the same company.

##### *6.3.2.3.6.3.2. Reverse Transcription (RT)*

During the reverse transcription, the enzyme reverse transcriptase is used to make a double-stranded cDNA copy of the mRNA molecules. To perform the reverse transcription of the samples a QuantiTect Reverse Transcription kit (QIAGEN, Germany) was used following the manufacturer's protocol.

##### *6.3.2.3.6.3.3. Polymerase chain reaction*

The resulting cDNA was then amplified using the SYBR Green method. This requires a double-stranded DNA dye in the PCR reaction which binds to the newly synthesized double-stranded DNA and gives it fluorescence. The QuantiFast SYBR Green kit (QIAGEN, Germany) was used for this purpose.

The gene amplification was carried out using a StepOne™ Real-Time PCR System (Applied Biosystems, Life Technologies, USA) for performance and monitoring purposes. The StepOne™ Software v2.2.1 was used applying the following amplification protocol:

- 95 °C 10 min.
- 40 cycles of:
    - 95 °C 30 sec.
    - 55 °C 1 min.
    - 72 °C 1 min.
- Melting/ dissociation curve
    - 55° to 95°

To analyze the gene expression results the $2^{\Delta\Delta Ct}$ method was followed [64] calculating the expression of the target normalized to reference = $2^{(Cttarget\ -\ Ctreference)}$ divided by the control sample which in our case was the expression of β-actin on the first day of culture for the NIH/3T3 fibroblasts and on the second day for the MC3T3-E1 pre-osteoblasts. Corrections and normalization of the efficiency of each primer were performed to obtain reliable results.

#### 6.3.2.3.6.4. Differentiation of human mesenchymal stem cells

In order to evaluate the alkaline phosphatase and osteocalcin protein expression of cells seeded on our titanium surfaces, human mesenchymal stem cells were selected. Prior to the assay, the hMSC cell of pass 0 were cultured to ensure obtaining the amount needed to perform the experiments. Thus, the cells were cultured in 80 $cm^2$ culture flasks (Nunc, Thermo Scientific, USA) with mesenchymal stem cell expansion medium provided by the manufacturer and supplemented with 8 ng/ml of recombinant FGF-2. The media were changed every two days. When the cells reached 80% confluence they were trypsinized and re-cultured for expansion. When the cells arrived at passage 4, they were dispersed in FBS with 10% DMSO and cryogenized until the assay.

To measure the expression of ALP and OC on human mesenchymal stem cells attached to the different titanium surfaces, 3 samples of each condition were prepared for each time of cell harvesting. The times selected to harvest the cells were 7, 14, and 21 days. The titanium samples were sterilized immersing them in 96% ethanol for 10 minutes and were then rinsed twice with PBS. 10,000 cells were seeded on each surface using Advance DMEM (Gibco, Life technologies, USA) supplemented with 1% penicillin/streptomycin, 1% L-glutamine, 5% FBS, 10 mM β-glycerol phosphate, 50 μg/ml ascorbic acid, 50 μM dexamethasone and 0.5 ng/ml TGF-β1.

#### *6.3.2.3.6.4.1. Alkaline phosphatase activity*

Alkaline phosphatase (ALP) catalyzes the hydrolysis of phosphate esters in alkaline buffer and produces an organic radical and inorganic phosphate. Changes in alkaline phosphatase level and activity are associated with various disease states in the liver and bone [65].

The measurement of ALP activity was performed using the Alkaline Phosphatase Assay Kit (Colorimetric) from Abcam (UK) and following the kit's protocol.

The kit uses p-nitrophenyl phosphate (pNPP) as a phosphatase substrate which turns yellow (λmax = 405 nm) when dephosphorylated by ALP. The kit can detect 10-250 µU ALP in samples.

#### *6.3.2.3.6.4.2. Osteocalcin production*

Osteocalcin or bone gla protein (B.G.P.) is the major non-collagenous protein of the bone matrix. It has a molecular weight of 5800 Da and contains 49 amino acids, including 3 residues of gamma carboxy glutamic acid. Osteocalcin is synthesized in the bone by the osteoblasts. After production, it is partly incorporated in the bone matrix and the rest is found in the blood circulation. The exact physiological function of osteocalcin is still unclear. Studies show that the circulating levels of osteocalcin reflect the rate of bone formation [66].

To measure the amount of osteocalcin produced by the cells, the Osteocalcin Human Direct ELISA kit (Invitrogen, Life Technologies, USA) was used.

The invitrogen human osteocalcin EASIA is a solid phase enzyme amplified sensitivity immunoassay (EASIA) performed on a microtiter plate. The assay uses monoclonal antibodies (Mabs) directed against distinct epitopes of human osteocalcin. Samples react with the capture monoclonal antibody (Mab 1) coated on the microtiter well and with a monoclonal antibody (Mab 2) labeled with horseradish peroxidase (HRP). After an incubation period allowing the formation of a sandwich: coated Mab 1 - human osteocalcin - Mab 2 - HRP, the microtiter plate is washed to remove unbound enzyme labeled antibody. Bound enzyme labeled antibody is

measured through a chromogenic reaction. Chromogenic solution (TMB ready for use) is added and incubated. The reaction is stopped with the addition of Stop Solution and the microtiter plate is then read at the appropriate wavelength. The amount of substrate turnover is determined colorimetrically by measuring the absorbance which is proportional to the human osteocalcin concentration. A standard curve is plotted and human osteocalcin concentration in a sample is determined by interpolation from the standard curve [67].

#### 6.3.2.4. Statistical analysis

The statistical treatment of the data was similar to that described in section 2.4.1.5.

# 6.4. Results

## 6.4.1. Inhibition of TGF-β1 activity

### 6.4.1.1. Phospho-SMAD2 activity by Western Blot

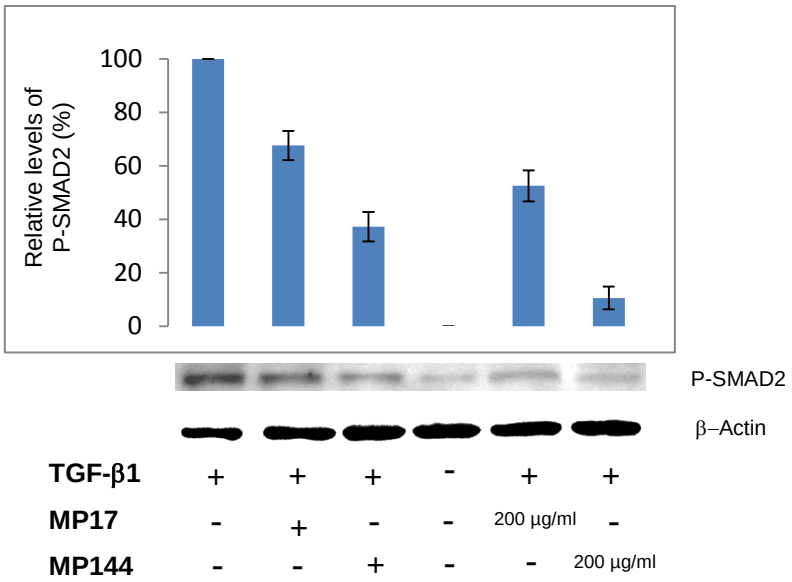


***Figure 6-2:*** *Western Blot results of expression of phospho-SMAD2 on MC3T3-E1 pre-osteoblasts. + implies that TGF-β1 was administered to the cells at 0.7 ng/ml. On the MP17 and MP144 rows, + implies that the titanium surface was biofunctionalized with the peptide. 200 µg/ml implies that the surface was not biofunctionalized but MP17 or MP144 was administered to the cells, in solution, at a concentration of 200 µg/ml. Signal of the non-treated sample without administration of exogenous TGF-β1 was used as background.*

Figure 6-2 shows the Western Blot results of the expression of phosphorylated SMAD2 protein. The expression of p-SMAD2 is the most reliable method to elucidate whether the TGF-β1 signalling is taking place. The graph shows that when the titanium surfaces were biofunctionalized with MP17 and MP144 peptides, the expression of p-SMAD2 was considerably reduced in comparison with a non-biofunctionalized surface, especially so on the surfaces functionalized with P144 on which the p-SMAD2 expression was reduced to about 40%. It is also possible to observe that when cells were attached to non-biofunctionalized titanium surfaces and the peptide was administered in solution at high concentrations, the inhibition effect was stronger. Finally, it can be seen that when exogenous TGF-β1 is not

administered to the cells, the p-SMAD2 production was very low but still detectable by Western Blot.

### 6.4.1.2. MV-1-Lu cell proliferation

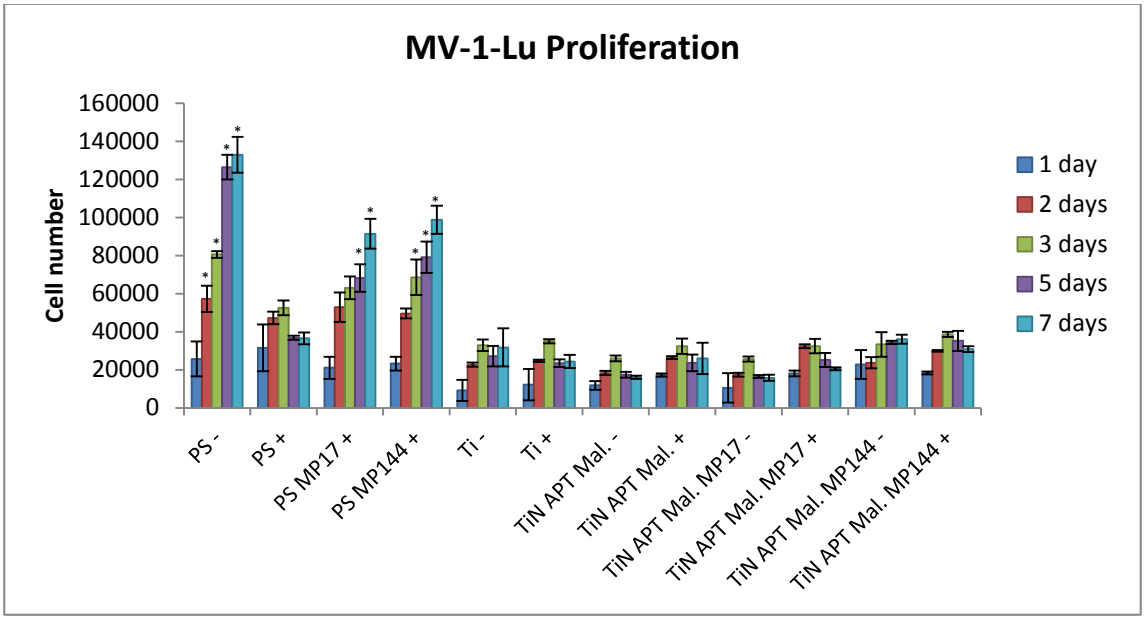


***Figure 6-3:*** *Cell proliferation on MV-1-Lu cell line. PS refers to cells seeded on a polystyrene well plate, PS MP17 and PS MP144 refers to cells seeded on a polystyrene well plate with daily administration of 200 ng/ml of MP17 or MP144 peptide. + refers to that 0,5 ng/ml of TGF-β1 which was daily administered to the cells. – refers to the cells that were not treated with TGF-β1. *: Statistically significant differences with respect to PS + given the same proliferation times ($\alpha$<0.05).*

Proliferation assay on MV-1-Lu cells (figure 6-3) gave unexpected results. It is well known that TGF-β1 inhibits MV-1-Lu proliferation [57] and this can be seen when the cells were seeded on the polystyrene well plate. It is also possible to observe that MP17 and MP144 in solution were capable of partially inhibit TGF-β1 from allowing the cells to proliferate. However, when the cells were seeded on titanium surfaces the initial cell adhesion was much lower than on the well plate. Moreover, the cells didn't proliferate over time after the second day, even on the samples where no TGF-β1 was added. This fact indicates that the effect of the peptides on MV-1-Lu cells gets masked by effect of the metallic surface on its proliferation. Therefore, it can be assumed that MV-1-Lu cell proliferation, which is an excellent test for TGF-β and its inhibition is not useful for cells seeded on titanium surfaces.

## 6.4.2. Cell adhesion of MC3T3 pre-osteoblasts

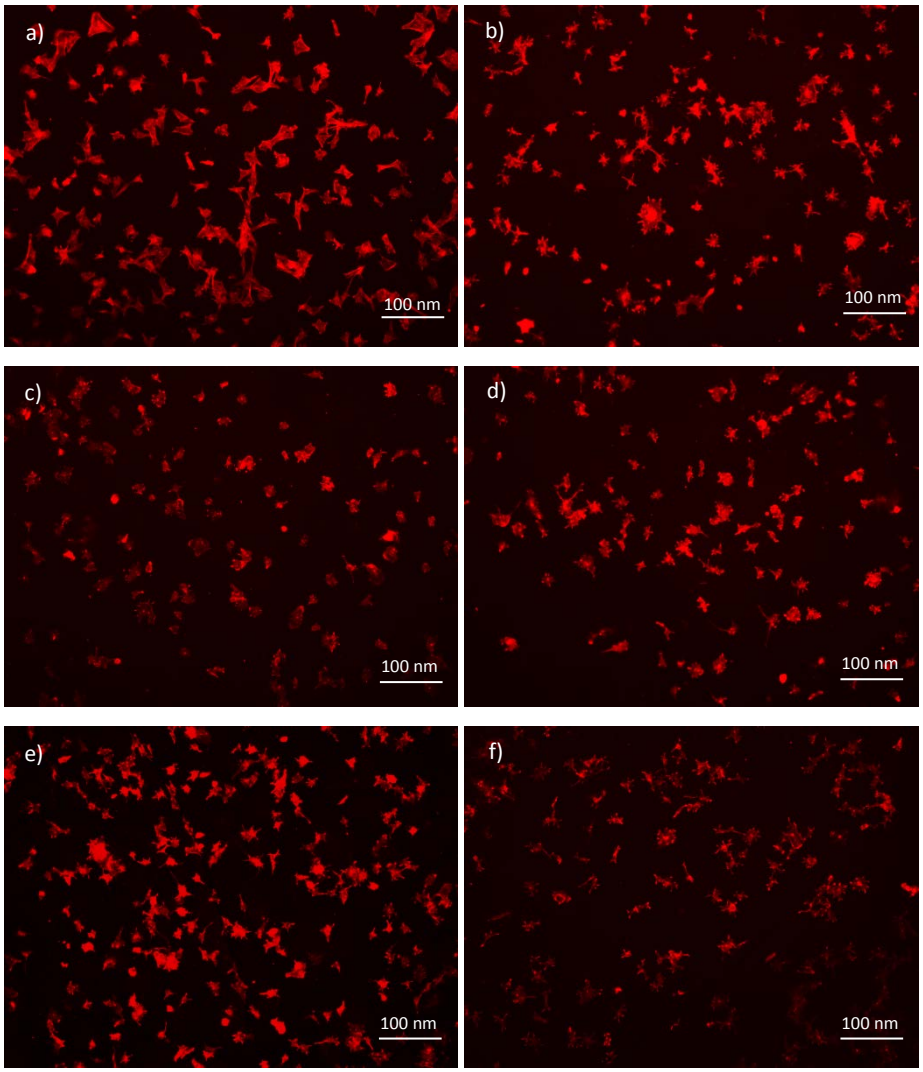


***Figure 6-4:*** *Overall morphology of adhered MC3T3-E1 cells after 3h in culture on the different titanium surfaces. a) Plain Ti, b) Ti NaOH, c) TiN APTES, d) TiN APT malonic a., e)TiN APT mal. MP17, f) TiN APT mal. MP144.*

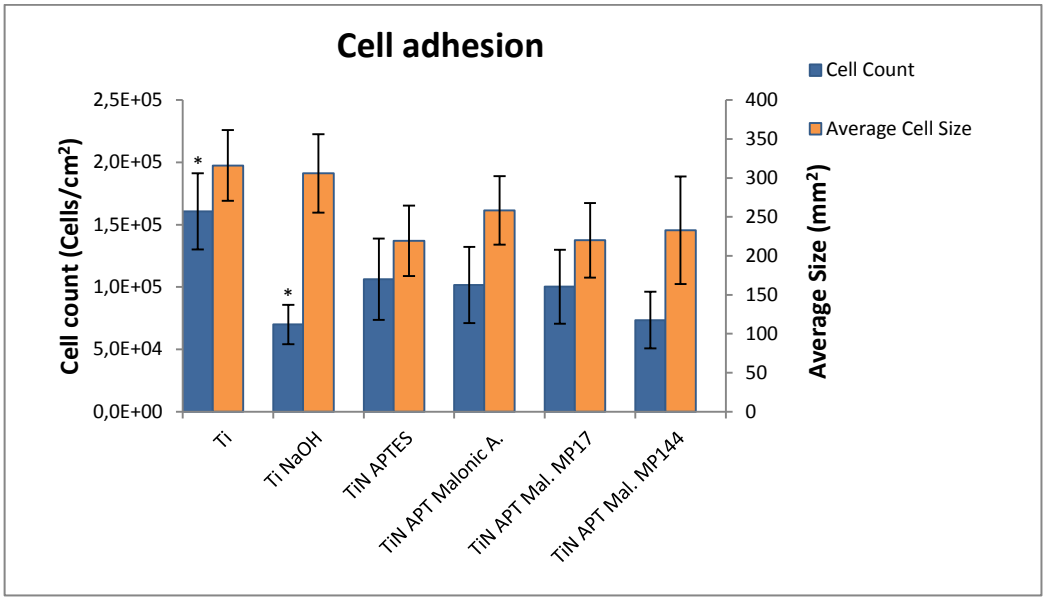


***Figure 6-5:*** *Cell adhesion of MC3T3-E1 pre-osteoblasts on the different Ti surfaces. PS refers to cells seeded on a polystyrene well plate. * means statistically significant differences between groups ($\alpha$<0.05).*

From the morphology micrographs of MC3T3-E1 cells (figure 6-4) it can be seen that the overall morphology of the cells attached to a plain Ti surface was sensibly different to the cells attached to the other surfaces. On Ti surfaces cells presented a spreaded morphology while cells on the other surfaces presented a round morphology with long philopodia connected to the surface. An exception to this tendency was the TiN APTES surface where cells showed an intermediate morphology between Ti and the other surfaces. It is well known that APTES silane can markedly affect the cell adhesion, actively promoting it [68-70].

MC3T3-E1 cells exhibit, in general, good adhesion to titanium surfaces. On smooth titanium, the cell number of adhered cells (figure 6-5) is higher than on the other surfaces. The NaOH treatment, which generates a high hydrophilicity and marked nanoroughness of the surface, probably provoked this reduction of the cell adhesion. The average cell size did not show marked differences in conditions which were not statistically significant.

### 6.4.3. Cell proliferation of MC3T3 pre-osteoblasts

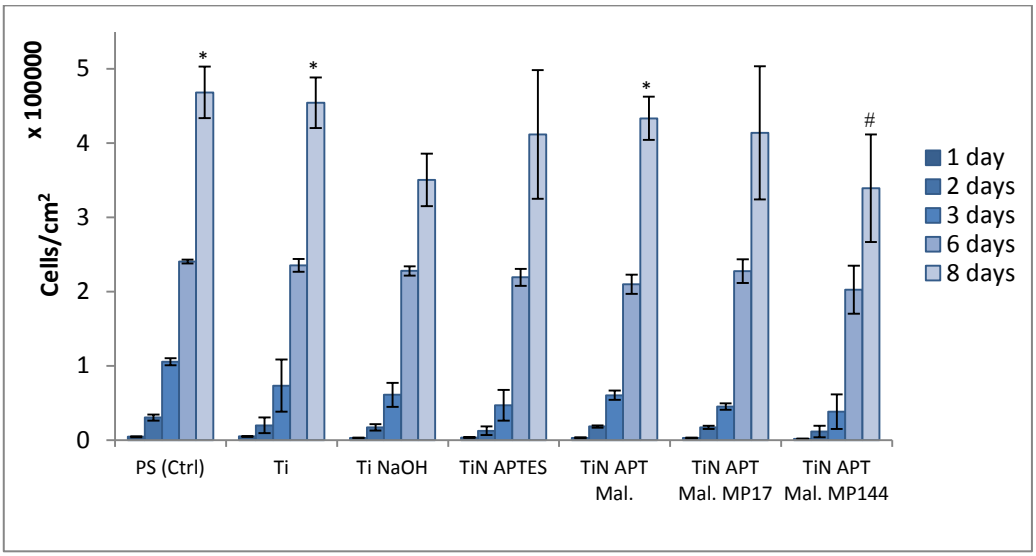


***Figure 6-6:*** *Cell proliferation on MC3T3-E1 pre-osteoblasts. PS refers to cells seeded on a Polystyrene well plate. *: Statistically significant differences with respect to Ti NaOH after 8 days. #: Statistically significant differences with respect to Ti after 8 days. ($\alpha$<0.05).*

The proliferation of MC3T3-E1 pre-osteoblastic cells (figure 6-6) reveals that it was not greatly affected by the surface where they were seeded. Nevertheless, it can be seen that, in the first days of the proliferation assay cells tended to proliferate faster on PS surfaces than on titanium surfaces. One also observes that Ti NaOH and TiN APT mal. MP144 surfaces showed a slightly lower proliferation rate than do plain Ti surfaces. It is known that sodium titanate surfaces provoke fast osteoblastic differentiation and this effect hinders the proliferation of cells since these then tend to differentiate rather than proliferate [71]. A similar effect may have happened on MP144 biofunctionalized surfaces, explaining a lower proliferation. Further results presented later in this chapter confirmed this point.

## 6.4.4. Cell differentiation of fibroblasts and pre-osteoblasts

### 6.4.4.1. Gene expression of fibroblasts and pre-osteoblasts

#### 6.4.4.1.1. *Fibroblastic response*

Normal fibroblasts are embedded within the fibrillar extracellular matrix (ECM) of the connective tissue. A normal fibroblast can acquire an 'activated' phenotype to synthesize large amounts of ECM constituents. Fibroblast activation is induced by various stimuli that arise when tissue injury occurs [72] including growth factors such as transforming growth factor-β (TGF−β), epidermal growth factor (EGF), platelet-derived growth factor (PDGF) and fibroblast growth factor 2 (FGF2). Activated fibroblasts express alpha-smooth-muscle actin, leading to the term 'myofibroblasts'. In addition, activated fibroblasts also secrete increased levels of ECM-degrading proteases such as matrix metalloproteinase 2 (MMP2), MMP3 and MMP9, facilitating increased ECM turnover and altered ECM composition [73]. Activated fibroblasts are found in healing wounds and sclerosing tissues, and are also associated with cancers. Importantly, in the context of wound healing, fibroblast activation is reversed once the activating stimulus is attenuated. However, in tissue fibrosis, fibroblasts sustain their activated state, often until organ death. Interestingly, fibroblasts that are isolated from fibrotic tissue maintain their activated phenotype when cultured *in vitro*. Fibroblasts in such a sustained state of activation typically continue to secrete ECM constituents, growth factors and cytokines [72].

The results of gene expression of differentiation markers on NIH/3T3 mouse fibroblasts are presented henceforth. There are two graphs per gene. Both graphs present the same results but in different order. Blue bars show the expression related to the conditions separated in blocks of time. Red lines show the gene expression related to the time of cell lysis separated into groups of surfaces treated differently. On these graphs, the results regarding the TCPS (Control) and TiN (NaOH treated samples) conditions have been suppressed in order to give a clearer depiction of the results. Although the TCPS are not shown, the results are still related to the expression of the cells on TCPS on day 1 of culture.

6.4.4.1.1.1. Collagen type 1 alpha 1 gene expression

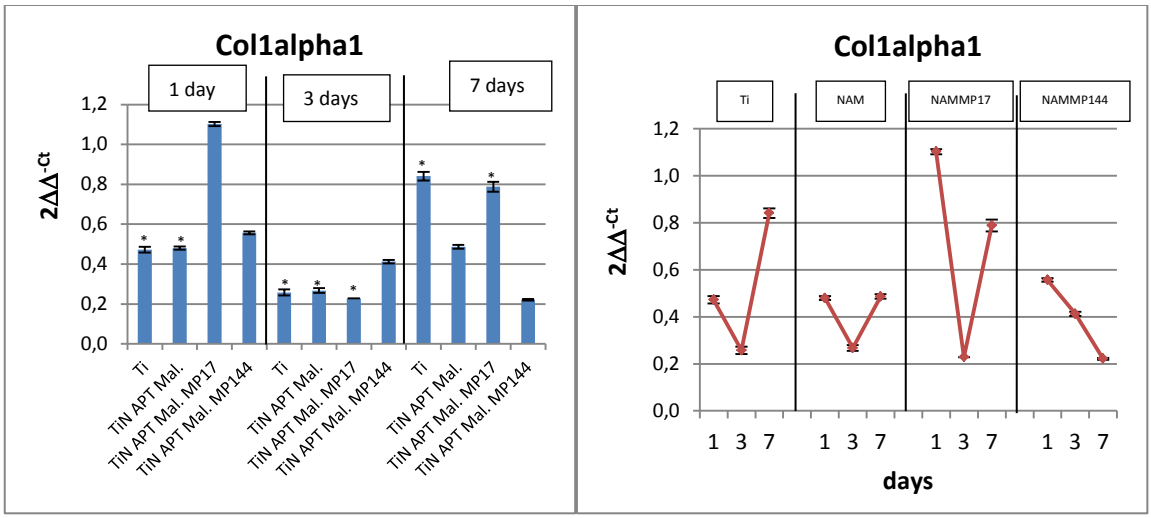


***Figure 6-7:*** *Collagen type 1 alpha 1 gene expression of NIH/3T3 fibroblasts on Ti surfaces with different surface treatments by qRT-PCR after 1, 3 and 7 days of cell culture. Ratios of target genes relative to housekeeping gene –β-actin- were expressed relative to tissue culture polystyrene after 1 day of cell culture. Left: data classified by time of cell culture. Right: data classified by surface treatment. Bars with same symbols (*) indicate that differences between them are not statistically significant when compared within the same culture time block.*

Collagen is one of the most common fibroblastic markers. However, collagen type I is not only secreted by fibroblasts, but also by condroblasts and osteoblasts. TGF-β1 seems to stimulate the production of collagen among other fibroblastic proteins like alpha-SMA and fibronectin [74-76]. From the graphs it is difficult to extract a response pattern. On day 1, P17 seemed to highly stimulate collagen production, whereas on day 3 the collagen production dropped intensely, to again rise on day 7. NAMMP144 slightly increased collagen production after 1 and 3 days in comparison with Ti and NAM, but markedly decreased after 7 days. It is interesting that for all samples except for NAMMP144 the lowest gene expression was found in day 3. Although, NAMMP144 surfaces still reduced the gene expression of their cells at day 7. This result suggest an inhibitory effect of the NAMMP144 surfaces on the expression of collagen according to the hypothesis estated in this chapter.

6.4.4.1.1.2. Alpha-Smooth Muscle Actin (α-SMA) gene expression

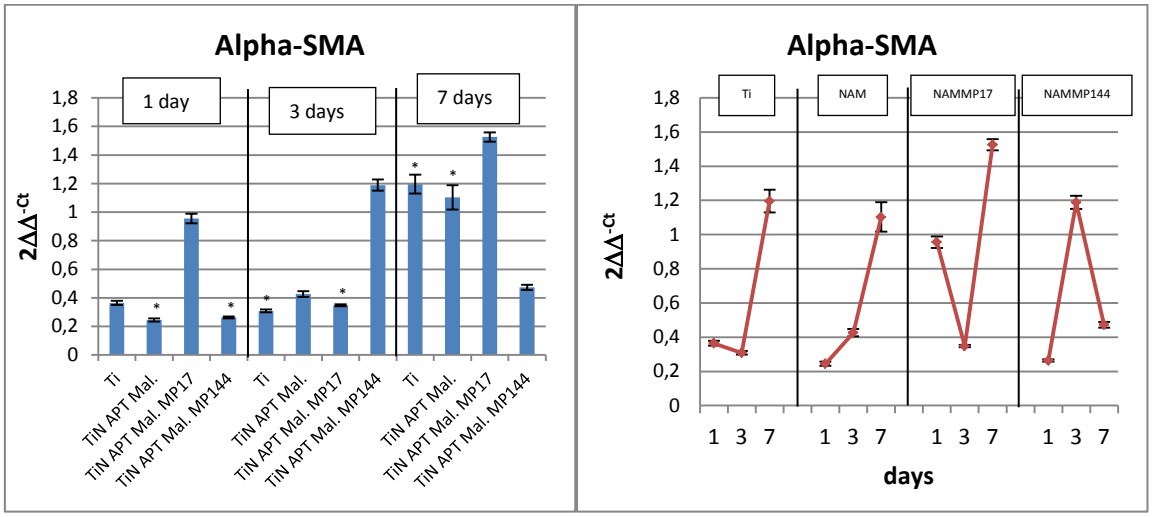


***Figure 6-8:*** *α-SMA gene expression of NIH/3T3 fibroblasts on Ti surfaces with different surface treatments by qRT-PCR after 1, 3 and 7 days of cell culture. Ratios of target genes relative to housekeeping gene –β-actin- were expressed relative to tissue culture polystyrene after 1 day of cell culture. Left: data classified by time of cell culture. Right: data classified by surface treatment. Bars with same symbols (*) indicate that differences between them are not statistically significant when compared within the same culture time block.*

Alpha-smooth muscle actin (α-SMA) is commonly used as a marker of myofibroblast formation [59,77]. Alpha-SMA is present in the contractile apparatus as well as in the fibrous tissue [78]. Like collagen, alpha-SMA also shows very variable response. NAMMP17 shows similar patterns to that of collagen expression, having the lowest value after 3 days. NAMMP144 shows the opposite behavior, being higher than Ti, NAM and P17 after 3 days but much lower after 7 days, suggesting that NAMMP144 surfaces have a sustained inhibitory effect over time.

6.4.4.1.1.3. Fibronectin gene expression

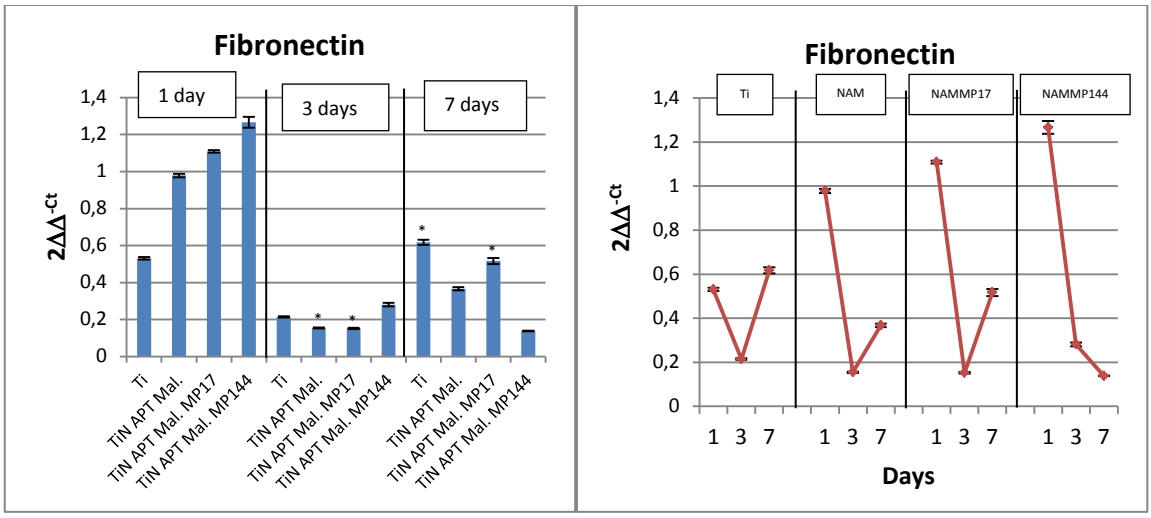


***Figure 6-9:*** *Fibronectin gene expression of NIH/3T3 fibroblasts on Ti surfaces with different surface treatments by qRT-PCR after 1, 3 and 7 days of cell culture. Ratios of target genes relative to housekeeping gene –β-actin- were expressed relative to tissue culture polystyrene after 1 day of cell culture. Left: data classified by time of cell culture. Right: data classified by surface treatment. Bars with same symbols (*) indicate that differences among them are not statistically significant when compared within the same culture time block.*

Insoluble cellular fibronectin is a major component of the extracellular matrix. It is secreted by various cells, primarily fibroblasts, as a soluble protein dimer and is then assembled into an insoluble matrix in a complex cell-mediated process [79]. Fibronectin plays a major role in cell adhesion, growth, migration and differentiation, and it is important for processes such as wound healing [80]. In this experiment, fibronectin expression shows a similar tendency over time for all surface treatment except for NAMMP144, which has its lowest value after 7 days. On the first day of culture the expression of fibronectin was higher on the surfaces that were treated. This effect could be associated to the sodium titanate on the surface of the treated titanium samples.

As it can be seen on the non-enzymatic protein expression, the gene expression of the three proteins studied gets hindered by NAMMP144 surfaces after 7 days of culture. These results suggest a sustained inhibitory effect of the fibrotic response by thy titanium surfaces treated with the NAMMP144 peptide.

6.4.4.1.1.4. Matrix metalloproteinase-2 (MMP-2) gene expression

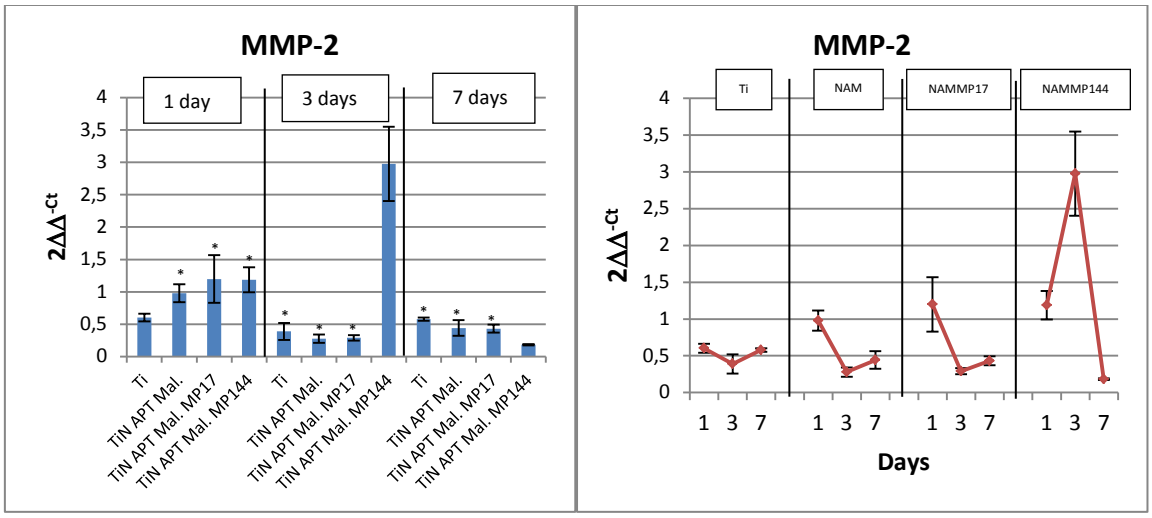


***Figure 6-10**: MMP2 gene expression of NIH/3T3 fibroblasts on Ti surfaces with different surface treatments by qRT-PCR after 1, 3 and 7 days of cell culture. Ratios of target genes relative to housekeeping gene –β-actin- were expressed relative to tissue culture polystyrene after 1 day of cell culture. Left: data classified by time of cell culture. Right: data classified by surface treatment. Bars with same symbols (*) indicate that differences between them are not statistically significant when compared within the same culture time block.*

MMPs are a family of enzymes that are secreted by connective tissue cells, inflammatory phagocytes, and a number of different transformed cells. They are called metallo because they all contain a zinc atom at their active site. MMPs are responsible for normal turnover and remodeling of the extracellular matrix, and are capable of breaking down most components in the extracellular matrix, including collagen, laminin, fibronectin, elastin, serpin, etc [81]. Proteins of the matrix metalloproteinase (MMP) family are involved in the breakdown of extracellular matrix in normal physiological processes, such as embryonic development, reproduction, and tissue remodeling, as well as in disease processes, such as arthritis and metastasis. Most MMPs are secreted as inactive pro-proteins which are activated when cleaved by extracellular proteinases [60]. Matrix metalloproteinase-2, also known as gelatinase A, readily digests the denatured collagens type I, II, and III [82] and is related to certain bone diseases, such as osteolisis and arthritis, when a mutation of the MMP-2 gene occurs [83]. TGF-β1 can induce the expression of this protein [84].

In this case, P144 shows similar behavior to the one shown on Alpha-SMA expression, having its maximum expression after 3 days. The other conditions do not show marked differences among each other.

6.4.4.1.1.5. Matrix metalloproteinase-3 (MMP-3) gene expression

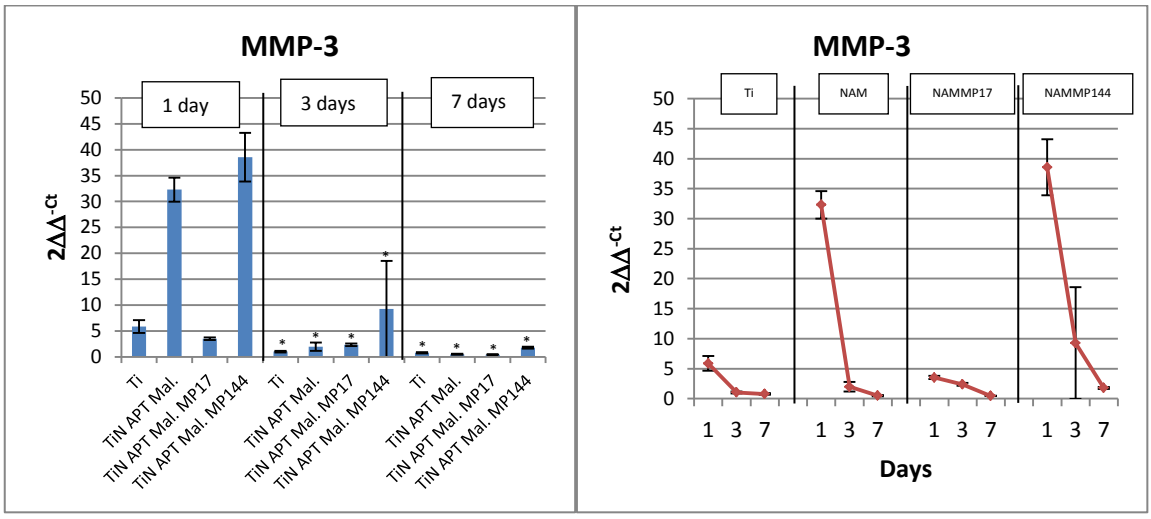


***Figure 6-11:*** *MMP3 gene expression of NIH/3T3 fibroblasts on Ti surfaces with different surface treatments by qRT-PCR after 1, 3 and 7 days of cell culture. Ratios of target genes relative to housekeeping gene –β-actin- were expressed relative to tissue culture polystyrene after 1 day of cell culture. Left: data classified by time of cell culture. Right: data classified by surface treatment. Bars with same symbols (*) indicate that differences between them are not statistically significant when compared within the same surface treatment group.*

Matrix metalloproteinase-3, also known as stromelysin-1, degrades collagen types II, III, IV, IX, and X, proteoglycans, fibronectin, laminin, and elastin. In addition, MMP-3 can also activate other MMPs such as MMP-1, MMP-7, and MMP-9, rendering MMP-3 crucial in connective tissue remodeling [85]. The enzyme is thought to be involved in wound repair, progression of atherosclerosis, and tumor initiation. The expression of MMP-3 is an indicator myofibroblastic activity and remodelation of the extracellular matrix.

NAMMP144 surfaces behave in a similar way in the different conditions studied throughout the time intervals established. The peak of expression of this enzyme is shown on day 1. P17

displays the lowest values, while P144 shows the highest ones. The high expression of MMP-2 and MMP-3 on NAMMP144 surfaces at day 3 correlates with the high expression of collagen, fibronectin and alpha-SMA at the same day of culture suggesting a correlation between the expression of extracellular matrix and the expression of the metalloproteinases for the remodelation of the new tissue.

6.4.4.1.1.6. Matrix metalloproteinase-9 (MMP-9) gene expression

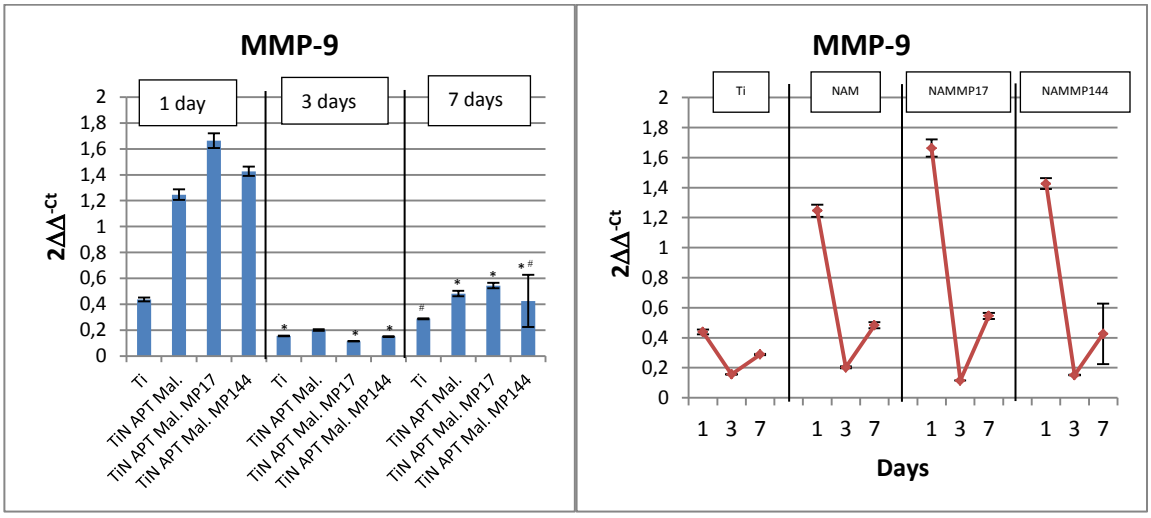


***Figure 6-12:*** *MMP9 gene expression of NIH/3T3 fibroblasts on Ti surfaces with different surface treatments by qRT-PCR after 1, 3 and 7 days of cell culture. Ratios of target genes relative to housekeeping gene –β-actin- were expressed relative to tissue culture polystyrene after 1 day of cell culture. Left: data classified by time of cell culture. Right: data classified by surface treatment. Bars with same symbols (*,#) indicate that differences among them are not statistically significant when compared within the same culture time block.*

Matrix metalloproteinase-9 enzyme, also known as gelatinase B, degrades type IV and V collagens [60]. Studies in rhesus monkeys suggest that the enzyme is involved in IL-8-induced mobilization of hematopoietic progenitor cells from bone marrow, and murine studies suggest a role in tumor-associated tissue remodeling [86]. Also, MMP-9 is related to inflammatory processes [87].

Finally, like MMP-3, MMP-9 shows the highest values of expression on the first day of culture. NAMMP144 shows similar patterns to those of the other metalloproteins studied except that

no overexpression of MMP-9 was detected at day 3. Being MMP-9 related to inflammatory processes it would suggest that cells expressed higher values of this protein at the beginning of the cell culture due to the fact that no extracellular matrix was already generated on the surface of the samples. After 3 days of culture the expression of MMP-9 lowered its signal significantly suggesting the inflammation process had ended.

#### 6.4.4.1.2. *Osteoblastic response*

The results of gene expression on differentiation markers of MC3T3-E1 mouse pre-osteoblasts are presented below. The setup of the graphs is parallel to that corresponding to 3T3 fibroblasts. We have suppressed the TCPS and N conditions because they didn't provide relevant information.

##### 6.4.4.1.2.1. Collagen Type 1 alpha 1 gene expression

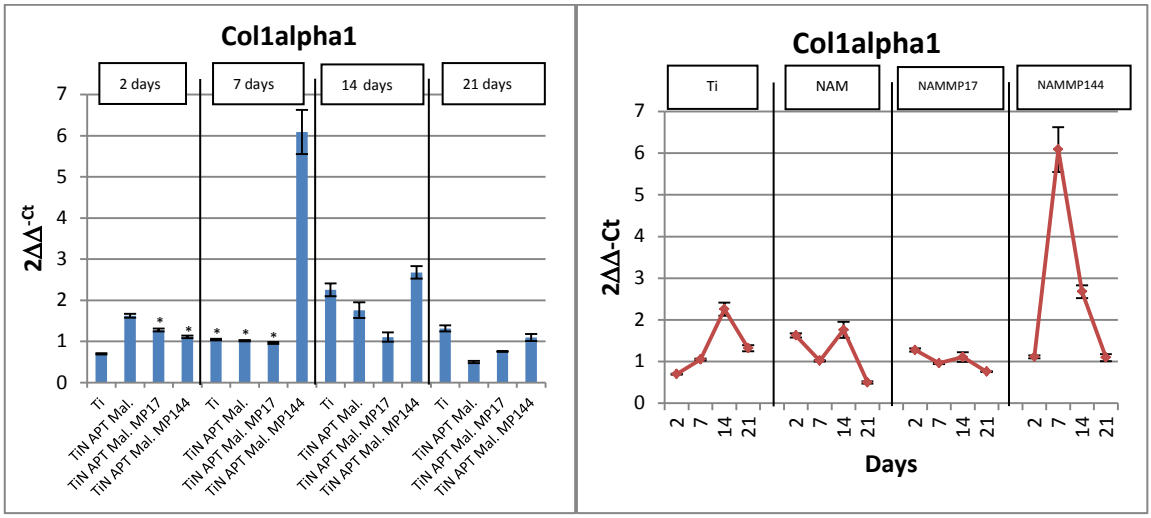


***Figure 6-13:*** *Col1alpha1 gene expression of MC3T3-E1 pre-osteoblasts on Ti surfaces with different surface treatments by qRT-PCR after 2, 7, 14 and 21 days of cell culture. Ratios of target genes relative to housekeeping gene β-actin- were expressed relative to tissue culture polystyrene after 2 days of cell culture. Left: data classified by time of cell culture. Right: data classified by surface treatment. Bars with same symbols (*) indicate that differences between them are not statistically significant when compared within the same culture time block.*

On a time basis, collagen is the first marker of osteoblastic differentiation [88]. Some authors propose that a collagen matrix is necessary for osteoblastic differentiation [89,90]. On the graphs above we can see that the peak of collagen expression in most of the samples is shown after 14 days except for P144, where the peak expression is found after 7 days. This result suggests that P144 surface is accelerating and greatly increasing the collagen expression that could entail a premature osteoblastic differentiation. From the left side graph it is difficult to draw conclusions because the collagen expression doesn't show any particular trend, and the progression is not the same for all samples.

6.4.4.1.2.2. Runt-related transcription factor-2 (RUNX2) gene expression

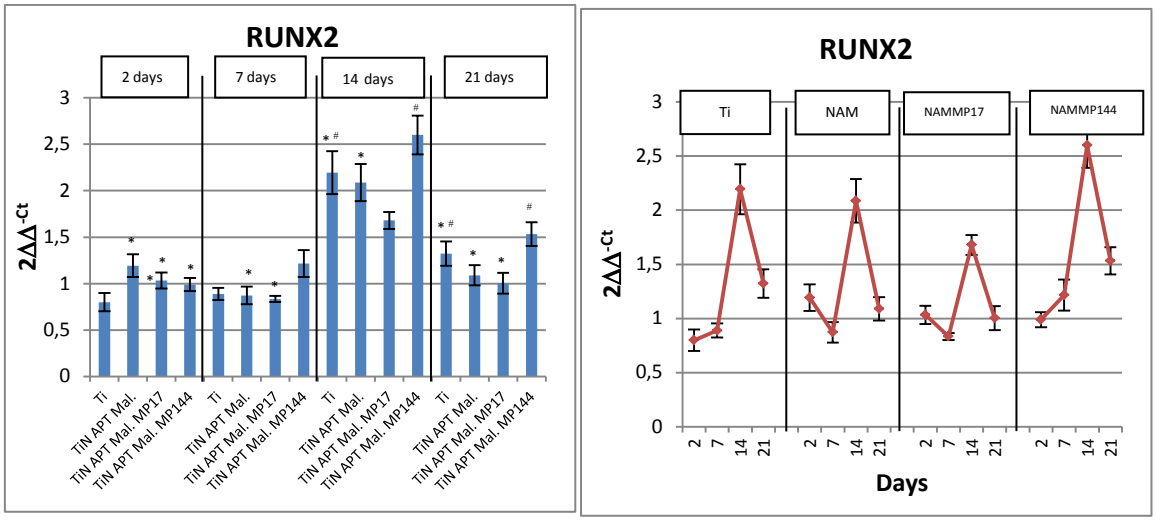


***Figure 6-14:*** *RUNX2 gene expression of MC3T3-E1 pre-osteoblasts on Ti surfaces with different surface treatments by qRT-PCR after 2, 7, 14, and 21 days of cell culture. Ratios of target genes relative to housekeeping gene –β-actin- were expressed relative to tissue culture polystyrene after 2 days of cell culture. Left: data classified by time of cell culture. Right: data classified by surface treatment. Bars with same symbols (*,#) indicate that differences are not statistically significant between them when compared in the same block culture time.*

RUNX2 is a transcription factor, essential for osteoblastic differentiation. The expression of RUNX is usually shown at the beginning of differentiation or just after the peak of collagen expression [91]. From the graphs, we can see that the peak of RUNX2 expression was invariably

obtained at 14 days, being at its maximum on functionalized MP144 samples. It is important to remark that functionalized MP17 surfaces showed the lowest expression of RUNX2. From the red graph, again, it is difficult to draw conclusions but it seems that Ti response pattern was similar to those of MP144, and the response pattern of TiN APT Mal. was similar to the one of P17. This trend was also displayed in the results of the collagen expression.

#### 6.4.4.1.2.3. Alkaline Phosphatase gene expression

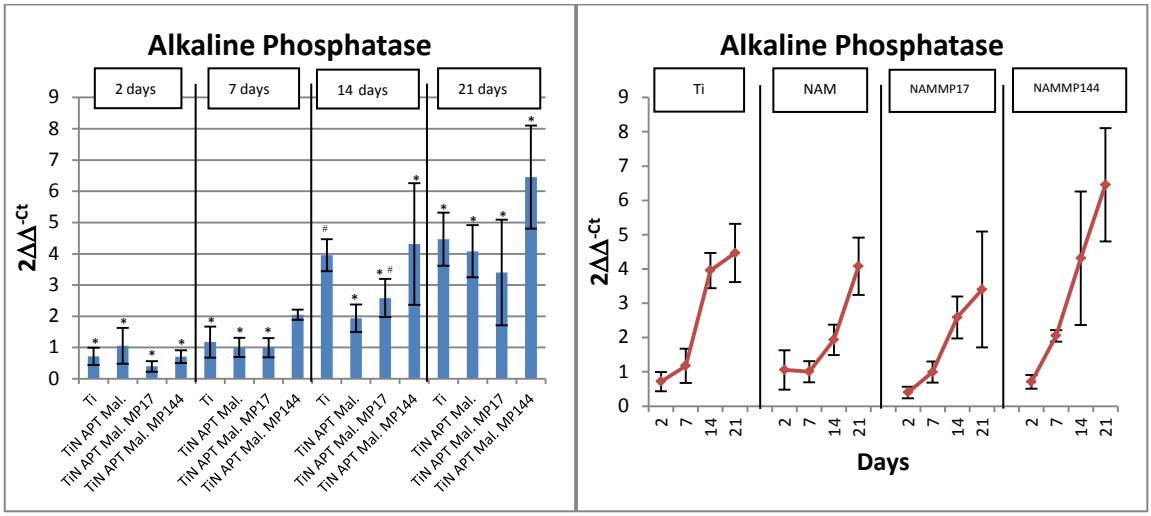


***Figure 6-15:*** *Alkaline phosphatase gene expression of MC3T3-E1 pre-osteoblasts on Ti surfaces with different surface treatments by qRT-PCR after 2, 7, 14, and 21 days of cell culture. Ratios of target genes relative to housekeeping gene β-actin- were expressed relative to tissue culture polystyrene after 2 days of cell culture. Left: data classified by time of cell culture. Right: data classified by surface treatment. Bars with same symbols (*,#) indicate that differences between them are not statistically significant when compared within the same culture time block.*

Alkaline phosphatase is the most common marker for osteoblastic differentiation. It is a hydrolase enzyme that has the role of dephosphorylating many types of molecules, including bone [92]. As can be seen on the red graph, ALP expression was increased over time, reaching its apex on day 21. Usually the peak of alkaline phosphatase *in vitro* is shown previously, between days 10 to 14. The specific clone of MC3T3-E1 used for this experiment is known to have a delayed expression of ALP [93]. Nevertheless, the results show that the highest ALP

expression occurred on P144 surfaces while P17 again showed the lowest values. Differences are not statistically significant but this result supports the findings obtained from the other genes.

6.4.4.1.2.4. Osteocalcin gene expression

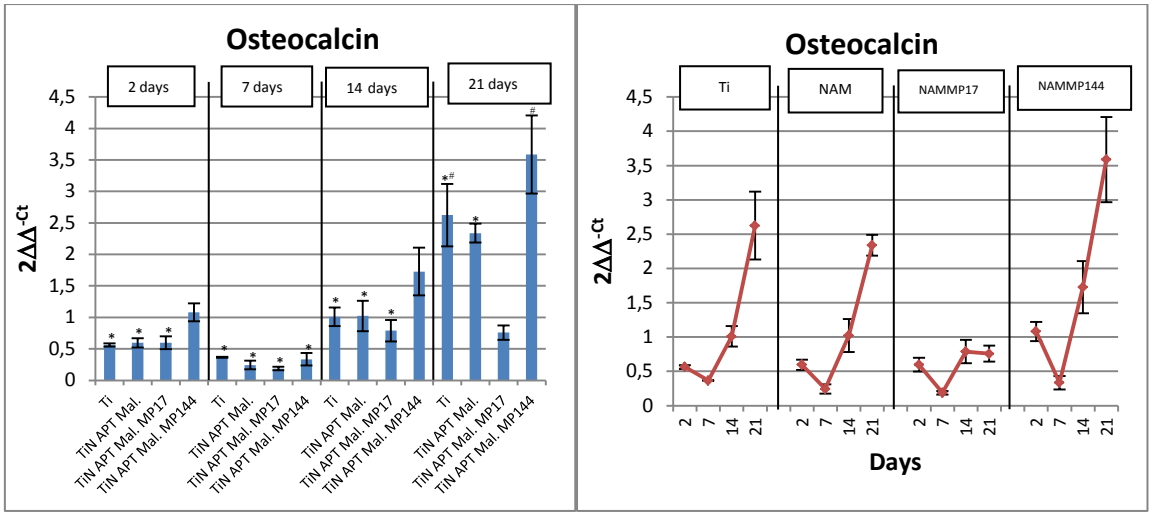


***Figure 6-16:*** *Osteocalcin gene expression of MC3T3-E1 pre-osteoblasts on Ti surfaces with different surface treatments by qRT-PCR after 2, 7, 14 and 21 days of cell culture. Ratios of target genes relative to housekeeping gene –β-actin- were expressed relative to tissue culture polystyrene after 2 days of cell culture. Left: data classified by time of cell culture. Right: data classified by surface treatment. Bars with same symbols (*,#) indicate that differences are not statistically significant between them when compared within the same culture time block.*

Osteocalcin is the ultimate marker for osteoblastic differentiation because it is solely secreted by osteoblasts [92]. It has many different functions related to bone and it is usually expressed and produced after ALP. From the red graph we can see that all the conditions revealed the same tendency to reach the expression peak after 21 days and exhibited the lowest expression after 7 days. It appears from the blue bars that MP17 functionalized surfaces hindered differentiation, showing very low values of OC expression, whereas MP144 functionalized samples again showed the highest expression levels of OC at all times.

### 6.4.4.2. Osteoblastic differentiation of human mesenchymal stem cells

#### 6.4.4.2.1. *Alkaline phosphatase (ALP) activity*

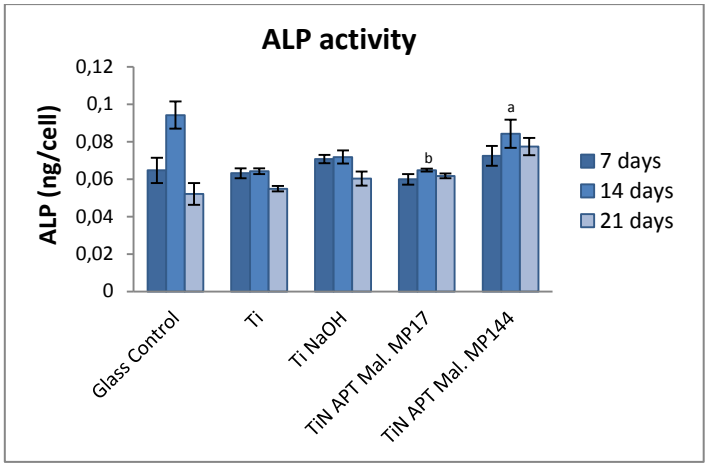


***Figure 6-17:*** *Alkaline phosphatase activity on human mesenchymal stem cells seeded on Ti surfaces with different surface treatments after 7, 14 and 21 days of culture.* [a:] *indicates that differences are not statistically significant with respect to Ti on day 14 of culture.* [b:] *indicates that differences are not statistically significant with respect to Ti NaOH on day 14 of culture.*

The activity of alkaline phosphatase on human mesenchymal stem cells shows that the peak of activity occurred after 14 days of culture with osteogenic media. At this time, MP144 surfaces exhibited higher ALP activity than Ti surfaces while MP17 surfaces displayed similar ALP activity with respect to Ti samples.

6.4.4.2.2. *Osteocalcin (OC) production*

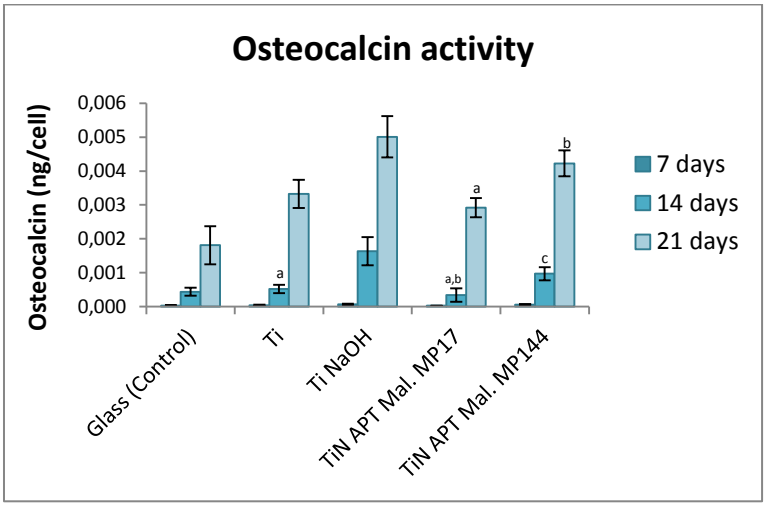


***Figure 6-18:*** *Osteocalcin concentration on human mesenchymal stem cells seeded on Ti surfaces with different surface treatments after 7, 14 and 21 days of culture. Differences are not statistically significant with respect to a: Glass, b: Ti, c: Ti NaOH, given the same culture time.*

It is possible to observe in figure 6-18 that osteocalcin concentration increased over culture time, reaching its peak after 3 weeks of culture. The biofunctionalized surfaces showed the same response as that of alkaline phosphatase activity. After 21 days, MP144 surfaces show a higher OC concentration than that shown by Ti surfaces, whereas MP17 surfaces showed a lower concentration than MP144 surfaces, similar to that of Ti surfaces.

# 6.5. Discussion

## 6.5.1. Inhibition of TGF-β1 activity

Western Blot results demonstrated the capability of the titanium surfaces biofunctionalized with MP17 and MP144 to hinder the expression of phosho-SMAD2 and, therefore, to inhibit the TGF-β1 signalling pathway. This result is of major relevance as it validates the most important of the hypothesis of this PhD dissertation. Results of gene expression of relevant markers for osteoblast and fibroblast differentiation as well as differentiation markers produced by osteoprogenitor cells further validated that the MP144 peptides on titanium surfaces allowed downregulation of fibroblastic activity and upregulation of osteoblastic activity. Overall, these results proved that the coatings produced with MP144 peptides are preferential candidates to be used in bone repair and regeneration applications with the ultimate purpose of accelerating osseointegration and improving the quality of interfacial interactions during the process of healing and regeneration after implantation. Although the peptides administered in solution had more effectiveness we have to bear in mind that the amount of peptide in solution was about 1 or two orders of magnitude larger than the amount of peptide present on the surface of a biofunctionalized surface. The fact that the biofunctionalized surface achieved this degree of effectiveness can be explained by the localization of the active principle next to the cells, thereby enabling it to react with the nearby TGF-β1 molecules which have a higher probability of interacting with the TGF-β1 cell receptors.

Another interesting fact is that MP144 surfaces are more effective than MP17 surfaces in inhibiting TGF-β1. Dotor et al. reported that the first lysine of the P17 peptide ($NH_2$-KRIWFIPRSSWYERA-OH) plays a crucial role in the interaction with TGF-β1 and the inhibition of this cytokine [45]. APTES silanized titanium surfaces treated with malonic acid via HBTU route are able to react readily with primary amines and produce a covalent bond between the malonic acid and the amines of the peptide. The MP17 peptide therefore contains 3 possible anchorage points to the malonic acid. These are: The N-Terminus, the lysine residue of the first amino acid of the MP17 sequence ($NH_2$- KGGGGGKRIWFIPRSSWYERA-OH), and the lysine residue of the first amino acid of the biologically active P17 sequence. If the last point of anchorage mentioned interacts with malonic acid creating an amide bond, it is possible that the

P17 peptide will become biologically inactive and, therefore, have its efficacy reduced. MP144 peptide doesn't have this problem since there are no residual primary amines in its biologically active sequence.

From the MV-1-Lu cell line proliferation, the results suggest that MV-1-Lu cell line, which is one of the most useful tools to test TGF-β1 activity [46,57], has a low affinity for titanium surfaces and its metabolism gets negatively affected when adhered to these surfaces. Nevertheless, no differences between plain titanium surfaces and biofunctionalized surfaces have been found. Therefore, no cytotoxicity from the biofunctionalization process was assessed.

### 6.5.2. Fibroblastic response

NIH/3T3 fibroblasts response can be somewhat confusing. During the first day, the cells were cultured on the surfaces with serum-free medium supplemented with 0.5 ng/ml of exogenous TGF-β1. After the first day, 10% of FBS was added to the medium in order to avoid cell starvation. Given that serum is able to block TGF-β1 due to hydrophobic interactions between them, we can assume that TGF-β1 was more effective stimulating target gene expression on the first day because no blocking from serum was possible. This could further explain the high expression of collagen, fibronectin, MMP2, MMP3 and MMP9 on the first day.

From what can be gleaned of the gene expressions measured, the fibroblast differentiation after 7 days of culture seems to be consistently reduced on MP144 functionalized surfaces. MP17 functionalized surfaces show similar tendencies to those of non-functionalized titanium surfaces. These results suggest that MP17 surfaces were not affecting the fibroblast behavior significantly whereas MP144 functionalized surfaces had the ability to inhibit fibroblastic differentiation after 3 days in culture with a maximum expression of the inhibitory effect after 7 days in culture. Results about the inhibition of TGF-β1 activity demonstrated that MP144 functionalized surfaces were considerably more effective than MP17 surfaces. It is important to remark that Western Blot was used to test the inhibition of TGF-β1 activity for cell response after a 1 hour period whereas fibroblast differentiation lasted 7 days. A sustained inhibition effect of the functionalized surfaces was unexpected due to the remodelation that suffers the

surface after seeding the cells on it, such protein adsorption, surface coverage by the cells and enzymatic activity. Despite the fact that surfaces tend to become biologically inactive over time, it is possible that MP144 surfaces could inhibit TGF-β1 for longer periods of time than MP17 surfaces given the greater effectiveness they've shown. Authors believe that two key factors are responsible for the high efficacy and sustainability of the inhibitory effect of the MP144 surfaces. One is the high amount of peptide on the surface achieved by the methodology developed in chapter 2 and studied in chapter 5. The second is the high stability of the peptides on the surfaces achieved by means of the APTES + Malonic acid route as explained in chapters 4 and 5.

### 6.5.3. Osteoblastic response

From the results regarding differentiation of the mouse MC3T3-E1 pre-osteoblasts, a similar effect than the one of the fibroblastic response could have taken place after 2 days in culture. In this case, the cells remained serum-free during the first 2 days but the medium was loaded with osteogenic precursors during the whole experiment.

In general, MP144 functionalized surface showed strong osteoinductive effect that promoted the expression of all osteoblastic differentiation markers. These somehow unexpected results can be explained due to the fact that inhibition of TGF-β1 has been proven to promote osteoblast differentiation in MC3T3 cells [51] and some studies report the negative effect of exogenous TGF-β1 on the differentiation of osteoblasts [28,33-35]. On the other hand, MP17 surfaces showed the opposite effect and hindered osteoblast differentiation. Although this effect is not very acute, previous results suggest that the reduction of the expression of the osteogenic markers is not connected with the inhibition of TGF-β since MP17 has shown a low TGF-β inhibition effect.

MP144 functionalized surfaces clearly induced osteoblastic differentiation while also apparently inhibiting fibroblastic activity. These results make MP144 surfaces a good candidate for its application in bone implants and prostheses.

Alkaline phosphatase and osteocalcin expression in human mesenchymal stem cells supported the results shown by MC3T3 cells regarding gene expression which have been used in several works for study the effect on TGF-β1 and its inhibition [3,32,51]. MP144 surfaces had the potential to induce osteoblastic differentiation while MP17 surfaces seemed to inhibit it.

Although the results show non-significant differences between groups, the fact that human mesenchymal stem cells have responded well to the biofunctionalized surfaces implies that the biofunctionalization process, the MP17 and MP144 peptides, and the biofunctionalized surfaces are not noxious for human cells and can even be beneficial for osteoblast differentiation in the case of MP144 biofunctionalized surfaces.

The results presented in this chapter are valuable to develop new strategies for implant osseointegration. The achievement of a surface that can inhibit the TGF-β1 effect on cells has been possible thank to the work and achievements accomplished in the previous chapters of this thesis. A high amount of peptide on the surface and a good anchorage of the peptides is necessary for having a significant effect of the surfaces on the inhibition of the TGF-β1. Moreover, a new titanium surface that can hinder the production of fibrous tissue and enhance osteoblastic differentiation has been generated, being an important candidate for its application in the field of osseointegration.

# 6.6. Conclusions

The following conclusions can be extracted from the results obtained in this chapter:

- A new titanium surface, with TGF-β1 inhibitory activity *in vitro*, has been developed. Specifically, titanium surfaces biofunctionalized with MP144 peptide showed a strong inhibition of the activity of the cytokine.

- The new developed surfaces did not hinder cell adhesion or proliferation in comparison with the control biocompatible titanium surfaces.

- The proved TGF-β1 inhibitory effect of MP144-functionalized surfaces notably reduced fibroblastic differentiation of NIH/3T3 cells.

- Titanium surfaces biofunctionalized with MP144 notable favored osteoblast and osteoprogenitor cell differentiation.

Overall, these results proved that the coatings produced with MP144 peptides are preferential candidates to be used in bone repair and regeneration applications with the ultimate purpose of accelerating osseointegration and improving the quality of interfacial interactions during the process of healing and regeneration after implantation.

# 6.7. References

1. Sporn MB, Roberts AB. Introduction: What is TGF-beta? Ciba foundation Symposium 1991;157:1-6.

2. Branton MH, Kopp JB. TGF-β and fibrosis. Microb Infect 1999;1:1349-1365.

3. Spinella-Jaegle S, Roman-Roman S, Faucheu C, Dunn F-, Kawai S, Galléa S, Stiot V, Blanchet AM, Courtois B, Baron R, Rawadi G. Opposite effects of bone morphogenetic protein-2 and transforming growth factor-[beta]1 on osteoblast differentiation. Bone 2001;29:323-330.

4. Schmidmaier G, Lucke M, Schwabe P, Raschke M, Haas NP, Wildemann B. Collective review: bioactive implants coated with poly(D,L-lactide) and growth factors IGF-I, TGF-beta1, or BMP-2 for stimulation of fracture healing. Journal of Long-Term Effects of Medical Implants 2006;16:61-69.

5. Peralta-Zaragoza O, Lagunas-Martínez A, Madrid-Marina V. Factor de crecimiento transformante beta-1: estructura, función y mecanismos de regulación en cáncer. Salud Pública de México 2001;43:340-351.

6. Letterio JJ, Roberts AB. Regulation of immune responses by TGF-β. Annu Rev Immunol 1998;16:137-161.

7. Li Y, Wang M, Carra C, Cucinotta FA. Modularized Smad-regulated TGFbeta signaling pathway. Math Biosci 2012;240:187-200.

8. Massague J. The Transforming Growth Factor-beta Family. Annu Rev Cell Biol 1990;6:597-641.

9. Sporn MB, Roberts AB. Transforming growth factor-beta: recent progress and new challenges. The Journal of Cell Biology 1992;119:1017-1021.

10. Barnard JA, Lyons RM, Moses HL. The cell biology of transforming growth factor β. Biochimica et Biophysica Acta (BBA) - Reviews on Cancer 1990;1032:79-87.

11. Streuli CH, Schmidhauser C, Kobrin M, Bissell MJ, Derynck R. Extracellular matrix regulates expression of the TGF-beta 1 gene. The Journal of Cell Biology 1993;120:253-260.

12. LeRoy E, Trojanowska M, Smith E. Cytokines and human fibrosis. Eur Cytokine Netw 1990;1:215-219.

13. Kane CJ, Hebda PA, Mansbridge JN, Hanawalt PC. Direct evidence for spatial and temporal regulation of transforming growth factor beta 1 expression during cutaneous wound healing. J Cell Physiol 1991;148:157-173.

14. Schmid P, Itin P, Cherry G, Bi C, Cox DA. Enhanced expression of transforming growth factor-beta type I and type II receptors in wound granulation tissue and hypertrophic scar. Am J Pathol 1998;152:485-493.

15. Diez-Marques L, Ortega-Velazquez R, Langa C, Rodriguez-Barbero A, Lopez-Novoa JM, Lamas S, Bernabeu C. Expression of endoglin in human mesangial cells: modulation of extracellular matrix synthesis. Biochimica et Biophysica Acta (BBA) - Molecular Basis of Disease 2002;1587:36-44.

16. Lin RY, Sullivan KM, Argenta PA, Meuli M, Lorenz HP, Adzick NS. Exogenous transforming growth factor-beta amplifies its own expression and induces scar formation in a model of human fetal skin repair. Ann Surg 1995;222:146-154.

17. Shah M, Foreman DM, Ferguson MW. Neutralising antibody to TGF-beta 1,2 reduces cutaneous scarring in adult rodents. J Cell Sci 1994;107 ( Pt 5):1137-1157.

18. Mead AL, Wong TTL, Cordeiro MF, Anderson IK, Khaw PT. Evaluation of Anti-TGF-β2 Antibody as a New Postoperative Anti-scarring Agent in Glaucoma Surgery. Investigative Ophthalmology & Visual Science 2003;44:3394-3401.

19. Leask A, Abraham DJ. TGF-β signaling and the fibrotic response. The FASEB Journal 2004;18:816-827.

20. Shi Y, Massagué J. Mechanisms of TGF-beta Signaling from Cell Membrane to the Nucleus. Cell 2003;113:685-700.

21. Odell W. TGF beta signaling pathway. http://www.biocarta.com/pathfiles/h_tgfbpathway.asp. 2012.

22. Alberts B, Johnson A, Lewis J, Raff M, Roberts K, Walter P. Molecular biology of the cell. : Garland Science Taylor & Francis Group, 2002.

23. Chen W, Kirkbride KC, How T, Nelson CD, Mo J, Frederick JP, Wang X, Lefkowitz RJ, Blobe GC. {beta}-Arrestin 2 Mediates Endocytosis of Type III TGF-{beta} Receptor and Down-Regulation of Its Signaling. Science 2003;301:1394-1397.

24. Souchelnytskyi S, Ronnstrand L, Heldin CH, ten Dijke P. Phosphorylation of Smad signaling proteins by receptor serine/threonine kinases. Methods Mol Biol 2001;124:107-120.

25. Noda M, Camilliere JJ. In Vivo Stimulation of Bone Formation by Transforming Growth Factor-β. Endocrinology 1989;124:2991-2994.

26. Joyce ME, Roberts AB, Sporn MB, Bolander ME. Transforming growth factor-beta and the initiation of chondrogenesis and osteogenesis in the rat femur. The Journal of Cell Biology 1990;110:2195-2207.

27. Erlebacher A, Derynck R. Increased expression of TGF-beta 2 in osteoblasts results in an osteoporosis-like phenotype. The Journal of Cell Biology 1996;132:195-210.

28. Alliston T, Choy L, Ducy P, Karsenty G, Derynck R. TGF-[beta]-induced repression of CBFA1 by Smad3 decreases cbfa1 and osteocalcin expression and inhibits osteoblast differentiation. EMBO J 2001;20:2254-2272.

29. Maeda S, Hayashi M, Komiya S, Imamura T, Miyazono K. Endogenous TGF-[beta] signaling suppresses maturation of osteoblastic mesenchymal cells. EMBO J 2004;23:552-563.

30. Schmidmaier G, Wildemann B, Ostapowicz D, Kandziora F, Stange R, Haas NP, Raschke M. Long-term effects of local growth factor (IGF-I and TGF-β1) treatment on fracture healing: A safety study for using growth factors. Journal of Orthopaedic Research 2004;22:514-519.

31. Sodek J, Li IWS, Li H, Bellows CG, McCulloch CAG, Tenenbaum HC, Ellen RP. The role of TGF-β and BMP-7 in regenerating bone and soft tissues. Materials Science and Engineering: C 1994;2:19-26.

32. Kahai S, Vary CPH, Gao Y, Seth A. Collagen, type V, α1 (COL5A1) is regulated by TGF-β in osteoblasts. Matrix Biology 2004;23:445-455.

33. Bosetti M, Boccafoschi F, Leigheb M, Cannas MF. Effect of different growth factors on human osteoblasts activities: A possible application in bone regeneration for tissue engineering. Biomol Eng 2007;24:613-618.

34. Fischer U, Hempel U, Becker D, Bierbaum S, Scharnweber D, Worch H, Wenzel K-. Transforming growth factor β1 immobilized adsorptively on Ti6Al4V and collagen type I coated Ti6Al4V maintains its biological activity. Biomaterials 2003;24:2631-2641.

35. Nikolidakis D, Meijer GJ, Oortgiesen DAW, Walboomers XF, Jansen JA. The effect of a low dose of transforming growth factor β1 (TGF-β1) on the early bone-healing around oral implants inserted in trabecular bone. Biomaterials 2009;30:94-99.

36. Clokie CML, Bell RC. Recombinant Human Transforming Growth Factor [beta]-1 and Its Effects on Osseointegration. J Craniofac Surg 2003;14:268-277.

37. Halder SK, Beauchamp RD, Datta PK. Smad7 induces tumorigenicity by blocking TGF-β-induced growth inhibition and apoptosis. Exp Cell Res 2005;307:231-246.

38. Copple BL, Allen K, Welch TP. 9.11 - mechanisms of liver fibrosis. In: Editor-in-Chief: Charlene A. McQueen, editor. Comprehensive Toxicology (Second Edition)Oxford: Elsevier, 2010. p. 263-274.

39. Dawson DG. Corneal scars. In: Editor-in-Chief: Darlene A. Dartt, editor. Encyclopedia of the EyeOxford: Academic Press, 2010. p. 499-514.

40. Tansey MG, Kernie SG. Inflammation in neurodegenerative disease and injury. In: Editor-in-Chief: Larry R. Squire, editor. Encyclopedia of NeuroscienceOxford: Academic Press, 2009. p. 131-136.

41. Hermida N, López B, González A, Dotor J, Lasarte JJ, Sarobe P, Borrás-Cuesta F, Díez J. A synthetic peptide from transforming growth factor-β1 type III receptor prevents myocardial fibrosis in spontaneously hypertensive rats. Cardiovascular Research 2009;81:601-609.

42. Serrati S, Margheri F, Pucci M, Cantelmo AR, Cammarota R, Dotor J, Borràs-Cuesta F, Fibbi G, Albini.A, Del Rosso M. TGFb1 antagonistic peptides inhibit TGFb1-dependent angiogenesis. Biochemical Pharmacology 2009;77:812-825.

43. Santiago B, Gutierrez-Cañas I, Dotor J, Palao G, Lasarte JJ, Ruiz J, Prieto J, Borrás-Cuesta F, Pablos JL. Topical application of a peptide inhibitor of transforming growth factor-beta1 ameliorates bleomycin-induced skin fibrosis. J Invest Dermatol 2005;125:450-455.

44. Reiss M. TGF-β and cancer. Microb Infect 1999;1:1327-1347.

45. Dotor J, López-Vázquez AB, Lasarte JJ, Sarobe P, García-Granero M, Riezu-Boj J, Martínez A, Feijoó E, López-Sagaseta J, Hermida J, Prieto J, Borrás-Cuesta F. Identification of peptide inhibitors of transforming growth factor beta 1 using a phage-displayed peptide library. Cytokine 2007;39:106-115.

46. Ezquerro I, Lasarte J, Dotor J, Castilla-Cortázar I, Bustos M, Peñuelas I, Blanco G, Rodríguez C, Lechuga MdCG, Greenwel P, Rojkind M, Prieto J, Borrás-Cuesta F. A synthetic peptide from transforming growth factor β type III receptor inhibits liver fibrogenesis in rats with carbon tetrachloride liver injury. Cytokine 2003;22:12-20.

47. Ruiz-de-Erenchun R, Herrerías JDdl, Hontanilla B. Use of the Transforming Growth Factor-β1 Inhibitor Peptide in Periprosthetic Capsular Fibrosis: Experimental Model with Tetraglycerol Dipalmitate. Plast Reconstr Surg 2005;116:1370-1378 10.1097/01.prs.0000181694.07661.0d.

48. Arribillaga L, Dotor J, Basagoiti M, Riezu-Boj JI, Borrás-Cuesta F, Lasarte JJ, Sarobe P, Cornet ME, Feijoó E. Therapeutic effect of a peptide inhibitor of TGF-β on pulmonary fibrosis. Cytokine 2011;53:327-333.

49. Levy L, Hill CS. Alterations in components of the TGF-β superfamily signaling pathways in human cancer. Cytokine Growth Factor Rev 2006;17:41-58.

50. Shen Z, Kook Kim S, Youn Jun D, Park W, Ho Kim Y, Malter JS, Jo Moon B. Antisense targeting of TGF-β1 augments BMP-induced upregulation of osteopontin, type I collagen and Cbfa1 in human Saos-2 cells. Exp Cell Res 2007;313:1415-1425.

51. Takeuchi K, Abe M, Hiasa M, Oda A, Amou H, Kido S, Harada T, Tanaka O, Miki H, Nakamura S, Nakano A, Kagawa K, Yata K, Ozaki S, Matsumoto T. TGF-β Inhibition Restores Terminal Osteoblast Differentiation to Suppress Myeloma Growth. PLoS ONE 2010;5:e9870.

52. Mohammad KS, Chen CG, Balooch G, Stebbins E, McKenna CR, Davis H, Niewolna M, Peng XH, Nguyen DHN, Ionova-Martin S, Bracey JW, Hogue WR, Wong DH, Ritchie RO, Suva LJ, Derynck R, Guise TA, Alliston T. Pharmacologic Inhibition of the TGF-β Type I Receptor Kinase Has Anabolic and Anti-Catabolic Effects on Bone. PLoS ONE 2009;4:e5275.

53. Yamaguchi T, Chattopadhyay N, Kifor O, Butters RR, Sugimoto T, Brown EM. Mouse Osteoblastic Cell Line (MC3T3-E1) Expresses Extracellular Calcium (Ca2+o)?Sensing Receptor and Its Agonists Stimulate Chemotaxis and Proliferation of MC3T3-E1 Cells. Journal of Bone and Mineral Research 1998;13:1530-1538.

54. ATCC. 3T3-Swiss albino. http://www.atcc.org/ATCCAdvancedCatalogSearch/ProductDetails/tabid/452/Default.aspx?ATCCNum=CCL-92&Template=cellBiology. 2012.

55. altogen I. NIH 3T3. http://nih3t3.com/. 2012.

56. Spearman M, Taylor WR, Greenberg AH, Wright JA. Antisense oligodeoxyribonucleotide inhibition of TGF-β1 gene expression and alterations in the growth and malignant properties of mouse fibrosarcoma cells. Gene 1994;149:25-29.

57. Sjöblom T, Yakymovych I, Heldin C-, Östman A, Souchelnytskyi S. Smad2 suppresses the growth of Mv1Lu cells subcutaneously inoculated in mice. Eur J Cancer 2004;40:267-274.

58. Neman J, Persson A, Ho A, Levy ML, Snyder EY, Jandial R. Stem cells. In: Editors-in-Chief: Katie Kompoliti, Leo Verhagen Metman, editors. Encyclopedia of Movement DisordersOxford: Academic Press, 2010. p. 159-166.

59. Martinez EF, Araújo VC, Sousa SOM, Arana-Chavez VE. TGF-β1 Enhances the Expression of α–Smooth Muscle Actin in Cultured Human Pulpal Fibroblasts: Immunochemical and Ultrastructural Analyses. J Endod 2007;33:1313-1318.

60. Birkedal-Hansen H, Moore WGI, Bodden MK, Windsor LJ, Birkedal-Hansen B, DeCarlo A, Engler JA. Matrix Metalloproteinases: A Review. Critical Reviews in Oral Biology & Medicine 1993;4:197-250.

61. Li W, Xu S, Lin S, Zhao W. Overexpression of runt-related transcription factor-2 is associated with advanced tumor progression and poor prognosis in epithelial ovarian cancer. J Biomed Biotechnol 2012;2012:456534.

62. Aparicio C, Rodriguez D, Gil FJ. Variation of roughness and adhesion strength of deposited apatite layers on titanium dental implants. Materials Science and Engineering: C 2011;31:320-324.

63. Nakanishi T, Kokubun K, Oda H, Aoki M, Soma A, Taniguchi M, Kazuki Y, Oshimura M, Sato K. Bioluminescence imaging of bone formation using hairless osteocalcin-luciferase transgenic mice. Bone 2012;51:369-375.

64. Hunt M. Real Time PCR Tutorial. http://pathmicro.med.sc.edu/pcr/realtime-home.htm. 2010.

65. Jean G, Souberbielle J, Zaoui E, Lorriaux C, Mayor B, Hurot J, Deleaval P, Chazot C. Total and bone-specific alkaline phosphatases in haemodialysis patients with chronic liver disease. Clin Biochem 2012;45:436-439.

66. Nakanishi T, Kokubun K, Oda H, Aoki M, Soma A, Taniguchi M, Kazuki Y, Oshimura M, Sato K. Bioluminescence imaging of bone formation using hairless osteocalcin-luciferase transgenic mice. Bone 2012;51:369-375.

67. Invitrogen I. Human osteocalcin ELISA kit manual. 2010.

68. Lee MH, Ducheyne P, Lynch L, Boettiger D, Composto RJ. Effect of biomaterial surface properties on fibronectin–α5β1 integrin interaction and cellular attachment. Biomaterials 2006;27:1907-1916.

69. Acarturk TO, Peel MM, Petrosko P, LaFramboise W, Johnson PC, DiMilla PA. Control of attachment, morphology, and proliferation of skeletal myoblasts on silanized glass. J Biomed Mater Res 1999;44:355-370.

70. Kapur R, Rudolph AS. Cellular and Cytoskeleton Morphology and Strength of Adhesion of Cells on Self-Assembled Monolayers of Organosilanes. Exp Cell Res 1998;244:275-285.

71. Lee TM, Tsai RS, Chang E, Yang C,Y., Yang MR. The cell attachment and morphology of neonatal rat calvarial osteoblasts on the surface of Ti-6Al-4V and plasma-sprayed HA coating: Effect of surface roughness and serum contents. J Mater Sci Mater Med 2002:341-350.

72. Kalluri R, Zeisberg M. Fibroblasts in cancer. Nat Rev Cancer 2006;6:392-401.

73. Rodemann HP, Muller GA. Characterization of human renal fibroblasts in health and disease: II. In vitro growth, differentiation, and collagen synthesis of fibroblasts from kidneys with interstitial fibrosis. Am J Kidney Dis 1991;17:684-686.

74. Silverio-Ruiz KG, Martinez AET, Garlet GP, Barbosa CF, Silva JS, Cicarelli RMB, Valentini SR, Abi-Rached RSG, Junior CR. Opposite effects of bFGF and TGF-β on collagen metabolism by human periodontal ligament fibroblasts. Cytokine 2007;39:130-137.

75. Kegui W, Liangdi X, Shuilong C. Effects of TGF—β1 and PDGF on collagen synthesis of cardiac fibroblasts from spontaneously hypertensive rats. American Journal of Hypertension 2001;14:A172.

76. Moir LM, Burgess JK, Black JL. Transforming growth factor β1 increases fibronectin deposition through integrin receptor α5β1 on human airway smooth muscle. J Allergy Clin Immunol 2008;121:1034-1039.e4.

77. Mohan RR, Gupta R, Mehan MK, Cowden JW, Sinha S. Decorin transfection suppresses profibrogenic genes and myofibroblast formation in human corneal fibroblasts. Exp Eye Res 2010;91:238-245.

78. Kisseleva T, Brenner DA. Anti-fibrogenic strategies and the regression of fibrosis. Best Practice & Research Clinical Gastroenterology 2011;25:305-317.

79. Pankov R, Yamada KM. Fibronectin at a glance. Journal of Cell Science 2002;115:3861-3863.

80. Williams C, Engler A, Slone R, Galante L, Schwarzbauer J. Fibronectin expression modulates mammary epithelial cell proliferation during acinar differentiation. Cancer Res 2008;68:3185-3192.

81. Rasmussen HS, McCann PP. Matrix Metalloproteinase Inhibition as a Novel Anticancer Strategy: A Review with Special Focus on Batimastat and Marimastat. Pharmacol Ther 1997;75:69-75.

82. Visse R, Nagase H. Matrix metalloproteinases and tissue inhibitors of metalloproteinases: structure, function, and biochemistry. Circ Res 2003;92:827-839.

83. Martignetti JA, Aqeel AA, Sewairi WA, Boumah CE, Kambouris M, Mayouf SA, Sheth KV, Eid WA, Dowling O, Harris J, Glucksman MJ, Bahabri S, Meyer BF, Desnick RJ. Mutation of the matrix metalloproteinase 2 gene (MMP2) causes a multicentric osteolysis and arthritis syndrome. Nat Genet 2001;28:261-265.

84. Xie J, Wang C, Huang D, Zhang Y, Xu J, Kolesnikov SS, Sung KLP, Zhao H. TGF-beta1 induces the different expressions of lysyl oxidases and matrix metalloproteinases in anterior cruciate ligament and medial collateral ligament fibroblasts after mechanical injury. J Biomech 2013;46:890-898.

85. Ye S, Eriksson P, Hamsten A, Kurkinen M, Humphries SE, Henney AM. Progression of Coronary Atherosclerosis Is Associated with a Common Genetic Variant of the Human Stromelysin-1 Promoter Which Results in Reduced Gene Expression. Journal of Biological Chemistry 1996;271:13055-13060.

86. Nagase H, Woessner JF. Matrix Metalloproteinases. Journal of Biological Chemistry 1999;274:21491-21494.

87. Halade GV, Jin Y, Lindsey ML. Matrix Metalloproteinase (MMP)-9: A proximal biomarker for cardiac remodeling and a distal biomarker for inflammation. Pharmacol Ther .

88. zur Nieden NI, Kempka G, Ahr HJ. In vitro differentiation of embryonic stem cells into mineralized osteoblasts. Differentiation 2003;71:18-27.

89. George J, Kuboki Y, Miyata T. Differentiation of mesenchymal stem cells into osteoblasts on honeycomb collagen scaffolds. Biotechnol Bioeng 2006;95:404-411.

90. Zhu B, Lu Q, Yin J, Hu J, Wang Z. Alignment of osteoblast-like cells and cell-produced collagen matrix induced by nanogrooves. Tissue Eng 2005;11:825-834.

91. Alliston T, Choy L, Ducy P, Karsenty G, Derynck R. TGF-[beta]-induced repression of CBFA1 by Smad3 decreases cbfa1 and osteocalcin expression and inhibits osteoblast differentiation. EMBO J 2001;20:2254-2272.

92. Aparicio Bádenas C. Tratamientos de superficie sobre titanio comercialmente puro para la mejora de la osteointegración de los implantes dentales.

93. Wang D, Christensen K, Chawla K, Xiao G, Krebsbach PH, Franceschi RT. Isolation and Characterization of MC3T3-E1 Preosteoblast Subclones with Distinct In Vitro and In Vivo Differentiation/Mineralization Potential. Journal of Bone and Mineral Research 1999;14:893-903.

# 7. Further work

The use of TGF-β inhibitor peptides to functionalize a surface is a novel concept in the field of biomimetic surfaces since the general approach is to functionalize surfaces with bioactive molecules that act directly on cells to induce cell differentiation and thus, tissue regeneration. Functionalization with RGD containing peptides for improving cell adhesion, anchoring directly to the cell integrins, or with antibacterial molecules to kill bacteria or inhibit bacterial growth interacting with the cell membrane are also alternative approaches that have been thoroughly pursued. In contrast, TGF-β inhibitor peptides that are anchored to the surface will not act directly on the cell but indirectly through the external TGF-β molecules around the cell to inhibit its interaction with it. This approach opens a new perspective of research where a number of possibilities for improvement arise.

Additionally, during this thesis some new research perspectives have been elucidated, such as the fact that MP144 peptides induced differentiation of cells into the osteoblastic lineage, which will deserve special attention in future research work.

### *New methodology for anchoring short peptides to surfaces*

Our work on silanization and functionalization of titanium surfaces has been successful since we could demonstrate a good anchorage and a high amount of peptide on the surface. However, the APTES + Malonic acid route of attaching peptides to the surface through the amino groups of the peptide can be improved by alternatively using other silane molecule characterized by including a head carboxylate group instead of an amino group. This approach would potentially overcome several drawbacks that the APTES + Malonic acid route present:

- The functionalization process can be shorten by one step . If the silane on the surface already contains a carboxylic group it won't be necessary to add the malonic acid as a crosslinker to, subsequently, bind an amino group of the peptide.
- The possibility of the malonic acid of anchoring two amino groups of the APTES surfaces, staying unreactive and capping two amino groups for anchoring of other molecules would be avoided, improving the efficiency of the process.
- More active silane molecules on the surface would be available to react directly with the peptides. This is desired to increase the efficiency of the process as malonic acid cannot anchor to all APTES molecules available at the silanized surface.

The problem of the silanes which have a carboxylic acid as a terminal reacting group is that the carboxilates are able to react with the ethoxy and methoxy groups of the silane polymerizing the silane in solution and thus, hindering good surface coverage on silanization. A solution for this problem would be the use of a silane containing an acid anhydride (Figure 7-1) instead of a carboxylic acid as a terminal group.

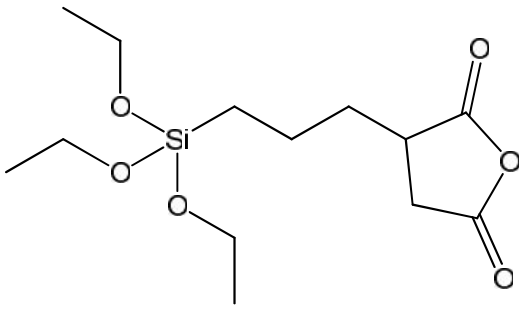


***Figure 7-1**: Structure of 3-(triethoxysilyl)propylsuccinic anhydride (TSP).*

The use of such silane would disable the polymerization of the silane when the silanization is done in dry conditions. After silanization, it is possible to open the anhydride ring by hydrolysing it, for example, immersing the silanized sample in water. The breakage of the anhydride ring will leave two carboxylic groups per each silane molecule, having, therefore, two anchorage groups (compared to one in APTES) per anchored silane molecule.

Activation of the carboxylic group by esterification would be still necessary to bind an amino group to this type of surface. This can be accomplished by adding to the water solution a water soluble coupling reagent such as dicyclohexylcarbodiimide (DCC), ethyl(dimethylaminopropyl) carbodiimide (EDC), N-Hydroxysuccinimide (NHS) or a mixture of them during the hydrolysis of the anhydride.

This approach will let a fast and reliable surface where it is possible to covalently attach primary amines and thiols just by dissolving them in water and immersing the surface in such a solution.

### *Effect of the TGF-β inhibitor peptides on the activity of osteoblasts*

P17 and P144 have been widely studied as to influence fibroblasts and cancer cell biological activity [1-7]. There are on-going studies of the effect of these two peptides on condroblasts. However no studies before our work here explored the effect of these two peptides on bone cell response and bone tissue regeneration.

The successful results of this thesis with P144 peptides to induce osteoprogenitor cells differentiation have been obtained with the peptides as functional coatings on titanium surfaces. However, there is lack of knowledge of the effect of the peptides in solution on the cell behaviour since the surface itself can play a big role on the cell response that can somehow mask the effects that are exclusively attributed to the P144 peptide.

It will be very interesting to elucidate more deeply what are the mechanisms of these peptides on the improvement of the osteoblastic differentiation as well as the extent of its effectiveness in doing so in solution, which we hypothesize that it will be more notable than attached to a surface.

### *In vivo studies of the new developed TGF-β inhibitory surfaces*

The next natural step on the development of a new bio-surface, after its successful physic-chemical and in vitro characterization, is to test the surface in vivo. Selection of an appropriate animal model is key and previous studies in our group to test other promising surfaces have proved that the use of pigs as animal model is a reliable model for assessing potential osseointegration benefits.

Currently, an in vivo experiment to study the effect of the titanium surfaces functionalized with the P144 peptide is being designed.

## 7.1. References

1. Santiago B, Gutierrez-Cañas I, Dotor J, Palao G, Lasarte JJ, Ruiz J, Prieto J, Borrás-Cuesta F, Pablos JL. Topical application of a peptide inhibitor of transforming growth factor-beta1 ameliorates bleomycin-induced skin fibrosis. J Invest Dermatol 2005;125:450-455.

2. Vicent S, Luis-Ravelo D, Antón I, García-Tuñón I, Borrás-Cuesta F, Dotor J, De Las Rivas J, Lecanda F. A novel lung cancer signature mediates metastatic bone colonization by a dual mechanism. Cancer Res 2008;68:2275-2285.

3. Ezquerro I, Lasarte J, Dotor J, Castilla-Cortázar I, Bustos M, Peñuelas I, Blanco G, Rodríguez C, Lechuga MdCG, Greenwel P, Rojkind M, Prieto J, Borrás-Cuesta F. A synthetic peptide from transforming growth factor [beta] type III receptor inhibits liver fibrogenesis in rats with carbon tetrachloride liver injury. Cytokine 2003;22:12-20.

4. Hermida N, López B, González A, Dotor J, Lasarte JJ, Sarobe P, Borrás-Cuesta F, Díez J. A synthetic peptide from transforming growth factor-β1 type III receptor prevents myocardial fibrosis in spontaneously hypertensive rats. Cardiovascular Research 2009;81:601-609.

5. Dotor J, López-Vázquez AB, Lasarte JJ, Sarobe P, García-Granero M, Riezu-Boj J, Martínez A, Feijoó E, López-Sagaseta J, Hermida J, Prieto J, Borrás-Cuesta F. Identification of peptide inhibitors of transforming growth factor beta 1 using a phage-displayed peptide library. Cytokine 2007;39:106-115.

6. Gil-Guerrero L, Dotor J, Huibregtse IL, Casares N, López-Vázquez AB, Rudilla F, Riezu-Boj JI, López-Sagaseta J, Hermida J, Van Deventer S, Bezunartea J, Llopiz D, Sarobe P, Prieto J, Borrás-Cuesta F, Lasarte JJ. In Vitro and In Vivo Down-Regulation of Regulatory T Cell Activity with a Peptide Inhibitor of TGF-β1. The Journal of Immunology 2008;181:126-135.

7. Arribillaga L, Dotor J, Basagoiti M, Riezu-Boj JI, Borrás-Cuesta F, Lasarte JJ, Sarobe P, Cornet ME, Feijoó E. Therapeutic effect of a peptide inhibitor of TGF-β on pulmonary fibrosis. Cytokine 2011;53:327-333.

# Annex A: Description of the characterization techniques

## CONTENTS

# Topography

## White Light Interferometry

White light interferometry (LIM) has been used for many years as a reliable non-contact optical profiling system for measuring step heights and surface roughness in many precision engineering applications. Recent developments in both instrumentation and in measurement software for this technique have increased the vertical (i.e. height) resolution of these instruments to give a capability better than 0,01 nm (i.e. 0,1 Angstrom). The ultimate lateral resolution is limited to around 0,35 µm [1].

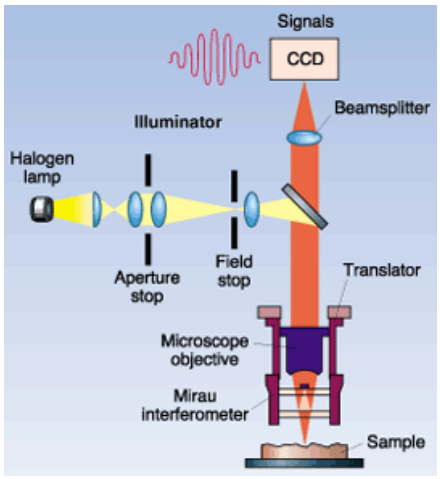


**Figure A-1:** Graphical schematic diagram of an interference microscope [2].

Several amplitude, spacing and hybrid roughness parameters exist to describe surface topography [3-5]. In this study, the following parameters to describe the surface have been used: Ra, Rq, Rt and Surface index;

- Ra (Arithmetic average roughness): Arithmetic average of the absolute values of all points of the profile.

$$R_a = \frac{1}{n}\sum_{i=1}^{n}|y_i| \qquad \textbf{Equation A-1}$$

- Rq (Root mean square): Is a statistical measure of the magnitude of the variation of the highness of the peaks. It is more sensitive to the variation of the peaks than Ra.

- $R_q = \sqrt{\frac{1}{n}\sum_{i=1}^{n} {y_i}^2}$ **Equation A-2**

- Rt (Maximum Height of the Profile): The difference in height between the peak of maximum value and the valley of maximum depth.

## Spectroscopic ellipsometry

### Ellipsometry

Ellipsometry is an optical technique for the investigation of the dielectric properties (complex refractive index or dielectric function) of thin films [6].

It has applications in many different fields, from semiconductor physics to microelectronics and biology, from basic research to industrial applications. Ellipsometry is a very sensitive measurement technique and provides unequalled capabilities for thin film metrology. As an optical technique, spectroscopic ellipsometry is non-destructive and contactless.

Upon the analysis of the change of polarization of light, which is reflected off a sample, ellipsometry can yield information about layers that are thinner than the wavelength of the probing light itself, even down to a single atomic layer. Ellipsometry can probe the complex refractive index or dielectric function tensor, which gives access to fundamental physical parameters and is related to a variety of sample properties, including morphology, crystal quality, chemical composition, or electrical conductivity. It is commonly used to characterize film thickness for single layers or complex multilayer stacks ranging from a few angstroms or tenths of a nanometer to several micrometers with an excellent accuracy.

The name "ellipsometry" stems from the fact that light reflected at angle from a sample has Elliptical polarization. The technique has been known since 1888 [7], and has many applications today.

## Spectroscopic ellipsometry

Single-wavelength ellipsometry employs a monochromatic light source. This is usually a laser in the visible spectral region, for instance, a HeNe laser with a wavelength of 632.8 nm. Therefore, single-wavelength ellipsometry is also called laser ellipsometry. The advantage of laser ellipsometry is that laser beams can be focused on a small spot size. Furthermore, lasers have a higher power than broad band light sources. Therefore, laser ellipsometry can be used for imaging (see below). However, the experimental output is restricted to one set of $\Psi$ and $\Delta$ values per measurement. Spectroscopic ellipsometry (SE) employs broad band light sources, which cover a certain spectral range in the infrared, visible or ultraviolet spectral region. By that the complex refractive index or the dielectric function tensor in the corresponding spectral region can be obtained, which gives access to a large number of fundamental physical properties. Infrared spectroscopic ellipsometry (IRSE) can probe lattice vibrational (phonon) and free charge carrier (plasmon) properties. Spectroscopic ellipsometry in the near infrared, visible up to ultraviolet spectral region studies the refractive index in the transparency or below-band-gap region and electronic properties, for instance, band-to-band transitions or excitons.

## Principles of Ellipsometry

### *Experimental setup*

Electromagnetic radiation is emitted by a light source and linearly polarized by a polarizer. It can pass through an optional compensator (retarder, quarter wave plate) and falls onto the

sample. After reflection the radiation passes a compensator (optional) and a second polarizer, which is called an analyzer, and falls into the detector. Instead of the compensators some ellipsometers use a phase-modulator in the path of the incident light beam. Ellipsometry is a specular optical technique (the angle of incidence equals the angle of reflection). The incident and the reflected beam span the *plane of incidence*. Light which is polarized parallel to this plane is named *p-polarized* (p-polarised). A polarization direction perpendicular is called *s-polarized* (s-polarised), accordingly. The *"s"* is contributed from the German *"senkrecht"* (perpendicular).

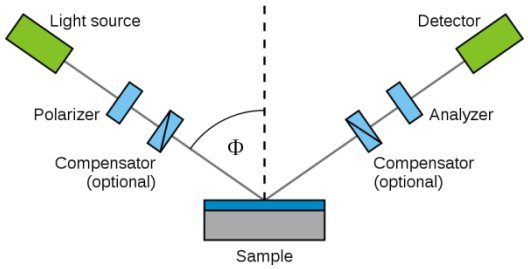


***Figure A-2:*** *Experimental setup of an ellipsometry experiment [8]*

*Materials*

Two values are used to describe the optical properties which determine how light interacts with a material. They are generally represented as a complex number. The complex refractive index (ñ) consists on the refractive index (*n*) and extinction coefficient (*k*):

$$\tilde{n} = n + ik \qquad \textbf{Equation A-3}$$

Alternatively, the optical properties can be represented as the complex dielectric function:

$$\tilde{\varepsilon} = \varepsilon_1 + i\varepsilon_2 \qquad \textbf{Equation A-4}$$

with the following relation between conventions:

$$\tilde{\varepsilon} = \tilde{n}^2 \qquad \textbf{Equation A-5}$$

The index describes the phase velocity of light as it travels in a material compared to the speed of light in vacuum, *c*:

$$v = \frac{c}{n} \qquad \textbf{Equation A-6}$$

Light slows as it enters a material with higher index. Because the frequency of light waves remains constant, the wavelength will shorten. The extinction coefficient describes the loss of wave energy to the material. It is related to the absorption coefficient, $\alpha$, as:

$$\alpha = \frac{4\pi k}{\lambda} \qquad \textbf{Equation A-7}$$

Light loses intensity in an absorbing material according to Beer's Law:

$$I(z) = I(0)e^{-i\omega t} \qquad \textbf{Equation A-8}$$

Thus, the extinction coefficient relates how quickly light vanishes in a material. These concepts are demonstrated in Figure A-3 where a light wave travels through two different materials of varying properties before returning to the ambient.

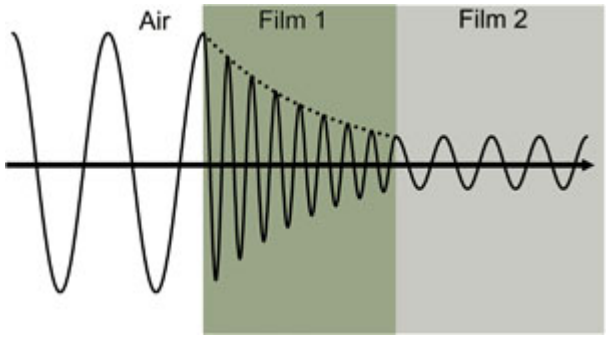


***Figure A-3:*** *Wave travels from air into absorbing Film 1 and then transparent Film 2. The phase velocity and wavelength change in each material depending on index of refraction (Film 1: n=4, Film 2: n=2).*

The optical constants for $TiO_2$ from the ultraviolet (UV) to the infrared (IR), as shown in. The optical constants are determined by wavelength with absorption (k>0) occurring in both UV and IR due to different mechanisms that take energy from the light wave. IR absorption is commonly caused by molecular vibration, phonon vibration, or free-carriers. UV absorption

is generally due to electronic transitions, where light provides energy to excite an electron to an elevated state. A closer look at the optical constants in Figure A-4 shows that real and imaginary optical constants are not independent. Their shapes are mathematically coupled through Kramers-Kronig consistency.

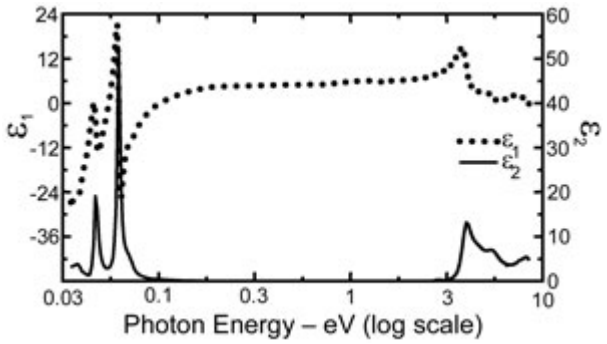


***Figure A-4:*** *Complex dielectric function for TiO2 film covering wavelengths from the infared (small eV) to the ultraviolet (high eV).*

## Interactions between light and materials

Maxwell's equations must remain satisfied when light interacts with a material, which leads to boundary conditions at the interface. Incident light will reflect and refract at the interface, as shown in figure A-2. The angle between the incident ray and sample normal (*fi*) will be equal to the reflected angle, (*fr*). Light entering the material is refracted at an angle (*ft*) given by:

$$n_0 \sin \phi_i = n_1 \sin \phi_t \qquad \textbf{Equation A-9}$$

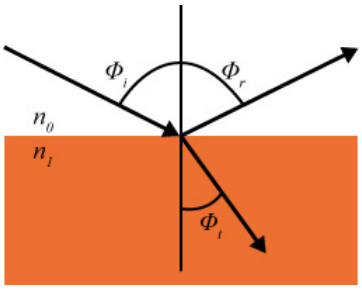


***Figure A-5**: Light reflects and refracts according to Snell's law [6]*

The same occurs at each interface where a portion of light reflects and the remainder transmits at the refracted angle. This is illustrated in Figure A-5. The boundary conditions provide different solutions for electric fields parallel and perpendicular to the sample surface. Therefore, light can be separated into orthogonal components with relation to the plane of incidence. Electric fields parallel and perpendicular to the plane of incidence are considered *p*- and *s*- polarized, respectively. These two components are independent and can be calculated separately. Fresnel described the amount of light reflected and transmitted at an interface between materials:

$$r_s = \left(\frac{E_{0r}}{E_{0i}}\right)_s = \frac{n_i \cos(\phi_i) - n_t \cos(\phi_t)}{n_i \cos(\phi_i) + n_t \cos(\phi_t)} \qquad \textbf{Equation A-10}$$

$$r_p = \left(\frac{E_{0r}}{E_{0i}}\right)_p = \frac{n_t \cos(\phi_i) - n_i \cos(\phi_t)}{n_i \cos(\phi_t) + n_t \cos(\phi_i)} \qquad \textbf{Equation A-11}$$

$$t_s = \left(\frac{E_{0t}}{E_{0i}}\right)_s = \frac{2n_i \cos(\phi_i)}{n_i \cos(\phi_i) + n_t \cos(\phi_t)} \qquad \textbf{Equation A-12}$$

$$t_p = \left(\frac{E_{0t}}{E_{0i}}\right)_p = \frac{2n_i \cos(\phi_i)}{n_i \cos(\phi_i) + n_t \cos(\phi_t)} \qquad \textbf{Equation A-13}$$

Thin film and multilayer structures involve multiple interfaces, with Fresnel reflection and transmission coefficients applicable at each. It is important to track the relative phase of each light component to determine correctly the overall reflected or transmitted beam. For this purpose, we define the film phase thickness as:

$$\beta = 2\pi \left(\frac{t_1}{\lambda}\right) n_1 \cos(\phi_1) \qquad \textbf{Equation A-14}$$

The superposition of multiple light waves introduces interference that depends on the relative phase of each light wave. Figure A-6 illustrates the combination of light waves in the reflected beam and their corresponding Fresnel calculations.

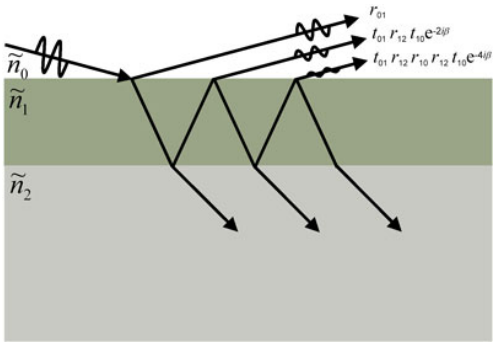


***Figure A-6:*** *Light reflects and refracts at each interface, which leads to multiple beams in a thin film. Interference between beams depends on relative phase and amplitude of the electric fields. Fresnel reflection and transmission coefficients can be used to calculate the response from each contributing beam [6]*

## Film thickness calculation

The development for the calculation of film thickness by ellipsometry was developed by Mario Ghezzo in 1967 [9]. Here, the development of the equations is presented.

Brewster's angle for the air-film interface, $\phi_0$, is

$$\tan \phi_0 = \frac{n_1}{n_0} \qquad \textbf{Equation A-15}$$

where $n_o$ and $n_1$, are the indices of refraction of air and the film, respectively. As $n_1$ is larger than $n_o$, $\phi_0$ must be more than 45° and, therefore, for example, an ellipsometer can be set at such an angle of incidence without mechanical interference between the collimator and telescope arms.

The combination of Snell's law

$$n_0 \sin \phi_0 = n_1 \sin \phi_1 \qquad \textbf{Equation A-16}$$

with Equation A-15 yields the important relations

$$\sin \phi_1 = \cos \phi_0 \qquad \textbf{Equation A-17}$$

$$\cos \phi_1 = \sin \phi_0 \qquad \textbf{Equation A-18}$$

Application of Equation A-15 and equation **A-17** to the expressions for the reflection coefficients for the air-film interface rs and rp (Equation A-10 and Equation **A-11**, respectively) allows for their calculation at Brewster's angle $\phi_0$. Results are

$$r_{p_{(0,1)}} = 0 \qquad \textbf{Equation A-19}$$

$$r_{s_{(0,1)}} = cos2\phi_0 \qquad \textbf{Equation A-20}$$

It is interesting to observe that, because $\phi_0$ is larger than 45º and less than 90°, $cos2\phi_0$ must be negative and $r_s$ can be expressed by

$$r_{s_{(0,1)}} = -cos2\phi_0 \qquad \textbf{Equation A-21}$$

The values of $r_{p_{(0,1)}}$ and $r_{s_{(0,1)}}$, given by Equation A-19 and Equation **A-20**, are then inserted in the expressions for the total reflection coefficients, which become

$$r_p = \frac{r_{p_{(0,1)}} + r_{p_{(1,2)}e^{-2i\delta}}}{1 + r_{p_{(0,1)}} r_{p_{(1,2)}e^{-2i\delta}}} = r_{p_{(1,2)}} \qquad \textbf{Equation A-22}$$

$$r_s = \frac{r_{s_{(0,1)}} + r_{s_{(1,2)}e^{-2i\delta}}}{1 + r_{s_{(0,1)}} r_{s_{(1,2)}e^{-2i\delta}}} = \frac{-|cos2\phi_0| + r_{s_{(1,2}}}{1 - |cos2\phi_0| r_{s_{(1,2}}} \qquad \textbf{Equation A-23}$$

where $r_{p_{(1,2)}}$ and $r_{s_{(1,2)}}$ are the reflection coefficients for the film-substrate interface and $2\delta$ is the phase shift of the light beam in traversing the film. As the substrate is generally absorbing, $r_{p_{(1,2)}}$ and $r_{s_{(1,2)}}$ are complex numbers, expressed by the relations

$$r_{p_{(1,2)}} = \frac{n_2 \cos(\phi_1) - n_1 \cos(\phi_2)}{n_2 \cos(\phi_1) + n_1 \cos(\phi_2)} \quad \textbf{Equation A-24}$$

$$r_{s_{(1,2)}} = \frac{n_1 \cos(\phi_1) - n_2 \cos(\phi_2)}{n_1 \cos(\phi_1) + n_2 \cos(\phi_2)} \quad \textbf{Equation A-25}$$

where $n_2$ and $\phi_2$ are, respectively, the refractive index and the complex angle of refraction of the substrate. Because the film is assumed to be transparent, $\Delta$ is real and is expressed by the relation

$$\delta(deg) = \left(\frac{360}{\lambda}\right) n_1 \cos\phi_1 d \quad \textbf{Equation A-26}$$

Where d is the thickness of the film and $\lambda$ is the wavelength of the light in vacuum. Introduction into Equation A-22 and Equation **A-23** of the expressions for $r_{p_{(1,2)}}$ and $r_{s_{(1,2)}}$ in polar form

$$r_{p_{(1,2)}} = \left|r_{p_{(1,2)}}\right| e^{i\, arg\left(r_{p_{(1,2)}}\right.} \quad \textbf{Equation A-27}$$

$$r_{s_{(1,2)}} = \left|r_{s_{(1,2)}}\right| e^{i\, arg\left(r_{s_{(1,2)}}\right.} \quad \textbf{Equation A-28}$$

results in the following relations

$$r_p = \left|r_{p_{(1,2)}}\right| e^{i\, arg\left(r_{p_{(1,2)}}\right) - i} \quad \textbf{Equation A-29}$$

$$r_s = \frac{-|cos2\phi_0| + \left|r_{s_{(1,2)}}\right| e^{i\, arg\left(r_{s_{(1,2)}}\right) - 2\delta}}{1 - |cos2\phi_0| \left|r_{s_{(1,2)}}\right| e^{i\, arg\left(r_{s_{(1,2)}}\right)}} \quad \textbf{Equation A-30}$$

where all of the angles are expressed in degrees, by convention. The definitions of the quantities

$$\gamma = 2\delta - arg\left(r_{s_{(1,2)}}\right) \qquad \textbf{Equation A-31}$$

$$\alpha = arg\left(r_{p_{(1,2)}}\right) - arg\left(r_{s_{(1} \qquad \textbf{Equation A-32}$$

permit writing Equation A-29 and Equation A-30 in the form

$$r_{p=}\left|r_{p_{(1,2)}}\right| e^{i(\alpha-\gamma)} \qquad \textbf{Equation A-33}$$

$$r_s = \frac{-|cos2\phi_0|+\left|r_{s_{(1,2)}}\right|^{e^{(-i\gamma)}}}{1-|cos2\phi_0|\left|r_{s_{(1,2)}}\right|^{e^{(-i\gamma)}}} \qquad \textbf{Equation A-34}$$

Use of Equation A-33 and Equation A-34 in connection with the fundamental ellipsometric equation

$$\rho = \frac{r_p}{r_s} = \tan(\Psi)e^{i\Delta} \qquad \textbf{Equation A-35}$$

where $\Psi$ and $\delta$ are quantities easily evaluated from the ellipsometric measurements, yields the formula

$$\tan(\Psi)e^{i\Delta} = \frac{\left|r_{p_{(1,2)}}\right|^{e^{i(\alpha-\gamma)}}}{\frac{-|cos2\phi_0|+\left|r_{s_{(1,2)}}\right|^{e^{(-}}}{1-|cos2\phi_0|\left|r_{s_{(1,2)}}\right|^{e^{(-i\gamma)}}}} \qquad \textbf{Equation A-36}$$

The definition of the angle β

$$\beta = \Delta - \alpha \qquad \textbf{Equation A-37}$$

allows writing Equation A-36

$$\tan(\Psi)e^{i\beta} = \frac{\left|r_{p_{(1,2)}}\right|e^{(-i\gamma)}}{\frac{-|cos2\phi_0|+\left|r_{s_{(1,2)}}\right|e^{(}}{1-|cos2\phi_0|\left|r_{s_{(1,2)}}\right|e^{(-i\gamma)}}} \qquad \textbf{Equation A-38}$$

By equating the squares of the moduli of both members of Equation A-38 we can derive the following equation

$$tan^2\ \Psi = \frac{\left|r_{p_{(1,2)}}\right|^2}{\frac{\left|r_{p_{(1,2)}}\right|^2 + |cos2\phi_0|^2 - 2\left|r_{s_{(1,2)}}\right||cos2\phi_0|\,c}{1+|cos2\phi_0|^2\left|r_{s_{(1,2)}}\right|^2 - 2\left|r_{s_{(1,2)}}\right||cos2\phi_0|\cos\gamma}} \qquad \textbf{Equation A-39}$$

A simple rearrangement of the terms in the above equation yields this expression for cos $\gamma$

$$\cos\gamma = \frac{|cos2\phi_0|^2 + \left|r_{s_{(1,2)}}\right|^2}{2|cos2\phi_0|\left|r_{s_{(1,2)}}\right|} \times \left( \frac{tan^2\ \Psi - \left|r_{p_{(1,2)}}\right|^2 \left( \frac{1+\left|r_{s_{(1,2)}}\right|^2 |cos2\phi_0|^2}{|cos2\phi_0|^2 + \left|r_{s_{(1,2)}}\right|^2} \right)}{tan^2\ \Psi + \left|r_{p_{(1,2)}}\right|^2} \right) \qquad \textbf{Equation A-40}$$

The right-hand member of Equation A-40 is called "a" and it can be calculated from the value of $\Psi$ when $n_o$, $n_1$, and $n_2$ are known and $\phi_0$ has been set at Brewster's angle for the air-film interface. The thickness of the film, d, appears in Equation A-40 only through $\gamma$ and, therefore, the determination of $\gamma$ provides also the determination of d by means of Equation A-31 and Equation A-26.

# Wettability

## Contact angle goniometry

Wettability or wetting is the actual process when a liquid spreads on a solid substrate. The wettability of a solid with a liquid is usually determined from their contact angle, CA, or wetting angle. The shape of a liquid front in contact with a solid substrate can be explained by the relative strength of the cohesive (Liquid/Liquid) and adhesive (Solid/Liquid) and is determined

by the interfacial forces of the participating phases (Figure A-7). The possible interfaces can be summarized in terms of the three states of matter solid, liquid and vapor as follows:

· Vapor/liquid

· Vapor/solid

· Liquid/solid

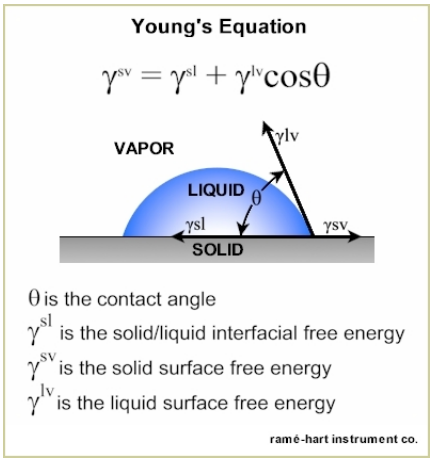


***Figure A-7:*** *Different interfaces between a liquid drop and a solid surface [10].*

Strong adhesion with weak cohesion produces very low contact angles with nearly complete wetting. As the solid/liquid interactions weaken, wetting diminishes and contact angle increases. Wetting (hydrophilic) or non-wetting (hydrophobic) of a solid by water is a qualitative criterion since all surfaces of condensed-phase materials attract water molecules to a considerable degree [11]. As shown on Figure A-8, an elevated contact angle defines a hydrophobic drop while a low value is considered a hydrophilic drop.

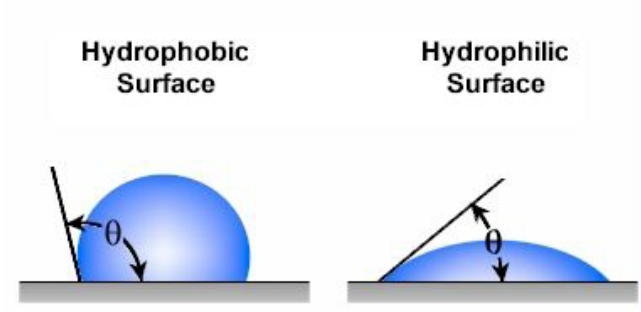


***Figure A-8:*** *Hydrophobic and a hydrophilic drop with its respective contact angle. [10].*

The hydrophilicity of a surface is related to its affinity to water [12] and by extension to its capability to form hydrogen bonds and, indirectly, the amount of $OH^-$ groups on the surface. Some authors [13] suggested defining the hydrophobicity as a repulsive force between non-polar molecules and water, also called the hydrophobic effect.

# Chemical composition

## X-Ray Photoelectron Spectroscopy (XPS)

X-ray photoelectron spectroscopy (XPS or ESCA) is a surface analytical technique based on the phenomena of photoelectric effect, by which Albert Einstein received the Nobel Prize in 1921. XPS was developed in the mid 1960s by K. Siegbahn and his research group. K. Siegbahn was awarded the Nobel Prize for Physics in 1981 for his work in XPS.

In XPS, the sample is irradiated with low-energy (~1.5 keV) X-rays, in order to provoke the photoelectric effect. The energy spectrum of the emitted photoelectrons is determined by means of a high-resolution electron spectrometer.

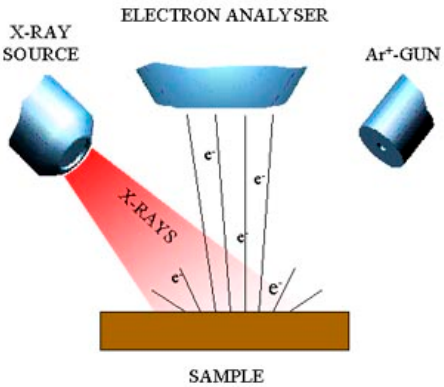


**Figure A-9:** Principle of XPS [14]

The photoemision process is extremely fast, $10^{-16}$ s, and its basic physics is described by means of Einstein's equation:

$$E_B = h\nu - KE \qquad \textbf{Equation A-41}$$

Where $E_B$ is the binding energy of the electron in the atom, $hv$ is the X-ray energy of the source and KE is the kinetic energy of the displaced electron which is measured by the XPS spectrometer. With the Equation A-41 it is possible to know the binding energies of the electrons pullet out from the surface. A negatively charged electron is bound to the atom by attraction with its positive nucleus. The internal energy levels of the atom are more energetic than the external. The binding energy of an electron will vary depending on the atom type, the energy level, and the atoms which will be combined with (which can alter the electronic distribution)

The sample analysis is conducted in a vacuum chamber, under the best vacuum conditions achievable, typically ~$10^{-10}$ torr. This facilitates the transmission of the photoelectrons to the analyzer but more importantly minimizes the re-contamination rate of a freshly cleaned sample [15].

XPS is used to determine quantitative atomic composition and chemistry. It is a surface analysis technique with a sampling volume that extends from the surface to a depth of approximately 50-70 Angstroms. Alternatively, XPS can be utilized for sputter depth profiling to characterize thin films by quantifying matrix-level elements as a function of depth. XPS is an elemental analysis technique that is unique in providing chemical state information of the detected elements, such as distinguishing between sulfate and sulfide forms of the element sulfur. The process works by irradiating a sample with monochromatic x-rays, resulting in the emission of photoelectrons whose energies are characteristic of the elements within the sampling volume [16].

## Fourier Transform Infrared Spectroscopy (FTIR)

FTIR (Fourier Transform Infrared) Spectroscopy, or simply FTIR Analysis, is an analysis technique that provides information about the chemical bonding or molecular structure of materials, whether organic or inorganic.

The technique works on the fact that bonds and groups of bonds vibrate at characteristic frequencies. A molecule that is exposed to infrared rays absorbs infrared energy at frequencies which are characteristic to that molecule.

During FTIR analysis, a spot on the specimen is subjected to a modulated IR beam. The specimen's transmittance and reflectance of the infrared rays at different frequencies is translated into an IR absorption plot consisting of reverse peaks. The resulting FTIR spectral pattern is then analyzed and matched with known signatures of identified materials in the FTIR library [17].

In infrared spectroscopy, IR radiation is passed through a sample. Some of the infrared radiation is absorbed by the sample and some of it is passed through (transmitted) or reflected. The resulting spectrum represents the molecular absorption and transmission/reflection, creating a molecular fingerprint of the sample. Like a fingerprint no two unique molecular structures produce the same infrared spectrum. This makes infrared spectroscopy useful for several types of analysis.

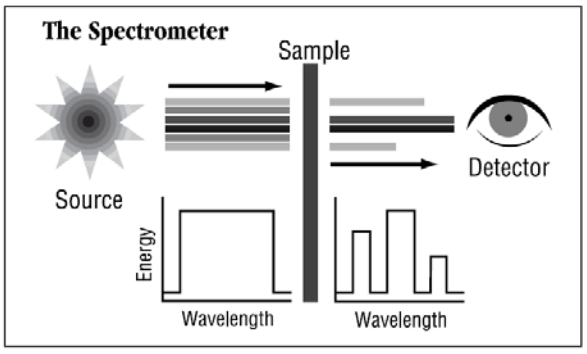


**Figure A-10:** Principle of infrared spectroscopy [18].

Figure A-10 shows a scheme of the principle of FTIR on an IR transparent sample. Samples that are opaque to IR radiation can be, also, analysed by FTIR if they are able to reflect the IR beam. To analyse the IR opaque sample several variations of the original FTIR spectroscopy have been developed. Next, a summary of these variations is shown:

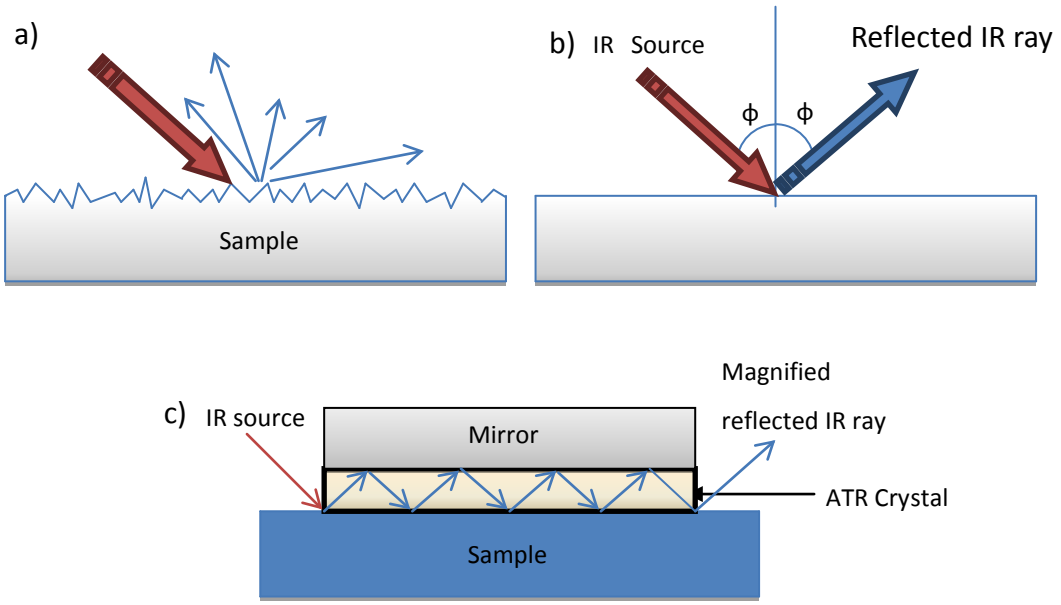


***Figure A-11:*** *FTIR reflection techniques. a) Difusse reflectance, b) Specular reflection, a) Attenuated Total Reflection (ATR)*

When incident light strikes a surface, the light that penetrates is reflected in all directions and this is called Diffuse Reflectance. As the light that leaves the surface has passed through a thin layer of the reflecting material, its wavelength content will have been modified by the optical properties of the matrix. Consequently, the wavelength and intensity distribution of the reflected light will contain structural information on the substrate. It is especially effective on rough surfaces where other techniques cannot be applied [19].

Light that reflects back at the same angle as the angle of incidence is known as "specular reflection light." The FTIR method that exploits specular reflection light is called the "specular reflection method." When using the specular reflection method, the sample can be irradiated with infrared light from an almost vertical angle of incidence or an almost horizontal angle of incidence. A specular reflection accessory that irradiates the sample with infrared light from an almost vertical angle is used to measure the infrared spectra of comparatively thick, μm-order, metal coatings or to measure the film thickness on epitaxial wafers using interference fringes [20].

ATR uses a property of total internal reflection resulting in an evanescent wave. A beam of infrared light is passed through the ATR crystal in such a way that it reflects at least once off

the internal surface in contact with the sample. This reflection forms the evanescent wave which extends into the sample. The penetration depth into the sample is typically between 0.5 and 2 micrometers, with the exact value being determined by the wavelength of light, the angle of incidence and the indices of refraction for the ATR crystal and the medium being probed [21]. The number of reflections may be varied by varying the angle of incidence. The beam is then collected by a detector as it exits the crystal. Most modern infrared spectrometers can be converted to characterize samples via ATR by mounting the ATR accessory in the spectrometer's sample compartment. The accessibility of ATR-FTIR has led to substantial use by the scientific community. Typical materials for ATR crystals include germanium and zinc selenide, while silicon is ideal for use in the Far-IR region of the electromagnetic spectrum. The excellent mechanical properties of diamond make it an ideal material for ATR, particularly when studying very hard solids, but its much higher cost means it is less widely used.

## Time of Flight Secondary Ion Mass Spectroscopy (ToF SIMS)

Time-of-Flight Ion Mass spectroscopy lets to determine and identify different organic species on the surface of a simple. This technique is very versatile since a smooth surface is not needed to obtain a reliable result.

ToF SIMS is based on the ion sputtering phenomena. The target particles are bombed by ions, atoms, or molecules. Depending on the range of energy of the source beam, elastic and inelastic collisions may occur:

- Within the range of keV, the dominant interactions are the elastic ones.
- The inelastic collisions increase when the energy increases. Inelastic collisions are more common in the range of MeV.

The dispersion process produces secondary ions in the range of the kinetic translational energies. The energy distributions are different for atomic ions and molecular ions. The ionization efficiency of SIMS is defined by the fraction of the ionized atoms. The efficiency

varies with respect to the element of analysis in several magnitude scales. Other parameters that have influence on the efficiency are the ionization potential and the electronic affinity of the negative ions [22].

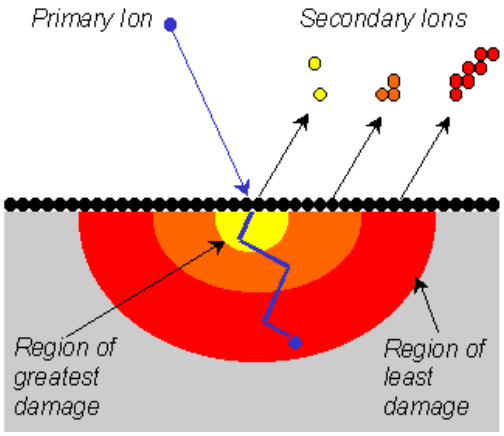


**Figure A-12:** Schematic diagram of the SIMS process [23]

The mass of the secondary ions is detected by means of the time of flight that passes from the collision of the ion beam on the surface to the moment that secondary ion gets the detector. Because of this fact, the technique gets the name of ToF SIMS (Time of Flight Secondary Ion Mass Spectroscopy).

# Surface charge

## ζ Potential

According to Stern's model [24], if charged surfaces are contacted with polyelectrolyte solution, the charge is balanced by counter ions (Figure A-13). The layer of the counter ion adsorbed on the surface is called Stern layer and the remainder of the counter ions are distributed in the diffuse layer. In case of negatively charged surface, the electric potential on the surface is the highest and it decreases rapidly until the Stern Plane due to the adsorbed positive ions. Outside the Stern Plane, the magnitude of potential decreases slowly.

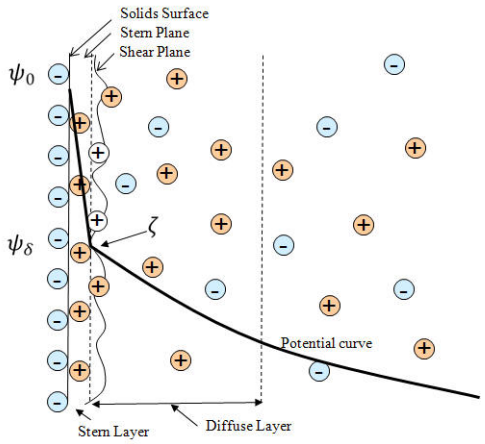


**Figure A-13:** Electric double layer according to Stern's model (after Shaw, 1969) [25]

The magnitude of the zeta potential gives an indication of the potential stability of the colloidal system. A colloidal system is when one of the three states of matter: gas, liquid and solid, are finely dispersed in one of the others. For this technique we are interested in the two states of: a solid dispersed in a liquid, and a liquid dispersed in a liquid, i.e. an emulsion [26].

If all the particles in suspension have a large negative or positive zeta potential then they will tend to repel each other and there is no tendency to flocculate. However, if the particles have low zeta potential values then there is no force to prevent the particles coming together and flocculating.

The most important factor that affects ζ potential is pH. A zeta potential value on its own without a quoted pH is a virtually meaningless number. Therefore, the measurement of the ζ potential is usually performed in a titration basis, obtaining the ζ potential for each value of pH in a range (figure A-14).

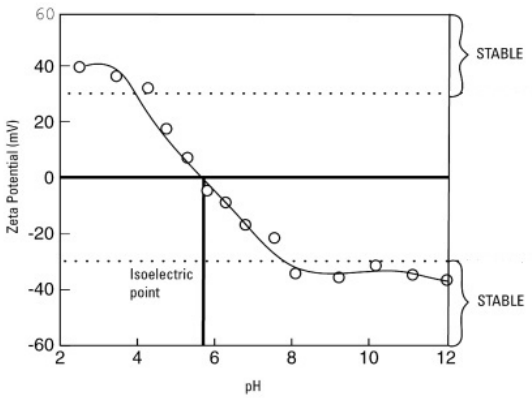


**Figure 0-14:** Titration of the ζ potential of a hypothetical sample [27].

## Iso-electric point

The formation of the electrochemical double layer depends on the characteristics of the electrolyte solution and, among other properties, its pH. The iso-electric point is an important quantity that may be determined from the pH dependence of zeta potential.

The isoelectric point, IEP, corresponds to the pH where zeta-potential becomes zero (z=0); i.e. the pH at which the net charge is zero as it is shown in figure Figure 0-14 [1].

## Electrokinetic effects

An important consequence of the existence of electrical charges on the surface of particles is that they will exhibit certain effects under the influence of an applied electric field. These effects are collectively defined as electrokinetic effects. There are four distinct effects depending on the way in which the motion is induced [28]. These are:

***Electrophoresis*** **:** The movement of a charged particle relative to the liquid it is suspended in under the influence of an applied electric field.

***Electroosmosis*:** The movement of a liquid relative to a stationary charged surface under the influence of an electric field.

***Streaming potential:*** The electric field generated when a liquid is forced to flow past a stationary charged surface.

***Sedimentation potential:*** The electric field generated when charged particles move relative to a stationary liquid.

The streaming potential method is the most convenient method for determining the zeta potential of macroscopic solid surfaces owing to its versatility that allows working with planar surfaces [1].

The streaming potential of surface is measured based on the voltage developed along the charged surface while electrolyte solution is flowing. Depending on the electric potential in Stern plane, the delay of counter ions varies and as a result varying degree of potential differences develop between upstream and downstream. Since the counter ion density near Stern Plane is affected by the flow velocity, the Stern potential is always affected by the experimental condition and cannot be measured accurately. Therefore, electrokinetic zeta potential is measured instead, which represents the potential in shear plane of which thickness is affected by the hydrodynamic conditions of experiment [29-31].

# Molecule quantification

## Spectrofluorophotometry

Spectrofluorophotometry (also called fluorometry or spectrofluorimetry) is an electromagnetic type of spectroscopy that analyzes the fluorescence of a sample. It involves using a beam of light, typically ultraviolet light, which excites electrons from molecules of certain compounds and causes them to emit light of lower energy, usually visible light (but not necessarily).

The molecules have different states or energy levels. Fluorescence Spectrometry refers mainly to vibrational and electronic states. In general, the species under consideration have a baseline electronic state (a state of low energy) of interest, and an excited electronic state of higher energy. Within each of these electronic states are different vibrational states.

In fluorescence spectroscopy, the sample is first excited by absorbing a photon of light, from baseline to one electronic state of the different vibrational states of the excited electronic state. Collisions with other molecules cause the excited molecule loses vibrational energy until it reaches the lowest vibrational state of the excited electronic state.

The molecule then drops back to one of several vibrational levels of basal electronic state, emitting a photon in the process. As the molecules can fall to any of the different levels of vibration in the basal state, the emitted photons have different energies and therefore, frequencies. Thus, by analyzing the different frequencies of light emitted by fluorescence spectroscopy, together with their relative intensities, can determine the structure of different levels of vibration.

In a typical experiment, different frequencies are measured fluorescent light emitted by a sample, maintaining the excitation light at a constant wavelength. This is called the emission spectrum. An excitation spectrum was measured by recording a series of emission spectra using light of different wavelengths.

## Instruments

In fluorescence spectrometry using two general types of instruments:

- Fluorometers filter. Filters used to isolate the incident light and fluorescent light.
- Spectrofluorometers. Using diffraction grating monochromators for isolating the incident light and fluorescent light.

Both types of instruments use the following scheme. The light from an excitation source passes through a filter or monochromator, and impinges on the sample. A portion of incident light is absorbed by the sample, and some of the sample molecules produce fluorescence. The fluorescent light is emitted in all directions. Part of this fluorescent light passes through a second filter or a monochromator and reaches the detector, which very often is 90° to the incident light beam to minimize the risk of incident light reflected or transmitted reaches the detector.

Various light sources can be used as excitation sources, including lasers, photodiodes and lamps, xenon arc lamps and mercury vapor. A laser emits light only high irradiance in a very narrow range of wavelengths, typically at 0.01 nm, which makes unnecessary the excitation monochromator or filter. The disadvantage of this method is that the wavelength of a laser cannot be changed much. A mercury vapor lamp is a linear lamp, which means that emits light near the peak wavelength. By contrast, a xenon arc has a continuous emission spectrum with almost constant intensity in the range of 300-800 nm, and an irradiance measurements sufficient to just above 200 nm.

Fluorometers can be used in filters and / or monochromators. A monochromator transmits light of a wavelength and adjustable tolerance. The most common type of monochromator using a diffraction grating, ie, the collimated light enters and exits a grating with a different angle depending on the wavelength. The monochromator can then select which transmits wavelengths. To enable measurements of anisotropy adds two polarizing filters, one after the excitation monochromator or filter, and another before the emission monochromator or filter.

As mentioned above, the fluorescence is measured more often at an angle of 90° relative to the excitation light. This geometry is used instead of placing the sensor in the line of the excitation light at an angle of 180° to avoid interference of the excitation light transmitted. The monochromator is not perfect and transmit light with wavelengths other than those set. A monochromator ideal only transmits light in the specified range and has an independent transmission wavelength. When measuring at an angle of 90°, only the light scattered by the sample causes light. This results in a better signal to noise ratio and reduces the detection limit

by a factor of about 10,000, compared with the geometry of 180°. Moreover, the fluorescence can also be measured from the front, which method is often used to turbid samples.

The detector can be single channel or multiple channels. The detector of a single channel can only detect the intensity of a wavelength at all times while the multi-channel detects the intensity at all wavelengths simultaneously, so that the emission monochromator or filter is unnecessary. The different types of detectors have their advantages and disadvantages.

The fluorimeter more versatile with double monochromator and an excitation light source continuously, it can record both an excitation spectrum and a fluorescence spectrum. By measuring the fluorescence spectra, the wavelength of the excitation light is kept constant, preferably in a high-wavelength absorption and the emission monochromator scans the spectrum. To measure the excitation spectra, the wavelength that passes through the filter or emission monochromator is kept constant and the excitation monochromator is scanned. The excitation spectrum is generally identical to the absorption spectrum, since the intensity of fluorescence is proportional to absorption.

# Biological in vitro charaterization

## Western Blot

Western blot test is a technique used to detect specific proteins from samples such as cell extracts or tissue homogenates, also analyze recombinant proteins synthesized in vitro. Western blot can also be used to identify a target protein on the basis of the special affinity between a certain antigen and its relative antibody. Western blot generally contains three main steps, SDS-PAGE firstly, then blot of samples, and finally immunology test. Qualitative and semi-quantitative data can be acquired about the target protein through western blot.

## SDS-PAGE

The separation of macromolecules in an electric field is called *electrophoresis*. A very common method for separating proteins by electrophoresis uses a discontinuous polyacrylamide gel as a support medium and sodium dodecyl sulfate (SDS) to denature the proteins. The method is called sodium dodecyl sulfate polyacrylamide gel electrophoresis (SDS-PAGE). The most commonly used system is also called the Laemmli method after U.K. Laemmli, who was the first to publish a paper employing SDS-PAGE in a scientific study [32].

SDS (also called lauryl sulfate) is an anionic detergent, meaning that when dissolved its molecules have a net negative charge within a wide pH range. A polypeptide chain binds amounts of SDS in proportion to its relative molecular mass. The negative charges on SDS destroy most of the complex structure of proteins, and are strongly attracted toward an anode (positively-charged electrode) in an electric field.

Polyacrylamide gels restrain larger molecules from migrating as fast as smaller molecules. Because the charge-to-mass ratio is nearly the same among SDS-denatured polypeptides, the final separation of proteins is dependent almost entirely on the differences in relative molecular mass of polypeptides. In a gel of uniform density the relative migration distance of a protein is negatively proportional to the logarithm of its mass. If proteins of known mass are run simultaneously with the unknowns, the relationship between relative migration distance and mass can be plotted, and the masses of unknown proteins estimated.

Protein separation by SDS-PAGE can be used to estimate relative molecular mass, to determine the relative abundance of major proteins in a sample, and to determine the distribution of proteins among fractions [33].

## Sample blotting

Sufficiently separated proteins in an SDS-PAGE can be transferred to a solid membrane for Western blot analysis. For this procedure, an electric current is applied to the gel so that the

separated proteins transfer through the gel and onto the membrane in the same pattern as they separate on the SDS-PAGE. All sites on the membrane which do not contain blotted protein from the gel can then be non-specifically "blocked" so that antibody (serum) will not non-specifically bind to them, causing a false positive result. Often the membrane is cut into strips to facilitate testing of a large number of samples for antibodies directed against the blotted protein (antigen) [34].

## Inmunology test

To detect the antigen blotted on the membrane, a primary antibody (serum) is added at an appropriate dilution and incubated with the membrane. If there are any antibodies present which are directed against one or more of the blotted antigens, those antibodies will bind to the protein(s) while other antibodies will be washed away at the end of the incubation. In order to detect the antibodies which have bound, anti-immunoglobulin antibodies coupled to a reporter group such as the enzyme alkaline phosphatase are added (e.g. goat anti-human IgG-alkaline phosphatase). This anti-Ig-enzyme is commonly called a "second antibody" or "conjugate". Finally after excess second antibody is washed free of the blot, a substrate is added which will precipitate upon reaction with the conjugate resulting in a visible band (where the primary antibody bound to the protein [34].

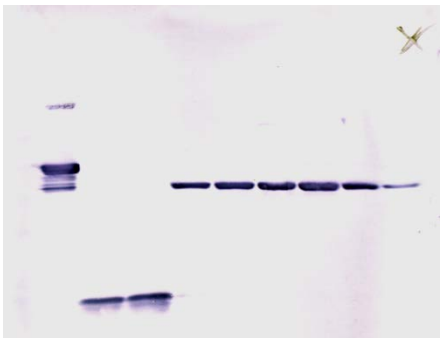

*Figure A-15: Revealed western Blot membrane.*

# Real Time RT-PCR

The real-time, fluorescence-based reverse transcription polymerase chain reaction (RT-PCR) is one of the enabling technologies of the genomic age and has become the method of choice for the detection of mRNA [35].

## PCR and RT-PCR

Polymerase chain reaction (PCR) is a method that allows exponential amplification of short DNA sequences (usually 100 to 600 bases) within a longer double stranded DNA molecule. PCR entails the use of a pair of primers, each about 20 nucleotides in length, that are complementary to a defined sequence on each of the two strands of the DNA. These primers are extended by a DNA polymerase so that a copy is made of the designated sequence. After making this copy, the same primers can be used again, not only to make another copy of the input DNA strand but also of the short copy made in the first round of synthesis. This leads to exponential amplification. Since it is necessary to raise the temperature to separate the two strands of the double strand DNA in each round of the amplification process, a major step forward was the discovery of a thermo-stable DNA polymerase (Taq polymerase) that was isolated from *Thermus aquaticus,* a bacterium that grows in hot pools; as a result it is not necessary to add new polymerase in every round of amplification. After several (often about 40) rounds of amplification, the PCR product is abundant enough to be detected with fluorescent stain. In order to measure messenger RNA (mRNA), the method was extended using reverse transcriptase to convert mRNA into complementary DNA (cDNA) which was then amplified by PCR and, again analyzed. In many cases this method has been used to measure the levels of a particular mRNA under different conditions but the method at best semi-quantitaive. Reverse transcriptase-PCR analysis of mRNA is often referred to as "RT-PCR" which is unfortunate as it can be confused with "real time-PCR".

## Real Time RT-PCR

Normal reverse transcriptase PCR is only semi-quantitative at best. Thus real time PCR was developed because of:

- The need to quantitate differences in mRNA expression
- The availability of only small amounts of mRNA in some procedures.

Quantitative PCR is carried out in a thermal cycler with ability to influence each sample with a beam of light of a wavelength determined and detect the fluorescence emitted by the fluorochrome excited. This thermal cycler is a device with the ability to heat and cool quickly the samples, so that the physical and chemical qualities of nucleic acids and the enzyme DNA polymerase are taken in advantage.

The PCR process usually consists of a cycles of temperature changes in 25-40 times, where each has a minimum of two stages: the first, around 95° C, allows the separation of double-stranded nucleic acids; the second, at a temperature around 50-60° C, allows the alignment of the primers DNA pattern [36].

Quantification can either be relative to an external standard curve or to one or more co-amplified internal control mRNAs. The former is based on the use of a dilution series of an external standard, which can be used to generate a standard curve of Ct
(threshold cycle) against initial target copy number [37]. The copy numbers of unknown samples can be calculated from the linear regression of that standard curve, with the y-intercept giving the sensitivity and the slope giving the amplification efficiency (Figure. Standard curves can be constructed from PCR fragments, in vitro T7-transcribed sense RNA transcripts, from commercially available universal reference RNAs [37].

Quantification relative to internal standards compares the Ct values from target RNAs to those of one or more internal reference genes and results are expressed as ratios of the target-specific signal to the internal reference. This produces a corrected relative value for the target specific RNA product that can be compared between samples and allows an estimate of the relative expression of target mRNA in those samples.

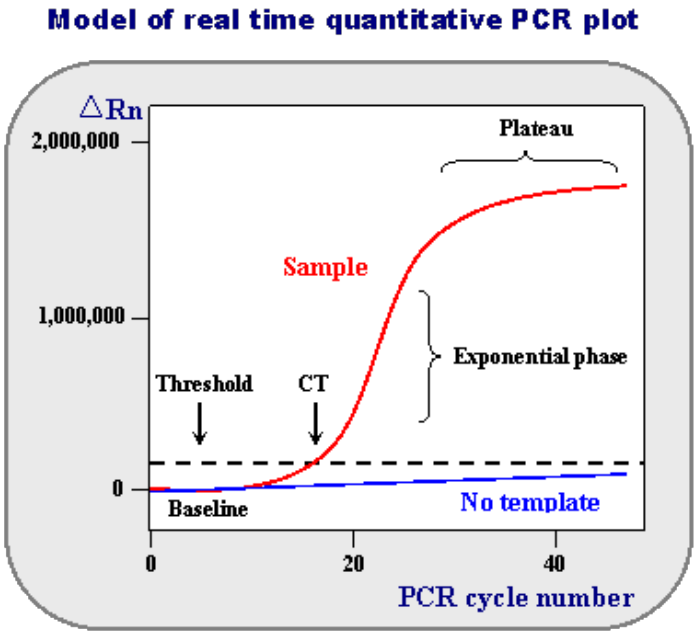


***Figure A-16:*** *Amount of target DNA created by the Real Time instrument (as measured by the fluorescence) is shown. The log (10) of concentration is plotted against the number of instrument cycles [38].*

# References

1. Pegueroles Neyra M. Interactions between titanium surfaces and biological components.

2. Olszak AG, Schmit J, Heaton MG. LaserFocusWorld. 2012.

3. Bagno A, Di Bello C. Surface treatments and roughness properties of Ti-based biomaterials. J Mater Sci Mater Med 2004;15:935-949.

4. Wieland M, Hänggi P, Hotz W, Textor M, Keller BA, Spencer ND. Wavelength-dependent measurement and evaluation of surface topographies: application of a new concept of window roughness and surface transfer function. Wear 2000;237:231-252.

5. Stout KJ, Blunt L. Three dimensional surface topography . : Elsevier, 2000.

6. Wollam JA. Ellipsometry tutorial. http://www.jawoollam.com/tutorial_1.html. 2012.

7. Azzam,R.,M.,A., Bashara N,M. Ellipsometry and Polarized Light. 1986.

8. DIFFER. Using distorted light to characterise surface layers. http://www.differ.nl/en/node/3035. 2012.

9. GHEZZO M. Thickness Calculations for a Transparent Film from Ellipsometric Measurements. J Opt Soc Am 1968;58:368-368.

10. Ramé-Hart. Information on Contact Angle. 2012.

11. van Oss CJ. Hydrophobicity and hydrophilicity of biosurfaces. Current Opinion in Colloid & Interface Science 1997;2:503-512.

12. Adamson AW, Gast AP. Physical chemistry of surfaces. : Wiley, 1997.

13. Médout-Marère V, El Ghzaoui A, Charnay C, Douillard JM, Chauveteau G, Partyka S. Surface Heterogeneity of Passively Oxidized Silicon Carbide Particles: Hydrophobic–Hydrophilic Partition. J Colloid Interface Sci 2000;223:205-214.

14. SCKCEN. *X-ray Photoelectron Spectroscopy at SCK•CEN*.

15. Paynter R. XPS Theory. 2000.

16. EAG Labs. X-Ray Photoelectron Spectroscopy / Electron Spectroscopy for Chemical Analysis (XPS / ESCA). 2012.

17. Siliconfareast. FTIR Spectroscopy. 2005.

18. Thermo Nicolet. Introduction to Fourier Transform Infrared Spectrometry. 2001.

19. Scott RPW. Analytical spectroscopy. 2006.

20. Shimadzu. ABC's of the Specular Reflection Method and Kramer's-Koenig Analysis. 2012.

21. Mirabella FM. Internal Reflection Spectroscopy. Applied Spectroscopy Reviews 1985;21:45-178.

22. Takeda S, Fukawa M. Role of surface OH groups in surface chemical properties of metal oxide films. Materials Science and Engineering B 2005;119:265-267.

23. Physical Electronics. TOF-SIMS<br />What is TOF-SIMS? 2012.

24. Shaw D. Introduction to colloid and surface chemistry. 4th ed. : Butterworth-Heinemann, 1992.

25. Yoon S. Theory - Streaming zeta potential. http://onlinembr.info/Principles/ZetaPotential.htm. 2011.

26. NBTC. Zeta Potential theory. http://www.nbtc.cornell.edu/facilities/downloads/Zetasizer%20chapter%2016.pdf. 2011.

27. Gibbs R. Silver Colloids, http://www.silver-colloids.com/Tutorials/Intro/pcs13.html. 2012.

28. Haynes CA, Sliwinsky E, Norde W. Structural and Electrostatic Properties of Globular Proteins at a Polystyrene-Water Interface. J Colloid Interface Sci 1994;164:394-409.

29. Pegueroles M, Gil FJ, Planell JA, Aparicio C. The influence of blasting and sterilization on static and time-related wettability and surface-energy properties of titanium surfaces. Surface and Coatings Technology 2008;202:3470-3479.

30. Zaucha M, Adamczyk Z, Barbasz J. Zeta potential of particle bilayers on mica: A streaming potential study. J Colloid Interface Sci 2011;360:195-203.

31. Szymczyk A, Fievet P, Mullet M, Reggiani JC, Pagetti J. Comparison of two electrokinetic methods – electroosmosis and streaming potential – to determine the zeta-potential of plane ceramic membranes. J Membr Sci 1998;143:189-195.

32. Laemmli UK. Cleavage of structural proteins during the assembly of the head of bacteriophage T4. Nature 1970;227:680-685.

33. Roitt IM, Brostoff J, Male DK. Inmunología. 5a ed. Madrid; Barcelona etc.: Harcourt, 2000.

34. Burnette WN. "Western blotting": electrophoretic transfer of proteins from sodium dodecyl sulfate--polyacrylamide gels to unmodified nitrocellulose and radiographic detection with antibody and radioiodinated protein A. Anal Biochem 1981;112:195-203.

35. Bustin SA, Benes V, Nolan T, Pfaffl MW. Quantitative real-time RT-PCR--a perspective. J Mol Endocrinol 2005;34:597-601.

36. Rychlik W, Spencer WJ, Rhoads RE. Optimization of the annealing temperature for DNA amplification in vitro. Nucleic Acids Res 1990;18:6409-6412.

37. Bustin SA, Mueller R. Real-time reverse transcription PCR (qRT-PCR) and its potential use in clinical diagnosis. Clin Sci (Lond) 2005;109:365-379.

38. NCBI. Probe, http://www.ncbi.nlm.nih.gov/projects/genome/probe/IMG/PCR_plot.gif. 2012.